DEPARTMENT OF ANALYTICAL CHEMISTRY

Development of separation methods and measurement protocols for Sr and Pb isotopic analysis of archaeological artefacts by means of single-collector and multi-collector ICP-mass spectrometry

Thesis submitted in fulfillment of the requirements for the degree of Doctor (Ph.D.) in Sciences : Chemistry

by

David De Muynck

PROMOTER : PROF. DR. F. VANHAECKE

June 2008

Acknowledgements

After the first lessons in chemistry I had in secondary school, I was interested in this science. A few years later, I started studying Chemistry at Ghent University. During these studies, I became convinced that chemistry is everywhere, and especially analytical chemistry drew my attention. After finishing my Master thesis in analytical chemistry, I had the chance to start a Ph.D. research in the same field. It started with a description of a not so well defined project: 'method development for isotope ratio analysis using (MC-)ICP-MS'. A new interesting challenge for me. Soon, I was working on three different projects requiring a lot of analytical chemistry followed by an attempt to answer a specific archaeological question. The results of four years Ph.D. research are summarized in this thesis. Of course, this thesis could not have evolved into what it is now without the input and the help of a number of people.

First of all, I want to express my gratitude towards my promoter, Prof. dr. Frank Vanhaecke, for offering me the possibility to carry out this research in his lab. I had the feeling to be really appreciated and trusted and received many possibilities to present my work on international meetings, which was always a wonderful experience.

My gratitude also goes to Prof. dr. Karel Strijckmans, the chairman of the Department of Analytical Chemistry, for making available the labs and the equipment.

This Ph.D. research consisted of multidisciplinary studies. I want to thank dr. Liesbeth Smits for providing the archaeological samples investigated in the framework of the Roman Bone and the Servatius projects. Em. Prof. dr. Freek de Wolff is thanked for sharing important considerations on the toxicology of lead and his enthusiasm concerning the lead study. Dr. Parsival Delrue is thanked for providing a (huge!) collection of metallic artefacts for the ed-Dur project. Further, I want to thank Liesbeth, Freek and Parsival for many email and/or personal communications that were most valuable for bringing all the analyses to a good end and for a proper interpretation of the isotope ratio data.

During my Ph.D. research, I had the opportunity to meet and work together with dr. Christophe Cloquet. Christophe, although your stay in Ghent was unfortunately quite short, I have learnt a lot from you and would like to express my sincere gratitude for sharing your considerable knowledge on isotopes and so much more. Further, I enjoyed the coffee breaks and it was great to have someone in the lab that also likes metal music. And the Goldschmidt 2007 conference in Cologne was my best conference so far!

Besides learning many things myself, I also tried to transfer some of my knowledge to last-year master students. I would like to acknowledge Karen, Pieter, Gonzalo and Sylvia for the nice and mostly smooth cooperations. Gonzalo, I really enjoyed working with you and going for a beer on Friday, followed by another metal gig in the weekend. You will

probably remember the E-17 between Ghent and Antwerp forever! Further, Karolina Danielewska is thanked for her big smile and for being a nice colleague and also great company for going out!

I also want to mention Roger Van Tittelboom in this acknowledgement. Without his quick interventions, patience and large knowledge about the electronics and delicate parts of an ICP – mass spectrometer, the instruments would have been out of operation much more often. Roger, your enthusiasm and optimism were always a pleasure to enjoy. Thank you for the many conversations about all kind of things! Also Bart is thanked for his quick help on all kind of computer-related problems.

Further, I want to acknowledge all the colleagues that left or joined the Department of Analytical Chemistry, and in particular the Atomic and Mass Spectrometry unit, during the period I was there.

Last, but not least, I want to thank my parents for the infinite trust and faith they have always had in me, and for always supporting me in whatever I do. Thank you!

David

Table of contents

Acknowledgements iii

Table of contents vii

CHAPTER I – Introduction and objectives 1

I.1 – Theoretical aspects 3

I.2 – Method development 4

I.3 – Archaeological applications 5

CHAPTER II – Inductively coupled plasma – mass spectrometry (ICP-MS) 7

II.1 – Operating principle 9

II.2 – Sample introduction system 10

II.2.1 – Pneumatic nebulization systems 12

II.2.1.1 – Nebulizers 12

II.2.1.1.1 – Concentric nebulizer 12

II.2.1.1.2 – Crossflow nebulizer 13

II.2.1.1.3 – Microconcentric nebulizer 13

II.2.1.2 – Spray chambers 13

II.2.1.2.1 – Cyclonic spray chamber 14

II.2.1.2.2 – Double-pass Scott-type spray chamber 14

II.2.1.3 – Performance 14

II.2.2 – Aridus aerosol desolvating device 15

II.2.3 – Alternative sample introduction systems 16

II.2.3.1 – Electrothermal vaporization (ETV) 16

II.2.3.2 – Laser ablation (LA) 16

II.3 – Inductively coupled plasma (ICP) 16

II.4 – Interface region 18

II.5 – Mass spectrometers 18

II.5.1 – Quadrupole filter 20

II.5.1.1 – Description 20

II.5.1.2 – Operating principle 21

II.5.1.3 – Performance 24

II.5.2 – Sector field mass spectrometer 24
II.5.2.1 – Description 24
II.5.2.2 – Magnetic sector 24
II.5.2.3 – Electrostatic sector 25
II.5.2.4 – Double focusing setup 26
II.5.2.5 – Performance 28
II.6 – Collision/reaction cell technology 28
II.6.1 – History of collision/reaction cells 29
II.6.2 – Dynamic reaction cell (DRC) 30
II.6.2.1 – Description 31
II.6.2.2 – Ion-molecule interactions 32
II.6.2.2.1 – Collisional processes 32
II.6.2.2.2 – Ion-molecule reactions 33
II.6.2.2.3 – Ion-molecule reaction types 34
II.6.2.2.4 – Non-reactive collisions 35
II.6.2.2.5 – Control of sequential chemistry 36
II.7 – Detection system 38
II.7.1 – Ion counting systems 39
II.7.2 – Analogue collection 39
II.7.3 – Dual detection systems 40
II.7.4 – Performance 40
II.8 – ICP-MS instruments used in this work 41
II.9 – ICP-MS for trace element determination 42
II.9.1 – Semi-quantitative elemental analysis 43
II.9.2 – Quantitative elemental analysis 44
II.9.2.1 – External standardization 44
II.9.2.2 – Standard addition 44
II.9.2.3 – Isotope dilution (ID) 45
II.9.3 – Internal standardization 45

CHAPTER III – Isotope ratio analysis via ICP-MS 47
III.1 – General concepts of isotopic analysis 49
III.2 – Stable isotope fractionation 52
III.2.1 – History 53
III.2.2 – Equilibrium isotopic fractionation 54
III.2.3 – Kinetic isotopic fractionation 54

III.3 – ICP-MS for isotope ratio applications 55
III.3.1 – Single-collector ICP-MS 55
III.3.2 – Multi-collector ICP-MS 56
III.4 – Uncertainty factors in isotope ratio determination via ICP-MS 59
III.4.1 – Sources of noise 59
III.4.2 – Mass discrimination 60
III.4.2.1 – Origin of mass discrimination 61
III.4.2.2 – Correction for mass discrimination 62
III.4.2.2.1 – Internal and external normalization 62
III.4.2.2.2 – External standardization 64
III.4.3 – Mass scale shift 65
III.4.4 – Background and contamination 65
III.4.5 – Detector dead time 67
III.4.5.1 – Definition 67
III.4.5.2 – Experimental determination of the detector dead time 67

CHAPTER IV – Target elements and sample types investigated in this work 73
IV.1 – Rubidium/strontium isotope system 75
IV.1.1 – Occurrence and properties of Rb and Sr 75
IV.1.2 – Rb-Sr dating 77
IV.2 – Uranium/thorium/lead isotope system 79
IV.2.1 – Occurrence and properties of U and Th 79
IV.2.2 – U-Th-Pb dating 81
IV.2.3 – Occurrence and properties of lead 82
IV.3 – Sr and Pb isotopes in archaeological studies 83
IV.3.1 – Sr isotope studies 84
IV.3.2 – Pb isotope studies 85
IV.4 – Sample types investigated in this work 87
IV.4.1 – Soils 87
IV.4.2 – Bone and dental tissues 89
IV.4.3 – Ceramics 91
IV.4.4 – Metallic artefacts 91

CHAPTER V – Sample pretreatment and digestion procedures 93

V.1 – Sample pretreatment procedures 95

V.1.1 – Sample cleaning and cutting 95

V.1.2 – Sample homogenization: microdismembrator 96

V.1.3 – Sampling of metallic artefacts: miniature-drill setup 97

V.2 – Sample digestion approaches 98

V.2.1 – Hotplate digestion 98

V.2.2 – Microwave-assisted acid digestion 99

V.2.2.1 – Absorption of microwave energy and heating 99

V.2.2.2 – Operating principle 99

V.2.2.3 – Performance 101

V.3 – Acid chemistry 101

V.3.1 – Nitric acid 102

V.3.2 – Hydrochloric acid 102

V.3.3 – Hydrofluoric acid 103

V.3.4 – Sulfuric acid 103

V.3.5 – Hydrogen peroxide 104

V.3.6 – Perchloric acid 104

V.4 – Development and validation of digestion procedures 105

V.4.1 – Soil digestion procedure 106

V.4.2 – Bone digestion procedure 107

V.4.3 – Enamel and dentine digestion procedure 107

V.4.4 – Ceramics digestion procedure 108

V.4.5 – Metallic artefacts digestion procedure 110

V.5 – Certification of Pb in bone candidate reference materials ... 111

V.6 – Conclusions 113

CHAPTER VI – Isolation procedures for strontium and lead 115

VI.1 – Pitfalls in obtaining accurate and precise isotope ratio results 117

VI.1.1 – Spectral interferences 117

VI.1.2 – Matrix effects 119

VI.1.3 – Other factors 119
VI.2 – Analyte separation prior to isotopic analysis 120
VI.2.1 – Interferences on strontium and lead 120
VI.2.2 – Requirements for analyte isolation 121
VI.2.3 – Existing isolation techniques for strontium 122
VI.2.4 – Existing isolation techniques for lead 123
VI.2.5 – Strontium and lead isolation techniques used in this work 123
VI.3 – Extraction chromatography using Sr spec™ 124
VI.3.1 – Description of the resin 124
VI.3.2 – Evaluation and optimization of the use of Sr spec™ resin 125
VI.3.2.1 – Isolation of Sr from its concomitant matrix 125
VI.3.2.2 – Separation of rubidium and strontium 128
VI.4 – Extraction chromatography using Pb spec™ 130
VI.4.1 – Description of the resin 130
VI.4.2 – Evaluation and optimization of the use of Pb spec™ resin 130
VI.5 – Isotopic fractionation on the Sr and Pb resins 134
VI.6 – Multiple use of extraction chromatographic resins 136
VI.7 – Conclusions 140

CHAPTER VII – Single-collector – and multi-collector ICP-MS measurement protocols 141
VII.1 – Quadrupole-based ICP-MS – elemental assay 143
VII.2 – ICP-DRC-MS – P, Ca and Sr determination 143
VII.2.1 – Selection of the target isotopes of P, Ca and Sr 144
VII.2.2 – Optimization of ICP-DRC-MS for P, Ca and Sr determination 147
VII.2.2.1 – Optimization of the NH_3 gas flow rate 148
VII.2.2.2 – Optimization of the rejection parameter q (RPq) 152
VII.2.2.3 – Determination of phosphorus 153
VII.2.3 – Validation of the ICP-DRC-MS measurement protocol 154
VII.2.4 – Conclusions 155
VII.3 – MC-ICP-MS – Sr isotopic composition 156
VII.4 – MC-ICP-MS – Pb isotopic composition 158
VII.5 – SC-ICP-DRC-MS – Pb isotopic composition 160
VII.5.1 – Selection of a collision gas and optimization of the flow rate 161
VII.5.2 – Measurement protocol 163

VII.5.3 – Validation of the SC-ICP-DRC-MS measurement protocol 165
VII.5.3.1 – Duplicate analyses 166
VII.5.3.2 – Comparison of single-collector – and multi-collector ICP-MS results 166
VII.5.3.3 – Pb isotope ratio determination in certified reference materials 169
VII.5.4 – Conclusions 171

CHAPTER VIII – Provenancing pre-Islamic metallic artefacts excavated at ed-Dur and Khor Rori 173
VIII.1 – Geography, history and archaeology 175
VIII.1.1 – The archaeological site of ed-Dur 175
VIII.1.2 – The archaeological site of Khor Rori 177
VIII.1.3 – Historical written sources on trade 177
VIII.2 – Samples investigated in this work 178
VIII.3 – Analytical methodology 179
VIII.4 – Pb isotope ratio results 184
VIII.5 – Provenance determination of artefacts 184
VIII.5.1 – Fragments BS 1466 and Z 019 (lead) and KR 009 (bronze) 187
VIII.5.2 – Copper-based artefacts 189
VIII.5.3 – Silver and lead artefacts 191
VIII.6 – Conclusions and implications on trade 195

CHAPTER IX – Investigation of infant exposure to lead during the Roman Era 199
IX.1 – Toxicological and historical background 201
IX.1.1 – Toxicology of lead 201
IX.1.2 – The use of lead in the Roman Era 202
IX.2 – Sampling site and history of research 203
IX.3 – Samples investigated in this work 204
IX.4 – Analytical methodology 205
IX.5 – Pb concentration and Pb isotope ratio results 205
IX.5.1 – Pb concentration results 205
IX.5.2 – Pb isotope ratio results 210
IX.6 – Conclusions 218

CHAPTER X – Investigation of the grave field population around the Servatius complex 219
X.1 – History of Servatius 221
X.2 – Samples investigated in this work 223
X.3 – Analytical methodology 224
X.4 – Evaluation of diagenetic alteration 224
X.5 – Sr concentration and Sr isotope ratio results 227
X.6 – Conclusions and future 231

CHAPTER XI – Summary and conclusions 235
XI.1 – Analytical methodologies developed 237
XI.2 – Archaeological projects 240

HOOFDSTUK XII – Samenvatting en besluit 243
XII.1 – Ontwikkelde analytische strategie 245
XII.2 – Archeologische projecten 248

References 253

CHAPTER I

Introduction and objectives

The aim of this work is to answer specific archaeological questions by means of isotope ratio analysis of strontium and lead. A first phase of this work consisted of the development of an appropriate analytical methodology, while in a second phase, the methodologies developed were applied to the archaeological applications.

I.1 – Theoretical aspects

Inductively coupled plasma – mass spectrometry (ICP-MS) is a powerful technique for (ultra)trace element determination. One of the advantages of ICP-MS is that this technique can provide information on the isotopic composition of the target element(s). For applications of isotope ratio analysis that require a high isotope ratio precision, single-collector ICP-MS (SC-ICP-MS) cannot compete with thermal ionization – mass spectrometry (TI-MS), a technique that has long been regarded as the reference technique for isotope ratio determinations of the "heavier" elements. However, ICP-MS has gained growing importance in the field of isotope ratio analysis after the introduction of multi-collector ICP-MS (MC-ICP-MS), a combination of the ICP as an ion source and a detector array consisting of multiple Faraday cups and electron multipliers for ion detection. Since the ICP is a more powerful ion source than a thermal ion source, elements that are difficult to ionize via thermal ionization became accessible to isotopic studies, with an isotope ratio precision similar to that offered by TI-MS. Additional important benefits of (MC-)ICP-MS over TI-MS are the continuous nebulization of sample solution into the ion source at atmospheric pressure and a higher sample throughput. Hence, MC-ICP-MS has evolved into a dedicated tool for isotopic analysis. In this work, both single-collector ICP-MS and multi-collector ICP-MS have been used for isotope ratio determination. In chapter II, the various components of present-day ICP – mass spectrometers are discussed. Chapter III provides general concepts and theory regarding isotope ratio analysis and isotopic fractionation, and further considers the use of ICP-MS for isotope ratio analysis.

The target elements in this work are strontium and lead. The isotopic composition of both of these elements is prone to small variations, since at least one isotope of each of these elements is an end-product of the radioactive decay of naturally occurring and long-lived radionuclides. One of the strontium isotopes, ^{87}Sr, is formed by the beta-decay of ^{87}Rb. The lead isotopes ^{206}Pb, ^{207}Pb and ^{208}Pb are the end-product of the decay series of ^{238}U, ^{235}U and ^{232}Th, respectively. These isotope systems are discussed in more detail in chapter IV. The variations in the isotopic composition of strontium and lead can be used

for a number of archaeological applications, some of which were carried out in this work. Strontium isotopic variations in dental tissues can be used to trace population migration between distinct geological areas. The isotopic composition of lead can be used for the provenance determination of archaeological artefacts and the investigation of lead exposure in the past. In chapter IV, these applications are highlighted. Most of the samples of archaeological origin investigated in this work are characterized by a complex matrix composition (*e.g.*, soil, bone and dental tissues). Chapter IV summarizes the characteristics and typical elemental composition of the various sample types studied in this work: soil, bone and dental tissues, ceramics and metallic objects with high copper, silver and/or lead contents.

I.2 – Method development

In its standard configuration, ICP-MS is suited for the analysis of solutions. This implies that solid samples need to be digested prior to analysis. Further, in order to improve the speed and performance of the digestion process, the conversion of the solid particles or fragments into a homogeneous and finely dispersed powder is beneficial. The first part of chapter V focuses on the pretreatment of the solid samples supplied: cleaning, rinsing, homogenization and sampling of metallic fragments and coins. The second part of chapter V is dedicated to the digestion procedures that were developed to dissolve the various sample types. Hereto, a suitable combination of acids was added to the powdered samples, followed by a hotplate digestion or a microwave-assisted acid digestion. The digestion procedures aimed at a complete dissolution of the samples to assure that no strontium or lead isotopic fractionation is introduced by the digestion process. Certified reference materials were used for validation of the digestion protocols developed.

Most of the sample types under study (soil, bone and dental tissues, ceramics and metallic objects) are characterized by a complex matrix composition. Especially in the case where MC-ICP-MS is used for isotope ratio analysis, it is required to isolate the target element from its concomitant matrix prior to isotopic analysis, in order to obtain accurate and precise isotope ratio results. In this work, the target elements Sr and Pb were isolated by means of an extraction chromatographic separation, based on a crown ether. It was the intention to obtain the pure Sr or Pb fraction of the sample and to establish a quantitative recovery so that no isotopic fractionation of Sr or Pb is introduced by the separation process. The separation procedures developed are described in chapter VI.

Multi-collector ICP-MS was used in this work for Sr and Pb isotopic analysis. However, in the cases where the very high precision as offered by MC-ICP-MS is not required, also single-collector ICP-MS can provide valuable results. The use of a collision gas in the dynamic reaction cell (DRC) of a quadrupole-based ICP – mass spectrometer allows isotope ratio precisions to be obtained that are better than those attainable with standard quadrupole-based ICP-MS. A single-collector ICP-DRC-MS measurement protocol, using a quadrupole-based ICP-MS instrument equipped with a dynamic reaction cell, was hence developed for Pb isotope ratio analysis. Validation of the measurement protocol was performed by comparison of the experimental results with the corresponding results obtained by multi-collector ICP-MS and the analysis of samples with a known isotopic composition, as is described in chapter VII.

The use of a gas in the dynamic reaction cell of a quadrupole-based ICP – mass spectrometer is not only useful in the case of isotopic analysis, but also allows the selective removal of spectral interferences when an appropriate reaction gas is chosen. A measurement protocol was developed for the simultaneous determination of P, Ca and Sr in dental tissues in order to evaluate the biogenic integrity of these tissues. The development and validation of this measurement protocol is also discussed in chapter VII.

I.3 – Archaeological applications

The digestion procedures, separation methods and measurement protocols developed were applied to Sr or Pb isotope ratio analysis in the context of three archaeological projects, each having its own specific question.

A first project aimed at obtaining insight into the trade relations between the Roman Empire and the Indian subcontinent in the period 1st century BC – 1st half 2nd century AD, and the position of the coastal site of ed-Dur in the international metal trading network of this period. The samples investigated originate from the archaeological site of ed-Dur, located in the Emirate of Umm al-Qaiwain (United Arab Emirates). Excavations conducted on this site have revealed the presence of an enormous amount of imported goods, such as metallic objects, pottery and glasswork, witnessing an international orientation. A large collection of metallic objects and fragments (unalloyed copper, brass, bronze, silver, lead, litharge) excavated at the site of ed-Dur was available for investigation and submitted to Pb isotope ratio analysis. For comparison purposes, also the Pb isotopic composition of a few metallic samples excavated at the archaeological site of Khor Rori (Oman) was studied. Single-collector ICP – dynamic reaction cell – MS was used for Pb isotope ratio

analysis of the metallic artefacts, and an attempt was made to determine the provenance of the metallic objects studied on the basis of their Pb isotopic composition. This project was carried out in collaboration with the research unit Near Eastern Archaeology of the Department of Languages and Cultures of the Near East and North-Africa (Ghent University), and the results of this study are presented in chapter VIII.

In a second study, the origin of high lead concentrations, retrieved in infant bone tissue dating from the Roman Era, is investigated. Archaeological artefacts, excavated at the remains of a cemetery of a Roman settlement dating from the 1^{st} – 3^{rd} century AD in the village of Valkenburg (The Netherlands), are in the centre of attention. The sample set under investigation consists of infant bone tissue, along with samples from the surrounding soil and additional potential sources of bone lead, such as fish bones, lead fragments and ceramics. The aim of the project is to elucidate whether the high bone lead concentrations arise from the process of diagenesis by post-mortem lead exchange between the bone tissue and the surrounding soil, or if *in vivo* lead exposure can be identified as the cause of the high Pb content in the bone tissue of the infants. To this purpose, the artefacts were investigated for their Pb isotopic composition using multi-collector ICP-MS. This research was carried out in collaboration with the Amsterdam Archaeological Center (University of Amsterdam) and the Toxicology Laboratory of the Leiden University Medical Center, and the results obtained are summarized in chapter IX.

The third archaeological question deals with the grave field population excavated around the basilica dedicated to Saint Servatius in Maastricht (The Netherlands). The Servatius complex witnesses of 1 600 years of religion and is one of the most important monuments of the Low Countries. An explorative study was carried out to obtain insight into the heterogeneity of the populations from two grave fields, Pandhof and Vrijthof. Hereto, the strontium isotopic composition of the dental tissues (enamel and dentine) of a number of individuals from the buried populations were determined via multi-collector ICP-MS. The strontium isotopic composition of enamel is a reflection of the geological area of residence during childhood, while that of dentine reflects the geological area where the individual under study resided during the last years of his/her life. Hence, when enamel and dentine display a different strontium isotopic composition, this indicates that the individual has relocated during his/her life. The results of this explorative study, carried out in collaboration with the Amsterdam Archaeological Center (University of Amsterdam) are presented in chapter X.

CHAPTER II

Inductively coupled plasma – mass spectrometry (ICP-MS)

Since its commercial introduction in 1983, inductively coupled plasma – mass spectrometry (ICP-MS) has continuously gained importance as an elemental detection technique. This is owing to its (i) extremely low detection limits (ng L^{-1} and even sub-ng L^{-1} range), (ii) multi-element character, (iii) high sample-throughput, (iv) wide linear dynamic range and (v) relatively simple spectra [Houk *et al.*, 1980; Gray, 1986; Gray, 1989]. These excellent figures of merit make ICP-MS one of the most powerful techniques for trace element ($< 10^{-4}$ g g^{-1}) and ultratrace element ($< 10^{-8}$ g g^{-1}) determination. Furthermore, ICP-MS offers the possibility to obtain information on the isotopic composition of the target element(s). Especially with the introduction of multi-collector ICP – mass spectrometers, combining an excellent isotope ratio precision with the possibility of continuous nebulization of sample solution into an ion source at atmospheric pressure and the high ionization efficiency of the ICP [Walder and Freedman, 1992; Walder and Furuta, 1993], ICP-MS also gained growing importance in isotope ratio analysis. Next to the standard introduction system, consisting of a pneumatic nebulizer and a spray chamber for analysis of sample solutions (digests), the use of alternative sample introduction systems such as electrothermal vaporization (ETV) and laser ablation (LA) allow direct analysis of solid samples [Darke and Tyson, 1994]. Furthermore, hyphenation with separation techniques such as capillary electrophoresis (CE), gas chromatography (GC) and high performance liquid chromatography (HPLC) allows the use of ICP-MS in elemental speciation studies [Zoorob *et al.*, 1998]. Obviously, the application range of ICP-MS is immense and this technique has become a valuable partner throughout the analytical world, for both academic and industrial purposes.

II.1 – Operating principle

In ICP – mass spectrometry, an argon inductively coupled plasma (ICP) is deployed as an ion source. The sample under investigation, in many cases an aqueous solution, is converted into an aerosol by means of a suited sample introduction system, and led into the plasma. Energy transfer from plasma to sample aerosol results in desolvation of the aerosol, atomization of the molecules and ionization of the atoms. Since the ICP is working at atmospheric pressure, while the mass spectrometer (MS) operates under high vacuum conditions, an interface, offering a stepwise decrease in pressure, is needed. The interface allows only a part of the plasma gas – consisting of ions, electrons and neutrals – to pass. After the interface, a lens (or lens system) extracts the positive ions from the bundle and also deflects the anions and electrons. Both the neutrals and the

negatively charged species extracted by the interface are pumped away by vacuum pumps. The positive ion beam is then focused towards the mass spectrometer, in which the ions are separated according to their mass-to-charge (m/z) ratio, or simplified, by mass, when only singly positively charged ions (M^+) are considered. Finally, the ions that had a stable trajectory through the mass spectrometer are detected, resulting in a signal intensity that is proportional to the amount of ions registered, and thus the concentration of the target element in the sample investigated [Evans *et al.*, 1995]. A schematic representation of a conventional quadrupole-based ICP – mass spectrometer is given in figure II.1. What follows, is a detailed description of the principal components found in present-day ICP-MS instrumentation.

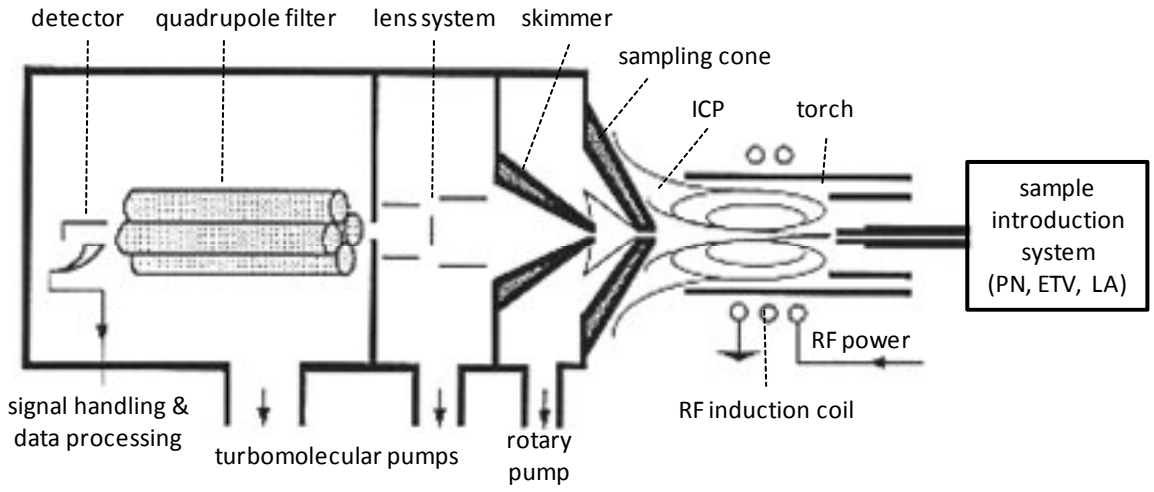

Figure II.1 – Schematic representation of a conventional quadrupole-based ICP – mass spectrometer

II.2 – Sample introduction system

The sample introduction system serves two purposes: (i) the conversion of the sample into an aerosol, and (ii) guiding a representative part of the sample into the plasma. In its standard configuration, an ICP – mass spectrometer is equipped with a pneumatic nebulizer mounted onto a spray chamber, and is suited for analysis of liquid samples, or solid samples that have been dissolved prior to analysis. The liquid sample is converted into an aerosol, and only the smallest droplets are transported to the plasma. Since in this way, both the analyte (M^+) and the matrix and solvent enter the plasma, the occurrence of spectral and non-spectral interferences is triggered.

Spectral interferences occur when ions having the same nominal mass as the analyte are formed [Horlick and Montaser, 1998]. This type of interferences is also called 'additive

interferences', since they alter the intercept of the calibration curve with the Y-axis. A sample matrix can induce two types of spectral interference: (i) plasma- and/or matrix-induced molecular species, such as oxide-, nitride-, argide- and dimer ions (*e.g.*, N_2^+, NO^+, NOH^+, O_2^+, ArN^+, ArO^+, $ArOH^+$, Ar_2^+, ArM^+) and (ii) singly charged ions from the matrix elements themselves (*e.g.*, M^+ and M'^+) and/or their oxides and hydroxides (*e.g.*, MO^+, MOH^+) [Evans and Giglio, 1993]. In order to prevent spectral interferences from occurring, various approaches can be followed [Dams *et al.*, 1995]. The most drastic one is to separate the analyte from the species at the origin of the interfering ion by a chemical separation method. However, this approach is not suitable for interferences originating from, *e.g.*, argon. In this case, the formation of the interference in the plasma itself can be prevented by operating the plasma under so-called 'cold plasma' or 'cool plasma' conditions, which means that the plasma is operated at low power and high injector flow rate. As a result, the distribution of the ionic species after the plasma is totally changed, suppressing in particular the interfering species originating from argon (*e.g.*, Ar^+ and Ar-containing molecular ions) [Douglas and Tanner, 1998]. Alternatively, a plasma relying on another gas than argon, *e.g.*, helium, can be used [Sheppard *et al.*, 1990]. Further in the instrument, the mass analyzer itself can be of such a design that the mass resolving power (mass resolution) is high enough to distinguish the interfering ion from the analyte. In low-resolution (quadrupole-based) mass spectrometers, a collision/reaction cell can be installed in-between the plasma and the mass analyzer, providing a reactor in which the interference is chemically suppressed.

Non-spectral interferences, or matrix effects, refer to matrix-induced changes in signal intensity that are unrelated to the presence of a spectral component [Horlick and Montaser, 1998]. A high concentration of concomitant may suppress or enhance the signal in a complex fashion, depending on the concomitant's concentration. In general, the presence of a high concentration of a concomitant suppresses the analyte signal, although under certain conditions, enhancement has been established as well. The suppression is usually more serious with heavier matrix elements, and light analytes are more severely influenced. This type of interferences is also called 'multiplicative interferences', since they alter the slope of the calibration curve. They play a role in, *e.g.*, the ionization equilibrium and charge distribution in the plasma. Intensive research has been carried out with the aim of avoiding or correcting for these effects. Replacing the standard sample introduction system by, *e.g.*, a desolvating system or electrothermal vaporization (ETV) were shown as valuable alternatives. In view of the analytical problem to deal with, the best suited sample introduction system can be selected, based on aggregation state of the sample,

matrix composition, amount of sample available, desired analysis speed and analyte concentration.

II.2.1 – Pneumatic nebulization systems

Liquid sample introduction is the most common way to bring a sample into the plasma [Montaser *et al.*, 1998-a]. Generally, liquids are dispersed into fine aerosols before being introduced into the ICP. Typically, the quality of the aerosol is improved by removing the large droplets from the aerosol stream by means of a spray chamber.

II.2.1.1 – Nebulizers

The most widespread sample introduction device in ICP – (optical and mass) spectrometry is the pneumatic nebulizer (PN). Below, three types of nebulizers are discussed: (i) the concentric nebulizer, (ii) the crossflow nebulizer and (iii) the microconcentric nebulizer. More information on other nebulizer devices available, such as the ultrasonic nebulizer, the thermospray nebulizer and the direct injection nebulizer, can be found in dedicated sources, *e.g.*, [Montaser *et al.*, 1998-a].

II.2.1.1.1 – Concentric nebulizer

One of the most frequently used nebulizers is the concentric nebulizer of the Meinhard type (figure II.2.a) [Meinhard *et al.*, 1992]. This nebulizer consists of 2 glass or quartz capillaries that are mounted in a concentric setup. The liquid sample solution flows in the inner capillary, and an Ar gas stream flows in the outer capillary. At the tip of the nebulizer, where both capillaries join, the outer (gas) capillary narrows, causing an acceleration of the Ar flow and thus a decreased pressure in the inner (liquid) capillary. This effect is known as the Venturi effect. The interaction between the accelerated gas flow and the liquid flow at the nebulizer tip breaks up the liquid into an aerosol. The sample solution is spontaneously aspirated into the liquid capillary owing to the Venturi effect (self-aspiration or auto-aspiration). Despite this phenomenon, in most cases a peristaltic pump is used because in this way, the sample uptake rate is independent of the viscosity of the sample solution, and hence, the sample flow can be controlled. This results in a better long-term stability.

II.2.1.1.2 – Crossflow nebulizer

In a crossflow nebulizer [Kniseley *et al.*, 1974], two adjustable capillary tubes (GemTips) are mounted at right angles with respect to each other in a polytetrafluoroethylene (PTFE) body. The vertical capillary guides the liquid sample, while the horizontal capillary guides an argon gas stream. The relative positions of the capillaries can be adjusted to achieve optimal performance, what, in its turn, negatively affects the long-term stability of the nebulizer if the capillaries move. The interaction between the liquid flow and the perpendicular gas flow causes the liquid sample to be broken up into an aerosol. Regarding the absence of the Venturi effect, this type of nebulizer is always used in combination with a peristaltic pump for sample delivery.

II.2.1.1.3 – Microconcentric nebulizer

The microconcentric nebulizer (MCN) is a highly efficient nebulizer for operation at low sample uptake rates (< 1 mL min^{-1}). Different types are available, manufactured from quartz or a HF-resistant material. It was shown for a MCN-100 microconcentric nebulizer (figure II.2.b) that when operated at a solution uptake rate of 30 µL min^{-1}, the MCN can provide detection limits similar to those of a PN consuming sample solution at a rate of 1000 µL min^{-1} [Vanhaecke *et al.*, 1996-a].

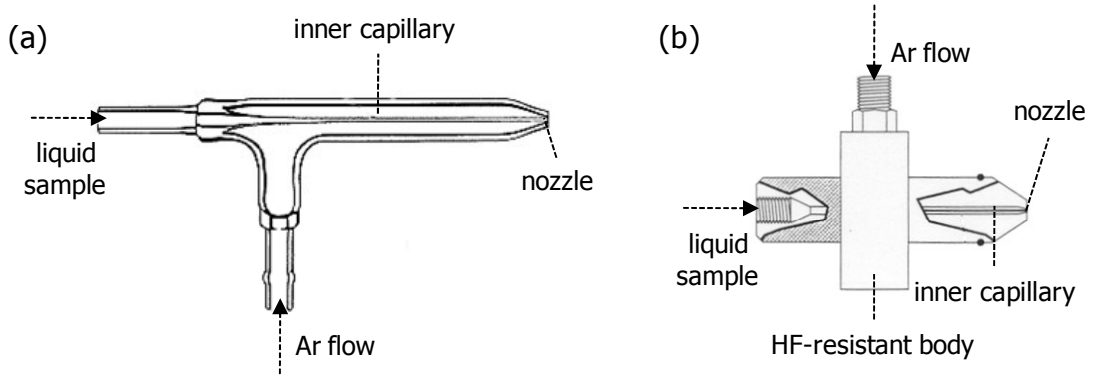

Figure II.2 – Nebulizers – (a) concentric nebulizer of the Meinhard type; (b) MCN-100 microconcentric nebulizer

II.2.1.2 – Spray chambers

Nebulizers produce aerosols that are very dispersed in diameter, up to 100 µm, while only droplets with a diameter less than 10 µm lead to an efficient desolvation, atomization and ionization in the plasma [Montaser *et al.*, 1998-a]. Hence, a spray chamber is needed to remove the large droplets from the aerosol that will be transported to the plasma. In this

way, a stable and efficient plasma operation is guaranteed. Below, the cyclonic and the double-pass Scott-type spray chambers are described.

II.2.1.2.1 – Cyclonic spray chamber

A cyclonic spray chamber (figure II.3.a) [Vieira *et al.*, 1986] has a conical shape, and the aerosol enters through a tangential inlet on the periphery of the spray chamber body and flows in a downward spiral motion. This motion leads to a centrifugal force acting on the droplets. The larger (heavier) droplets impact against the side of the spray chamber and are evacuated. In the lower region of the spray chamber, the aerosol changes direction and moves upward in an even tighter spiral, concentric with the original path. Finally, the finest droplets pass through the outlet tube towards the plasma.

II.2.1.2.2 – Double-pass Scott-type spray chamber

The double-pass spray chamber of the Scott-type [Scott *et al.*, 1974] is shown in figure II.3.b. In this type of spray chamber, the larger droplets are removed by turbulent deposition on the inner walls of the spray chamber, and by gravity. The inner concentric tube reduces random fluctuations in signal intensity, much of which originate from aerosol density changes in the spray chamber.

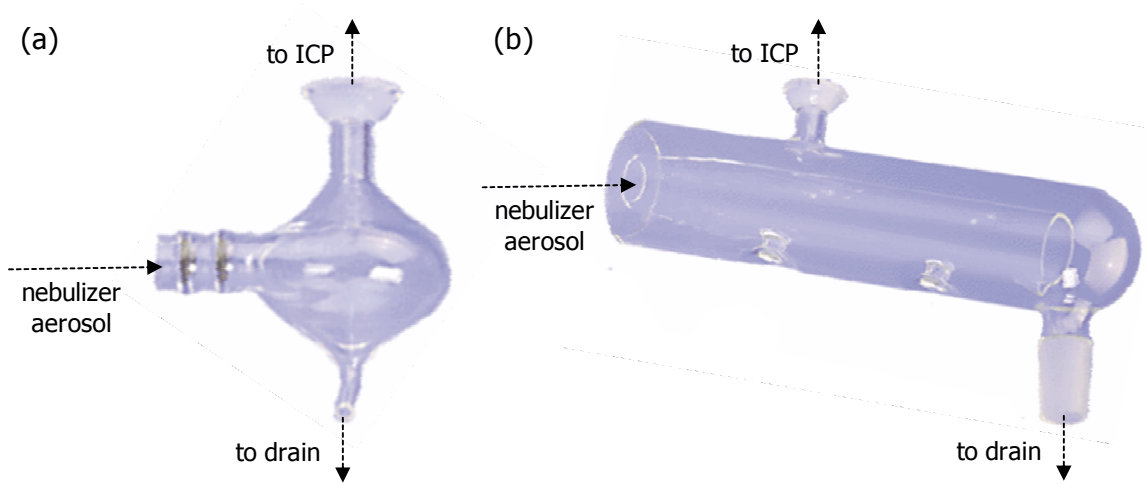

Figure II.3 – Spray chambers – (a) cyclonic spray chamber;
(b) double-pass Scott-type spray chamber

II.2.1.3 – Performance

The combination of a pneumatic nebulizer and a spray chamber is characterized by its (i) relatively low cost, (ii) instrumental simplicity, (iii) high sample-throughput and (iv) good

stability. Despite these advantages, (i) the transport efficiency of this introduction system is limited to 1-2 % [Olesik and Bates, 1995], (ii) the simultaneous introduction of analyte(s) and matrix can give rise to spectral interferences and matrix effects and (iii) the application range of this setup is limited to sample solutions.

II.2.2 – Aridus aerosol desolvating device

One of the drawbacks of using pneumatic nebulization is that they transport so much solvent into the plasma that it may extinguish the plasma or alter the plasma's properties significantly. Reducing the water content results in improved detection limits, higher ionization temperatures and affects the electron number density [Walters and Barnardt, 1988], illustrating the importance of controlling the solvent load in ICP – (optical and mass) spectrometry. Desolvation is achieved by heating the aerosol so that the solvent evaporates from the aerosol. Heating is accomplished either in a heated spray chamber [Veillon and Margoshe, 1968] or in a separately heated tube [Peters and Beauchemin, 1993]. An Aridus aerosol desolvating system [Botto and Zhu, 1994] is schematically presented in figure II.4 and consists of a microconcentric nebulizer and a heated spray chamber, both manufactured from polytetrafluoroethylene (PTFE). By heating the spray chamber (± 70 °C), initially larger droplets can be transported to the plasma, so that the analyte transport efficiency – and along with it, the sensitivity – increases. This also implies that larger amounts of solvent can be introduced into the ICP, leading to plasma instability and decreasing analyte ionization efficiency. In order to avoid this effect, the aerosol is passed from the spray chamber through a heated (± 160 °C) microporous membrane. The

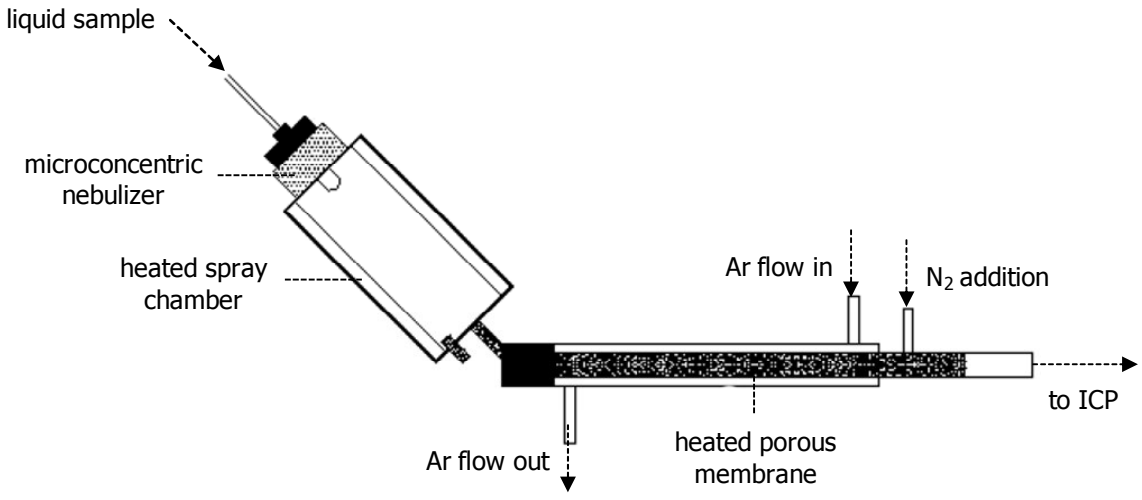

Figure II.4 – Schematic representation of an Aridus desolvating device

solvent vapors penetrate through the membrane and are evacuated by means of a heated argon gas stream. In this way, the occurrence of solvent-based interferences (*e.g.*, oxide and hydroxide ions) is strongly reduced. Drawbacks of this sample introduction system are (i) loss of volatile elements in the desolvating system, (ii) increasing risk on memory effects and (iii) clogging of the nebulizer or the membrane pores owing to solid particles present in the sample solution.

II.2.3 – Alternative sample introduction systems

II.2.3.1 – Electrothermal vaporization (ETV)

In electrothermal vaporization (ETV) [Carey and Caruso, 1992], the sample is deposited into a graphite tube which acts as an oven. The oven temperature can be raised stepwise, up to 3000 °C. Depending on its evaporation temperature, the analyte will evaporate before or after the matrix. When the aerosol that contains the analyte is formed, this aerosol is transmitted to the ICP by means of an argon gas stream. Benefits of this technique are (i) the possibility of direct analysis of solid samples, (ii) matrix-free introduction of the analytes into the plasma, avoiding spectral interferences and matrix effects from occuring and (iii) a high transport efficiency (gas) and consequently, a high sensitivity. Drawbacks are (i) the loss of multi-element character due to the transient signals generated and (ii) the limited precision in solid sample analysis of 5-20 % RSD compared to 1-2 % RSD with sample introduction via pneumatic nebulization.

II.2.3.2 – Laser ablation (LA)

Next to ETV, also laser ablation (LA), introduced by Gray [Gray, 1985], can be applied for direct analysis of solid samples. Here, a highly energetic laser beam is focused onto the sample surface, causing the ablation of a limited amount of the solid sample. The sample aerosol, formed by impact of the laser beam, is guided to the plasma by means of an argon or helium gas flow. More detailed information on laser ablation can be found in dedicated sources, *e.g.*, [Günther *et al.*, 1999].

II.3 – Inductively coupled plasma (ICP)

The ion source in ICP – mass spectrometry is an inductively coupled plasma (ICP), which is a gaseous mixture of molecules, atoms, ions and electrons at a high temperature

(6 000-8 000 K) [Montaser *et al.*, 1998-b]. The ICP is generated at the end of a plasma torch, usually manufactured from quartz and consisting of three concentric tubes. A schematical representation is given in figure II.5. Argon gas is passed through each tube, but in every tube at a different flow rate. The plasma gas or cool gas (flow rate 10-20 L min^{-1}) passes between the outer and middle tube, maintains the plasma and acts as a thermal barrier between the plasma and the torch, preventing the torch from melting. The auxiliary gas (flow rate 1-1.5 L min^{-1}) passes between the middle and inner tube and is used to change the position of the base of the plasma relative to the torch. In the inner tube, or injector tube, the nebulizer gas (flow rate 0.8-1.2 L min^{-1}) carries the sample aerosol generated by the sample introduction system. This nebulizer gas flow punctures the plasma, causing a toroidal plasma shape. When argon gas is flowing through the torch, the plasma can be ignited by a high-voltage spark, or Tesla discharge, which causes some electrons to be stripped from argon atoms. Owing to the presence of charged particles, the plasma can be supplied with energy from a radiofrequent (RF) alternating current passing through the induction coil around the torch.

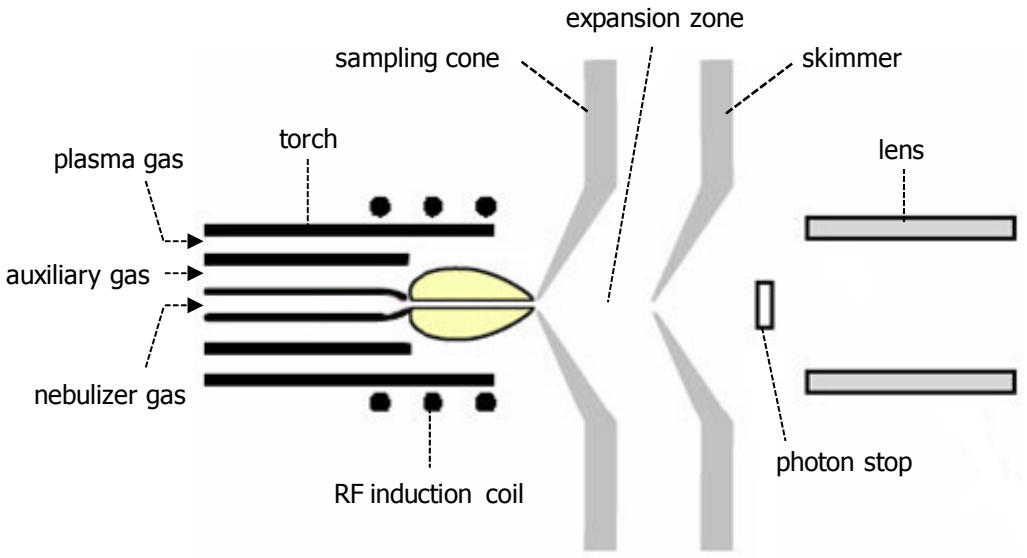

Figure II.5 – Schematic representation of plasma torch and interface region

Energy transfer from plasma to sample aerosol results in desolvation of the aerosol, atomization of the molecules and ionization/excitation of the atoms [Gray, 1975]. The latter process can occur via different mechanisms; the most important mechanisms are:

- Thermal ionization/excitation; collisions between atoms, ions and electrons:

$$M + e^- \rightarrow M^+ + 2e^- \; ; \; M + A \rightarrow M^+ + A + e^-$$

- Penning ionization/excitation; collisions between atoms in ground state and metastable argon species:

$$Ar^m + M \rightarrow Ar + M^+ + e^- \; ; \; Ar^m + M \rightarrow Ar + M^{+*} + e^-$$

- Ionisation/excitation by charge transfer; charge transfer between atoms and ions:

$$Ar^+ + M \rightarrow Ar + M^+ \; ; \; Ar_2^+ + M \rightarrow 2Ar + M^{+*}$$

II.4 – Interface region

The role of the interface is to transport the ions efficiently, consistently and with electrical integrity from the plasma, operating at atmospheric pressure, to the mass spectrometer region, operating at high vacuum [Houk *et al.*, 1980]. The interface consists of a sampling cone and a skimmer, two metallic, water-cooled cones with a small central orifice that are coaxially mounted (figure II.5). When the plasma gas enters the space between sampling cone and skimmer (expansion zone), the bundle consisting of ions, electrons and neutral species is expanded due to the higher vacuum (lower pressure) in the expansion zone. The central part of the beam leaves the expansion zone through the skimmer orifice, entering a subsequent higher vacuum stage. At every vacuum stage, a vacuum pump pumps away residual components. After passing the interface cones, an electrostatic lens (or lens system) deflects anions and electrons while positively charged ions are focused and directed towards the mass spectrometer.

II.5 – Mass spectrometers

In ICP – mass spectrometry, the ions that are formed in the plasma and extracted by the interface are separated according to their mass-to-charge (m/z) ratio. Since only singly positively charged ions are considered (z = 1), this implies a separation according to mass. Different types of mass spectrometers have been developed [Turner *et al.*, 1998], so that ICP-MS instruments can be distinguished according to their mass separating device: (i) a quadrupole filter (± 90 %), (ii) a sector field (SF) mass spectrometer (≤ 10 %) or (iii) a time-of-flight (TOF) analyzer (a few instruments). The quadrupole filter and the sector field mass spectrometer are discussed below, while information on time-of-flight analyzers can be found in dedicated sources, *e.g.*, [Myers *et al.*, 1994; Myers *et al.*, 1995-a; Myers *et al.*, 1995-b].

Probably the most important characteristics of a mass spectrometer are (i) its scanning speed, (ii) its mass resolution, or its capability to distinguish adjacent peaks of neighboring masses, and (iii) its abundance sensitivity. In general, resolution R can be defined as (figure II.6.a):

$$\mathrm{R} = \frac{\mathrm{m}}{\Delta\mathrm{m}} \qquad \text{(equation II.1)}$$

with m the analyte mass and $\Delta\mathrm{m}$ the peak width at 5% of the peak height.

Two adjacent peaks of the same height at masses m_1 and m_2 are considered to be separated (resolved) when the valley between them is less than 10 % of the peak height. This leads to the alternative definition for mass resolution, the so-called '10 % valley' definition (figure II.6.b), according to which the mass resolution is expressed as:

$$R = \frac{\frac{m_1 + m_2}{2}}{m_2 - m_1} \qquad \text{(equation II.2)}$$

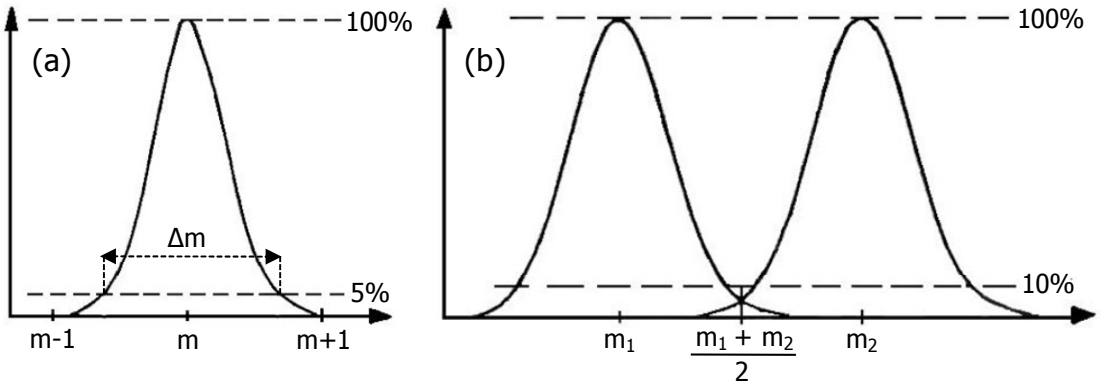

Figure II.6 – Mass resolution – (a) traditional definition; (b) '10% valley' definition

Typical resolutions are 300 for quadrupole mass spectrometers, and 300 (low resolution), 4 000 (medium resolution) and up to 10 000 (high resolution) for sector field mass spectrometers.

When a small peak is measured adjacent to a larger peak, not only must that peak be resolved, but any tailing from the larger peak affecting the smaller peak should be minimal. The abundance sensitivity of a mass spectrometer is a measure for the extent of this tailing, and can be expressed in terms of peak heights and peak areas. The height h and area a of a peak at mass m, $\mathrm{m}+1$ and $\mathrm{m}-1$ is $\mathrm{h_m}$ and $\mathrm{a_m}$, $\mathrm{h_{m+1}}$ and $\mathrm{a_{m+1}}$, and $\mathrm{h_{m-1}}$ and $\mathrm{a_{m-1}}$, respectively. The low-mass abundance sensitivity, expressed in terms of peak height or peak area, is given by the respective ratios:

$\frac{h_{m-1}}{h_m}$ (peak height) and $\frac{a_{m-1}}{a_m}$ (peak area) (equation II.3)

while the high-mass abundance sensitivity, expressed in terms of peak height or peak area, is given by the respective ratios:

$\frac{h_{m+1}}{h_m}$ (peak height) and $\frac{a_{m+1}}{a_m}$ (peak area) (equation II.4)

II.5.1 – Quadrupole filter

II.5.1.1 – Description

A quadrupole filter (figure II.7) consists of four cylindrical rods, positioned at the corners of a square [Turner *et al.*, 1998]. The diagonally opposed rods are electrically connected, so that two electrode pairs are formed. Each electrode pair is supplied with a combination of a direct current (DC) and a radiofrequent (RF) voltage. The magnitude of the voltage on both electrode pairs is the same while the sign is opposite. The quadrupole acts as a mass filter. Ions entering the quadrupole can either traverse according to a stable trajectory and finally reach the detector, or they can follow an unstable trajectory and be removed from the quadrupole prior to arrival at the detector. In this way, a quadrupole only allows the passage of ions within a narrow bandpass, typically 1 atomic mass unit (u) in width.

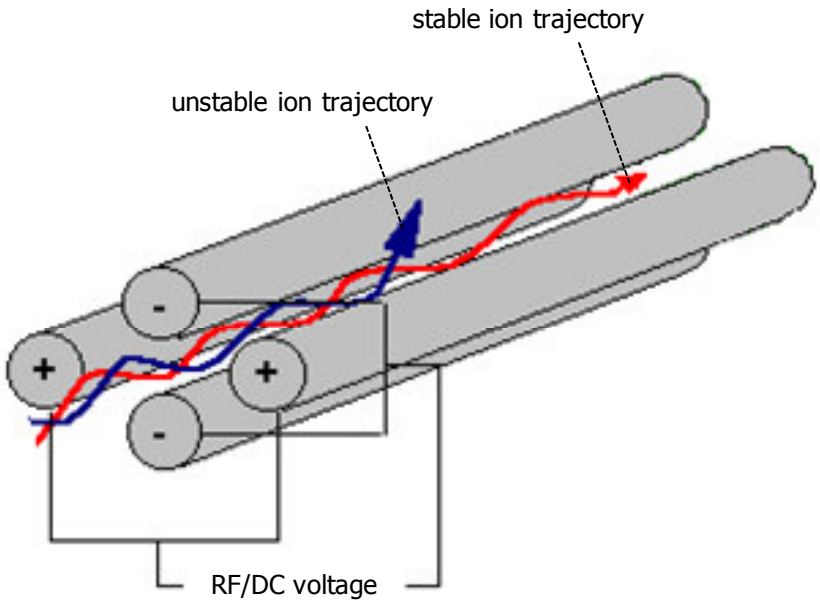

Figure II.7 – Quadrupole filter

II.5.1.2 – Operating principle

In order to understand the operating principle of the quadrupole filter, the ion trajectories in both the X-Z and Y-Z planes need to be examined, as illustrated in figure II.8 [De Hoffmann *et al.*, 1996]. In the X-Z plane, with a positive DC voltage on the rods, ions are subsequently focused towards and defocused from the central (Z-) quadrupole axis due to the RF component. The fact whether or not a defocused ion is removed from the ion beam depends on the time needed to reach a quadrupole rod, which is on its turn determined by (i) the magnitude of the negative potential of the RF component on the electrode, (ii) the frequency of the RF component and (iii) the position, speed and m/z of the ion. As the heavy ions are quasi only influenced by the average potential on the electrodes, they are only influenced by the DC component, leading to focusing of the ion towards the central axis of the quadrupole. Light ions, on the other hand, are mainly influenced by the RF component and whether or not they are defocused depends on their acceleration caused by the RF component. As a consequence, in the X-Z plane, only ions with an m/z above a certain value reach the detector. In the Y-Z plane, only ions with an m/z below a certain value reach the detector, since the voltage on the rods in the Y-Z plane has the same magnitude but the opposite sign (negative), leading to defocusing of heavy ions. Combining the effects of both the X-Z and Y-Z planes results in a mass bandpass filter: only ions with an m/z within a narrow range will pass through the quadrupole.

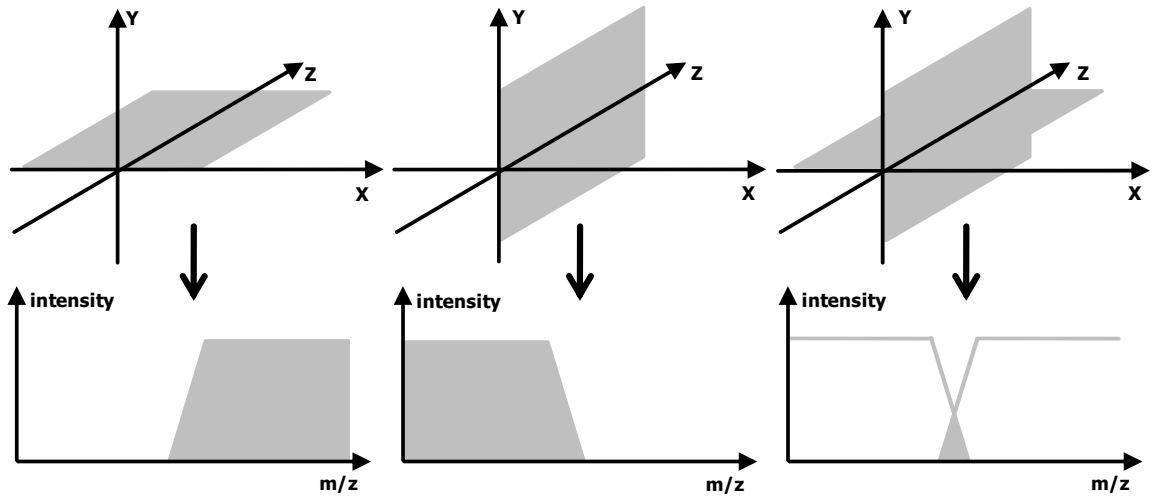

Figure II.8 – Operating principle of a quadrupole filter

During operation of the mass filter, the potential field in the quadrupole Φ is given by [Turner *et al.*, 1998]:

$$\Phi = \frac{(x^2 - y^2)}{r_0^2} [V \cos(\omega t) + U] \quad \text{(equation II.5)}$$

with x and y the distance to the X- and Y-axis respectively, r_0 the distance from the rods to the central (Z-)axis, V the amplitude of the RF voltage, ω the RF frequency, t the time and U the DC voltage offset.

The full equations of motion along the X-, Y- and Z-axis of the quadrupole are given by:

$$\frac{d^2x}{dt^2} - \frac{2e}{mr_0^2} [U + V \cos(\omega t)] x = 0 \quad \text{(equation II.6)}$$

$$\frac{d^2y}{dt^2} + \frac{2e}{mr_0^2} [U + V \cos(\omega t)] y = 0 \quad \text{(equation II.7)}$$

$$\frac{d^2z}{dt^2} = 0 \quad \text{(equation II.8)}$$

with e and m the charge and mass of the ion, respectively.

These equations result in a sinusoidal trajectory along the X- and Y-axis. By the substitution:

$$\omega t = 2\xi \quad \text{(equation II.9)}$$

and the introduction of the Mathieu parameters a and q where

$$a \equiv a_x = -a_y = \frac{8eU}{m\omega^2 r_0^2} \quad \text{(equation II.10)}$$

$$q \equiv q_x = -q_y = \frac{4eV}{m\omega^2 r_0^2} \quad \text{(equation II.11)}$$

the Mathieu equation becomes:

$$\frac{d^2u}{d\xi^2} - [a + 2q \cos(2\xi)] u = 0 \quad \text{(equation II.12)}$$

where $u = x$ or y.

The solutions of the Mathieu equation fall apart into two categories:

- The 'stable' ion trajectories describe the paths of ions passing along the full length of the quadrupole filter without hitting the rods.
- The 'unstable' ion trajectories represent the paths of ions that hit the quadrupole rods and are therefore lost from the system.

The magnitude of the DC and RF components is critical for proper operation of the bandpass filter. The ratio U/V determines the width of the bandpass filter, while the

absolute values of U and V determine its position. A stability diagram can be constructed, showing the values for the Mathieu parameters a and q that lead to a stable ion trajectory (figure II.9.a). Several stable regions can be distinguished, but in commercially available ICP-MS instruments, the quadrupole is operated in the first stability region only. A line, representing the ratio $a/q = 2U/V$ can be drawn on the stability diagram (figure II.9.a). This line represents the situation where the ratio of the amplitudes of the RF and DC components is held constant, while their absolute values are increased. Such a line is known as a mass scan line, and consists of all the values of a and q occurring in the scan. When the parameters e, ω, r_0, U and V are kept constant, the mass scan line can be considered as a line of points, each representing a certain mass. Since m is inversely proportional to a and q, the low masses are to be found in the right upper corner and the high masses in the lower left corner. The slope of the mass scan line can be adjusted by appropriate parameter settings so that only a small segment of the mass scan line intersects the stable region. As a consequence, only ions with an m/z corresponding to the masses in the stable segment of the mass scan line will travel a stable trajectory through the quadrupole. A mass scan can be performed by a linear increase of the DC – and RF components while their ratio is kept constant. When one point of the mass scan line, inside the stable region, is considered when U and V are increased, this point corresponds to an increasing m/z, so that the position of the bandpass window is moved across the mass range. The a versus q stability diagram can be replaced by a U versus V diagram (figure II.9.b) since ω and r_0 are constant and only singly charged positive ions are considered. This diagram is only valid for one particular mass. In figure II.9.b, the stability diagrams for 4 masses are displayed, and when scanning according to the scanline, a mass spectrum is obtained.

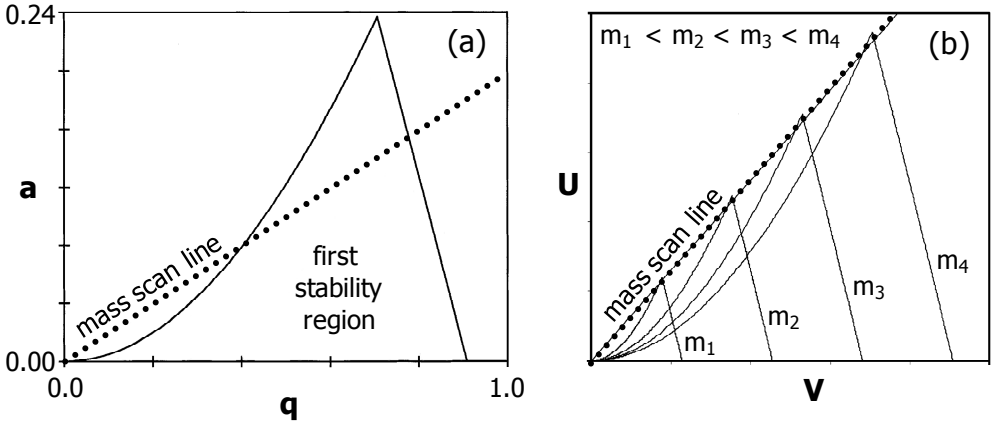

Figure II.9 – First stability region of a quadrupole mass filter and mass scan line – (a) a versus q stability diagram; (b) U versus V diagram

When the voltages applied on the quadrupole rods are continuously varied, a selected mass range is scanned (mass scan). In case of a discrete variation of the applied voltages, only selected masses are registered (peak hopping).

II.5.1.3 – Performance

Advantages of a quadrupole filter are its (i) robustness, (ii) limited dimension, (iii) high scanning speed, (iv) maintenance of resolution in the case where the introduced ions have an energy distribution and (v) relatively low price. As drawbacks, its limited mass resolution (± 300) and the triangular peak shapes can be noted.

II.5.2 – Sector field mass spectrometer

II.5.2.1 – Description

The full potential of ICP-MS cannot be exploited to the fullest extent by conventional quadrupole-based instrumentation because of spectral overlap. To overcome this problem, different techniques have been developed and applied with varying levels of success. A very effective approach for the improvement of ICP-MS analysis, is the combination of an inductively coupled plasma with a sector field – or high resolution mass spectrometer [Jakubowski *et al.*, 1998; Moens and Jakubowski, 1998; Turner *et al.*, 1998]. This type of mass separating device is essentially a combination of a magnetic sector and an electrostatic sector in such a way that so-called 'double focusing' is achieved.

II.5.2.2 – Magnetic sector

A magnetic sector analyzer [Turner *et al.*, 1998] consists of a curved flight tube located in the gap between the poles of an electromagnet. The ions produced in an ion source are accelerated into the magnetic field $\vec{B}$ through the entrance slit (source slit). The magnetic field is perpendicular to the flight direction of the ions and has a mass-dispersing and direction-focusing effect on ions. Due to the acceleration by the lens system, the ions obtain an amount of kinetic energy, E_k, given by:

$$E_k = \frac{mv^2}{2} = qV \qquad \text{(equation II.13)}$$

with m the mass of the ion, v its velocity, q its charge and V the potential difference leading to acceleration.

These ions will undergo the Lorentz force, $\vec{F}_L$, given by:

$$\vec{F}_L = q\left(\vec{v} \times \vec{B}\right) \qquad \text{(equation II.14)}$$

which is perpendicular to the direction of motion and the magnetic field. Its magnitude is given by:

$$F_L = qvB \qquad \text{(equation II.15)}$$

Under the influence of this force, an ion is deflected into a circular path with radius r, resulting into the relation:

$$F = \frac{mv^2}{r} = qvB \qquad \text{(equation II.16)}$$

It follows that the radius r of the circular path described by the ion is given by:

$$r = \frac{mv}{qB} \qquad \text{(equation II.17)}$$

and that this radius increases with increasing ion mass and increasing speed at the time the ion enters the magnetic sector. The radius decreases with increasing ion charge and increasing magnitude of the magnetic field. After elimination of the unknown parameter v by means of equation II.13, the radius can be expressed in terms of known parameters as follows:

$$r = \sqrt{\frac{2Vm}{q}}\, B \qquad \text{(equation II.18)}$$

From this expression, it is clear that ions with a different mass-to-charge ratio (m/q in this case) are following a different circular trajectory, and hence are separated in space. When detection is performed by means of a photo plate, the impact of the ions in different points will generate a mass spectrum. In the case where detection is done with a fixed detector, ions with the desired m/z can be selected by adjusting the magnitude of the accelerating potential V or the magnetic field B. At a given magnetic field B, only ions with a particular m/z ratio will travel along a stable trajectory through the magnetic sector and leave the sector via the exit slit (collector slit).

II.5.2.3 – Electrostatic sector

The energy spread of an ion beam limits the resolving power of a magnetic sector analyzer. Only when all the ions have the same kinetic energy at the moment they enter

the magnetic sector, ions with the same m/z will be focused into the same point. In practice, there is always a distribution in kinetic energy among the ions, which may result in focusing of ions with the same kinetic energy but different m/z in the same point. To overcome the problem of ion kinetic energy spread in high resolution mass spectrometry, energy focusing by means of an electrostatic sector is necessary [Turner *et al.*, 1998]. This sector consists of two curved plates with an electric field $\vec{E}$ applied between them. Generally, the outer plate is positive, the inner plate is negative and the centerline is at ground. Ions passing between these plates are subject to an electric force $\vec{F}_E$, given by:

$$\vec{F}_E = q\vec{E} \qquad \text{(equation II.19)}$$

with magnitude:

$$F_E = qE \qquad \text{(equation II.20)}$$

and are forced to move according to a circular trajectory. Thus:

$$F = \frac{mv^2}{r} = qE \qquad \text{(equation II.21)}$$

Taking into account the expression for the kinetic energy (equation II.13), it follows that:

$$r = \frac{mv^2}{qE} = \frac{2E_k}{qE} \qquad \text{(equation II.22)}$$

The higher the kinetic energy of an ion, the higher the radius of its circular path in the electrostatic sector. As a consequence, ions with the same m/z but a different kinetic energy will be focused in different points according to their kinetic energy, while ions with a different m/z but the same kinetic energy are focused in the same point. When a plate with a narrow slit is placed after the electrostatic sector, this setup can be used as an energy filter: only ions with a kinetic energy in a narrow range will leave the electrostatic sector, and the spread in kinetic energy is governed by the slit width. Placing such an energy filter before or after the magnetic sector considerably enhances the attainable mass resolution.

II.5.2.4 – Double focusing setup

The combination of a magnetic and electrostatic sector results in high resolution, but since a large fraction of the ion beam is eliminated, the transmission efficiency is low. Therefore, the sectors are designed and are positioned relative to each other in such a

way that the dispersions of the magnetic and electrostatic fields compensate one another and that a high resolution is achieved with minimal intensity loss. As a result, all the ions with the same m/z but a different kinetic energy are finally focused in the same point. This is called 'double focusing', and here, both directional focusing and energy focusing occur [Turner *et al.*, 1998]. Several setups result in double focusing:

- Mattauch-Herzog geometry: the electrostatic sector is placed before the magnetic sector, and the sectors are positioned relative to each other in such a way that the bundles corresponding to ions with a different m/z are all focused on the same plane (focal plane).
- Nier-Johnson geometry: the electrostatic sector is placed before the magnetic sector, and double focusing is obtained in one point.
- Reverse Nier-Johnson geometry: the electrostatic sector is placed after the magnetic sector (figure II.10). In this way, the largest fraction of the bundle is eliminated before entering the electrostatic sector, resulting in a lower instrumental background, enhanced abundance sensitivity (equations II.3 and II.4) and reduced space-charge effects (chapter III, § III.4.2.1).

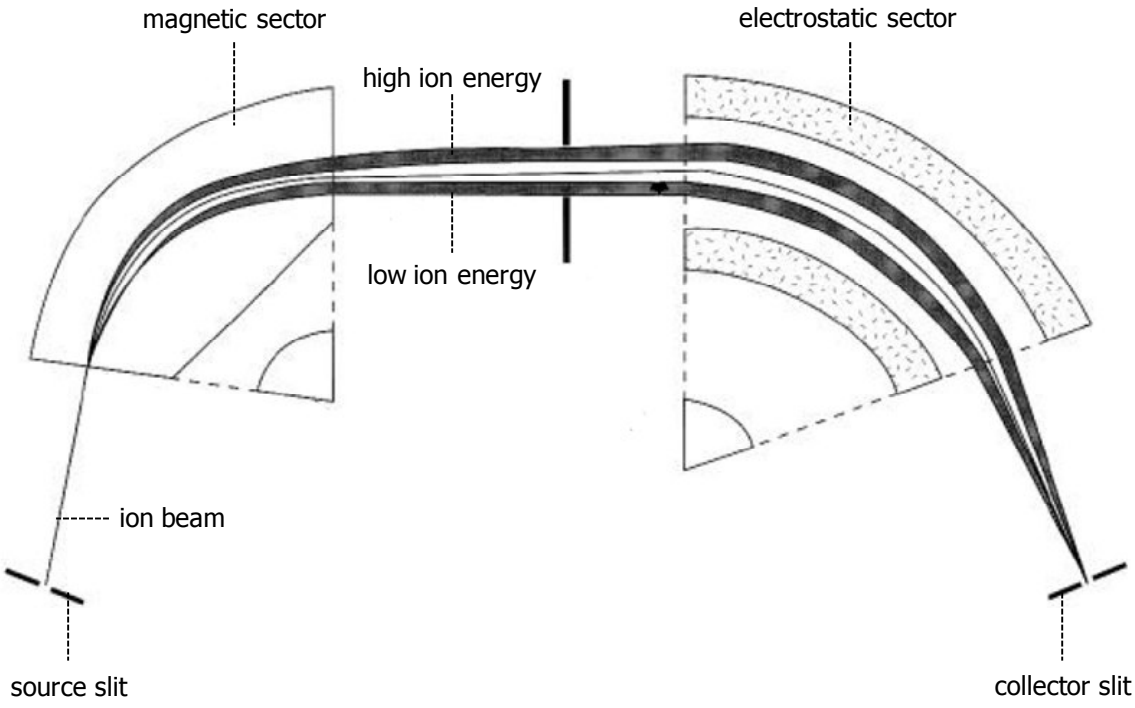

Figure II.10 – Double focusing in a sector field mass spectrometer of reverse Nier-Johnson geometry

In the (reverse) Nier-Johnson geometry, the ions with a particular m/z that reach the detector can be selected by adjusting either the magnetic field B (B-scan or magnetic scanning), or the acceleration potential V (E-scan or electric scanning) [Giessmann and Greb,

1994]. A disadvantage of magnetic scanning is that, due to magnet hysteresis, a 'settling time' is needed when jumping from one m/z to another. This settling time scales linear to the mass difference in the jump. In electric scanning, hysteresis is avoided, allowing the fast scanning of a mass range, however within a range of 30 % around the selected m/z only.

II.5.2.5 – Performance

The most important advantage of high resolution mass spectrometers is their excellent mass resolution compared to quadrupole devices, and the possibility to work at increased mass resolution depending on the analytical problem. However, the resolution attainable depends on the width of the source and collector slits. The higher the resolution, the smaller the width of the slits, and thus the lower the transmission efficiency. The sensitivity is decreased by a factor of 10 when changing from low (300) to medium (4 000) resolution [Moens *et al.*, 1995]. Another disadvantage of this type of mass spectrometers is the high cost and the fact that even the maximal resolution attainable is not sufficient to remove all spectral interferences (*e.g.*, isobaric nuclides). An important advantage of sector field mass spectrometers over quadrupole devices for isotopic analysis is the fact that the former provides flat-topped peak shapes when operated in low resolution mode [Vanhaecke *et al.*, 1996-b], while the peak shape for the latter is triangular. When the resolution is increased, however, the peak shape changes from flat-topped (trapezoidal) to triangular.

II.6 – Collision/reaction cell technology

As already stated in § II.2, the major drawback of ICP-MS is the occurrence of spectral interferences and matrix effects. Although sector field ICP-MS offers an elegant solution to cope with most spectral interferences, it is not able to resolve the signals of isobaric nuclides. For example, the resolution required to separate the signals of the isobaric nuclides $^{87}Rb^{+}$ and $^{87}Sr^{+}$ is ~ 300 000, while the maximum attainable resolution with modern sector field instrumentation is ~ 10 000. As opposed to physical resolution with a sector field mass spectrometer, quadrupole-based ICP-MS with chemical resolution in a dynamic reaction cell offers a valuable solution, as was illustrated for the $^{87}Rb^{+}/^{87}Sr^{+}$ case [Moens *et al.*, 2001].

The principle of this technology is the presence of a gas-filled cell that is placed in-between the interface and the quadrupole mass analyzer. The reduction of spectral interferences by means of this cell is based on a different reaction behavior between the gas in the cell on one hand, and the analyte ion and interfering ion, on the other hand. This phenomenon is addressed as 'chemical resolution'.

II.6.1 – History of collision/reaction cells

Multipole collision cells [Turner *et al.*, 1997] in quadrupole-based instrumentation offer a quite general approach to cope with the problem of spectral interferences. These multipole collision cells replace the traditional ion lens system and consist of n rods (where n = 4 for a quadrupole, n = 6 for a hexapole and n = 8 for an octopole) to which an RF voltage is applied. If an appropriate gas is used (*e.g.*, H_2 for the reduction of Ar^+ and ArX^+ and Xe for the reduction of MO^+), the signal of interfering ions can be reduced by means of charge transfer reactions and/or collision-induced dissociation (CID).

The application of collision cells has a long history in organic mass spectrometry, where they have been used in tandem mass spectrometry arrangements to study the fragmentation of complex organic molecules due to collision-induced dissociation (CID) [Busch *et al.*, 1988]. The application of such triple quadrupole setups in analytical plasma spectrometry was first performed in glow discharge – mass spectrometry (GD-MS), where an intermediate collision cell was used to dissociate $ArFe^+$ and Fe_2^+ [King *et al.*, 1988]. This approach was later extended to the dissociation of TaO^+, an extremely refractory oxide ion [King and Harrison, 1989]. Significant reduction of molecular interferences could be achieved by collision-induced dissociation when the collisional energy was sufficiently high to break the molecule bond. Douglas first described the use of CID in ICP-MS, and showed that strong losses of both the analyte and interfering ions can be expected because of charge transfer between the ions and scattering effects [Douglas, 1989]. This result was only partly corroborated in another contemporary study. The use of an arrangement with two quadrupoles where the first quadrupole acts as collision cell and the second quadrupole acts as mass analyzer, showed that low-energy gas phase collisions with a reaction gas such as Xe or CH_4 can be successfully applied for reduction of polyatomic interfering ions, while retaining a signal intensity of 60-70 % of the signal intensity without a reaction gas [Rowan and Houk, 1989]. Rowan and Houk recognized that useful ion-molecule reactions were occurring and the removal of interfering ions was partly attributed to such reactions. They also deduced that the energy of the reaction

product ions would be lower than that of ions from the extracted plasma beam and showed that these ions could be discriminated against by biasing the mass filter positive relative to the collision cell. They thus established the basis for what is at present known as 'kinetic energy discrimination' techniques. However, the practical use of these ion-molecule reactions remained questionable as a result of the loss of ions from the first quadrupole due to scattering events. Moreover, the introduction of high resolution mass spectrometers captured much attention in the following years. After a period of relative silence concerning this topic, it was shown that H_2 could be successfully used in the reduction of the Ar^+ signal [Eiden *et al.*, 1996]. From this moment on, the ion-molecule reaction approach was adopted by other research groups and commercialized by several manufacturers of ICP-MS instruments. Additional information on the collision/reaction cell technology can be found in dedicated sources, *e.g.*, [Feldmann *et al.*, 1999-a; Feldmann *et al.*, 1999-b; Koppenaal *et al.*, 2004].

II.6.2 – Dynamic reaction cell (DRC)

Also by means of a dynamic reaction cell (DRC) [Tanner and Baranov, 1999; Tanner *et al.*, 2002], spectral interferences can be chemically resolved. In this case, an RF/DC quadrupole assembly is used. Baranov and Tanner first described the use of a quadrupole cell, in which reactions take place between the ions extracted from the plasma and a reactive gas at elevated pressure [Baranov and Tanner, 1999]. In contradiction to traditional collision cells, the incidence of collisions is very high due to the elevated pressure inside the cell. As a consequence, ions that enter the cell lose their energy so that all the ions present inside the DRC, both the ones extracted from the plasma, and these newly formed inside the cell, have the same energy (so-called 'thermal' conditions). Since the reaction efficiency increases exponentially with the number of collisions, a reaction cell is characterized by a very high reaction efficiency, which is beneficial for the removal of spectral interferences. However, also the formation rate of new ions inside the reaction cell (sequential or secondary chemistry) is increased. Working in thermal conditions does not allow to distinguish the ions formed inside the cell from the ions that are extracted from the plasma by means of their kinetic energy, as is the case in collision cells (so-called 'non-thermal' conditions). In a dynamic reaction cell however, the sequential chemistry can be controlled by dynamic bandpass tuning (DBT) [Latino *et al.*, 2001].

Despite the fact that the terms 'collision cell' and 'reaction cell' are often mixed, both cell types can be distinguished according to the operating conditions. A collision cell aims at

endothermic fragmentation with the cell being operated at high ion energy and low pressure. A dynamic reaction cell is operated at elevated pressure and a low ion energy, aiming at exothermic ion-molecule reactions. In view of the different reaction conditions, the cells can also be considered according to the energy distribution of the ions inside. After passing through a collision cell, analyte ions and newly formed ions in the cell can be distinguished, based on their energy distribution. When no distinction in kinetic energy is possible between analyte and newly formed ions, the cell is a reaction cell.

II.6.2.1 – Description

A dynamic reaction cell (DRC) consists of a closed quadrupole-unit that is placed in-between the extraction lens and the quadrupole mass analyzer. A schematic representation of an ICP – mass spectrometer equipped with a dynamic reaction cell is given in figure II.11. High purity reaction gases (*e.g.*, CH_4, NH_3, CO, O_2, CH_3F) can be introduced into the DRC via two entrance gates at a carefully controlled gas flow rate, regulated by two mass flow controllers. These mass flow controllers are calibrated for use with argon gas, and the gas flow rate as set in the instrument is expressed in argon-equivalent units. A correction factor, calculated as the ratio of the molar specific heat for argon gas to that of the reaction gas used, is needed to obtain the true gas flow rate of the reaction gas used.

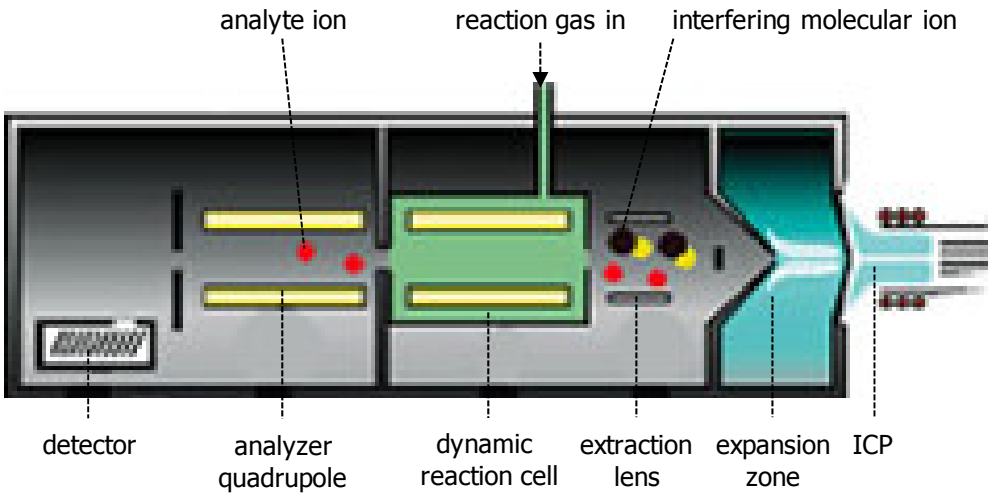

Figure II.11 – Schematic representation of an ICP – mass spectrometer equipped with a dynamic reaction cell (DRC)

The ion beam that is extracted from the plasma by the interface is focused towards the dynamic reaction cell by the extraction lens. The ion beam consequently passes through

and leaves the DRC towards the analyzer quadrupole. The reaction gas can leave the DRC via both apertures.

When no gas is led into the dynamic reaction cell, the cell just guides the ions extracted from the plasma towards the quadrupole analyzer. In this operation mode, called 'standard mode' or 'vented mode', the ICP – mass spectrometer behaves as a convential quadrupole-based instrument.

II.6.2.2 – Ion-molecule interactions

The dynamic reaction cell relies on the principle of chemical resolution. Owing to the difference in reactivity of the analyte ions and the interfering ions with respect to the reaction gas, spectral interferences can be prevented from occurring. To assure the selectivity and specificity of ion-molecule reactions, a carefully controlled and nearly-thermal environment is necessary, which can be obtained by working at low ion energies and a relatively high reaction gas pressure (1.3-2.7 Pa).

II.6.2.2.1 – Collisional processes

All interactions of ions with molecules are collisional processes, where energy transfer, as discussed below, and collisional fragmentation can be considered as reaction processes [Tanner *et al.*, 2002]. In an elastic, non-reactive collision of an ion of mass m_1 and kinetic energy E_1 with a stagnant neutral of mass m_2 and kinetic energy E_2 $(E_2 = 0)$, the respective energies after collision, E_1' and E_2', are given by:

$$E_1' = E_1 \frac{m_1^2+m_2^2}{(m_1+m_2)^2} \qquad \text{(equation II.23)}$$

$$E_2' = E_1 - E_1' \qquad \text{(equation II.24)}$$

Multiple collisions of the ion result in sequential losses of kinetic energy and in a reduction in the width and magnitude of the kinetic energy distribution (energy damping). The extent of ion energy damping depends on (i) the ion/neutral mass ratio, (ii) the ion energy at the moment of entrance into the cell and (iii) the number of collisions. A lower ion/neutral mass ratio increases the rate of energy damping of the ion. Complete damping to the thermal condition means that the ion executes a 'random walk' through the cell. A high ion energy at the moment of entrance into the cell requires more collisions for energy damping. For a given cell pressure, a higher initial energy also results in a reduction in efficiency because the ion progresses further into the cell before the energy

is damped, and hence the number of reactive collisions is reduced. Further, higher energy lowers the probability of reaction during collision, compromises the specificity of the thermal chemistry and increases the potential for sputtering cell materials. Information on collisional fragmentation processes is given in dedicated sources, *e.g.*, [Tanner *et al.*, 2002].

II.6.2.2.2 – Ion-molecule reactions

As for any chemical reaction, it can be assumed that, under thermal conditions, ion-molecule reactions only take place when (i) they are thermodynamically allowed and (ii) the reaction kinetics are favorable [Tanner *et al.*, 2002].

Since the system is dynamic, it cannot reach equilibrium because of the constant flow originating from the plasma through the reaction cell. Nevertheless, the only practical approach possible is to determine whether the Gibbs energy of reaction, given by:

$$\Delta G = \Delta H - T\Delta S \qquad \text{(equation II.25)}$$

is negative after the equilibrium is reached, or in other words, if the reaction is spontaneous. In most cases, the reactions that occur are bimolecular reactions with small-particle or charge transfer, so that the entropy term ΔS is negligible. Consequently, the thermochemistry of the reactions is correctly described by ΔH. Of course, this approximation is not valid for condensation reactions and reactions where the number of reaction products is higher than the number of reactants. The change of enthalpy, ΔH, in a reaction $A^+ + B \rightarrow C^+ + D$ can be calculated using the heats of formation, ΔH_f, of the reactants and reaction products as follows:

$$\Delta H = \Delta H_f(C^+) + \Delta H_f(D) - \Delta H_f(A^+) - \Delta H_f(B) \qquad \text{(equation II.26)}$$

If the enthalpy of reaction is negative, the reaction is exothermic and might proceed under thermal conditions. If the enthalpy of reaction is positive, the reaction is endothermic and will not take place unless additional energy is contributed to the process, *e.g.*, by an excess of axial kinetic energy before relaxation in a collision/reaction cell, or by the RF voltage that is applied on the quadrupole in the cell. The contribution of this RF energy to the reaction energy favors endothermic reactions. It was shown that this RF energy contribution is minimized by operating at a low RF amplitude (V), a high RF frequency (ω) and a large number of collisions per RF cycle [Baranov and Tanner, 1999]. Positioning the mass window of the DRC quadrupole is hence performed by varying the

RF frequency at a constant amplitude, in contradiction to the analyzer quadrupole, where the RF frequency is kept constant and the RF amplitude is varied for mass selection.
Although there is no correlation between the enthalpy of reaction and the reaction rate, it can be stated that when an exothermic small-particle transfer reaction takes place under thermal conditions, this reaction takes place at a high reaction rate, mainly due to the low energy of activation for this type of reactions. Ions are charged, and can interact with a polar molecule, or induce a dipole in an apolar molecule. These ion-dipole interactions are, in most cases, strong enough to overcome the activation energy of exothermic reactions. As a consequence, the exothermicity usually determines whether a simple ion-molecule reaction in which small particles are exchanged, will take place, or not [Tanner *et al.*, 2002].

II.6.2.2.3 – Ion-molecule reaction types

The generic ion-molecule reaction of the form $A^+ + B \rightarrow C^+ + D$ includes several types of processes [Tanner *et al.*, 2002]. In the context of ICP-MS, the most important reactions are charge transfer reactions of the type:

$$A^+ + B \rightarrow A + B^+, \textit{e.g.}, Ar^+ + NH_3 \rightarrow Ar + NH_3^+$$

Indeed, the first applications were the resolution of argon-based interferences (Ar^+ and ArX^+, with X = N, O, Ar). The corresponding neutral argides have high ionization energies and their charge transfer reactions often proceed with high efficiency near the collision rate. However, with further development of the reaction cell technology, it has become apparent that the scope of application is considerably broader than simple charge transfer reactions. A second important class of reactions involves hydrogen-containing species:

- proton transfer:

$$AH^+ + B \rightarrow A + BH^+, \textit{e.g.}, ArH^+ + H_2 \rightarrow H_3^+ + Ar$$

- hydrogen atom transfer:

$$A^+ + BH \rightarrow AH^+ + B, \textit{e.g.}, Ar^+ + H_2 \rightarrow ArH^+ + H$$

- hydride ion transfer:

$$A^+ + BH \rightarrow B^+ + AH$$

So-called condensation reactions involve transfer of atoms other than hydrogen, and sometimes result in rearrangement to a thermodynamically stable form. Oxidation reactions are promising due to their apparent selectivity and speed:

$$A^+ + BO \rightarrow AO^+ + B, \textit{ e.g.}, Ce^+ + N_2O \rightarrow CeO^+ + N_2$$

This type of ion-molecule reaction is very sensitive to the thermodynamic stabilities of the product oxide ions and of the neutral molecule. For example, N_2O is attractive as an oxidizing agent because the corresponding reactions include N_2 as a product molecule. CO_2 is also a promising reactant due to the thermodynamic stability of CO as a leaving group. In contrast, it was also shown that ArO^+ molecular ions can be removed by the use of CO as a reaction gas, according to the reaction:

$$ArO^+ + CO \rightarrow Ar^+ + CO_2$$

O_2 has a different application because a very strong A^+–O bond is required for this reaction to proceed. As a result, some reactions with oxygen have a very high specificity. Finally, clustering is a common reaction between many electron donor molecules and ions (ligand-ion mutual electron donation). Association or clustering reactions of the type:

$$A^+ + B \rightarrow AB^+$$

generally play a negative role in reaction cell ion chemistry when applied to ICP-MS. Ammonia is a good clustering ligand, meaning that it forms adducts readily and hence can be an analytical complication, unless steps are taken to control the appearance of cluster ions (dynamic bandpass tuning, § II.6.2.2.5). This type of reaction is often observed with water molecules, which are present in many reaction gases in trace quantities. Water also facilitates oxidation, hydroxylation and hydrogen and proton transfer reactions.

II.6.2.2.4 – Non-reactive collisions

Self-evidently, the essential reason of using a dynamic reaction cell in quadrupole-based ICP – mass spectrometry is to suppress spectral interferences by means of selective ion-molecule reactions. Next to the collisions that lead to reactions, many collisions occur between ions and gas molecules that do not result in reaction. These 'non-reactive' collisions are at the basis of side effects such as thermalization, collisional focusing and scattering that occur in the dynamic reaction cell [Tanner *et al.*, 2002] and deliver important benefits for isotope ratio determinations (chapter III, § III.3.1).

Under usual operating conditions, ions must be accelerated through a counter flow of gas in order to enter the cell. In this instance, the ions enter the cell with a relatively large axial kinetic energy. In most collisions, the ion transfers a fraction of its kinetic energy to the neutral, and the ion energy is damped. In the case of ICP-MS, the axial kinetic energy of the ion is significantly greater than the radial energy, and the first step in the collisional damping of the ion's axial energy is the conversion of axial to radial energy, so that the ion tends to move away from the central axis. In this regard, an advantage of an RF-driven reaction cell is that the restoring force provided by the RF voltage drives the radially excited ions back towards the cell axis. Transfer of energy from axial to radial excitation continues until the two modes approach equilibrium, and then both translational degrees of freedom relax together. Eventually, the axial energy should be completely relaxed to nearly-thermal, while the radial energy does not completely relax, as it continues to be excited by the RF field. At pseudo-equilibrium, the ion energy is a function of the Mathieu parameters a and q, and of the number of collisions per RF cycle (and is thus dependent on the pressure and RF frequency) [Baranov and Tanner, 1999; Tanner *et al.*, 2002]. The over-all consequence of energy damping and thermalization is that the ions are focused towards the central axis and that the transmission efficiency is increased. This phenomenon is known as collisional focusing and can be used in order to increase the analyte ion intensity by a factor of 2 to 5. However, several aspects should be considered if the benefits of collisional focusing are to be employed. To improve sensitivity, non-reactive gases ought to be selected carefully: (i) the mass of the collision gas used should be below that of the analyte ion in order to minimize scattering, (ii) the gas should be thoroughly dried to avoid any reactions with concomitant water vapors and (iii) the gas flow control manifold should be sufficiently stable with respect to flow and composition of the gas in the cell.

II.6.2.2.5 – Control of sequential chemistry

The gas that fills the cell is usually reactive with at least some of the ions. Even if an intentionally non-reactive gas is used, reactive contaminants are commonly present either as an impurity or from entrainment of plasma gas into the cell. As long as ions and reactive gas components are in the cell, reactions may take place resulting in the formation of new ions that may be isobaric with an analyte of interest. If multiple collisions are provided, as required for efficient suppression of plasma-based interfering

ions, secondary reactions that may produce an ubiquitous chemical background are promoted [Tanner *et al.*, 2002].

An average ion experiences some 20 collisons when passing through a dynamic reaction cell of 12.5 cm in length and operated at a pressure of approximately 1.3 Pa. If the ion reacts on its first collision, the product ion on average may suffer a further 19 collisions. In this instance, there are some 20 levels of sequential chemistry. As an example, the reactions that can occur when methane is used as a reaction gas can be considered. It is known that methane can react with Ar^+ via dissociative charge transfer [Anicich, 1993]:

$$Ar^+ + CH_4 \rightarrow Ar + CH_4^+ \rightarrow Ar + CH_3^+ + H \rightarrow Ar + CH_2^+ + H_2$$

The products of this reaction, if retained by the reaction cell, react further, *e.g.*:

$$CH_3^+ + CH_4 \rightarrow C_2H_5^+ + H_2$$

or in general:

$$C_nH_x^+ + CH_4 \rightarrow C_mH_y^+ + \text{neutrals}$$

with $m = 1,2,\dots,n+1$ and $y = 0,1,\dots,x+4$

A reaction cell can be operated in such a manner that plasma-based interfering ions are efficiently removed by ion-molecule reactions. This raises the issue of the three forms of efficiency that are required of the reaction cell: (i) efficient removal of plasma-based interfering ions, (ii) efficient transmission of analyte ions of interest and (iii) efficient suppression of the appearance of new interference ions produced in sequential (secondary) chemistry in the reaction cell.

Two means to control the appearance of secondary reaction product ions in the mass spectrum are used in present-day instruments [Tanner *et al.*, 2002]. First, the well-defined stability boundaries of a quadrupole mass filter remain reasonably well-defined when the quadrupole is pressurized as is the case in the dynamic reaction cell. Hence, a dynamic reaction cell can be operated in a bandpass mode in which the low-mass and high-mass cutoff boundaries are determined principally by the Mathieu parameters a and q of its quadrupole (equations II.10 and II.11). The position of the stability boundary relative to the analyte ion is conveniently selected by adjustment of either the RF voltage (V), as is typical for the mass filter, or the frequency of operation (ω). Because the RF contribution to the reaction energy, which is important in the establishment of thermal conditions, is a strong function of the RF amplitude, it is convenient to use the frequency for this purpose in the reaction cell. The dynamic aspect of the dynamic reaction cell is comprised in the

tunable mass bandpass window of its quadrupole. The use of the DRC quadrupole as a dynamic bandpass is defined as 'dynamic bandpass tuning' (DBT) [Latino *et al.*, 2001; Tanner *et al.*, 2002].

Alternatively, kinetic energy discrimination after the cell allows operation of the cell as a passive device (meaning that the chemistry is allowed to proceed). Resolution of the plasma ions from cell-produced ions is based on the kinetic energy difference between these. A potential barrier is established downstream of the cell and provides a degree of resolution of plasma polyatomic ions from atomic ions [Tanner *et al.*, 2002].

In some instances, it is more convenient to convert the analyte ion, generally by atom transfer, into another ionic species than to reactively remove the interfering ion. Most often, this situation will arise when the thermochemistry is unfavorable for charge transfer. Such an instance arises when it is desired to chemically resolve certain isobaric atomic ions, *e.g.*, $^{87}Rb^+$ and $^{87}Sr^+$. If heavy-atom transfer is an option, the m/z of the product ion should be relatively free of interference, or the interference should also react at a sufficient rate so that it no longer interferes with the determination of the analyte as the MX^+ ion. Of course, it is necessary to allow the secondary chemistry by including both the reacting (atomic) analyte ion and the (molecular) product ion in the bandpass. This approach was successfully applied by Moens *et al.* to Rb/Sr geochronology, using methyl fluoride (CH_3F) in a neon buffer. It was demonstrated that Sr^+ reacts with CH_3F by F-atom transfer, forming SrF^+, while Rb^+ is unreactive. The neon buffer was used to homogenize the ion temporal distribution and yielded isotope ratios the precision of which approximated the counting statistics limit [Moens *et al.*, 2001].

II.7 – Detection system

After passage through the quadrupole or sector field mass spectrometer, the ion beam must be detected and measured by an appropriate system. The magnitude of the signal to be detected is in the range of a few ions per second for ultratrace components up to 10^{10} ions per second for major components. Because the charge of an electron is $1.6\ 10^{-19}$ C, this ion density corresponds to a current in the range of 10^{-20} to 10^{-9} A. To cover this dynamic range, a variety of detectors are used. For low signal ranges ($< 10^6$ ions/s), an ion counting system (electron multiplier) is usually employed, while for the higher count rates, an analogue measurement is used [Turner *et al.*, 1998].

II.7.1 – Ion counting systems

When ions leaving the mass spectrometer are directed towards a suitable surface at a highly negative voltage, electrons will be released by the resulting impact. These primary electrons may be directed, by a suitably applied voltage, onto a further surface from which secondary electrons are released. The energy, supplied by an electric potential of a few thousand volts that is applied across the ends of the multiplying surface (dynode), is sufficiently high to release in average three electrons per impact. After many repetitions of this impact process, a huge number of electrons will have been generated. A device operating in this way is called a secondary electron multiplier (SEM), and the multiplication factor will typically be on the order of 10^8 [Turner *et al.*, 1998] At the end of this device, the electrons are directed onto a collector electrode, and the resulting pulse is electronically processed by the data system. Electron multipliers exist with either a continuous dynode (figure II.12.a), or several discrete dynodes (figure II.12.b).

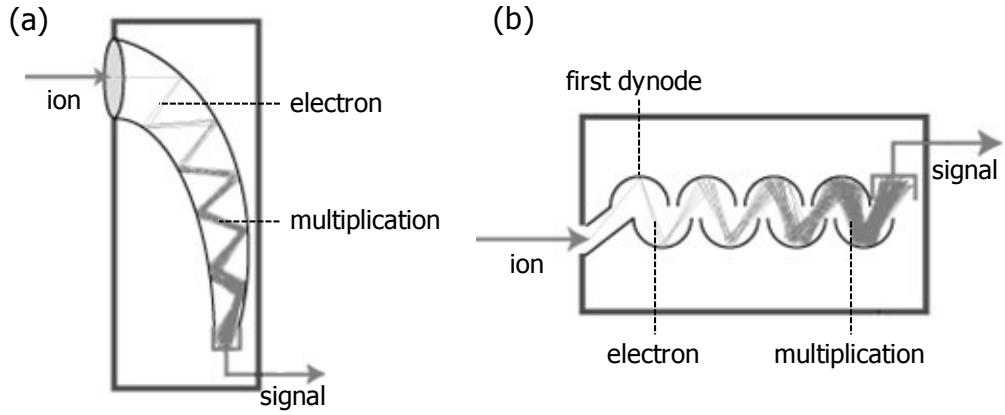

Figure II.12 – Secondary electron multiplier (SEM) with (a) a continuous dynode and (b) several discrete dynodes

If the rate of ion arrival at the collector is very high, the period between detected ions will become comparable to the pulse length of the output. During this output period, some ions will arrive and will not be detected by the counting system. This period, which is the multiplier dead time (τ) limits the maximum ion count rate where the detection stays in a linear mode. Especially for isotope ratio measurements, a correction for this dead time is mandatory [Ingle and Crouch, 1972].

II.7.2 – Analogue collection

Large signals require an analogue device, because ion counters cannot be used for ion rates above 10^6 ions/s [Turner *et al.*, 1998]. This can be accomplished in two ways. First, the

voltage applied to the secondary electron multiplier used in the ion counting systems can be reduced so that the average gain is reduced to about 10^3 instead of 10^8. The collector's output current can be used as a direct measure of the input current. Alternatively, the ion beam may be directed into a Faraday collector (Faraday cup), which is a metal beaker (cup) grounded with a high resistance (*e.g.*, 10^{11} Ω). When a positive ion beam impacts on the cup, the ions are neutralized with electrons coming from the ground, inducing a potential difference over the resistance according to Ohm's law $(U = IR)$. This device can be used for direct measurement of currents down to 10^4 ions/s (10^{-15} A), so there is overlap with the upper range for ion counting systems [Turner *et al.*, 1998].

II.7.3 – Dual detection systems

In order to deal with the large range of signals arriving at the detection system – ranging from a background < 1 count/s for sector field mass spectrometers to high count rates for major elements – the analogue mode of a secondary electron multiplier can be utilized instead of a Faraday cup. For low signals, the normal pulse counting output is recorded at the end of the multiplier chain. In the case of high signals, an analogue output signal can be obtained partway down the multiplier chain. An automatic monitoring system can be used to select the appropriate registration mode.

II.7.4 – Performance

The dead time (τ) of a secondary electron multiplier (SEM) requires correction of the count rates obtained and limits the use of ion counting. The damage rate of the multiplier is considerable because ion counting systems operate at high gain. On the other hand, a secondary electron multiplier is characterized by a high sensitivity, and a dual detection system allows a rapid changeover between pulse counting and analogue mode within a single scan. This rapid changeover is not possible on a Faraday collector. However, the multiplier analogue mode is somewhat less stable than the Faraday system and suffers from mass bias. The Faraday cup is extremely robust, does not suffer from damage to the multiplier system at high count rates and has no dead time. The linearity is excellent, so that isotope ratio measurements can be conducted with improved accuracy, and without instrumental mass bias. On the other hand, a Faraday collector has a slow time constant precluding fast scanning, and is characterized by a lower sensitivity.

II.8 – ICP-MS instruments used in this work

In previous paragraphs, the principal components of an ICP – mass spectrometer were described. Below, the design of the ICP – mass spectrometers used in this work, will be discussed. Instruments can be distinguished according to (i) the device used for mass separation, resulting in quadrupole-based ICP-MS (ICP-Q-MS) either with or without dynamic reaction cell (ICP-DRC-MS), and sector field ICP-MS or high resolution ICP-MS (ICP-SF-MS or HR-ICP-MS), and (ii) the detection system, resulting in single-collector ICP-MS (SC-ICP-MS) and multiple collector or multi-collector ICP-MS (MC-ICP-MS). In the field of isotopic analysis, the most relevant distinction between instruments is on the basis of the detection system, or single-collector – versus multi-collector ICP-MS instruments.

Single collector ICP – mass spectrometers are equipped with one electron multiplier for ion detection. In this work, two single-collector quadrupole-based ICP – mass spectrometers were used. A PerkinElmer SCIEX Elan 5000 was used for elemental assay. The sample introduction system consisted of a multichannel peristaltic pump (Minipuls-3), a GemTip cross flow nebulizer, a PerkinElmer type II double pass spray chamber of the Scott-type made of Ryton, and a corrosion resistant torch with alumina injector. An electrostatic lens system, consisting of six individual lenses focuses the ion beam towards the quadrupole analyzer. Detection of ions is performed by a channeltron continuous dynode electron multiplier. Single-collector isotope ratio determinations and elemental assay were carried out using a PerkinElmer SCIEX Elan DRC*plus*. The sample introduction system consisted of a multichannel peristaltic pump, a Meinhard concentric nebulizer mounted onto a cyclonic spray chamber, both made from quartz, and a PerkinElmer quartz torch with quartz injector. In one experiment, a GeoLas 200M 193 nm excimer laser ablation unit was used. A single extraction lens focuses ions towards the dynamic reaction cell that is placed in-between the interface and the mass analyzing quadrupole. A secondary electron multiplier with discrete dynodes is used for registration of the ion signals.

The technique multiple collector – or multi-collector ICP-MS (MC-ICP-MS) was developed specifically for isotopic analysis [Rehkämper *et al.*, 2001]. Two multi-collector ICP – mass spectrometers have been used in this work: Nu Instruments' Nu Plasma 500 and Thermo Electron's Neptune, which are represented schematically in figure II.13. The Nu Plasma 500 is a double focusing Nier-Johnson arrangement with a fast-scanning magnet and allows operation at a mass resolution of 450. The detector array consists of 12 fixed Faraday collectors and 3 fixed ion counters. The mass dispersion of the ion beam is varied

using a zoom lens system situated between the magnet and collector array. The sample introduction system consisted of an Aridus desolvating system to which sample delivery was accomplished via an auto-aspirating microconcentric nebulizer. The Thermo Electron Neptune used provides double focusing with a Nier-Johnson geometry and allows operation at a resolving power up to 8 000 in pseudo-high resolution mode. A retardation lens provides an excellent abundance sensitivity. The multicollection arrangement consists of a fixed center Faraday cup along with 8 movable Faraday cups and 3 secondary electron multipliers. Sample delivery was accomplished via an auto-aspirating low-flow PFA nebulizer at a flow rate of 50 μL min^{-1}, mounted onto a spray chamber that is a combination of a cyclonic spray chamber and a double-pass spray chamber.

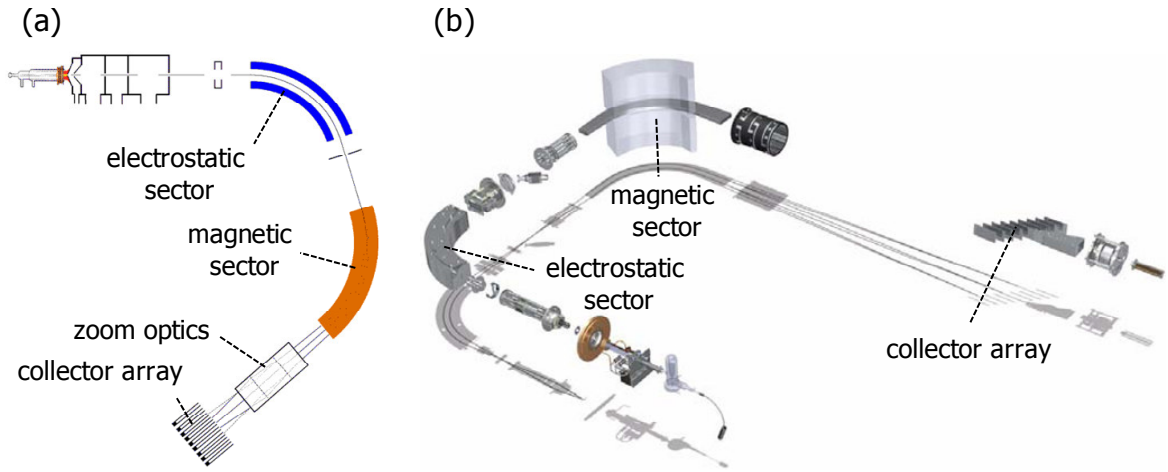

Figure II.13 – multi-collector ICP – mass spectrometers used in this work – (a) Nu Instruments' Nu Plasma 500 (b) Thermo Electron's Neptune

II.9 – ICP-MS for trace element determination

The use of the inductively coupled plasma as an ion source for analytical mass spectrometry was first described by Houk and coworkers [Houk *et al.*, 1980] and Date and Gray [Date and Gray, 1981; Date and Gray, 1983-a; Date and Gray, 1983-b; Date and Gray, 1983-c; Gray and Date, 1983; Date and Gray, 1985; Gray, 1985; Gray, 1989]. In an argon ICP, most chemical elements are converted into singly charged ions, because the ionizing power of an atmospheric pressure Ar plasma is dominated by the first ionization energy of Ar (15.8 eV). Most elements have first ionization energies well below 16 eV [Moore, 1970], and the degree of ionization of most elements in the plasma is 90 % or higher [Houk *et al.*, 1980]. As a consequence, an abundant population of singly charged ions is produced in the ICP. Similarly, few elements have second ionization energies below 16 eV (except, *e.g.*,

Ba) [Moore, 1970], which implies that the formation of doubly charged ions is rare in the plasma. Consequently, a relatively simple mass spectrum results from an argon ICP, dominated by peaks from the singly positively charged isotopes of the analyte elements. The simplicity of the mass spectrum obtained is however sometimes compromised by the occurrence of spectral interferences (§ II.2). With few exceptions however (*e.g.*, In), at least one isotope of each element is free of isobaric interference [Taylor *et al.*, 1998].

In this work, (semi-)quantitative analysis was regularly performed, using both the Elan 5000 and Elan DRC*plus* ICP – mass spectrometers. In what follows, calibration methods for semi-quantitative and quantitative concentration determinations are discussed. The application of ICP-MS to isotope ratio analysis will be discussed in detail in chapter III.

II.9.1 – Semi-quantitative elemental analysis

Analytical determinations with an accuracy of 30-50 % are known as 'semi-quantitative' [Taylor *et al.*, 1998]. A semi-quantitative analysis requires the measurement of a single multi-element standard solution. After registering the isotope intensities for a calibration standard containing a few elements so that the full mass range (6 to 238 amu) is covered, a relative sensitivity factor can be calculated for each element measured as follows:

$$RF_X = \frac{I_X}{C_x} \qquad \text{(equation II.27)}$$

with RF_X the sensitivity factor for element X, I the isotope intensity and C the concentration of element X.

The sensitivity factors for elements that are not present in the calibration standard can be graphically derived by fitting a curve through the data points obtained for the calibration standard in a diagram where the intensity is plotted versus the analyte mass. Hereby, the isotopic abundance and ionization energy of the isotopes involved also has to be taken into account. These relative sensitivity factors will vary for each element depending on the abundance of the specific isotope measured and the operating conditions selected for the determination. Concentrations of analytes in unknown samples can be estimated by dividing the measured isotope intensities by the predetermined relative sensitivity factors for the specific isotope of the element under investigation. Because relative sensitivity factors are dependent on the specific operating conditions, they should be reestablished whenever adjustments or modifications are made to instrumental parameters [Taylor *et al.*, 1998].

II.9.2 – Quantitative elemental analysis

Analytical determinations with an accuracy better than 10 % are known as quantitative analyses [Taylor *et al.*, 1998]. Mostly, a quantitative analysis is performed for the accurate determination of the level of one or a limited number of analytes. Below, three calibration approaches for quantitative analysis are discussed: (i) external standardization, (ii) standard addition and (iii) isotope dilution (ID).

II.9.2.1 – External standardization

In quantitative analysis via external standardization, several multiple concentration standards containing the analyte(s) of interest are involved. Scans of these standards are performed immediately before, during and after samples are scanned under the same operating conditions, and a relationship is established between signal intensity and concentration. By closely matching the bulk chemical composition of the calibration standards to the known matrix of the samples by the use of, *e.g.*, element standards or salts (so-called 'matrix matching'), an improved accuracy is obtained, since the matrix effects occurring in the samples are similar to that in the calibration standards [Beauchemin *et al.*, 1988; Taylor *et al.*, 1998].

II.9.2.2 – Standard addition

An improved form of matrix matching is standard addition. In this approach, a sample is split into two aliquots, and to one aliquot, a known amount of analyte is added. The amount added should be higher than the amount of analyte already present in the sample. As in external standardization, a relationship is established between the signal intensity and the standard concentration, where in this case the standard is added directly to the sample. Since in this case the standard is a sample spiked with a known amount of analyte, the standard signal is measured in the sample matrix itself. As a consequence, the standard undergoes the same signal influence as the analyte in the matrix, so that a very accurate correction for matrix effects can be performed [Taylor *et al.*, 1998].
In this work, both external standardization and standard addition were applied as a calibration strategy for quantitative elemental assay. Regarding the heavy sample matrices dealt with (*e.g.*, bone, soil), the results obtained by standard addition were considered as the most reliable.

II.9.2.3 – Isotope dilution (ID)

Isotope dilution – mass spectrometry (ID-MS) is a quantitative technique to determine the number of atoms, and thus, the concentration, of a trace element in a diverse range of samples. To accomplish this, an accurately known number of atoms of the same element, but a different isotope, a so-called 'spike', is added to the sample. The mixture is then isotopically equilibrated and the ratio of the unknown number of atoms to the known number of spike atoms is measured [Heumann, 1988; Platzner, 1997]. Contrary to the quantitative analysis approaches described higher, isotope dilution (ID) thus makes full use of the existence of isotopes. The ability of ICP-MS to independently measure the ion intensities of different isotopes allows quantification via ID-ICP-MS [Heumann, 1988; Platzner, 1997; Vanhaecke *et al.*, 2006].

The equation applicable for isotope dilution effects does not contain a sensitivity factor, as is the case in all other calibration strategies. Most analytical instrumentation is susceptible to temporal and/or matrix-induced changes in sensitivity. This effect is orders of magnitude smaller for isotope dilution compared to other calibration methods and therefore it is not measurable in most cases. Since isotope ratios can be determined with a high precision (chapter III, § III.3), also the concentration result obtained from ID experiments is characterized by a high precision [Vanhaecke *et al.*, 2006].

II.9.3 – Internal standardization

In order to correct for temporal and/or matrix induced changes in sensitivity and when no isotope dilution is used, an internal standard is often added in the same concentration to blanks, standards and samples. The use of one or more internal standards is highly recommended to achieve maximum precision and accuracy [Vandecasteele *et al.*, 1988; Vanhaecke *et al.*, 1992] and in this work, one or more internal standards were always used when determining elemental concentrations. Separate internal standards were selected for the various mass ranges where analyte elements occur in the mass spectrum. An element is suited as an internal standard when (i) it is not present in the sample under investigation, (ii) it is preferably mono-isotopic and (iii) it displays similar characteristics (*e.g.*, mass, ionization energy) as the analyte(s). By referencing the analyte signal intensities to the signal intensity for the internal standard, the analyte signals can be corrected for matrix effects, signal drift and instrument instabilities [Vanhaecke *et al.*, 1992; Taylor *et al.*, 1998].

CHAPTER III

Isotope ratio analysis via ICP-MS

From its introduction in 1983 on, ICP-MS has been used for isotope ratio measurements. However, its application range was limited to measuring either induced changes in the isotopic composition of a target element, or pronounced natural variations, as is the case for Pb. This was because the isotope ratio precision attainable with most ICP-MS instruments was rather poor compared to that achievable using thermal ionization – mass spectrometry (TI-MS). The introduction of multi-collector ICP-MS for isotopic analysis however, has not only bridged this gap in isotope ratio precision, but has also opened previously inaccessible application ranges. In this chapter, general concepts of isotopic analysis and the use of (MC-)ICP-MS as a tool for isotopic analysis are described, followed by a discussion of the sources of noise and bias in isotopic analysis using ICP-MS.

III.1 – General concepts of isotopic analysis

Of the eighty-three naturally occurring elements that are not radioactive or have half lives long enough to be considered as stable (half life > 10^9 years), nearly three quarters have two or more isotopes. Variations in the isotopic ratios of a number of these elements, including H, C, N, O and S, provide the foundation for the field of stable isotope geochemistry. Investigations of variations in the isotopic compositions of these 'traditional' elements have provided important constraints on their sources in rocks, minerals and fluids. Much less attention, however, has been paid to stable isotope variations of other elements that are also geochemically important, such as certain metals and halogens ('non-traditional' elements). This can be attributed to the analytical challenges, although first-order variations for several systems have been established using gas source – and thermal ionization – mass spectrometry. With the advent of multi-collector ICP – mass spectrometry, large portions of the periodic table are now accessible to stable isotope studies [Johnson *et al.*, 2004-a].

Generally speaking, isotopic abundances are constant in nature [De Laeter *et al.*, 2003]. As a consequence, a variety of problems can be studied by using compounds in which a particular element shows an isotopic composition sufficiently different from the corresponding natural one, *e.g.*, in the case of artificially produced radionuclides (^{99}Tc, ^{129}I, ^{236}U). Many isotope applications are based on the assumption that the behavior of different isotopes is chemically and physically identical. This is a prerequisite for tracer and isotope dilution (ID) experiments often practiced in ICP-MS. Nevertheless, small isotopic or mass fractionation effects do occur in both natural and industrial processes [Roth, 1997]. The origin of such fractionation effects can be either kinetic or thermodynamic

[Schauble, 2004] (§ III.2), and the isotopic variation they give rise to is especially observed for the lighter elements such as H, C, N, O and S, occurring due to the relatively large mass difference between their isotopes [Coplen *et al.*, 2002]. Most of these elements are typically studied using gas source – mass spectrometry (GS-MS), which is therefore also often referred to as isotope ratio – mass spectrometry (IR-MS). With the increasing isotope ratio precision offered by TI-MS, and later also by MC-ICP-MS, however, natural variations in the isotopic composition are established for an increasing number of 'heavier' elements and turned out not to be restricted to light elements only. Additionally, variations in the isotopic composition of some elements may also occur as a consequence of the radioactive decay of naturally occurring long-lived radionuclides (as is the case for Sr and Pb, the target elements in this work (chapter IV, § IV.1 and § IV.2)), nuclear reactions resulting from the interaction of cosmic rays with matter, producing mainly short-lived isotopes [Leya *et al.*, 2000] and anthropogenic activities [Cloquet *et al.*, 2006-a]. In addition, in some meteoritic samples, some elements show deviations from the natural isotopic composition, unknown in terrestrial samples [Birck, 2004]. Because of these variations, the representative isotopic composition in normal terrestrial materials cannot be defined precisely for some elements, such as Li, Sr and Pb, but covers a small range [De Laeter *et al.*, 2003].

Of all the isotope-specific analytical techniques (mass spectrometry, activation analysis, spectroscopic methods and nuclear magnetic resonance (NMR-) spectroscopy), mass spectrometry is by far the most versatile and powerful [Roth, 1997], since it allows the relative abundances of different isotopes to be measured with a high precision and accuracy. An isotope ratio R of an element M, which is in fact a ratio of amounts of isotopes of mass i and j, is experimentally accessible using mass spectrometry, since ion currents corresponding to the isotopes under consideration are easily measured:

$$R = \frac{n(^{i}E)}{n(^{j}E)} \approx \frac{I(^{i}E^{+})}{I(^{j}E^{+})} \qquad \text{(equation III.1)}$$

An isotope ratio is a well-defined and robust property. However, there are some mass-dependent processes that cause a small, but measurable, bias due to the difference in mass between the isotopes measured, as a consequence of a different transmission efficiency through the mass spectrometer for ions of different mass [Vanhaecke *et al.*, 2006]. This can be mathematically expressed as:

$$R = \frac{n(^{i}E)}{n(^{j}E)} = \frac{I(^{i}E^{+})}{I(^{j}E^{+})} K \qquad \text{(equation III.2)}$$

with K the product of the correction factors for the different sources of bias.

In general, K is fairly close to unity and is known with a relatively small uncertainty. Depending on the objective of the measurement and the effort that goes into the determination of the correction factors, different situations arise: (i) the correction factor is determined and applied, (ii) small correction factors are ignored, as is the case in tracer experiments; (iii) correction factors are assumed to stay constant during the measurement and no effort is performed to quantify them, *e.g.*, in isotope dilution experiments and (iv) a constant bias is assumed in differential isotopic measurement, where the aim is to find out how different the isotope ratio measured in the sample is, compared to the corresponding ratio in a reference sample. Such differences are often small, and therefore, a high reproducibility is desired. Assuming a constant bias is convenient, but for critical applications, *e.g.*, the preparation of certified reference materials, the bias should be checked independently, and the availability of calibrated isotope ratios is required [De Bièvre *et al.*, 1993].

The vast majority of isotopic data are expressed in 'delta-notation' (δ), where the isotopic composition is cast as the deviation of an isotope ratio relative to the same ratio in a standard:

$$\delta\,{}^{i}E_X = \left(\frac{R_X^{i/j} - R_{std}^{i/j}}{R_{std}^{i/j}}\right) 10^3 \qquad \text{(equation III.3)}$$

with i and j the mass of the isotopes used in the ratio R of an element E, X the sample of interest and std the standard reference material or reservoir.

The units for the $\delta\,{}^{i}E_X$ value are in parts per thousand, or 'per mil', commonly noted as ‰. In the case of the $\delta\,{}^{18}O$ value, $R = {}^{18}O/{}^{16}O$, following the traditional protocol of expressing $R^{i/j}$ as the abundance ratio of the rare isotope to the major isotope, which corresponds in the case of the traditional isotope systems, to heavy over light isotope, *e.g.*, $\delta\,{}^{15}N$ and $\delta\,{}^{34}S$ use the isotope ratios ${}^{15}N/{}^{14}N$ and ${}^{34}S/{}^{32}S$, respectively. This convention implies that a positive $\delta\,{}^{i}E_X$ value refers to a sample that is relatively enriched in the heavy isotope [Johnson *et al.*, 2004-a].

The motivation for expressing $\delta\,{}^{i}E_X$ values as rare isotope over major isotope lies in the fact that the mathematics of mixing relations are greatly simplified in cases where the rare isotope i is very low in abundance, which leads to the simplification that the abundance of isotope j may be treated as invariant, particularly when the range in isotopic compositions is relatively restricted. When mixing two components, A and B, that contain an amount of an element E with a different isotopic composition, the isotopic composition of E in the resulting mixture is given by:

$$\frac{M_A}{M_B} = -\left(\frac{C_B}{C_A}\right)\frac{R^*_{mix} - R^*_B}{R^*_{mix} - R^*_A} \qquad \text{(equation III.4)}$$

with M_A and M_B the masses of components A and B respectively, C_A and C_B the concentrations of the element in components A and B respectively, and R^* the ratio of the mass of the rare isotope over the total mass of the element E.

In the case of O, where the abundances of ^{18}O and ^{16}O are 0.20 % and 99.76 % respectively, R^* is very nearly equal to the $^{18}O/^{16}O$ ratio, so that the exact mixing equation can be directly related to the measured isotopic compositions and simplified using the delta-notation:

$$\delta\,^{i}E_{mix} \approx \delta\,^{i}E_A\, f + \delta\,^{i}E_B\,(1 - f) \qquad \text{(equation III.5)}$$

with f the fraction of component A in the two-component mixture.

It is important to note that equation III.5 is only valid for cases where the abundance of the isotope in the numerator of R is very low and/or when the difference between $\delta\,^{i}E_A$ and $\delta\,^{i}E_B$ is small [Johnson *et al.*, 2004-a].

When working with non-traditional isotopes, it is not always possible to follow at the same time the convention of rare isotope over major isotope on one hand and heavy isotope over light isotope on the other hand. Both conventions are met in the case of, *e.g.*, Mg ($^{25}Mg/^{24}Mg$ and $^{26}Mg/^{24}Mg$) and Ca ($^{44}Ca/^{40}Ca$), but not in the case of, *e.g.*, Li ($^{6}Li/^{7}Li$) and Fe ($^{54}Fe/^{56}Fe$). If the rare over major isotope definition is maintained, there will be inconsistencies in the sign of the $\delta\,^{i}E_X$ value, so that a positive value will sometimes reflect an enrichment in the heavier isotope, and sometimes a depletion. Given the fact that some nucleosynthetic processes produce values of R that approach unity with increasing atomic number, and that the simplifications of mixing and other equations become less accurate as R approaches unity, it is preferred to define R for the new isotope systems as heavy isotope over light isotope. This maintains the same convention as used for traditional isotope systems, where a positive $\delta\,^{i}E_X$ value indicates a relative enrichment in the heavy isotope relative to a standard [Johnson *et al.*, 2004-a].

III.2 – Stable isotope fractionation

Isotopic fractionation, *i.e.*, minor changes in the isotopic composition of an element, between species or phases depends on a number of factors, including the relative mass difference, the nature of the bonding environment and the redox state. Generally, it is expected that the range in isotopic variations will decrease with increasing atomic number

Z because the relative mass difference also decreases [Johnson *et al.*, 2004-a]. The relatively large mass differences for the traditional stable isotopes are in part responsible for the relatively large ranges in isotopic ratios (10's-100's ‰) that have been measured in natural samples for these elements. Despite relatively small mass differences on the order of ~ 1 %, significant isotopic variations are seen for heavier elements such as Mo (z=42) [Anbar, 2004] and even Hg (z=80) [Jackson, 2001] and Tl (z=81) [Rehkämper *et al.*, 2002].

III.2.1 – History

The theory of stable isotope fractionation precedes the development of modern mass spectrometry, and includes a number of studies in the early-mid 20th century [Lindemann, 1919; Lindemann and Aston, 1919; Urey and Greiff, 1935; Bigeleisen and Mayer, 1947; Urey, 1947]. The most studied elements were H, C, N, O and S, and theoretical calculations successfully predicted the directions, magnitudes and temperature sensitivities of isotopic fractionations. A key point is that all these theoretical treatments result from a simplified thermodynamic model of the quantum mechanics of molecular vibration and rotation, making calculations feasible for many substances, while maintaining enough accuracy to be quantitatively useful [Schauble, 2004].

In stable isotope fractionation processes, a distinction between thermodynamic or equilibrium isotope fractionation and kinetic isotope fractionation can be made. For most elements, and typical terrestrial temperature and pressure conditions, equilibrium isotopic fractionations are caused by the sensitivities of molecular and condensed-phase vibrational frequencies to isotopic substitution. Some kinetic isotopic fractionations are controlled by molecular or atomic translational velocities; this class includes many evaporative and diffusive fractionations [Rodushkin *et al.*, 2004; Richter *et al.*, 2006].

The discovery of oxygen and sulfur fractionations that appear to have an unusual mass dependence has renewed interest in variations in the mass dependence of different fractionation mechanisms [Young *et al.*, 2002]. However, recent measurements in non-traditional stable isotope systems appear to confirm that mass-dependent fractionation is the norm in geochemical processes and typical chemical reactions. In addition, theoretical calculations suggest that different mass-dependent fractionation mechanisms will follow slightly different laws, so that it may be possible to distinguish equilibrium and kinetic fractionations [Young *et al.*, 2002].

III.2.2 – Equilibrium isotopic fractionation

From an examination of both observed and theoretically calculated isotope fractionations, it is clear that there are a number of qualitative chemical rules that can be used to estimate which substances will tend to be enriched in heavy isotopes in a given geochemical system. Five characteristics are shared by the elements that show large variations in isotopic composition in nature: (i) low atomic mass, (ii) large relative mass difference between stable isotopes, (iii) tendency to form highly covalent bonds, (iv) multiple oxidation states or other chemical variability and (v) availability of multiple isotopes with sufficient abundance to make measurements feasible [O'Neil, 1986]. Although 'non-traditional' stable isotopes in general fail to meet one or more of these criteria, the rules are strongly supported by theoretical considerations [Bigeleisen and Mayer, 1947] and form the basis for a qualitative guide to stable isotopic fractionations in all elements [Schauble, 2004].

Equilibrium stable isotope fractionation is a quantum-mechanical phenomenon, driven mainly by differences in the vibrational energies of molecules and crystals containing atoms of differing masses [Urey, 1947]. In fact, a list of vibrational frequencies for two isotopic forms of each substance of interest, along with a few fundamental constants, is sufficient to calculate an equilibrium isotope fractionation with reasonable accuracy, as is shown for the $^{35}Cl/^{37}Cl$ swap between the diatomic gas ClO and an isolated Cl atom [Schauble, 2004]. When dealing with condensed phases, additional assumptions have to be made in order to deal with the complexities and uncertainties arising in that situation.

Also a handful of non-vibrational mechanisms have been proposed to be responsible for equilibrium isotopic fractionations, including effects of nuclear spin or shape on electronic energies [Bigeleisen, 1998]. These non-vibrational phenomena can, in principle, be distinguished from the conventional fractionations because they are not expected to be mass-dependent. However, it is not yet clear how important these unconventional mechanisms are in natural systems [Schauble, 2004].

III.2.3 – Kinetic isotopic fractionation

Kinetic isotopic fractionations also show systematic behavior, although they are more difficult to predict with a list of widely applicable rules. The term kinetic is being used loosely to describe a host of basically one-directional processes occurring under conditions of incomplete isotopic exchange. One common feature in many kinetic fractionation processes is that the lighter isotopes are concentrated in reaction products, since the

transport of the lighter isotopes is more efficient than that of the heavier isotopes. This behavior is observed, *e.g.*, in rapid precipitations of Fe^{3+} oyhydroxide and oxide minerals from Fe^{3+} solutions [Skulan *et al.*, 2002], in evaporation of many substances including silicate melts [Davis *et al.*, 1990], in diffusion processes [Rodushkin *et al.*, 2004; Malinovskiy *et al.*, 2007], and in numerous biological reactions [Johnson *et al.*, 2004-b]. Kinetic fractionations are usually sensitive to a host of factors, such as reaction rates, activation energies and the presence of exchange catalysts, in addition to temperature [Schauble, 2004].

III.3 – ICP-MS for isotope ratio applications

As stated in chapter II (§ II.8), the most relevant distinction between ICP-MS instruments in the field of isotopic analysis is on the basis of their detection system, i.e., single-collector (SC) – versus multi-collector (MC) – ICP-MS instrumentation.

III.3.1 – Single-collector ICP-MS

Single collector ICP – mass spectrometers are equipped with one electron multiplier for ion detection. This implies that, for isotope ratio determinations, the isotopes of interest are sequentially detected so that the isotope ratio precision attainable is inferior to that attainable with thermal ionization – mass spectrometry (TI-MS), a technique that has long been regarded as the reference technique for isotope ratio determinations of the heavier elements [Walczyk, 2004] and offers an isotope ratio precision down to < 0.01 % RSD [Heumann *et al.*, 1998; Taylor *et al.*, 1998]. However, for isotope ratio applications where an extremely high precision is not required, ICP-MS offers important benefits over TI-MS, such as the continuous nebulization of sample solution into the ion source at atmospheric pressure, the higher sample throughput and the high ionization efficiency of the ICP [Houk *et al.*, 1980; Gray, 1986].

In traditional single-collector quadrupole-based ICP-MS (SC-ICP-Q-MS), the isotope ratio precision attainable is limited to 0.1-0.5 % RSD [Heumann *et al.*, 1998], a precision that is not sufficiently high for many isotope ratio applications. This inferior precision can be attributed to instabilities in the formation, transmission and detection of the ions and the sequential detection of the isotopes of interest. The occurrence of spectral interferences is another drawback, further limiting the application field of conventional quadrupole-based ICP-MS for isotopic studies. However, by the introduction of collision/reaction cells [Feldmann *et al.*, 1999-a, Feldmann *et al.*, 1999-b; Koppenaal *et al.*, 2004] including the dynamic

reaction cell (DRC) [Tanner and Baranov, 1999; Tanner *et al.*, 2002] in quadrupole-based ICP-MS (SC-ICP-DRC-MS), considerable progress has been made in terms of both the battle against interferences (chapter II, § II.6) and the isotope ratio precision attainable. Thermalization of the ions in the dynamic reaction cell does not only result in an improved transmission efficiency (collisional focusing), but can also improve the isotope ratio precision attainable. In standard quadrupole-based ICP-MS without DRC or with DRC used in vented mode, the time it takes an ion to travel from the extraction lens downstream to the detector is of the order of 100 µs. During the time the intensity for one isotope is registered (*e.g.*, 1 ms), the other isotopes formed at exactly the same moment and under the same conditions in the plasma, are not detected. For measuring the signal intensity of the second isotope, an ion population sampled at a later moment from the plasma is monitored, and thus the measured isotope ratio is biased by fluctuations in the ion beam. Bandura and coworkers [Bandura and Tanner, 1999; Bandura *et al.*, 2000] simulated these fluctuations in a continuous ion beam originating from the plasma by applying a pulsed voltage to the extraction lens. The individual ion packets, 200 µs long in vented mode, were broadened up to 4 ms when the cell was pressurized. It was assumed that this broadening also occurs when working with a continuous ion beam, as was demonstrated by comparing the RSDs obtained upon isotope ratio measurement under vented and pressurized conditions, respectively. From the results of the modulated beam experiments, it can be assumed that ion density fluctuations of the continuous ion beam, that occur in a timeframe of a few milliseconds or less, are damped in the cell, and therefore, ions are redistributed in time. This temporal redistribution of the ions should improve the correlation between populations of isotope ions selected sequentially by the downstream quadrupole analyzer, leading to an improved isotope ratio precision.

Single-collector sector field ICP-MS or high resolution ICP-MS (SC-ICP-SF-MS or SC-HR-ICP-MS) [Jakubowski *et al.*, 1998] can be operated at a higher mass resolution, providing an elegant way to resolve analyte signals from those of molecular ions with nearby mass [Vanhaecke *et al.*, 1996-b] and provides an isotope ratio precision of 0.05-0.2 % RSD [Vanhaecke *et al.*, 1997; Heumann *et al.*, 1998]. Isotope ratio precisions of 0.05-0.5 % RSD have been reported for TOF-ICP-MS [Vanhaecke *et al.*, 1999].

III.3.2 – Multi-collector ICP-MS

The technique multiple collector – or multi-collector ICP-MS (MC-ICP-MS) was developed specifically to overcome the limitations of TI-MS on one hand and single-collector ICP-MS

on the other hand for isotope ratio analysis [Rehkämper *et al.*, 2001]. To achieve this goal, the argon ICP ion source was combined with a magnetic sector mass spectrometer (chapter II, § II.5.2.2) and a Faraday cup array (chapter II, § II.7.2) as these were already used in TI-MS instrumentation. At the high temperatures attained in an inductively coupled argon plasma, elements with a first ionization energy < 10 eV are ionized to an extent of 75 % or more [Jarvis *et al.*, 1992]. Thus, with an ICP as an ion source, virtually all elements of the periodic table are accessible to isotopic analysis. This stands in contrast with TI-MS, where thermal ionization to positive ions is achieved for only a limited number of elements with low first ionization energies.

The mass spectrometers in MC-ICP-MS are similar to the sector field mass spectrometers used in single-collector ICP-SF-MS, but also aim at obtaining flat-topped peaks necessary for high-precision isotope ratio measurements. For this reason, most MC-ICP-MS instruments operate at a low mass resolution (~ 400) and at minimal loss of transmission by the use of wide source and collector slits. Self-evidently, the possibility to overcome spectral interferences by operating a sector field mass spectrometer at increased mass resolution is also desirable for MC-ICP-MS, while at the same time preserving flat-topped peaks and hence, assuring an isotope ratio precision still competitive with TI-MS. In the case where there is only one interfering ion, its signal will either be at the high mass or the low mass side of the analyte peak, and even if there are more molecular ions interfering with accurate measurement of the analyte peak intensity, very often, all of these ions are to be found at the same side of the analyte mass. In MC-ICP-MS, this fact is often taken advantage of by working in so-called 'pseudo-high resolution' mode [Vanhaecke and Moens, 2004]. While reducing the width of the source slit by moving one side only, the width of the collector slit is not adjusted. In this way, the mass range over which the analyte intensity is constant (the flat section of the spectral peak) is maximized [Weyer and Schwieters, 2003]. The isotope ratio precision obtained under these conditions is significantly better that that obtained at 'full' high resolution. Of course, the higher the mass resolution, the harder it becomes to maintain the trapezoidal peak shape. Therefore, the maximum resolving power offered by MC-ICP-MS is lower than that offered by single-collector sector field ICP-MS. It is worth pointing out that the traditional definition of resolution (chapter II, equation II.1), where Δm represents the peak width at 5 % of the maximum peak height, is not valid in this case. In pseudo-high resolution conditions, Δm represents the difference between the masses where the analyte intensity amounts to 95 % and 5 % of the maximal signal intensity, respectively. The mass resolution calculated using the latter approach exceeds that calculated using the former approach by

more than a factor of two, so that care has to be taken when comparing mass resolutions [Vanhaecke and Moens, 2004].

The use of a detector array with multiple Faraday cups permits the simultaneous collection of the separated isotopes. Despite its lower sensitivity, the Faraday collector is preferred over the secondary electron multiplier for ion detection in MC-ICP-MS instrumentation, because in the counting mode, the multiplier suffers from dead time effects which become increasingly important as the isotope ratio deviates more from unity [Russ, 1989]. Only if a higher sensitivity is required, one or more Faraday cups can be replaced by an electron multiplier. The multi-collection approach cancels out the effects of a 'noisy' signal on the isotope ratio measurement. Especially in ICP – mass spectrometry, this static multiple collection is critical because the ion beam that is produced in the plasma is significantly more unstable than the ion beam in TI-MS, mainly due to short-term intensity fluctuations. The collector incidences can be adjusted to permit isotopic analysis of a wide range of elements having isotopes that display different mass dispersions [Rehkämper *et al.*, 2001], either by zoom optics that focus the separated ion beams towards the respective fixed Faraday cups (*e.g.*, Nu Plasma 500), or by adjusting the positions of the Faraday cups (*e.g.*, Neptune).

The results obtained with the first prototype MC-ICP-MS instrument, built by VG Elemental in 1990, were impressive because they demonstrated that the isotopic composition of elements such as Sr and Nd could be determined with a precision similar to TI-MS [Walder and Freedman, 1992; Walder *et al.*, 1993]. Furthermore, isotope ratio measurements of elements with high ionization energies, such as Hf and W, were of superior quality and were obtained at much greater speed and ease [Halliday *et al.*, 1995]. Since its development, MC-ICP-MS has undergone a rapid evolution and has found application in a continuously growing number of laboratories world-wide. The immense interest of the geochemical community in MC-ICP-MS instrumentation is largely based on the high precision and extreme versatility of this mass spectrometric technique. The principal application of MC-ICP-MS can be found in the earth sciences, and more specifically, in the highly precise measurement of the isotopic composition of a wide range of elements. The application field focuses on (i) elements that are difficult to analyze by TI-MS, such as isotopic measurements in the context of long-lived (Lu-Hf) or extinct (Hf-W) radiogenic isotope systems, (ii) precise elemental analysis with isotope dilution of a number of trace elements, and, more recently, (iii) stable isotope ratio measurements [Halliday *et al.*, 1998; Rehkämper *et al.*, 2001; Collerson *et al.*, 2002].

III.4 – Uncertainty factors in isotope ratio determination via ICP-MS

The quality requirements and/or expectations of isotope ratio measurements are often very high. This implies the need of an adequate identification of the different sources of uncertainty. Although these different factors are often intertwined, a distinction is often made between factors affecting (i) presicion, or factors that contribute to the noise of the system [Begley and Sharp, 1994] and (ii) accuracy, or factors that create an offset or bias: mass discrimination, mass scale shift, background and contamination, and detector dead time [Begley and Sharp, 1997].

III.4.1 – Sources of noise

Inductively coupled plasmas are known as 'noisy' ion sources, compared to thermal ionization sources. Different parts of the instrument are responsible for producing noise, *e.g.*, pulsations of the peristaltic pump, variations in the nebulizer efficiency, the gasdynamic rotation of the plasma, changes in energy transfer from the plasma to the aerosol and variation in ion extraction efficiencies. Random events also occur in detectors and their associated electronics. More troublesome is noise picked up from inside the instrument or from external sources.

Source noise contributions can be minimized by selecting suitable data acquisition parameters for single-collector instruments [Begley and Sharp, 1994; Appelblad *et al.*, 2001], such as an increased measurement time, peak hopping instead of scanning, and a suited choice of the dwell time per acquisition point, number of acquisition points per spectral peak, number of sweeps and settling time. With single-collector ICP-MS instruments, the noisy character of the ICP is counteracted by using a high peak-hopping rate (short settling time) to eliminate low frequency noise from the plasma and the sample introduction system to the largest possible extent [Furuta, 1991]. In the 1980's, dwell times of typically 10-20 ms were advised. With shorter settling times and using a dwell time of a few milliseconds only, even higher peak-hopping rates can be used, allowing optimum isotope ratio precisions to be obtained in both quadrupole-based – [Bandura *et al.*, 2000; Moens *et al.*, 2001] and sector field [Vanhaecke *et al.*, 1996-b] single-collector ICP-MS. The measurement time can sometimes be used more efficiently by increasing the acquisition time for the low abundant isotope(s) relative to that of the higher abundant isotope(s) [Quétel *et al.*, 1997]. The most efficient way to minimize the effect of source noise, however,

is the use of a multi-collector ICP-MS instrument. The simultaneous monitoring of all the isotopes involved results in a superior isotope ratio precision, similar to that offered by TI-MS. Multi-collector ICP – mass spectrometers are operated in static mode, which means that neither the accelerating field, nor the strength of the magnetic field are changed during data acquisition.

The effect of all the processes introducing noise is that the arrival of ions at the detector is not a continuous process, but a random one, and is often assumed to be described using a Poisson distribution. On the basis of counting statistics, the minimum standard deviation σ_N on the number of counts N for ion counting systems is given by:

$$\sigma_N = \sqrt{N} \qquad \text{(equation III.6)}$$

Following error propagation, the standard uncertainty on the isotope ratio $R^{i/j} = I/J$, representing the best isotope ratio precision theoretically attainable since it only takes into account counting statistics, is given by [Vanhaecke *et al.*, 2006]:

$$\frac{\sigma_{R^{i/j}}}{R^{i/j}} = \sqrt{\left(\frac{\sigma_I}{I}\right)^2 + \left(\frac{\sigma_J}{J}\right)^2} \qquad \text{(equation III.7)}$$

III.4.2 – Mass discrimination

When an instrument produces a different response for ions of different mass, this systematic error is called 'mass discrimination' or 'mass bias'. Typically, the mass discrimination that occurs in ICP-MS instrumentation is about 1 % per mass unit (at mass 100), irrespective of the kind of instrumentation. As the ion kinetic energy is dependent on the mass [Niu and Houk, 1996], any energy-dependent process in the instrumentation (*e.g.*, sampling of ions from the ICP, transfer of ions, or detection) will result in mass discrimination. Compared to TI-MS, mass discrimination in ICP-MS is often larger, especially at lower mass. For example in the case of the $^6Li/^7Li$ isotope ratio, a mass discrimination of 16 % is observed for ICP-MS [Sun *et al.*, 1987] against less than 1 % mass fractionation for TI-MS [Michiels and De Bièvre, 1983]. For both quadrupole-based – and sector field instrumentation, the behavior and the magnitude of mass discrimination across the mass range is fairly similar. Contrary to TI-MS, in which a discrete amount of sample is brought into the ion source, there is a continuous introduction of new sample into the ICP. Therefore, systematic time-dependent fractionation as in TI-MS does not occur in ICP-MS.

III.4.2.1 – Origin of mass discrimination

Although not all the sources and mechanisms of mass discrimination in ICP-MS have been unequivocally identified, the sampling of ions from the ICP and the ion transfer lens system have been identified as the major contributors. A distinction can be made between space-charge effects and nozzle-separation effects [Heumann *et al.*, 1998], although the effects cannot be distinguished from each other at the detector side of an ICP – mass spectrometer since they both cause mass discrimination in the same direction (enrichment in heavier isotopes). It was also suggested that mass discrimination originates during ionization in the plasma itself [Maréchal *et al.*, 1999]. Regardless of the origin, the large mass bias associated with plasma source ionization necessitates that mass discrimination is carefully monitored during isotope ratio measurements if precise and accurate analytical results are to be obtained.

The space-charge effect is assumed to have the largest contribution to the mass discrimination in an ICP – mass spectrometer. Tanner *et al.* described the influence of the space-charge effects caused by the large matrix Ar^+ ion currents (μA) passing through the lens system [Tanner *et al.*, 1994]. After the positively charged ion beam leaves the skimmer cone, the mutual repulsion of ions limits the total number of ions which are transmitted by the ion optics. If an ion beam consists of light and heavy ions, the light ions are deflected more extensively than the heavy ions, whereas the heavy ions preferably remain in the central ion beam. Hence, mass discrimination in isotope ratio measurements depends on the matrix and therefore also on the total ion current produced by a sample [Heumann *et al.*, 1998]. The causal relation of these space-charge effects to mass discrimination was later experimentally confirmed by isotopic analysis of deposits of various elements on the ion lenses [Andrén *et al.*, 2004].

The nozzle-separation effect has been described as a reason of mass discrimination during plasma extraction via the sampling cone aperture [Heumann *et al.*, 1998]. The ion beam extracted from the ICP supersonically expands in the expansion zone between the sampling and skimmer cones. Independent of space-charge effects, the lighter ions should preferably be removed from the central beam compared to the heavier ions, resulting in an enrichment of the central beam in the heavier isotopes. This effect was later confirmed by carrying out isotopic analysis of B deposited onto the sampling and skimmer cones [Andrén *et al.*, 2004].

In the case of Cu and Zn isotopic analysis using multi-collector ICP-MS, it was observed that a varying mass fractionation factor was obtained for Zn depending on the relative

transmission of Cu and Zn. Herefrom, it was suggested that the competition of different elements for ionization in the plasma at different temperatures may induce mass discrimination [Maréchal *et al.*, 1999].

III.4.2.2 – Correction for mass discrimination

The mass bias is corrected for by either one of two methods. External standardization, wherein the isotope ratio of interest is measured in a standard solution, and the bias used to correct the same ratio in the sample, allows the mass bias to be measured at the same masses as the analyte, and at approximately the same abundances. The magnitude of mass bias, however, may change in the presence of the sample matrix and/or in the time elapsed between measurement of the sample and the standard [Ingle *et al.*, 2003]. In internal standardization approaches, the mass bias is determined in the sample solution either using a known isotope ratio of an element added to the sample for that purpose (external normalization), or using a pair of isotopes of the analyte element that display an invariant ratio in nature (internal normalization). The bias is then applied as part of a mathematical model to correct the analyte ratio. Internal standardization provides nearly continuous monitoring of the mass bias and can be used to correct matrix effects. However, inaccuracies may be introduced as the isotopes used to calculate the bias have masses, ionization characteristics and isotopic abundances that are different to the analyte isotopes [Ingle *et al.*, 2003].

III.4.2.2.1 – Internal and external normalization

Measurements of radiogenic isotope compositions (*e.g.*, $^{87}Sr/^{86}Sr$, $^{143}Nd/^{144}Nd$) are corrected for instrumental mass discrimination by normalization of the measured ratio to an invariant isotope ratio of the same element. This procedure, so-called 'internal normalization' employs empirically derived formulae, intended for the correction of TI-MS data for evaporation-induced fractionation. The lack of a causal law that is able to describe accurately the static mass discrimination effects of ICP – mass spectrometry has led to the use of the same laws in ICP-MS [Rehkämper *et al.*, 2004].

External normalization can be used for the determination of stable isotope compositions. Since the mass discrimination in ICP-MS is, to a first order, a relatively simple function of mass, elements with similar or overlapping mass ranges display a nearly identical mass bias. Using a solution containing a mixture of two elements with similar masses, the mass discrimination observed for an element of known isotopic composition can be used to

determine the mass discrimination affecting the unknown isotopic composition of the second element (*e.g.*, Tl in the case of Pb isotopic analysis [Rehkämper *et al.*, 2004], Cu in the case of Zn isotopic analysis [Maréchal *et al.*, 1999].

Several empirical laws are used, in which a factor K is calculated on the basis of the true isotope ratio R from the certificate or the IUPAC table, the observed isotope ratio r and the mass difference Δm for the isotopes considered. From this factor, a mass discrimination factor ε can be calculated. Three laws are distinguished: the linear law, the power law and the exponential law, respectively given by:

$$K = \frac{R}{r} = 1 + \varepsilon_{lin}\,\Delta m \qquad \text{(equation III.8)}$$

$$K = \frac{R}{r} = \left(1 + \varepsilon_{pow}\right)^{\Delta m} \qquad \text{(equation III.9)}$$

$$K = \frac{R}{r} = e^{\varepsilon_{exp}\,\Delta m} \qquad \text{(equation III.10)}$$

In these expressions, ε is defined and determined for a specific isotope pair. Subsequent incorporation of the calculated ε into one of the models implies two assumptions: (i) ε can be considered as a measure of the bias per mass unit, and is therefore constant over the mass range, and (ii) ε has additive properties, so that ε measured from isotopes having two mass units separation is equal to twice that for unit mass separation over the same interval. It is evident that these models cannot be completely correct, since they predict that the mass bias is dependent on the mass difference between the isotopes and not on their absolute mass [Ingle *et al.*, 2003]. This implies that the predicted bias in $^{6}Li/^{7}Li$ is the same as in $^{206}Pb/^{207}Pb$, contradicting common experience. Nevertheless, in MC-ICP-MS, internal normalization using the power and exponential laws have been shown to be most effective for the correction of mass bias in U measurements [Taylor *et al.*, 1995] and Pb measurements [Rehkämper and Mezger, 2000]. In quadrupole-based ICP-MS, the linear model appeared to be at least as suited as the two alternatives for the correction of Pt isotope ratios [Begley and Sharp, 1997]. The external normalization procedure was first suggested by Longerich *et al.* to improve the Pb isotope ratio precision with quadrupole-based ICP-MS using Tl as the reference element [Longerich *et al.*, 1987]. The three correction equations were found to be almost equally effective in SC-ICP-SF-MS when correcting the $^{111}Cd/^{112}Cd$ isotope ratio for the isobaric ^{112}Sn interference on m/z 112 via the mass-bias corrected $^{112}Sn/^{117}Sn$ ratio [Park *et al.*, 2000]. Also in MC-ICP-MS, the external normalization approach has been applied in several studies [Hirata, 1996; Belshaw *et al.*, 1998; Rehkämper and Halliday, 1998].

A different approach has been favored for the correction of mass bias in TI-MS, using an equation first described by Russell *et al.* [Russell *et al.*, 1978]:

$$K = \frac{R}{r} = \left(\frac{m_1}{m_2}\right)^{\beta} \qquad \text{(equation III.11)}$$

with m_1 and m_2 the masses of the isotopes in the ratios R and r and β the mass discrimination factor.

Here, the mass discrimination factor β is still determined for a specific isotope pair, but should be a better approximation as it indicates that the correction depends on the absolute masses of the isotopes in the ratio considered. This equation has been shown to be applicable to MC-ICP-MS for several isotope systems [Maréchal *et al.*, 1999; White *et al.*, 2000; Anbar *et al.*, 2001] as well. In these cases, it was found that the mass bias factors for the analyte and internal standard are not equal, but that the ratio of the two was constant during an analytical session, and could be used to successfully correct for mass bias.
It was shown that the power law (equation III.9) and the Russell expression (equation III.11) are particular cases of a generalized power law [Maréchal *et al.*, 1999], expressed as:

$$K = \frac{R}{r} = \frac{1}{g(m_2^n - m_1^n)} \qquad \text{(equation III.12)}$$

with g a mass-independent coefficient and n an arbitrary number.

The generalized power law is equivalent to the power law for $n = 1$ and approaches the Russell expression for $n \to 0$. The generalized power law was proven to be a valuable tool to correct for instrumental mass bias in the case of Nd isotope ratio determinations, where an optimum value of –0.23 was found for n [Wombacher and Rehkämper, 2003].

III.4.2.2.2 – External standardization

In TI-MS, the measured isotopic composition changes with time due to the progressive evaporation process, and mass fractionation is thus time-dependent. Since an ICP source operates at steady-state, mass discrimination in ICP-MS is not primarily a time-dependent process. This is beneficial for the correction of instrumental mass bias by external standardization, where the isotopic data obtained for a sample are referenced to the value obtained for an isotopic standard [Rehkämper *et al.*, 2004].
For heavy elements such as U, where the mass bias is ~ 0.5 % per mass unit, the mass discrimination generally varies by < 0.2 ‰ per hour. For light elements below mass 40,

the drift is significantly larger, up to ~ 5 ‰ per hour [Tomascak *et al.*, 1999]. Changes in mass discrimination with time thus appear to be more severe for the lighter elements, such that optimized application of external standardization will require different analytical protocols for different elements. At present, the most precise data have been collected by alternating sample and standard measurements, so that each sample is referenced only to the mean of the standards measured immediately before and afterwards. In the case of Pb isotope ratio measurements and using NIST SRM 981 Common Lead as a standard, the corrected ratio can be calculated as follows:

$$R_X = 2\, R_{NIST}\, \frac{r_X}{r_{NIST,before} + r_{NIST,after}} \qquad \text{(equation III.13)}$$

with R_X and r_X the true and measured isotope ratio in the sample, respectively and R_{NIST} and r_{NIST} the true and measured isotope ratio in the standard, respectively.

This technique of sample-standard bracketing is similar to the standardization method used in GS-MS. For light elements, where the drift in mass bias is particularly severe, the precision of sample measurements can be improved by performing multiple short analytical runs that are each bracketed by standard measurements. Switching between samples and standards can be very rapid if long washout protocols are not required, and mass spectrometric runs of a few minutes have been used to maximize the precision of, *e.g.*, Mg isotopic measurements by MC-ICP-MS [Galy *et al.*, 2001]. Longer data acquisition periods are more applicable for heavier elements, for which the drift in mass bias is less severe [Rehkämper *et al.*, 2004].

III.4.3 – Mass scale shift

Mass scale shift occurs in both quadrupole-based and sector field ICP-MS instruments. For quadrupole filters, the constancy of the RF and DC fields is the limiting factor [Begley and Sharp, 1997] but is improved by the introduction of solid state RF generators. In sector field equipment, mass scale shift occurs as a consequence of, *e.g.*, temperature fluctuations [Vanhaecke *et al.*, 2006].

III.4.4 – Background and contamination

Here, 'background' is defined as that part of the ion current measured at a certain mass-to-charge ratio, corresponding to the isotope under investigation, not originating from this

element. 'Contamination' is defined as that part of the ion current measured at a certain mass-to-charge ratio that does not originate from the same element, but for which the origin either lies within the instrument or the chemical procedure used. Distinction between background and contamination can be done by studying the mass spectral region of interest and measuring and comparing isotope ratios to the expected ones, as calculated from the IUPAC tables [De Laeter *et al.*, 2003].

Background can be either continuous over the mass spectral region, due to, *e.g.*, photons from the ICP arriving at the electron multiplier, or discontinuous, due to the presence of spectrally interfering species. The origin of spectrally interfering species can be either instrumental, *e.g.*, due to the formation of ArO^+ and Ar_2^+ ions or impurities present in the plasma gas (*e.g.*, Kr, Xe), or external, originating from concomitants in the sample, *e.g.*, $ArNa^+$ on $^{63}Cu^+$ [Vanhaecke *et al.*, 2006].

Contamination can also be instrumental or external. Instrumental contamination comprises, *e.g.*, memory effects occurring in the nebulizer tubing, nebulizer, spray chamber, and/or interface and can be caused by, *e.g.*, the volatility of the compound (*e.g.*, B, Os, Hg) and specific chemical features (*e.g.*, Pt in solution is easily reduced in Teflon tubings and refractory elements tend to deposit on the interface). External contamination can occur in any of the sample preparation steps, *e.g.*, sample pretreatment, sample digestion and separation procedures. For this reason, the preparation of a procedural blank is extremely important.

In order to correct for instrumental background and instrumental contamination, a representative blank needs to be measured, and the blank signal obtained has to be subtracted from the corresponding signal for all subsequent samples. Obviously, the magnitude of the correction should be limited. For a discontinuous background originating from the sample, the same approach can be followed when it is possible to prepare a matrix-matched blank. Also mathematical corrections can be used to correct the ion current observed for isotope ^{j}M (*e.g.*, ^{204}Pb interfered by ^{204}Hg) by measuring the ion current for another isotope (*e.g.*, ^{202}Hg) of the interfering element and calculating its effect at the mass-to-charge ratio of interest assuming natural isotopic composition for the interfering element. The same approach holds for corrections involving polyatomic species (*e.g.*, the abundance of $ArNa^+$ reflects that of Ar itself). Procedural contamination is best corrected for by measuring the isotope intensities (or concentration of M) in a number of independent blank samples.

III.4.5 – Detector dead time

III.4.5.1 – Definition

When using an electron multiplier in the pulse counting mode (chapter II, § II.7.1), pulse pile-up leads to biased isotope ratio results, at least for isotope ratios different from unity. This is commonly attributed to the detector dead time, which is the time required for the detection and the electronic handling of an ion pulse. If another ion strikes the detector surface within the time required for handling the first ion pulse, the second ion will not be detected and hence, the observed count rate will be lower than the actual count rate. Typically, the detector dead times reported for ICP-MS instrumentation range from 15 to 100 ns [Vanhaecke *et al.*, 2006]. If the detector dead time can be determined accurately, these signal losses can be appropriately corrected for by using the following equation:

$$N = \frac{N_0}{1 - N_0 \tau} \qquad \text{(equation III.14)}$$

with N the actual count rate, N_0 the observed count rate and τ the detector dead time.

The higher the count rate, the larger the bias that is observed. As isotope ratio measurements are often carried out at quite high count rates to improve the isotope ratio precision (counting statistics, equation III.6 and equation III.7), an accurate determination of the detector dead time is of great importance for reliable isotope ratio results. In addition, the detector dead time should be determined at regular time intervals since it has been observed to be influenced by the age of the detector [Seah, 1995] and previous exposure. As opposed to an electron multiplier, a Faraday cup does not suffer from dead-time effects (chapter II, § II.7.2 and § II.7.4).

III.4.5.2 – Experimental determination of the detector dead time

Several methods for determining the dead time of an electron multiplier are described in literature [Nelms *et al.*, 2001]. A first method used in this work was described by Russ [Russ, 1989]. For standard solutions of different concentration levels, a given isotope ratio differing from unity is determined with the dead time set at 0 ns. For each concentration level, the normalized isotope ratio, which is the measured isotope ratio corrected for the detector dead time divided by the true value, is plotted against the detector dead time used for correction. This results in a curve for each concentration level. The higher the

concentration, the more important the dead time effect will be, and the larger the slope of the resulting curve. The actual dead time corresponds to the intersection point of the curves, where the isotope ratio is independent of the concentration. Moreover, the ordinate of the intersection point provides an estimation of the mass discrimination. The experimental data obtained for the determination of the dead time of the PerkinElmer SCIEX Elan DRC*plus* equipped with a secondary electron multiplier with discrete dynodes using the $^{207}Pb/^{208}Pb$ ratio are displayed in figure III.1.

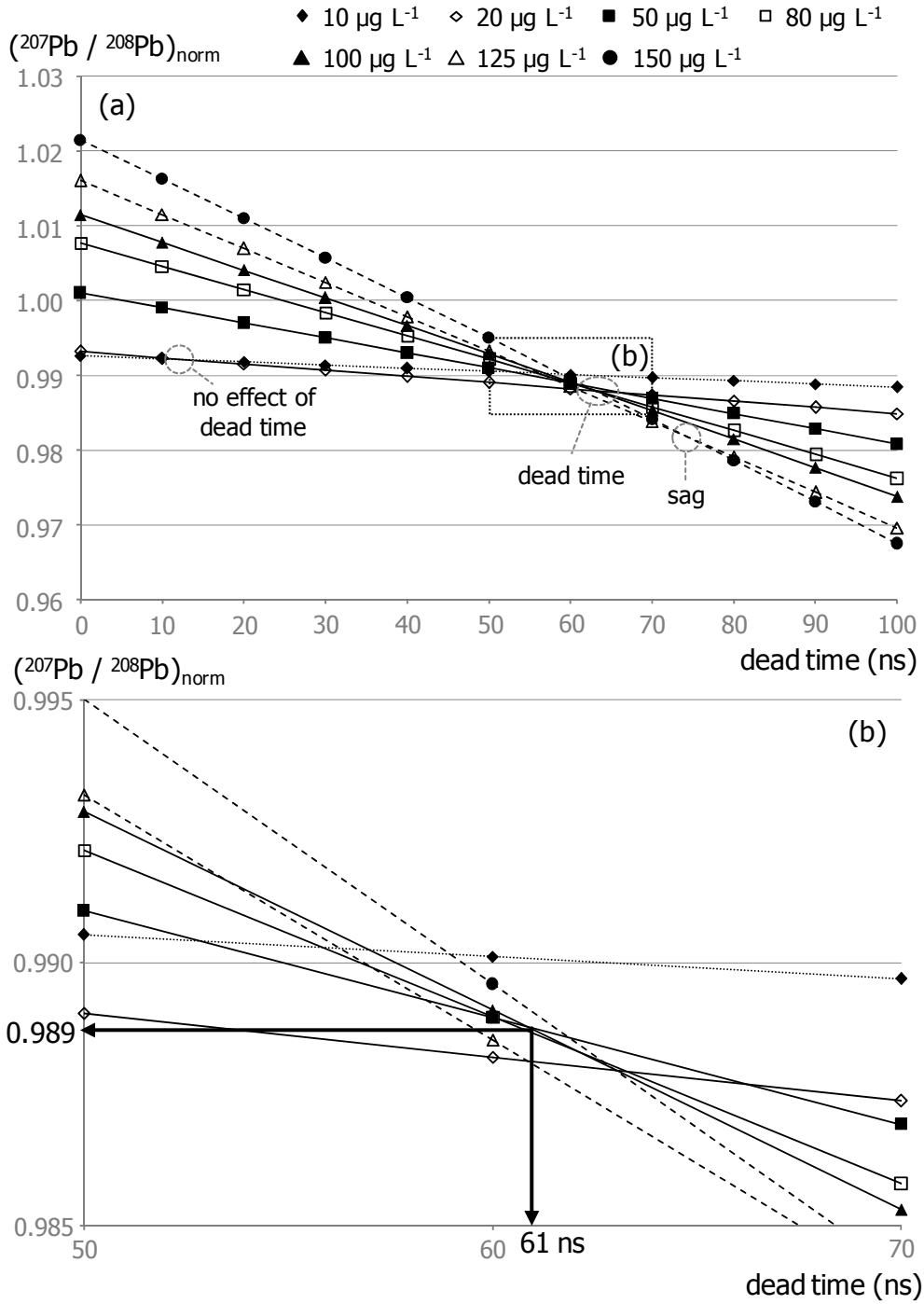

Figure III.1 – Dead time determination via the method of Russ –
(a) normalized $^{207}Pb/^{208}Pb$ ratio versus dead time for different Pb concentrations;
(b) zoom around the actual dead time area

As can be seen from figure III.1.a, the different curves corresponding to the various Pb concentrations do not intersect in exactly the same point, so that a definitive dead time cannot be visually determined. An average dead time can be determined from the dead times corresponding to each intersection point, and the standard deviation of this set of values can be used to estimate the uncertainty. In figure III.1, the curves corresponding to the lowest Pb concentrations (10 and 20 µg L^{-1}) intersect at a very low dead time (~ 12 ns), what can be explained by the fact that the signal intensity is not high enough for a considerable dead-time effect to take place. The curves corresponding to the highest Pb concentrations (125 and 150 µg L^{-1}) intersect at a considerably higher dead time than the average intersection point. This phenomenon is called 'sag' [Vanhaecke *et al.*, 1998]. In an electron multiplier operated in pulse-counting mode, the amplitude of a pulse has to be above a certain discriminator level in order to be considered as a signal instead of noise. It has been reported that, above a critical level, the gain of an electron multiplier decreases with the number of incident particles per time unit [Kurz, 1979]. As a result, at increasingly higher count rates, an increasing fraction of the output pulses shows an amplitude below the discriminator level and hence, these pulses are not detected [Dietz, 1965; Russ and Bazan, 1987], explaining the occurrence of sag. Measurement data that are influenced by sag should not be taken into account for the determination of the dead time. The detector dead time for Pb was calculated as the average of the intersection points of the curves corresponding to Pb concentrations of 50, 80 and 100 µg L^{-1} and was established to be 61 ± 2 ns. Following an analogous approach, a dead time of 48 ± 3 ns was found for Sr on the basis of the $^{86}Sr/^{88}Sr$ ratio.

At the actual dead time (61 ns for Pb), an estimation of the mass discrimination can be made, since at this point, the measured isotope ratio is corrected for the detector dead time. In the case of figure III.1.b, the mass discrimination amounts to 1.1 % per mass unit, since the normalized $^{207}Pb/^{208}Pb$ ratio equals 0.989 at the intersection point.

An alternative approach, also applied in this work, relies on the same experimental data as in the first method described, but a different way of graphical display [Koirtyohann, 1994; Quétel *et al.*, 2000]. In this case, the measured isotope ratio is plotted versus the Pb concentration for different dead times (figure III.2.a). The optimum dead time is determined by plotting linear regression lines through the data for each dead time and taking the value that yields a line through the data with a slope of zero. When the dead time is set at zero ns, in the case of the $^{207}Pb/^{208}Pb$ ratio where the abundance of ^{208}Pb is nearly twice the abundance of ^{207}Pb, an increasing curve will be obtained with increasing Pb concentrations, because more ^{208}Pb is lost relative to ^{207}Pb, resulting in a higher

$^{207}Pb/^{208}Pb$ ratio. With increasing dead time, the slope of the curve will decrease until, at the optimum dead time, the slope equals zero. In this case, the measured isotope ratio is independent of the Pb concentration. Further increasing the dead time will result in an over-correction (and thus, increase) of the ^{208}Pb intensity relative to the ^{207}Pb intensity, resulting in negative slopes in the $^{207}Pb/^{208}Pb$ ratio versus Pb concentration diagram.

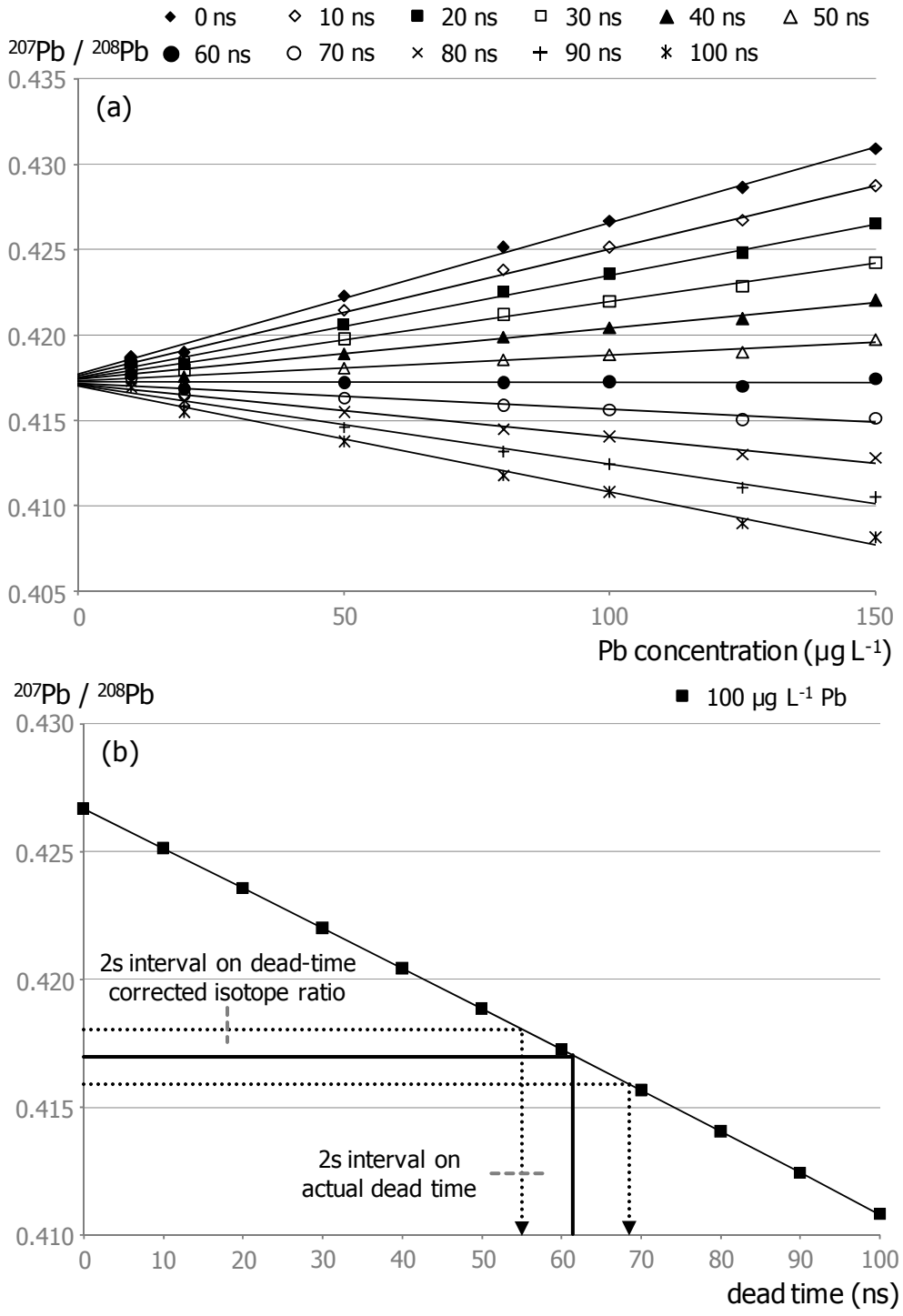

Figure III.2 – Alternative method for dead time determination –
(a) measured $^{207}Pb/^{208}Pb$ ratio versus concentration for different dead time values;
(b) graphical determination of the uncertainty on the actual dead time

It can be seen that around 60 ns, a curve with slope zero is obtained. However, regarding the fact that the optimum dead time is not easily derived on a visual basis, plotting the slope of the regression lines for different dead times versus the assumed dead time yields the actual dead time at the point where the curve intersects the dead-time axis. The equation of the latter curve turned out to be:

$$\text{slope} = 10^{-6}\,(-1.506\,\tau + 89.679),$$

from which the detector dead time τ could be calculated as 60 ns. The uncertainty on the experimentally determined dead time can be derived by first calculating the isotope ratio at the different concentrations with the optimum dead time, their average and the corresponding standard deviation (2s uncertainty interval). The uncertainty on the actual dead time can be graphically evaluated by projecting the uncertainty on the average dead-time corrected isotope ratio onto the dead-time axis, as is shown in figure III.2.b. The detector dead time for the secondary electron multiplier of the Elan DRC*plus* was established to be 60 ± 4 ns for Pb, and 49 ± 5 ns for Sr. The agreement between the dead time obtained via this method, and the method described by Russ, is excellent. The dead time was set at 61 ns for Pb isotope ratio measurents, and at 49 ns for Sr isotope ratio measurements.

The difference in dead time retrieved for Sr (49 ns) and Pb (61 ns) is small compared to the relative mass difference between these elements. Since the dead time was determined only for these two elements, no mass-dependent trend of the detector dead time could be established with certainty in this work for an electron multiplier with discrete dynodes. For a continuous dynode electron multiplier, it was shown that the detector dead time is mass-dependent, yielding dead times of ~ 80 ns for Sr and ~ 110 ns for Pb [Vanhaecke *et al.*, 1998].

The correction methods described above are relatively simple and fast, but do not take into account the occurrence of mass discrimination. A third approach incorporates mass discrimination correction, and is limited to elements that have a pair of isotopes of relative abundance 1:1, with a third isotope of relative abundance between 0.01 and 0.05 [Held and Taylor, 1999; Nelms *et al.*, 2001], ensuring that the target ratio is small enough to be clearly affected by dead time losses, while at the same time this isotope is sufficiently abundant to prevent blank subtraction or interference correction inducing a bias in the dead time calculations. These requirements are met in the Pb certified reference material NIST SRM 982 Equal Atom Lead (^{204}Pb: 1.0912 %; ^{206}Pb: 40.0890 %, ^{207}Pb: 18.7244 %; ^{208}Pb: 40.0954 %). When measuring this reference material, the ratios ^{204}Pb/^{206}Pb and

$^{204}Pb/^{208}Pb$ are influenced by both mass discrimination and dead time, while the $^{206}Pb/^{208}Pb$ ratio is quasi only influenced by mass discrimination. After mass discrimination correction via internal normalization for the standards with different concentrations, the ratio of the certified $^{204}Pb/^{206}Pb$ or $^{204}Pb/^{208}Pb$ isotope ratio and the mass discrimination corrected $^{204}Pb/^{206}Pb$ or $^{204}Pb/^{208}Pb$ ratio is plotted versus the observed count rate of the major isotope of the isotope pair under study. Such a plot results in a line of negative slope from which the optimum dead time can be determined from the relationship:

$$\tau = \frac{\text{slope}}{R - 1} \qquad \text{(equation III.15)}$$

with R the certified isotope ratio.

Recalculating the normalized isotope ratios using the optimum dead time and plotting the new ratios in the same way should result in a horizontal curve. The uncertainty on the slope of the regression line determines the uncertainty on the experimental dead time [Nelms *et al.*, 2001].

A fourth approach consists of plotting analog data versus the corresponding pulse count data across a range of increasing signal intensities [Nelms *et al.*, 2001]. This can be easily done on a quadrupole-based instrument by aspirating a single standard, varying the lens voltage over a preset range, measuring the intensities both in pulse counting and analog mode, and recalculating them for different dead times. For every dead time value, the analog signal is plotted versus the pulse counting signal, and a correlation coefficient is calculated. The optimum dead time is considered to be the average of those for which the correlation coefficient remains constant up to the sixth decimal place. The standard deviation of this range of dead times is an indication for the uncertainty on the determined dead time.

CHAPTER IV

Target elements and sample types investigated in this work

This chapter provides a general background on the target elements and on the sample types studied in this work. The methods developed in this work aim at the Sr or Pb isotopic analysis of archaeological artefacts, such as bone and dental tissues, soils, ceramics and metallic objects. The target elements in this work, Sr and Pb, both display variations in their isotopic composition due to the decay of radioactive parent elements: Sr evolves from Rb while Pb evolves from U and Th. In this chapter, the Rb-Sr and U-Th-Pb isotope systems are discussed and the use of Sr and Pb for archaeological studies is highlighted. Then, general characteristics and properties of the different sample types studied in this work, are given.

IV.1 – Rubidium/strontium isotope system

IV.1.1 – Occurrence and properties of Rb and Sr

Rubidium is an alkali metal, belonging to group IA of the periodic table. Its ionic radius (1.48 Å) is sufficiently similar to that of potassium (1.33 Å) to allow rubidium to substitute potassium in all K-bearing minerals. As a consequence, Rb is a dispersed element that occurs in easily detectable amounts in common K-bearing minerals such as micas (muscovite, biotite, phlogopite and lepidolite), K-feldspar (orthoclase and microcline), certain clay minerals, and in evaporate minerals such as sylvite and carnallite. Rubidium does not form any minerals of its own [Faure, 1986-a].

Rubidium has two naturally occurring isotopes: ^{85}Rb and ^{87}Rb. Information on the isotopes of rubidium is summarized in table IV.1.a. The ^{87}Rb isotope is radioactive and decays to stable ^{87}Sr by emission of a negative beta particle (electron) as follows:

$$^{87}_{37}\mathrm{Rb} \rightarrow {}^{87}_{38}\mathrm{Sr} + \beta^- + \bar{\nu} + \mathrm{Q}$$

with β^- a beta particle (electron), $\bar{\nu}$ an antineutrino and Q the decay energy of 0.275 MeV/atom.

Strontium is a member of the alkaline earths that constitute group IIA of the periodic table. Its ionic radius (1.13 Å) is slightly larger than that of Ca (0.99 Å), which it can replace in many minerals. As a consequence, also strontium is a dispersed element and occurs in Ca-bearing minerals such as plagioclase, apatite, and calcium carbonate, especially aragonite. The ability of strontium to replace calcium is somewhat restricted by the fact that strontium ions (Sr^{2+}) favor eight-fold coordinated sites, whereas calcium ions (Ca^{2+}) can be accommodated in both six- and eight-fold coordinated sites because of their

smaller size. Moreover, Sr^{2+} ions can be captured in place of K^+ ions by K-feldspar, but the replacement of K^+ by Sr^{2+} must be accompanied by the replacement of Si^{4+} by Al^{3+} to preserve electrical neutrality. Strontium is the major cation in strontianite ($SrCO_3$) and celestite ($SrSO_4$), both of which occur in hydrothermal deposits and in carbonate rocks [Faure, 1986-a].

Strontium has four naturally occurring isotopes: ^{84}Sr, ^{86}Sr, ^{87}Sr and ^{88}Sr, all of which are stable (table IV.1.b). The isotopic abundances of strontium isotopes are variable because of the formation of radiogenic ^{87}Sr by the decay of naturally occurring ^{87}Rb. For this reason, the isotopic composition of strontium in a rock or mineral that contains rubidium depends on its age and its Rb/Sr ratio.

Table IV.1 – Naturally occurring isotopes of (a) rubidium and (b) strontium. Uncertainties on the last digits indicated in parentheses. All data from [De Laeter *et al.*, 2003].

	naturally occurring isotopes	absolute atomic mass (u)	abundance (%)	half-life $t_{1/2}$ (years)	daughter(s)
(a) Rb	^{85}Rb	84.911792(3)	72.17(2)	(stable)	-
	^{87}Rb	86.909186(3)	27.83(2)	4.88(5) 10^{10}	^{87}Sr
(b) Sr	^{84}Sr	83.913426(4)	0.55 – 0.58	(stable)	-
	^{86}Sr	85.909265(3)	9.75 – 9.99	(stable)	-
	^{87}Sr	86.908882(3)	6.94 – 7.14	(stable)	-
	^{88}Sr	87.905617(3)	82.29 – 82.75	(stable)	-

The rubidium concentrations of common igneous and sedimentary rocks are correlated with that of potassium, and range from less than 1 µg g^{-1} (ultramafic rocks and carbonates) to more than 170 µg g^{-1} in low-calcium granitic rocks. The concentrations of strontium are correlated with that of calcium and range from a few µg g^{-1} (ultramafic rocks) to about 465 µg g^{-1} in basaltic rocks and reach up to 2 000 µg g^{-1} or more in carbonate rocks. Evidently, most common rocks contain appreciable concentrations of rubidium and strontium of the order of tens to several hundreds of µg g^{-1}. The Rb/Sr ratios of common igneous rocks vary in a wide range from 0.06 (basaltic rocks) to 1.7 or more in highly differentiated granitic rocks having low calcium concentrations [Faure, 1986-a]. The numerical values given above can vary considerably and are, at best, an average.

The exact Sr isotopic composition of a rock will depend on the original Rb/Sr ratio of the rock at crystallization, its age and hence, how much ^{87}Sr has been formed, as well as any subsequent mixing, fluid-mineral interaction or metamorphic activity that has occurred.

Consequently, older Rb-bearing rocks will tend to contain more radiogenic ^{87}Sr than younger rocks, whereas if no Rb was incorporated into the rock at formation, it will retain its original, unradiogenic Sr isotope ratio. The estimated $^{87}Sr/^{86}Sr$ ratio for 'primordial' Sr is 0.699 and, as ^{87}Sr has been continually produced since the Earth was formed, that of the present-day mantle is 0.704 ± 0.002. The Sr isotope ratio in whole rocks can vary from ~ 0.703 for young basaltic rocks to > 0.750 for K-rich (and hence Rb-rich) granites formed from older, crustal rocks [Graustein, 1989; Bentley, 2006].

Strontium is released from rocks primarily through chemical weathering. Any subsequent alteration of the Sr isotope ratio (isotopic fractionation; chapter III, § III.2) that occurs during this and ensuing low-temperature geolocial or biological processes is negligible [Capo *et al.*, 1998; Blum *et al.*, 2000]. Consequently, the isotope abundances that characterize a particular rock move unaltered from the source rock into soils, groundwater, plants and animals. However, this does not imply that the Sr isotope ratio measured in, *e.g.*, tooth enamel or river water, is exactly the same as that of the underlying whole rock. Two factors may complicate the process. Firstly, the isotopic composition of Sr released from a heterogeneous, polymineralic rock may not match that of the whole rock. Some components may weather more readily than other, resulting in Sr isotope ratios that are characteristic for, rather than an exact reflection of, the parent rock. Furthermore, since Rb-bearing (felsic) minerals are generally more resistant to weathering than the Sr-bearing (mafic) minerals, the $^{87}Sr/^{86}Sr$ isotope ratio of released Sr tends to be less radiogenic (lower) than that of the whole rock and thus, over time, the remaining rock becomes increasingly more enriched in radiogenic ^{87}Sr [Faure, 1986-a]. The second process that may alter a given $^{87}Sr/^{86}Sr$ isotope ratio is mixing of two or more sources. Strontium released from rocks into soil and water may be modified by non-local Sr derived from other rock types, transported and deposited by wind-blown dust, river water and precipitation, which has, on its turn, seawater as a source [Capo *et al.*, 1998; Blum *et al.*, 2000].

IV.1.2 – Rb-Sr dating

The Rb-Sr decay system has been widely used in geochronology and remains one of the most useful geochemical tracers, as $^{87}Sr/^{86}Sr$ is a function of the relative abundances of rubidium and strontium, and the age of the rocks. Specifically, the $^{87}Sr/^{86}Sr$ ratio in a rock mineral depends on: (i) the $^{87}Sr/^{86}Sr$ ratio at the time the rock crystallized, (ii) the $^{87}Rb/^{86}Sr$ ratio, which is directly proportional to the Rb/Sr ratio, and (iii) the time elapsed since formation [Bentley, 2006].

The growth of radiogenic ^{87}Sr in a Rb-rich mineral is a phenomenon of radioactivity, and thus, the total number of ^{87}Sr atoms in a mineral of age t given by:

$$^{87}\mathrm{Sr} = {}^{87}\mathrm{Sr_i} + {}^{87}\mathrm{Rb}\left(e^{\lambda t} - 1\right) \qquad \text{(equation IV.1)}$$

with $^{87}\mathrm{Sr}$ the total number of atoms of this isotope in a unit weight of the mineral at the present time, $^{87}\mathrm{Sr_i}$ the number of atoms of this isotope that was incorporated into the same unit weight of this mineral at the time of its formation, $^{87}\mathrm{Rb}$ the number of atoms of this isotope in a unit weight of the mineral at the present time, λ the decay constant (given by $\ln(2)/t_{1/2}$) and t the time elapsed in years since the time of formation of the mineral.

Each term of equation IV.1 can be divided by the number of ^{86}Sr atoms, which is constant because this isotope is stable and is not produced by the decay of a naturally occurring isotope of another element, resulting in:

$$\frac{^{87}\mathrm{Sr}}{^{86}\mathrm{Sr}} = \left(\frac{^{87}\mathrm{Sr}}{^{86}\mathrm{Sr}}\right)_i + \frac{^{87}\mathrm{Rb}}{^{86}\mathrm{Sr}}\left(e^{\lambda t} - 1\right) \qquad \text{(equation IV.2)}$$

The term $e^{\lambda t}$ can be expanded as a power (Taylor) series:

$$e^{\lambda t} = 1 + \lambda t + \frac{(\lambda t)^2}{2!} + \frac{(\lambda t)^3}{3!} + \cdots \qquad \text{(equation IV.3)}$$

Since the decay constant λ of ^{87}Rb is very small (table IV.1.a), the terms of higher order than 1 are negligible, and therefore the following approximation can be made:

$$\left(e^{\lambda t} - 1\right) \approx \lambda t, \qquad \text{(equation IV.4)}$$

so that equation IV.2 can be rewritten as:

$$\frac{^{87}\mathrm{Sr}}{^{86}\mathrm{Sr}} \approx \left(\frac{^{87}\mathrm{Sr}}{^{86}\mathrm{Sr}}\right)_i + \frac{^{87}\mathrm{Rb}}{^{86}\mathrm{Sr}}\lambda t \qquad \text{(equation IV.5)}$$

This equation has the form of a straight line in a $^{87}Sr/^{86}Sr$ versus t diagram, with a slope given by the product of the $^{87}Rb/^{86}Sr$ ratio and the decay constant of rubidium, and an intercept that equals the initial $^{87}Sr/^{86}Sr$ ratio. Equation IV.5 is the basis for age determinations via the Rb-Sr method, and is only valid for age determinations where the number of ^{87}Sr and ^{87}Rb atoms in the mineral have changed as a result of radioactive decay only. In other words, the mineral must have always behaved as a closed system with respect to rubidium and strontium [Faure, 1986-a].

The Rb-Sr decay system produces an array of values for the different minerals in a rock. Given measurements of $^{87}Sr/^{86}Sr$ and $^{87}Rb/^{86}Sr$ in a sample, two unknowns remain in equation IV.5: the age t and the initial $^{87}Sr/^{86}Sr$ ratio. Neither can be calculated from a

single sample. However, if $^{87}Sr/^{86}Sr$ and $^{87}Rb/^{86}Sr$ can be measured on a second mineral for which t and the initial $^{87}Sr/^{86}Sr$ are the same, two equations result with two unknowns, and the difference between equation IV.5 for each mineral yields:

$$\Delta\frac{^{87}Sr}{^{86}Sr} = \Delta\frac{^{87}Rb}{^{86}Sr}\,\lambda t \qquad \text{(equation IV.6)}$$

This relationship shows that a line results if the $^{87}Sr/^{86}Sr$ is plotted against the product of λ and the $^{87}Rb/^{86}Sr$ ratio. Such a line is known as an isochron (figure IV.1), with the age t as slope and the initial $^{87}Sr/^{86}Sr$ ratio as intercept. The older the system is, the steeper will be the isochron because the differences in $^{87}Sr/^{86}Sr$ are built up over time by differences in $^{87}Rb/^{86}Sr$. The slope of the isochron depends only on t, which can be solved for as:

$$t = \frac{1}{\lambda}\left(\frac{\Delta\frac{^{87}Sr}{^{86}Sr}}{\Delta\frac{^{87}Rb}{^{86}Sr}}\right) \qquad \text{(equation IV.7)}$$

If two minerals with a different Rb/Sr ratio formed within a rock at the same time with the same initial $^{87}Sr/^{86}Sr$ ratio, then the mineral with the higher Rb/Sr ratio will have a higher $^{87}Sr/^{86}Sr$ ratio. In other words, a single rock which partitioned into different minerals when it crystallized, yields a linear array of $^{87}Sr/^{86}Sr$ ratios, as described by its isochron.

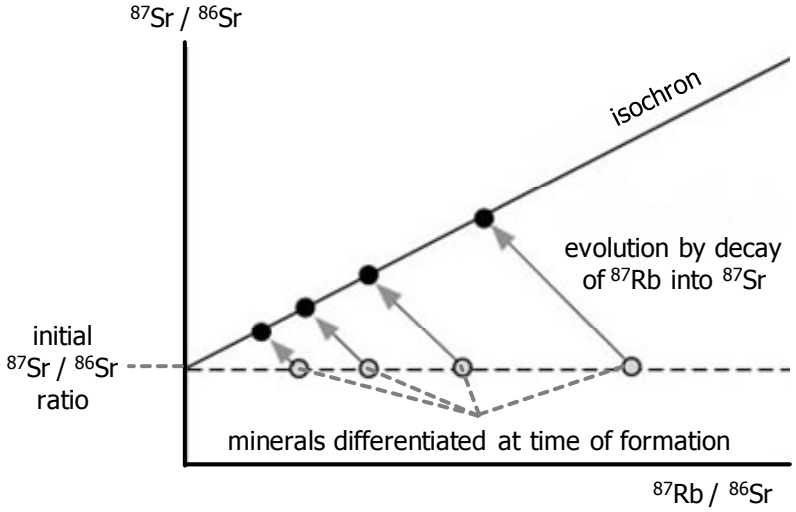

Figure IV.1 – Rb-Sr isochron

IV.2 – Uranium/thorium/lead isotope system

IV.2.1 – Occurrence and properties of U and Th

Uranium and thorium are members of the actinide series in the periodic table. Both elements occur in nature in the tetravalent oxidation state and their ions have similar radii

(U^{4+}: 1.05 Å, Th^{4+}: 1.10 Å). Consequently, the two elements can substitute each other, explaining their geochemical coherence. However, under oxidizing conditions, U forms the uranyl ion (UO_2^{2+}), and this ion forms compounds that are soluble in water. Therefore, U is a mobile element under oxidizing conditions and is separated from Th which exists only in the tetravalent state and whose compounds are generally insoluble in water [Faure, 1986-b].

The concentrations of U and Th in the common rock-forming silicate minerals are uniformly low, in the order of a few μg g^{-1}. Instead, these two elements occur primarily in certain accessory minerals in which they are either major constituents or replace other elements, *e.g.*, uraninite, thorianite, zircon, apatite and sphene [Faure, 1986-b].

Uranium has three naturally occurring isotopes: ^{234}U, ^{235}U and ^{238}U (table IV.2.b). Thorium exists primarily as one radioactive isotope, ^{232}Th (table IV.2.a). In addition, five radioactive isotopes of Th occur in nature as short-lived intermediate daughters of ^{232}Th, ^{235}U and ^{238}U.

Table IV.2 – Naturally occurring isotopes of (a) thorium, (b) uranium and (c) lead. Uncertainties on the last digits indicated in parentheses. All data from [De Laeter *et al.*, 2003].

	naturally occurring isotopes	absolute atomic mass (u)	abundance (%)	half-life $t_{1/2}$ (years)	daughter(s)
(a) Th	^{232}Th	232.038050(2)	100	1.40(1) 10^{10}	^{228}Th, ^{228}Ac, ^{228}Ra, ^{224}Ra, ^{220}Rn, ^{216}Po, ^{212}Po, ^{212}Bi, ^{212}Pb, **^{208}Pb**, ^{208}Tl
(b) U	^{234}U	234.040945(2)	(50 – 59) 10^{-4}	2.454(6) 10^5	equilibrium with ^{238}U
	^{235}U	235.043922(2)	0.7198 – 0.7207	7.037(11) 10^8	^{231}Pa, ^{231}Th, ^{227}Th, ^{227}Ac, ^{223}Ra, ^{223}Fr, ^{219}Rn, ^{219}At, ^{215}At, ^{215}Po, ^{211}Po, ^{215}Bi, ^{211}Bi, ^{211}Pb, **^{207}Pb**, ^{207}Tl
	^{238}U	238.050784(2)	99.274 – 99.275	4.468(5) 10^9	^{234}U, ^{234}Pa, ^{234}Th, ^{230}Th, ^{226}Ra, ^{222}Rn, ^{218}Rn, ^{218}At, ^{218}Po, ^{214}Po, ^{210}Po, ^{214}Bi, ^{210}Bi, ^{214}Pb, ^{210}Pb, **^{206}Pb**, ^{210}Tl, ^{206}Tl, ^{206}Hg
(c) Pb	^{204}Pb	203.973028(3)	1.04 – 1.65	(stable)	-
	^{206}Pb	205.974449(3)	20.84 – 27.48	(stable)	-
	^{207}Pb	206.975880(3)	17.62 – 23.65	(stable)	-
	^{208}Pb	207.976636(3)	51.28 – 56.21	(stable)	-

The decay of ^{238}U gives rise to the uranium series in which several intermediate daughters, *e.g.*, ^{234}U, undergo branched decay by emission of either an alpha (helium atom) or beta (electron) particle. The chain therefore splits into separate branches, but the stable end product of all possible decay paths is ^{206}Pb. The decay of ^{238}U to stable ^{206}Pb can be summarized as:

$$^{238}_{92}\mathrm{U} \rightarrow {}^{206}_{82}\mathrm{Pb} + 8\,{}^{4}_{2}\mathrm{He} + 6\,\beta^{-} + \mathrm{Q}$$

with Q = 47.4 MeV/atom.

The decay of ^{235}U gives rise to the actinium series, a series that also shows several decay paths but always ends with stable ^{207}Pb:

$$^{235}_{82}\mathrm{U} \rightarrow {}^{207}_{82}\mathrm{Pb} + 7\,{}^{4}_{2}\mathrm{He} + 4\,\beta^{-} + \mathrm{Q}$$

with Q = 45.2 MeV/atom

The decay of ^{232}Th leads to the formation of stable ^{208}Pb:

$$^{232}_{90}\mathrm{Th} \rightarrow {}^{208}_{82}\mathrm{Pb} + 6\,{}^{4}_{2}\mathrm{He} + 4\,\beta^{-} + \mathrm{Q}$$

with Q = 39.8 MeV/atom

Despite the fact that in the decay series of ^{232}Th, ^{235}U and ^{238}U together, a total of 43 isotopes of 12 elements are formed as intermediate daughters, none of these is a member of more than one series. In other words, each decay chain always leads to the formation of a specific isotope: ^{232}Th produces ^{208}Pb, ^{235}U produces ^{207}Pb and ^{238}U produces ^{206}Pb [Faure, 1986-b].

The half-lives of ^{232}Th, ^{235}U and ^{238}U are all very much longer than those of their respective daughters. In this case of so-called 'secular equilibrium', the production rate of the stable daughter at the end of a particular decay chain is equal to the rate of decay of its parent at the head of the chain. As a consequence, the decay of Th and U can be considered as if it occurred directly to the respective isotopes of Pb [Faure, 1986-b].

IV.2.2 – U-Th-Pb dating

Ordinary lead has four naturally occurring isotopes: ^{204}Pb, ^{206}Pb, ^{207}Pb and ^{208}Pb (table VI.2.c). Only ^{204}Pb is not radiogenic, and is treated as a stable reference isotope. The isotopic composition of Pb in minerals containing U and Th can be expressed in equations of the form of equation IV.2 as follows:

$$\frac{^{206}Pb}{^{204}Pb} = \left(\frac{^{206}Pb}{^{204}Pb}\right)_i + \frac{^{238}U}{^{204}Pb}\left(e^{\lambda_1 t} - 1\right) \quad \text{(equation IV.8)}$$

$$\frac{^{207}Pb}{^{204}Pb} = \left(\frac{^{207}Pb}{^{204}Pb}\right)_i + \frac{^{235}U}{^{204}Pb}\left(e^{\lambda_2 t} - 1\right) \quad \text{(equation IV.9)}$$

$$\frac{^{208}Pb}{^{204}Pb} = \left(\frac{^{208}Pb}{^{204}Pb}\right)_i + \frac{^{232}Th}{^{204}Pb}\left(e^{\lambda_3 t} - 1\right) \quad \text{(equation IV.10)}$$

Solving the three equations results in three independent dates based on the three decay series. In the case where the three decay series yield the same date, this date represents the age of the mineral, provided that the following requirements are met: (i) the mineral remained closed to U, Th, Pb and all the intermediate daughters throughout its history, (ii) correct values are used for the initial Pb isotope ratios, (iii) the decay constants of ^{232}Th, ^{235}U and ^{238}U are known accurately and (iv) the isotopic composition of U has not been modified by isotopic fractionation or by the occurrence of a natural chain reaction based on fission of ^{235}U [Faure, 1986-b]. However, as with Sr, the Pb isotope ratios of a given rock or ore deposit may not be simply a function of age and the concentrations of Pb, U and Th incorporated at formation. Rocks that do meet this so-called 'single stage' model or formation and have remained closed to subsequent mixing are known as 'ordinary' or 'conformable' lead, and their isotopes lie on a growth curve. Anomalous Pb, which does not lie on the growth curve and may even plot in the future, does so because it has been mixed with radiogenic U and Th-rich crustal lead at some time in its formation history, and hence, is not compatible with the assumption of a closed system [Faure, 1986-c]. In order to make the evolution of common lead compatible with U and Th mixing, a two-stage model [Stacey and Kramers, 1975] or even a multi-stage model can be addressed. A detailed discussion of these models and additional information on U-Th-Pb dating is described in detail in dedicated sources, *e.g.*, [Faure, 1986-c].

IV.2.3 – Occurrence and properties of lead

Lead is widely distributed throughout the Earth and occurs not only as the radiogenic daughters ^{206}Pb, ^{207}Pb and ^{208}Pb of U and Th, but exists also as a non radiogenic ^{204}Pb isotope (table IV.2.c). Lead is found in many types of rocks, both as a major constituent and as a trace element, not only in association with U and Th-bearing minerals but also by forming its own minerals, principally galena (PbS), from which U and Th are excluded. Pb^{2+} is known to replace K^+ in K-feldspar but, unlike Sr, there is no striking geological correlation with Ca-bearing minerals [Elias *et al.*, 1982]. Lead accumulates with the transition

metals zinc, cadmium and trace amounts of silver in ore deposits. The lead isotopic composition can vary considerably from the common-lead found in low U/Pb and Th/Pb minerals such as galena (PbS), sulfides of other base metals, K-feldspar and the relatively uncommon secondary Pb minerals such as cerusite ($PbCO_3$) and anglesite ($PbSO_4$), to the highly radiogenic Pb in ancient accessory minerals such as zircon and apatite or rocks like U and Th-bearing granites [Faure, 1986-c; Erel *et al.*, 1994]. As a consequence, the lead isotopic composition in different kinds of rocks contains a record of the chemical environments in which the Pb resided (*e.g.*, mantle, crustal rocks, Pb ores). Each of these environments has different U/Pb and Th/Pb ratios that affect the isotopic evolution of Pb. The isotopic composition of Pb may be modified both by decay of Th and U and by mixing with Pb having a different isotopic composition.

Lead isotopic fractionation in low-temperature biogeochemical processes has not been proven, so that the Pb isotope ratios that characterize a particular rock, ore or locality are transferred unaltered to soil and groundwaters by natural weathering processes. Isotope variations, which can originate from small spatial differences within one ore field or preferential weathering of heterogeneous rock phases are mixed within the soil and groundwater to create a homogeneous reservoir representative of the underlying local geology [Erel *et al.*, 1994].

IV.3 – Sr and Pb isotopes in archaeological studies

The isotope systems Sr and Pb have been used individually in both archaeological and modern source-tracing studies. Strontium isotope ratios are employed frequently in investigation of archaeological bone, often combined with isotope ratio data for light isotopes (*e.g.*, C, O), and in provenance determination of, *e.g.*, marble and glass [Freestone *et al.*, 2003; Brilli *et al.*, 2005; Degryse *et al.*, 2006]. Also lead is useful in provenance determination studies of archaeological artefacts, *e.g.*, ceramics and metallic objects.

Published studies that utilize archaeological skeletal remains tend to fall into two categories: (i) those that harness Sr or Pb isotope analysis to answer a specific archaeological question, such as diagenesis or migration, as is also the case in this work, and (ii) those that utilize archaeological remains as a resource to illustrate an analytical technique or provide time-depth to an environmental or geochemical investigation. Both approaches have drawbacks. In conducting such studies, one has to be cautious to (i) not over- or misinterpret data due to their complex nature or limitations and (ii) carefully consider the nature and limitations of the archaeological resource being utilized.

IV.3.1 – Sr isotope studies

The $^{87}Sr/^{86}Sr$ isotope ratio reflects the average of all strontium that has been contributed to the sample. In the case of a skeleton of archaeological interest, each Sr atom has its own history and may, *e.g.*, have been transferred from a partial melt of magma into a rock mineral, a stream, a soil, a plant leaf, a herbivore's diet and finally in the meal of a (pre-)historic person. Within that individual's skeletal tissue, it joins other strontium atoms that have journeyed a different route. After centuries or millennia underground, the strontium is finally released from the skeletal mineral in the modern laboratory and analyzed by mass spectrometry.

The application of Sr isotope ratios in archaeology is based on the finding that migrant individuals who moved between geologic regions can be identified by comparing the $^{87}Sr/^{86}Sr$ ratio in the tooth enamel, composed between four and twelve years of age, and in the tooth dentine and the bones, which remodel throughout life and are therefore representative of adulthood [Bentley, 2006]. In theory, if the teeth and bones of a skeleton have different signatures, the person spent his/her life in a different geochemical environment than during his/her youth [Ericson, 1985; Sealy *et al.*, 1991]. In cases involving modern skeletons, or archaeological skeletons that have been extraordinarily well preserved, bone and tooth $^{87}Sr/^{86}Sr$ ratios can be successfully compared and used to establish migration behavior, as was shown for, *e.g.*, modern elephants in Amboseli National Park, Kenya [Koch *et al.*, 1995] and the Alpine iceman Ötzi [Hoogewerff *et al.*, 2001; Müller *et al.*, 2003]. A better temporal resolution can even be obtained via measurements of bone, which undergoes continual replacement of its inorganic phase, so that different individual bones contain information on the age of a migrant person when he/she moved [Price *et al.*, 2002]. Dense cortical bone remodels over a period of decades, while trabecular bone remodels with turnover times as short as a few years.

If assuming that a migrant individual moves only once from one place to another, it is possible to quantitatively model how the $^{87}Sr/^{86}Sr$ ratios in the bone and dental tissues approach the local ratio at different rates [Beard and Johnson, 2000]. How close the bone value is to the local signature depends on both the turnover rate of the bone and the time that the migrant individual resided at the specific location [Schweissing and Grupe, 2003]. Several studies have been carried out using Sr isotope ratios to investigate modern animal mobility and migration away from the place of origin through natural Sr uptake [Koch *et al.*, 1995; Chamberlain *et al.*, 1997; Hobson, 1999]. Strontium isotope ratio analysis has also been extensively applied on hominid and animal fossils to identify both migration and different

feeding strategies [Koch *et al.*, 1992; Sillen *et al.*, 1995; Sillen *et al.*, 1998; Hoogewerff *et al.*, 2001; Müller *et al.*, 2003].

Unfortunately, a major issue is the reliability of the measured $^{87}Sr/^{86}Sr$ ratio at present, since archaeological bone is often contaminated during burial. The groundwater strontium, namely, penetrates the bone after burial and can overwhelm, or even replace, the *in vivo* strontium in its mineral portion [Price *et al.*, 1992; Hedges, 2002; Nielsen-Marsh and Hedges, 2000-a]. It has been argued that diagenetic strontium can often be removed from skeletal samples by proper sample cleaning with weak acid, *e.g.*, 5 % acetic acid [Price *et al.*, 1992; Sillen and Sealy, 1995; Nielsen-Marsh and Hedges, 2000-b]. This leaching process will dissolve away the diagenetic strontium present in carbonate and in pore spaces, while retaining the original dietary strontium that is more strongly bound in the Ca sites of the bone hydroxyapatite. This technique has proved valuable in some cases [Price *et al.*, 1994; Ezzo *et al.*, 1997], but when diagenesis has taken more insidious forms than just filling pore spaces, the weak acid treatment cannot isolate the biogenic Sr, which may even have been completely replaced during burial [Budd *et al.*, 2000]. Like bone, tooth dentine is also highly susceptible to contamination, because it contains pores as large as 1 µm, much larger than its phosphate crystals, which are smaller than 0.1 µm [Kohn *et al.*, 1999]. For a sample of prehistoric and medieval human teeth from the UK, Budd *et al.* found that 15 to 100 % of the Sr in dentine was diagenetic, accumulated from the burial environment [Budd *et al.*, 2000]. Unlike bone and dentine, the story is different for tooth enamel. Because tooth enamel is denser, harder and more inert than bone or dentine, it is more resistant to post-burial isotopic contamination than bone or dentine [Kohn *et al.*, 1999; Budd *et al.*, 2000], the main reason being that the phosphate crystals in enamel are relatively large (> 1 µm), and the structure is compact, with little pore spaces [Kohn *et al.*, 1999]. Repeated studies have proven that fossil tooth enamel contains much less diagenetic Sr than bone or dentine [Kohn *et al.*, 1999; Chiaradia *et al.*, 2003; Lee-Thorp and Sponheimer, 2003; Trickett *et al.*, 2003]. For the reason that archaeological bone and dentine are often too contaminated to be of much use for Sr isotopic studies, several current studies focus exclusively on tooth enamel, which forms during childhood and undergoes relatively little change after it is mineralized [Knudson *et al.*, 2004; Knudson *et al.*, 2005; Price and Gestsdottir, 2006; Price *et al.*, 2006].

IV.3.2 – Pb isotope studies

Source-tracing applications of archaeological material can use and interpret Pb isotope data in a way analogous to those of Sr. However, Pb exposure is less dependent on

geological origin and natural baseline levels, but serves more as an indicator of status, or what access to Pb and its products was available within a society, geographical location or just to a specific individual. A complication to archaeological studies occurs when the accumulating anthropogenic pollution becomes so prominent that it is blurring the link between the locality and the bio-available Pb isotope signature. Although also the Roman Era can be clearly identified from the Pb accumulation profile in ice cores and peat bogs [Shotyk *et al.*, 1998], modern large-scale atmospheric pollution only becomes a major complicating factor during the Industrial Revolution and prior to this, trade of Pb products was the dominant mechanism for Pb movement [Hong *et al.*, 1994; Brännvall *et al.*, 1999].

Lead isotopes have been primarily used to track changes in pollution and exposure through space and time as opposed to the movement of people into different exposure zones. Accordingly, there are many published studies that characterize and then identify the contemporary sources of Pb in cases of Pb poisoning, particularly in children [Yaffe *et al.*, 1983; Rabinowitz, 1987], or assess the relative contributions that different sources, such as paint or petrol, have made to human Pb burdens [Keinonen, 1992; Delves and Campbell, 1993; Farmer *et al.*, 1994]. A large body of work has been published on source tracing contemporary Pb exposure by Gulson and coworkers [Gulson and Wilson, 1994; Gulson *et al.*, 1995; Gulson, 1996; Gulson and Gillings, 1997]. These workers also exploited the principle of different Pb sources having characteristic signatures to identify migrants in a forensic context [Gulson *et al.*, 1997]. Whereas archaeological applications are based on the consumption of locally-derived diets, the latter study utilized the different industrial Pb sources that exist in different countries and which residents are thus exposed to throughout their lives. The principle of different Pb sources was successfully applied in numerous other studies [Reinhard and Ghazi, 1992; Ghazi, 1994; Ghazi *et al.*, 1994; Carlson, 1996; Yoshinaga *et al.*, 1998; Bower *et al.*, 2005; Bower *et al.*, 2007]. The extent to which diagenesis blurred the Pb ratios was evaluated to be minimal. In other studies however, Pb concentrations higher than biogenic ranges were attributed to diagenesis [Millard, 2006; Zapata *et al.*, 2006].

Besides lead present in (archaeological) skeletal tissues, also lead present as a trace or major element in archaeological artefacts, such as ceramics and ancient metals or metallic objects, comprises valuable information. In this case, lead isotope ratios can provide insight into the provenance of the raw materials used for the manufacturing of the ceramics [Habicht-Mauche *et al.*, 2002; Tunstall and Amarasiriwardena, 2002; Resano *et al.*, 2008] or metallic artefacts [Young *et al.*, 1997; Ponting and Segal, 1998; Klein *et al.*, 2004-a; Baker *et al.*, 2006] under study.

IV.4 – Sample types investigated in this work

In what follows, a section is given on the general characteristics and the typical matrix composition of the various sample types investigated in this work. The various matrices comprise soils, bone and dental tissues, ceramics and metallic artefacts with lead, copper and silver as the major elements.

IV.4.1 – Soils

The composition of soils is extremely diverse and governed by many different factors. However, climatic conditions and parent material predominate most commonly [Kabata-Pendias and Pendias, 1984-a]. Two stages are involved in the formation of soil from parent material: (i) physical and chemical weathering, and (ii) pedogenesis. Weathering can be chemically described as the processes of dissolution, hydration, hydrolysis, oxidation, reduction and carbonation. All of these processes are based on rules of enthalpy and entropy, and they lead to the formation of mineral and chemical components that are relatively stable and equilibrated in the particular soil environments. Chemical weathering leads to the destruction of parent minerals and to the passing of the elements from the minerals into solutions and suspensions [Kabata-Pendias and Pendias, 1984-a].

Pedogenesis involves specific reactions, in addition to those involved in weathering, and results in the formation of a soil profile from the weathered rock material, leading to the development of a mature zonal soil. Although there is a great diversity in pedogenic processes, they all include similar stages: (i) addition of organic and mineral materials to the soil, (ii) losses of these materials from the soil, (iii) translocation of these materials within the soil, both vertically and horizontally, and (iv) transformation of the organic and mineral matter in the soil. These processes can be either constructive or destructive in soil formation [Kabata-Pendias and Pendias, 1984-a].

Soil is composed of three phases – solid (mineral and organic), liquid and gaseous – and exhibits properties resulting from the physical and chemical equilibriums of these phases. Moreover, not only the chemical composition of the solid components of soil, but also its mineral structure and the state of dispersion are important factors influencing soil properties [Kabata-Pendias and Pendias, 1984-a].

Quartz (SiO_2) is the most common macroscopically distinguishable mineral in surface soils, constituting 50 to more than 90 % of the solid soil phase. Even in geochemical conditions favorable for the leaching of silicates, quartz remains as a basic soil mineral. Feldspars are

of low relative resistance to weathering in soil environments and their alteration usually provides materials for clay mineral formation. These clay minerals are a host to many trace elements (*e.g.*, Sr and Pb) and are more important than quartz in this respect, the latter being poor in trace element content. Carbonates (calcite, dolomite) and metal oxides are usually accessory minerals in soils of humid climatic soils, while in soils of arid climatic zones, they may be significant soil constituents. Quantitatively, trace elements are negligible constituents of the solid soil phase, but they play an important role in soil fertility [Kabata-Pendias and Pendias, 1984-b].

The primary form of Pb in soil is galena (PbS). Lead occurs mainly as Pb^{2+}, although the occurrence of Pb^{4+} is also known, and it forms several other minerals which are quite unsoluble in natural waters. During weathering, Pb sulfides slowly oxidize and have the ability to form carbonates and also to be incorporated in clay minerals, in iron- and manganese oxides, and in organic matter. The geochemical characteristics of Pb^{2+} somewhat resemble the divalent alkaline-earth group of metals, thus Pb has the ability to replace K, Ba, Sr and even Ca both in minerals and in sorption sites. The natural Pb content of soil is inherited from parent rocks. However, due to the widespread Pb pollution, most soils are likely to be enriched in this metal, especially in the top horizon. The natural Pb occurrence in top horizons of different soils from various countries ranges from 3 to 189 μg g^{-1}, while mean values for different soil types range from 10 to 67 μg g^{-1} with an average of 32 μg g^{-1}. An upper limit for the Pb content of a normal soil can be established at 70 μg g^{-1}, while lead levels above 100 μg g^{-1} most probably reflect the impact of pollution [Kabata-Pendias and Pendias, 1984-c]. The Pb concentration in the upper continental crust equals 20 μg g^{-1} [Taylor and McLennan, 1995].

In the terrestrial environment, strontium is very often associated with Ca, and to a lesser extent with Mg, because the geo- and biochemical characteristics of Sr are similar to those of Ca. Strontium is easily mobilized during weathering, especially in oxidizing acid environments, and then it is incorporated into clay minerals and strongly fixed by organic matter, but most Sr is precipitated as biogenic carbonates, largely in the form of invertebrate shell material. This element is known to occur mainly as Sr^{2+} ions; however its chelated forms play an important role in Sr cycling which is closely associated with Ca cycling. The strontium content of soils is highly controlled by parent rocks and climate, and is therefore highly variable. Strontium concentrations range from 18 to 3 500 μg g^{-1} in top horizons [Kabata-Pendias and Pendias, 1984-d], from 10 to 1 000 μg g^{-1} in soil minerals [Elias *et al.*, 1982; Bashkin, 2002; Bentley, 2006] and the average Sr content of the upper continental crust is around 370 μg g^{-1} [Capo *et al.*, 1998].

IV.4.2 – Bone and dental tissues

Enamel, dentine and bone are composite tissues of inorganic, organic and water fractions in varying amounts. The inorganic phase is the crystalline calcium phosphate mineral dahllite or carbonate hydroxyapatite, with the repeating unit cell formula $[(Ca,X)_{10}(P,C)_6(O,OH)_{26}]$, where X is considered to represent a variety of possible substitutions for Ca, such as Na, Mg, Sr, Ba and Pb [McConnell, 1973]. It is, although inaccurate, frequently referred to as 'hydroxyapatite' with the unit cell $[Ca_{10}(PO_4)_6(OH)_2]$ [Bigi *et al.*, 1997; Wopenka and Pasteris, 2005]. As dahllite or carbonate hydroxyapatite is almost exclusively found in vertebrate tissues, it is also often called 'biological apatite' or 'biogenic apatite', of which the unit formula has been described as $\sim [Ca_9(PO_4)_{4.5}(CO_3)_{1.5}(OH)]$ [Driessens and Verbeeck, 1990]. The crystals are hexagonal prisms, formed from the repeating unit cell, and are renowned for their non-stoichiometry, because the crystal lattice accommodates a wide variety of distortions, substitutions and vacancies, and hence rarely conform to any simple formula [Wopenka and Pasteris, 2005].

Tooth enamel contains ~ 96 % calcium phosphate, ~ 3 % water and ~ 1 % organic matter. Tooth dentine is 70-75 % calcium phosphate, 5-10 % water and ~ 20 % organic matter [Hillson, 1986; Driessens and Verbeeck, 1990; Kohn *et al.*, 1999]. Structurally, enamel is extremely compact, with little pore space, large phosphate crystals (> 1 µm long), and a decussate texture. In contrast, dentine is porous with tubules of ~ 1 µm in diameter and smaller crystals (< 0.1 µm in length) [Hillson, 1986; Kohn *et al.*, 1999].

Enamel phosphate has a composition of $\sim [Ca_{4.5}[(PO_4)_{2.7}(HPO_4)_{0.2}(CO_3)_{0.3}](OH)_{0.5}]$ [Driessens and Verbeeck, 1990], where CO_3^{2-} and HPO_4^{2-} substitution for PO_4^{3-} is charge balanced by vacancies in the Ca^{2+} and OH^- sites. Other important substitutions include additional Cl^- and CO_3^{2-} in the OH^- sites, and Na^+ and Mg^{2+} in the Ca^{2+} sites. Dentine phosphate has, in comparison with enamel, a lower Ca^{2+} and PO_4^{3-} content, and a higher Mg^{2+} and CO_3^{2-} content [Driessens and Verbeeck, 1990]. Although enamel and dentine contain approximately the same mineral phase, there are major differences between their organic fraction. Enamel is the most highly mineralized of all mammalian skeletal tissues and is almost entirely composed of inorganic mineral. Its organic phase contains no collagen but consists of what appears to be remnants of redundant protein that were incompletely removed during development [Robinson *et al.*, 1995]. The much smaller dentine phosphate crystals are found within and around collagen fibrils, and also many non-collagenous proteins are present [Butler *et al.*, 1997]. The larger organic content and the smaller crystal size of dentine make this tissue more susceptible to alteration than enamel [Kohn *et al.*,

1999]. Dentine is, in contrast to enamel, a living, cellular tissue that can respond to blood-borne substances. The composition of primary dentine is, like that of enamel, largely determined at the time of formation. Nevertheless, the cells of dentine, the odontoblasts, remain active so that the formation of new, secondary dentine continues throughout life [Veis, 1989].

The structure and elemental composition of bone is more easily compared to that of dentine than to that of enamel. The mineral content of mature bone amounts from 55 to 75 % [Barone, 1982]. Dentine, however, contains at least three proteins that are not found in bone [Butler *et al.*, 1997]. Bone, unlike dentine, contains blood vessels and is subject to the continual remodeling behavior of the bone cells, the osteoclasts and the osteoblasts.

Strontium is incorporated as Sr^{2+} in the carbonate hydroxyapatite lattice as a substituent for Ca^{2+} [Rokita *et al.*, 1993; Vukovic *et al.*, 1998], and is distributed relatively homogeneously in the skeleton. Concentrations of strontium in the skeletal and dental tissues from a single individual are very similar, with bone and dentine containing slightly more than enamel [Underwood, 1977-a; Aufderheide, 1989], probably resulting from the smaller carbonate hydroxyapatite crystals of bone and dentine, providing larger surface areas available for cation adsorption. The difference may also originate from post-formation increases due to bone remodeling or secondary dentine formation, given the fact that bone Sr concentrations are believed to increase with age [Underwood, 1977-a]. As is the case for Sr isotope ratios, also *in vivo* strontium concentrations in bone and teeth appear to vary geographically [Underwood, 1977-a]. This could be due to regional variations in bedrock geology, water and food or types of diet. Although specific values are highly variable, a rough indication of strontium concentrations in mammal bone and dental tissues is the range of 50 to 1 000 µg g^{-1} [Elias *et al.*, 1982; Burton *et al.*, 1999; Kohn *et al.*, 1999].

The vast majority of Pb in the body is located in the hard tissues of the skeleton where it is believed to occupy Ca^{2+} sites within the carbonate hydroxyapatite lattice as Pb^{2+} [Wallach and Chausmer, 1990]. The incorporation of Pb^{2+} in place of Ca^{2+} is thermodynamically more favorable [Patterson *et al.*, 1991]. Lead is not distributed homogeneously throughout the skeleton and Pb concentrations can vary considerably between different bones [Aufderheide, 1989, Erkkilä *et al.*, 1992] but typical modern adult Pb concentrations are usually at least an order of magnitude lower than Sr concentrations, ranging from 3 to 60 µg g^{-1} [Arnay-De-La-Rosa *et al.*, 1998; Yoshinaga *et al.*, 1998]. The skeletal lead concentration appears to accumulate, most notably in cortical bone, until ~ 50-60 years of age and also increases with increasing exposure [Underwood, 1977-b; Erkkila *et al.*, 1992].

IV.4.3 – Ceramics

The raw materials used for the manufacturing of ceramics, or more specifically in this work, pottery and amphorae, are derived from mainly the clay minerals of soils. The strontium and lead content of ceramics was, as expected, shown to be in the same concentration range as for soils. The (trace-)elemental composition of ceramics is highly versatile, and hence allows provenance studies of ceramics based on their trace elemental composition [Mallory-Greenough *et al.*, 1998; Barone *et al.*, 2004; Kennett *et al.*, 2004; Klein *et al.*, 2004-b; Little *et al.*, 2004; Barone *et al.*, 2005; Marengo *et al.*, 2005; Resano *et al.*, 2005], as well as their Pb isotope ratios [Tunstall and Amarasiriwardena, 2002; Habicht-Mauche *et al.*, 2002; Marzo *et al.*, 2007].

IV.4.4 – Metallic artefacts

The metallic artefacts investigated in this work can be divided in groups according to the major metal in the alloy: copper (unalloyed copper, brass and bronze), lead (lead and litharge fragments) and silver. Copper, lead and silver are extracted from the parent ores, and in the case that no lead is intentionally added to the alloy, the Pb isotopic composition of the object reflects that of the parent ore since Pb does not undergo isotopic fractionation in its route from ore to object. Hence, the Pb isotopic composition was shown as a valuable tool for fingerprinting ancient metallic artefacts, such as objects and coins [Young *et al.*, 1997; Ponting and Segal, 1998; Klein *et al.*, 2004-a; Baker *et al.*, 2006]. Below, a word follows on the extraction and treatment of copper, silver and lead from their respective ores in antiquity, regarding its relevance for this work (chapter VIII). It is, however, not the intention to give a detailed or a complete overview of the existing production techniques in antiquity or at present. The interested reader is referred to dedicated sources for a more detailed overview [Tylecote, 1962; Tylecote, 1976; Craddock, 1995].

Copper occurs in nature in ore deposits. The existence of native copper in copper ore deposits is well known, and was most probably the source for the very first copper objects. Further, copper is present in a number of minerals, such as cuprite (Cu_2O), malachite ($CuCO_3.Cu(OH)_2$), chalcocite (Cu_2S) and chalcopyrite ($CuFeS_2$). Refining copper from oxide- and carbonate-based ores can be accomplished by heating and reduction with charcoal or wood, combined with a blast of air and a suited furnace [Moorey, 1994], while sulfide ores are more difficult to reduce due to the presence of many impurities (*e.g.*, S, As, Sb). Removal of these impurities prior to refining was performed by roasting, which is prolonged heating to convert the copper sulphides into their oxide form [Tylecote, 1976].

After refining, unalloyed copper is obtained, which contains < 2 % tin and zinc, and < 4 % lead. However, copper is often alloyed in the presence of heat. An alloy is the result of the combination of two or more chemical elements, of which at least one is a metal. In antiquity, copper was often alloyed with tin and/or zinc. Alloying copper with tin results in bronze (> 5 % Sn), alloying with zinc results in brass (> 10 % Zn and < 5 % Sn), and alloying with both tin and zinc results in gunmetal (> 5 % Zn and Sn) [Ponting, 2002]. Alloys containing more than 4 % lead are considered as 'leaded' in this work. The addition of lead to an alloy improves its characteristics with respect to further handling, *e.g.*, it increases the fluidity of the alloy. This is beneficial if the alloy is to be used for casting complex objects such as statuettes [Rosenfeld *et al.*, 1997; Weeks, 2004]. A disadvantage however is that lead does not 'dissolve' into copper, but forms globules throughout the metal [Thornton and Ehlers, 2003], thus forming a rather heterogeneous mixture on the microscopic level and rendering the resulting alloy difficult or even impossible to be mechanically handled, either cold or hot.

Silver is widely dispersed in minerals in low levels (< 0.5 %) and is almost invariably found in sulfides, with argentite (Ag_2S) being the main silver mineral. However, the principle silver sources in antiquity were silver-containing lead ores, such as galena (PbS) that generally contains small amounts of silver (argentiferous galena) [Habashi, 1994], cerussite ($PbCO_3$) and anglesite ($PbSO_4$). Lead ores are widely dispersed and relatively easy to refine to the pure metal [Tylecote, 1962]. Herefore, it seems likely that lead may have been among the first metals to be smelted [Craddock, 1995]. Smelting galena under a moderately oxidizing atmosphere triggers the conversion of PbS to PbO and $PbSO_4$, followed by the formation of metallic lead. Cerussite was heated with charcoal and also resulted in metallic lead. The metal obtained via this relatively simple smelting process can contain substantial amounts of silver and other impurities (*e.g.*, Cu, As, Sb) but was probably never refined, except from the extraction of the silver. Lead absorbs silver, but the two metals do not mix. The absorbed silver can be separated from the lead by the process of cupellation, which is the removal of lead by selective oxidation to litharge (lead oxide, PbO). Silver remains unaffected by this process [Tylecote, 1962]. The cupellation process that is most efficient in separating impurities from silver could be repeated several times in order to further purify the silver obtained [Tylecote, 1962].

CHAPTER V

Sample pretreatment and digestion procedures

In this work, several archaeological artefacts with a different matrix composition (soil, bone and dental tissues, ceramics and metallic objects) were the subject of investigation. The first – and probably most important – step in the analysis is to sample the object under investigation in such a way that the outcome of the analysis is representative for the whole sample. Regarding the small amount of sample often retrieved at the archaeological site and, to some extent, the historical value of some archaeological artefacts, the sample amounts available were in most cases limited to less than 1 g, and in many cases even less than 0.5 g. The next step is the sample pretreatment, where the samples under investigation are prepared for digestion. This step consists of (i) cleaning of the sample to remove contamination and/or an altered chemical composition on the sample's surface due to burial and (ii) obtaining a homogeneous fraction of the solid sample, preferably as a fine powder in order to facilitate the subsequent digestion, representative for the total sample available. In this chapter, such sample pretreatment procedures are described for the various types of samples, along with the digestion procedures that were developed and validated to result in a complete dissolution of the respective sample types.

V.1 – Sample pretreatment procedures

V.1.1 – Sample cleaning and cutting

All the samples investigated in this work are of archaeological origin. Small amounts of soil samples, bone tissues, amphora and pottery samples were delivered. Tooth tissues were delivered as whole teeth, and metallic objects, including lead objects, were provided as fragments or whole objects.

Bone samples, taken from the femora from deceased and stillborn infants (chapter IX), were delivered as small pieces, typically 0.1-0.5 g in weight. The bone pieces were mechanically cleaned, rinsed in ethanol and dried in a drying stove at 105 °C. Also a sample of fish bones was delivered, this was treated in the same way as the human bone samples. The dried pieces were subsequently pulverized using a microdismembrator (§ V.1.2), as were the soil particles.

Whole teeth were mechanically cleaned and subsequently leached in 0.1 M acetic acid in order to remove surface contamination and soil-derived (diagenetic) strontium (chapter IV, § IV.3.1). Considering that the aim of the Servatius – project (chapter X) was to establish whether there is a difference in Sr isotopic composition between the enamel

(crown, white outer tissue) and the dentine (root, inner tissue), these tissues were carefully separated from one another by means of a dental saw (Department of dentistry, Ghent University). After obtaining the separate enamel and dentine fractions, they were rinsed with ethanol to remove contamination originating from the cutting process, and dried in a drying stove at 105 °C.

Powdered amphora samples were delivered (chapter IX). One pottery sample was delivered as a larger shard. A hammer was used to crush the piece into smaller fragments, the fragments were rinsed with ethanol to remove contamination originating from the crushing process, and prior to digestion, the ceramics samples were dried in a drying stove at 105 °C.

Lead fragments (chapter VIII and IX) were partially cut into curls with a razor blade and rinsed with ethanol to remove potential surface contamination present due to the cutting process, and dried in a drying stove at 105 °C. The curls from the outer surface of the fragments was discarded to assure that a subsample free of corrosion products was obtained. The metallic objects that did not mainly consist of lead (chapter VIII) were sampled using a miniature-drill setup developed to this purpose (§ V.1.3).

V.1.2 – Sample homogenization: microdismembrator

In order to convert the archaeological samples that were delivered as larger pieces (*e.g.*, soil, bone tissue) into a homogeneous powder, a microdismembrator (Mikro-Dismembrator II, Braun, Germany) was used. The so-called 'brittle fracture technique' [Iyengar, 1976] is mainly used in studies involving biological materials in order to pulverize frozen tissues [Peters *et al.*, 1986] or plant materials [Verstraete *et al.*, 1998]. To this purpose, an amount of sample is put in a recipient manufactured from polytetrafluoroethylene (PTFE) together with a ball, also made from PTFE. Cooling down this assembly to the temperature of liquid nitrogen (~ –200 °C) and sonicating it for about 1 minute at a high frequency in the microdismembrator unit results in pulverization of the frozen sample by the impact of the ball onto the frozen sample. The homogeneous sample powder obtained in this way was subsequently collected and dried in a drying stove at 105 °C. The PTFE recipients were cleaned by boiling in aqua regia for 6 hours, followed by boiling in milli-Q water for another 6 hours and subsequent drying in a drying stove at 105 °C.

The microdismembrator approach was successfully used in this work for the homogenization of soil samples and bone tissues, but was not capable of pulverizing dental tissues. Hence, the dentine and enamel were dissolved as such.

V.1.3 – Sampling of metallic artefacts: miniature-drill setup

In order to sample metallic artefacts that were not delivered as powders, a miniature drill, manufactured from tungstencarbide (Drill Service, UK) was used, in analogy with an approach followed by Ponting and Segal [Ponting and Segal, 1998]. The experimental setup that was developed, in which both drill and sample can move in all directions relative to each other, is shown in figure V.1. The metallic object (*e.g.*, a coin) is fixed between two Teflon holders and the drill is mounted in horizontal position, perpendicular to the object. By the use of a drill with a narrow diameter (*e.g.*, 0.5 mm), it is possible to sample coins from the side instead of from the coin's face, which is important in order not to cause visible damage to the coin's face. The drilling process results in a finely dispersed powder, that is collected by gravity by means of a funnel inserted into a polyethylene (PE) tube. The powder originating from the surface of the sampled coin or object was discarded, to assure the subsequent sampling of an area free of contamination and corrosion products. Several places from the side of the coin or the object were sampled in this way to obtain a homogeneous subsample that is as representative as possible of the object in its

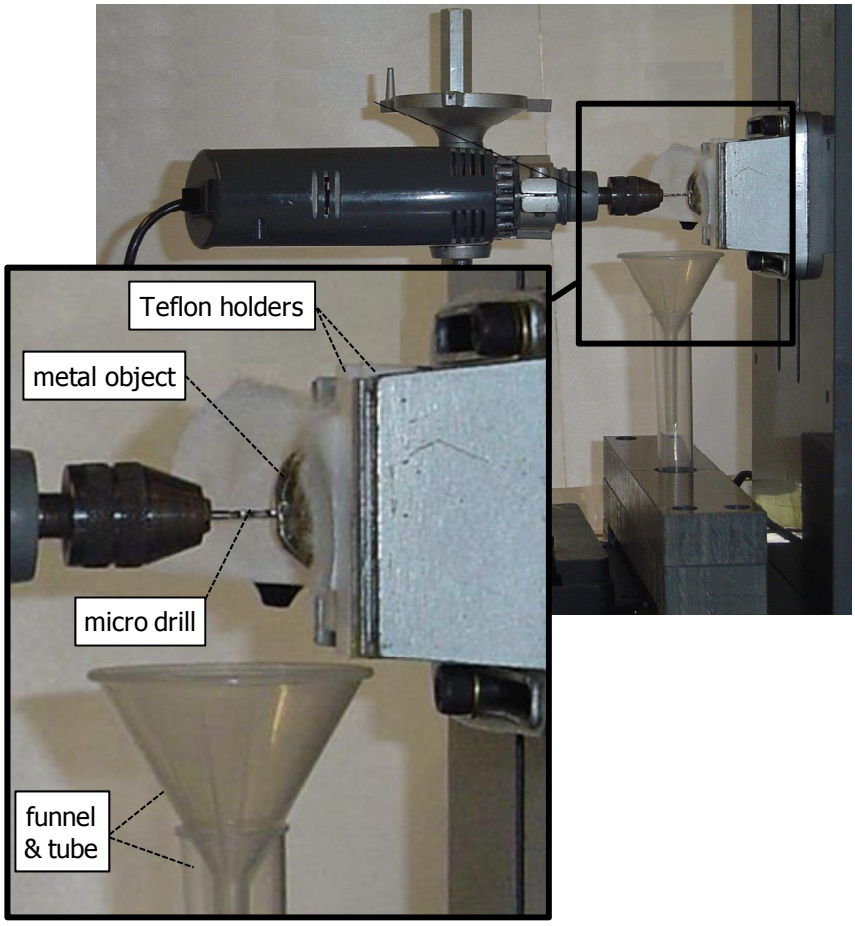

Figure V.1 – Miniature-drill setup for the sampling of metallic artefacts

totality. The powder collected was rinsed with ethanol to remove potential contamination that occurred during the sampling process and was subsequently dried in a drying stove at 105 °C. After the sampling of every coin or object, the drill was rinsed with 0.1 M HCl solution and dried in a drying stove at 105 °C to avoid cross-contamination between subsequent samples.

V.2 – Sample digestion approaches

The standard sample introduction system for an ICP – mass spectrometer is the combination of a pneumatic nebulizer (PN) and a spray chamber (chapter II, § II.2). This implies that the elemental analysis of nearly all matrices, including biological, geological, environmental and metallurgical materials, requires the dissolution of the sample prior to ICP-MS analysis. Dissolution of a heterogeneous sample provides a homogeneous solution. By powdering solid samples prior to analysis (§ V.1), homogeneity is already improved in the solid phase. The most common dissolution technique is the use of an open beaker with acid(s) heated on a hotplate. Another approach is the use of a microwave-assisted acid digestion procedure [Kingston and Walter, 1998].

V.2.1 – Hotplate digestion

In hotplate digestion, an amount of sample is weighed into a beaker, a suited combination of concentrated acids is added and the beaker is placed on a hotplate. Heating of the mixture results in dissolution of the solid sample. Despite their frequent use, hotplate dissolution procedures are limited by several factors: (i) long dissolution times, depending on the sample under investigation, (ii) the potential loss of volatile elements, (iii) contamination of the sample by excessive amounts of reagents and (iv) airborne contaminants [Kingston and Walter, 1998]. Depending on the target element and the matrix and when care is taken during laboratory practice however, a classical hotplate digestion can successfully be applied and give rise to excellent results.

In this work, sample dissolution was often accomplished by means of a final hotplate digestion step. The beakers used were manufactured from PTFE. In order to prevent contamination arising from airborne contaminants during digestion, the beakers were covered with a watch glass, also manufactured from PTFE. After use, the recipients and watch glasses were cleaned by boiling in aqua regia for 6 hours, followed by boiling in milli-Q water for another 6 hours and subsequent drying in a drying stove at 105 °C.

V.2.2 – Microwave-assisted acid digestion

V.2.2.1 – Absorption of microwave energy and heating

In microwave-assisted acid digestion procedures, microwave energy is applied to mineral acids, which are directly heated by coupling of the reagents with the electromagnetic field. Molecules have the ability to convert microwave energy into heat in an amount that is proportional to their dielectric constant ε, a measure for the molecule's ability to be polarized in an electric field. Since the dielectric constant is a function of the microwave frequency, the ability of a solvent to absorb microwave energy is a function of the frequency and the temperature. Solvents such as water, mineral acids and some organic solvents have dipole moments that can interact with an applied electric field. Dielectric polarization depends on the rapid alignment of polar molecules in solution and their relaxation and reorientation in a random pattern. This motion causes friction and converts the electromagnetic microwave energy into heat. The free ions in solutions such as ionized acids are attracted and repulsed by the electromagnetic field, which oscillates and reverses approximately 5 billion times per second [Kingston and Walter, 1998].

V.2.2.2 – Operating principle

In this work, a Milestone microwave labstation MLS-1200 mega, equipped with MDR^{TM} technology (microwave destruction rotor), was used. A schematical representation of the microwave unit is given in figure V.2. The magnetron produces microwaves that are radiated from its antenna into the waveguide. The waveguide is a microwave-reflective metal that directs the waves into the microwave cavity. As the microwaves enter the cavity, they are reflected by the mode stirrer to assist in homogenizing the microwave field inside the cavity. Despite the designs of the mode stirrer, a nonuniform standing pattern is established inside the cavity. To improve the homogeneity of the microwave field, the samples are rotated through the variable field [Kingston and Walter, 1998].

A representation of the vessel containing the sample, incorporated into a sarcophagus as it will be mounted onto the rotor inside the microwave unit, is given in figure V.3. From the onset of the experiment, the microwave energy heats the acid and the vessel in contact with the acid. The acid is below its atmospheric boiling point, its vapor phase is minimal, and no appreciable amount of vapor heats the vessel walls. When the temperature exceeds the atmospheric boiling point of the acid, a large quantity of gas phase acid is produced in the vessel. The gaseous acid cannot efficiently absorb

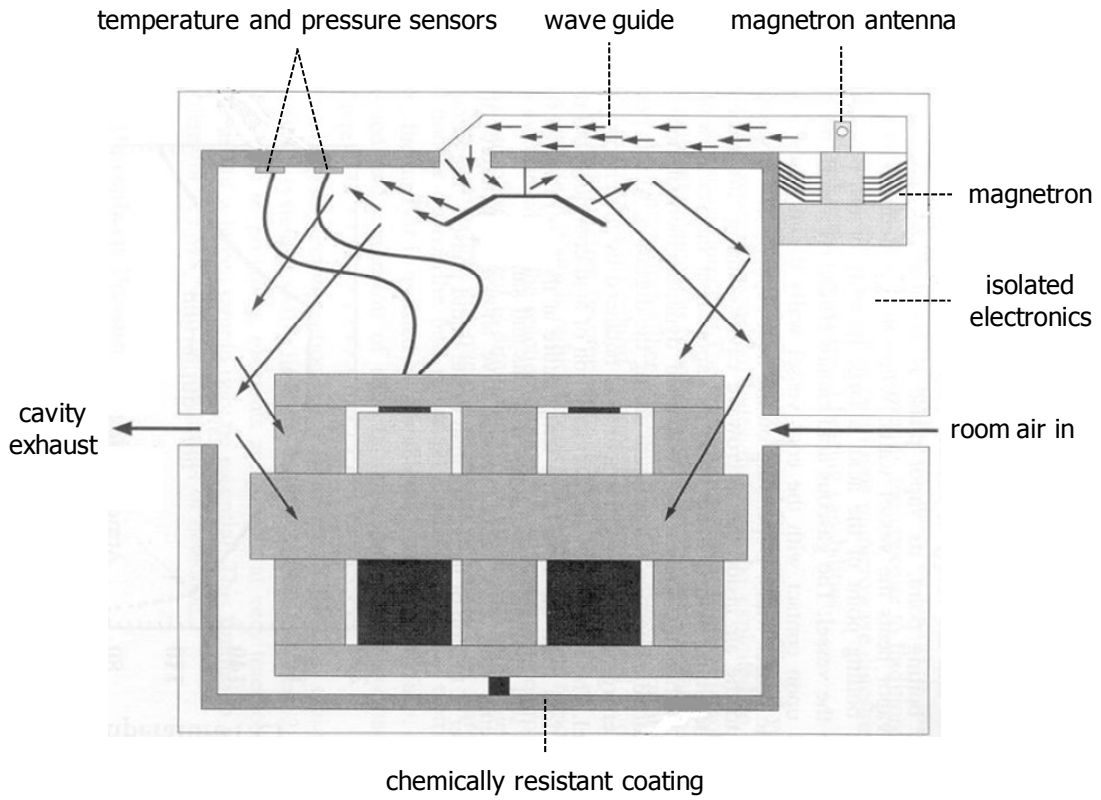

Figure V.2 – Schematical representation of a microwave unit for sample digestion

microwave energy, and upon contact with the cool vessel walls it condenses, releasing energy to the vessel walls. Depending on the heat capacity of the vessel, heat is released to the air inside the microwave cavity. During this stage of the digestion, the liquid acid is heated and its vapors heat the vessel walls. The final stage of heating, so-called 'sustained dynamic thermal non-equilibrium', maintains reaction temperature during the digestion. At this point, the microwave energy absorbed by the acid(s) is balanced by the energy released by the vessel. The evaporation and condensation of acid continues, but because of the heat loss from the vessel, the temperature at the top of the vessel can never reach that attained by the liquid reagents and sample. Experiments with PFA Teflon vessels have shown temperatures that are 100 °C lower at the top of the vessel than in the liquid phase. This tremendous temperature difference prevents the establishment of a normal thermodynamic equilibrium between the gas phase and the liquid. Owing to this heat loss, the microwave-assisted acid digestion system usually achieves a pressure much lower than otherwise attainable while maintaining a relatively high temperature for the acid solution. This behavior results in an efficient acid dissolution reaction. The energy is imported to the vessel through the acid reagents, exactly the opposite to traditional heating by convection or conduction [Kingston and Walter, 1998].

The microwave vessels used are made from tetrafluoromethaxil (TFM), a plastic that is transparent to microwave energy. These vessels incorporate pressure relief devices that vent excess pressure in a controllable manner through a resealable cap (figure V.3.a). When the internal pressure exceeds the applied external force, the resealable cap temporarily opens to expel the excess pressure and then reseals to retain the sample components (figure V.3.b). In this way, vessel over-pressurization is handled safely, and the occurrence of venting can be established by the user after the experiment is finished since the cap is not as tightly sealed as it was before the occurrence of venting.

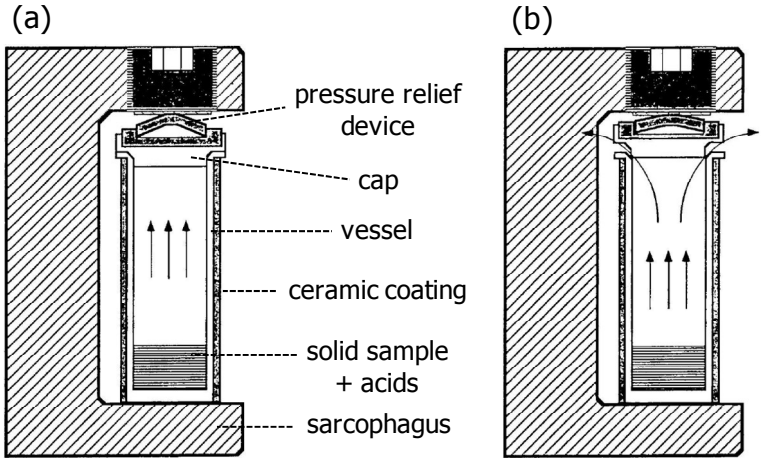

Figure V.3 – (a) sealing of the vessel into a resistant sarcophagus;
(b) pressure relief in the case of overpressure

V.2.2.3 – Performance

Closed vessel acid digestion has several unique attributes that may be exploited to improve the sample preparation process: (i) the higher temperature of the acid solution results in a kinetic advantage that is not duplicated at lower temperatures. Several acids exhibit improved oxidation potentials at elevated temperatures and therefore become more capable reagents. Furthermore, (ii) the risk of sample contamination during the digestion is decreased compared to a digestion on a hotplate since the digestion process takes place in a closed vessel and (iii) analytes that are transformed into volatile compounds during the digestion process are not lost, at least when no vessel over-pressurization has taken place.

V.3 – Acid chemistry

Acids are classified according to their major role in the digestion reaction: oxidizing or non-oxidizing. Examples of non-oxidizing acids are hydrochloric acid (HCl) and

hydrofluoric acid (HF); examples of oxidizing acids are nitric acid (HNO_3), concentrated sulfuric acid (H_2SO_4) and hydrogen peroxide (H_2O_2) [Kingston and Walter, 1998].

V.3.1 – Nitric acid

Nitric acid (HNO_3) is an oxidizing acid that will dissolve most metals to form the soluble metal nitrates. It has poor oxidizing strength at concentrations below 2 M, but is a powerful oxidizing agent in the concentrated form (14 M). Its oxidizing strength can be enhanced by the addition of, *e.g.*, chloride [Sulcek and Povondra, 1989] or by increasing the reaction temperature and pressure. Most metals and alloys are oxidized by nitric acid, but there are two exceptions: (i) gold and platinum are not oxidized, and (ii) some metals (*e.g.*, Al, Cr, Zr, Hf) form insoluble oxides when attacked by concentrated nitric acid [Marr, 1979]. These metals can be dissolved by the use of a combination of acids or by dilute nitric acid. Further, nitric acid is the most common acid for the oxidation of organic matrices. Its oxidation potential is directly proportional to temperature. When used in combination with a complexing acid, nitric acid is more powerful [Kingston and Walter, 1998].
For this work, *pro analysi* concentrated nitric acid (14 M) was purchased from Panreac, Spain and further purified by a subboiling distillation in quartz equipment.

V.3.2 – Hydrochloric acid

Hydrochloric acid (HCl) is a non-oxidizing acid that exhibits weak reducing properties during dissolution [Kingston and Walter, 1998]. Many metal carbonates, peroxides and alkali hydroxides are readily dissolved by hydrochloric acid, but dissolution is accelerated by the addition of another acid.
While hydrochloric acid reacts with most metals, it is frequently combined with a second acid. Aqua regia, a 3:1 mixture of hydrochloric and nitric acid, reacts to form the more reactive components nitrosylchloride and chlorine by the following reaction:

$$3\,\mathrm{HCl} + \mathrm{HNO_3} \rightarrow \mathrm{NOCl} + \mathrm{Cl_2} + 2\,\mathrm{H_2O}$$

The formation of these strong oxidizing agents enables aqua regia to dissolve several additional metals, including the noble metals not dissolved by hydrochloric acid and nitric acid individually.
For this work, *pro analysi* concentrated hydrochloric acid (12 M) was purchased from Panreac, Spain and further purified by a subboiling distillation in quartz equipment.

V.3.3 – Hydrofluoric acid

Hydrofluoric acid (HF) is a non-oxidizing acid, the reactivity of which is based on its strong complexing nature [Kingston and Walter, 1998]. It is most commonly used in inorganic analysis because it is one of the few acids that can dissolve silicates. The following reaction takes place:

$$SiO_2 + 6\,HF \rightarrow H_2SiF_6 + 2\,H_2O$$

Dissolution by hydrofluoric acid produces primarily soluble fluorides, except for the insoluble or sparingly soluble fluorides of the alkaline earths, lanthanides and actinides. To improve dissolution, hydrofluoric acid is routinely combined with another acid, such as nitric acid.

Following dissolution, many analyses require the removal of all hydrofluoric acid, to prevent damage to the equipment or to resolubilize insoluble fluorides. The fluorosilicic acid can be dissociated by heating the solution down to fumes in an open system (beaker on a hotplate) with another acid, *e.g.*, nitric acid:

$$H_2SiF_6 \rightarrow SiF_4 + 2\,HF$$

Another approach for the removal of hydrofluoric acid after digestion is to complex the fluoride anion with boric acid (H_3BO_3) [Sulcek and Povondra, 1989]. The reaction of boric acid with hydrofluoric acid is a two-step process:

$$H_3BO_3 + 3HF \rightleftharpoons HBF_3(OH) + 2H_2O$$

$$HBF_3(OH) + HF \rightleftharpoons HBF_4 + H_2O$$

For this work, the concentrated hydrofluoric acid (22 M, instra-analyzed) used, was purchased from JT Baker Chemicals, The Netherlands.

V.3.4 – Sulfuric acid

Dilute sulfuric acid does not exhibit any oxidizing properties, but the concentrated acid is capable of oxidizing many substances [Marr, 1979]. Concentrated sulfuric acid (H_2SO_4) has a boiling point of 338 °C, which is higher than the working ranges of all the Teflon materials commonly used in the construction of microwave vessels. Therefore, the reaction temperature must be monitored carefully to prevent damage to the microwave vessels.

Sulfuric acid is commonly used with other reagents, such as perchloric acid or hydrogen peroxide. Sulfuric acid will act as a dehydrating agent that will dramatically increase the

oxidizing power of the perchloric acid, but this mixture may react violently with organic matrices in closed vessels or if heated rapidly [Kingston and Walter, 1998].

For this work, *pro analysi* concentrated sulfuric acid (18 M) was purchased from Panreac, Spain and further purified by a subboiling distillation in quartz equipment.

V.3.5 – Hydrogen peroxide

Hydrogen peroxide (H_2O_2) can react explosively with many organics, especially in the more concentrated form. This acid is usually combined with another acid because its oxidizing power increases at higher acidity. Further, hydrogen peroxide is often added to the digestion solution to complete the digestion without the potential safety hazards of reacting a strong oxidizing reagent with an easily oxidizable material [Kingston and Walter, 1998].

For this work, the *pro analysi* concentrated hydrogen peroxide (10 M) used, was purchased from Merck, Germany.

V.3.6 – Perchloric acid

The oxidizing power of perchloric acid ($HClO_4$) is proportional to its concentration and temperature [Kingston and Walter, 1998]. Dilute aqueous perchloric acid is not an oxidizing acid, either cold or warm. Concentrated perchloric acid is not an oxidizing acid when cold, but becomes a powerful oxidizer when it is warm. Warm perchloric acid will readily decompose organic matter, sometimes violently. Because of its rapid, sometimes explosive, reaction with organic matrices, perchloric acid is generally mixed with nitric acid. Perchloric acid decomposes at 245 °C in a closed microwave vessel system, developing dangerous amounts of gaseous by-products and tremendous excess pressure [Kingston and Jassie, 1988]. It is recommended that in the case where perchloric acid is used for digestion, a two-step digestion is followed. In a first step, only acids other than perchloric acid are used in order to digest the sample as completely as possible. When the digestion vessels are cooled down, perchloric acid can be added and the vessels are heated another time. In this way, only the toughest part of the sample to dissolve will remain for the perchloric acid to decompose.

For this work, the concentrated perchloric acid (10 M, instra-analyzed) used, was purchased from JT Baker Chemicals, The Netherlands.

In the following text, the concentration of every acid mentioned is always that as given for the specific acid in the paragraph above, unless stated otherwise.

V.4 – Development and validation of digestion procedures

The general context of this work is isotopic analysis of Sr and Pb in archaeological artefacts. Two projects focus on Pb isotope ratio analysis. The ed-Dur – project (chapter VIII) focuses on metallic artefacts rich in copper, silver and/or lead, while in the Roman-bone – project (chapter IX), bone tissue, soil samples, ceramics and lead objects are the subject of investigation. The Servatius – project (chapter X) aims at comparative Sr isotopic analysis of human dental tissues (enamel and dentine). The procedures developed in this work for the digestion of the various sample types with a different matrix composition (chapter IV, § IV.4) aimed at (i) a total dissolution of the solid sample and (ii) a quantitative target element (Sr and/or Pb) recovery. In this way, isotopic fractionation during the digestion step can be ruled out.

The digestion procedures for the different matrices under investigation were optimized and validated by applying the proposed digestion protocol to a certified or standard reference material (CRM or SRM) with a similar matrix composition. The reference materials used in this work are available from the Community Bureau of Reference (BCR, Brussels, Belgium) and the National Bureau of Standards (NBS) which was renamed as National Institute of Standards and Technology (NIST) in 1988 (Gaithersburg, MD, USA). The following certified reference materials were used:

- NIST SRM 1400 Bone Ash and NIST SRM 1486 Bone Meal for validating digestion procedures for both bone and dental tissues
- BCR CRM 141 Calcareous Loam Soil and BCR CRM 142 Light Sandy Soil for validating digestion procedures for soil samples
- NBS SRM 500 Unalloyed Copper VII, NBS SRM 872 Phosphor Bronze and NBS SRM 875 Cupro-Nickel 10 % 'doped' for validating digestion procedures for metallic objects with various copper-silver-lead contents.

After digesting an amount of the certified reference materials according to the digestion protocol developed, lead elemental assay (chapter II, § II.9) was performed using the PerkinElmer SCIEX Elan 5000 quadrupole-based ICP – mass spectrometer (chapter II, § II.8). By comparing the experimentally obtained values to the corresponding certified values, the average recovery was calculated. Strontium, calcium and phosphorus recoveries for dental tissue digestions were determined by means of the PerkinElmer SCIEX Elan DRC*plus* quadrupole-based ICP – mass spectrometer (chapter II, § II.8 and § II.9) using a reaction gas in the dynamic reaction cell (chapter VII, § VII.2).

V.4.1 – Soil digestion procedure

Several microwave-assisted soil digestion procedures described in literature were tested for their ability to totally dissolve soil samples. A combination of 3 mL HNO_3 + 2 mL HCl in a 23 min microwave program [Prohaska *et al.*, 1999] and a combination of 2 mL HNO_3 + 6 mL HCl in a 14 min microwave program [Bettinelli *et al.*, 2000-a] did not result in a complete dissolution. Because of the high silicate content of soils (chapter IV, § IV.4.1), hydrofluoric acid is required for complete dissolution (§ V.3.3). Hence, in a next attempt, several HF-based procedures were tested. Although it was observed that the addition of HF resulted in dissolution of a larger soil fraction, 3 mL HNO_3 + 2 mL HCl + 1 mL HF in a 36 min microwave program [Prohaska *et al.*, 1999] or a 70 min microwave program [Engström *et al.*, 2004], 2 mL HNO_3 + 6 mL HCl + 2 mL HF in a 25 min microwave program [Bettinelli *et al.*, 2000-a; Bettinelli *et al.*, 2000-b] and 5 mL HNO_3 + 3 mL HF + 1 mL H_2O in a 40 min microwave program [Falciani *et al.*, 2000] resulted in Pb recoveries for BCR CRM 141 Calcareous Loam Soil and BCR CRM 142 Light Sandy Soil between 40 and 85 % only. In order to increase the power of the digestion process, $HClO_4$ was added. Ettler *et al.* used 10 mL HF + 0.5 mL $HClO_4$, followed by 5 mL HF + 0.5 mL $HClO_4$ after evaporation to dryness [Ettler *et al.*, 2004]. However, it was preferred not to add $HClO_4$ in the first step (§ V.3.6), so that an approach analogous to that described by Riondato *et al.* [Riondato *et al.*, 2001] was followed. The digestion procedure is summarized in table V.1.a and consisted of adding a concentrated acid mixture of 5 mL HNO_3 + 2 mL HCl + 2 mL HF to 0.2 g soil and submitting it to a 43 min microwave program. After this first microwave step, the vessels are cooled down, followed by addition of 1 mL $HClO_4$ and again submitted to a 43 min microwave program. Since the dissolution was not complete after the microwave treatment, the digest was transferred to a beaker containing a mixture of 2 mL HNO_3 + 2 mL HF + 2 mL $HClO_4$, followed by further digestion and evaporation to nearly dry on a hotplate. In this step, the remaining HF was removed as well (§ V.3.3). After this second step, complete dissolution of the soil sample was obtained. In the third step, the residue was taken up in concentrated HNO_3 and diluted to 1 M HNO_3 with milli-Q water.

Application of the described digestion procedure to the soil certified reference materials resulted in a Pb recovery of 94.9 ± 5.5 % for BCR CRM 141 Calcareous Loam Soil and 98.9 ± 6.3 % for BCR CRM 142 Light Sandy Soil, demonstrating that the digestion protocol results in a quantitative Pb recovery. A summary of the experimental Pb concentrations retrieved for the soil certified reference materials is given in table IV.1.b.

Table V.1 – Digestion of soil samples – (a) digestion procedure; (b) experimental Pb recoveries for 7 separate digestions. Uncertainties represent 2s uncertainty intervals.

(a) soil digestion procedure (± 0.2 g)

I. microwave-assisted acid digestion

acid combination	microwave programme
5 mL HNO_3 + 2 mL HCl + 2 mL HF	20 min 250 W, 8 min 600 W, 15 min 250 W
Cool down, + 1 mL $HClO_4$	20 min 250 W, 8 min 400 W, 15 min 250 W

II. transfer of digest to beaker, + 2 mL HNO_3 + 2 mL HF + 2 mL $HClO_4$, further digestion and evaporation on hotplate

III. uptake of residue in 1 mL HNO_3 under ultrasonic agitation, and subsequent dilution to 1 M HNO_3 with milli-Q water

(b) experimental recoveries

	$[Pb]_{exp}$ (µg g^{-1})	$[Pb]_{cert}$ (µg g^{-1})	recovery (%)
BCR CRM 141 Calcareous Loam Soil	27.9 ± 1.6	29.4 ± 2.6	94.9 ± 5.5
BCR CRM 142 Light Sandy Soil	37.4 ± 2.4	37.8 ± 1.9	98.9 ± 6.3

V.4.2 – Bone digestion procedure

Most bone digestion procedures reported on in literature make use of a hotplate digestion [Outridge *et al.*, 1996; May *et al.*, 1999] or Teflon bombs [Latkoczy *et al.*, 1998; Latkoczy *et al.*, 2001]. A microwave-assisted acid digestion procedure was developed in this work, based on that described for bone digestion by Hinners *et al.* [Hinners *et al.*, 1998]. A complete dissolution of bone could be achieved by adding 6 mL HNO_3 + 1.5 mL HCl to 0.2 g of pulverized bone and applying a 15 min microwave step (table V.2.a), followed by transfer to a beaker and evaporation to nearly dry on a hotplate. The residue was taken up in concentrated nitric acid and diluted to 1 M HNO_3 with milli-Q water. The certified reference materials NIST SRM 1400 Bone Ash and NIST SRM 1486 Bone Meal were used for validation of the digestion protocol. The experimental Pb recoveries turned out to be quantitative: 98.4 ± 3.6 % and 99.7 ± 7.2 %, respectively (table V.2.b).

V.4.3 – Enamel and dentine digestion procedure

In view of the similar elemental composition of bone tissue and dental tissues (chapter IV, § IV.4.2), it was expected that the digestion procedure for bone could also be used to digest enamel and dentine. However, this method succeeds in dissolving one of the two

Table V.2 – Digestion of bone tissue – (a) digestion procedure; (b) experimental Pb recoveries for 7 separate digestions. Uncertainties represent 2s uncertainty intervals.

(a) bone digestion procedure (± 0.2 g)

I. microwave-assisted acid digestion	
acid combination	microwave programme
6 mL HNO_3 + 1.5 mL HCl	5 min 250 W, 5 min 400 W, 5 min 250 W
II. transfer of digest to beaker, further digestion and evaporation on hotplate	
III. uptake of residue in 1 mL HNO_3 under ultrasonic agitation, and subsequent dilution to 1 M HNO_3 with milli-Q water	

(b) experimental recoveries

	$[Pb]_{exp}$ (µg g^{-1})	$[Pb]_{cert}$ (µg g^{-1})	recovery (%)
NIST SRM 1400 Bone Ash	8.92 ± 0.33	9.07 ± 0.12	98.4 ± 3.6
NIST SRM 1486 Bone Meal	1.330 ± 0.097	1.335 ± 0.014	99.7 ± 7.2

dental tissues only, namely dentine. The enamel, on the other hand, is not completely dissolved, what could be attributed to its very dense and compact structure, while dentine and bone have a more porous structure. Moreover, the enamel (and dentine) could not be pulverized using the microdismembrator (§ V.1.2), so that larger particles needed to be dissolved than in the case of bone. For this reason, another approach was searched for. It turned out that a hotplate digestion, summarized in table V.3.a, results in a complete dissolution. In a first step, 4 mL HNO_3 is added to 0.2 g dentine or enamel in a beaker and heated until nearly dry, followed by the addition of 2.5 mL HCl and again evaporation to nearly dry in a second step. The residue is finally taken up in concentrated nitric acid and diluted with milli-Q water. Also this approach was validated using the bone certified reference materials NIST SRM 1400 Bone Ash and NIST SRM 1486 Bone Meal, and resulted in a quantitative recovery for the target elements P, Ca, Sr and Pb (table V.3.b). The Pb recovery was determined by elemental assay using the Elan 5000 ICP – mass spectrometer; for the determination of P, Ca and Sr, the Elan DRC*plus* ICP – mass spectrometer was used.

V.4.4 – Ceramics digestion procedure

Because of the silicate matrix of ceramics (chapter IV, § IV.4.3), hydrofluoric acid is needed in order to obtain a complete dissolution. Mixtures of HF, HNO_3 and HCl have

Table V.3 – Digestion of dental tissues – (a) digestion procedure; (b) experimental recoveries for 7 separate digestions. Uncertainties represent 2s uncertainty intervals.

(a) dentine and enamel digestion procedure (± 0.2 g)
I. addition of 4 mL HNO_3, digestion by heating and evaporation on hotplate
II. addition of 2.5 mL HCl, further digestion by heating and evaporation on hotplate
III. uptake of residue in 1 mL HNO_3 under ultrasonic agitation and subsequent dilution with milli-Q water

(b) experimental recoveries

		$[target]_{exp}$ (µg g^{-1})	$[target]_{cert}$ (µg g^{-1})	recovery (%)
NIST SRM 1400 Bone Ash	Sr	246 ± 10	249 ± 7	99.0 ± 3.9
	Pb	8.94 ± 0.37	9.07 ± 0.12	98.6 ± 4.1
NIST SRM 1486 Bone Meal	Sr	263 ± 7	264 ± 7	99.6 ± 2.8
	Pb	1.351 ± 0.043	1.335 ± 0.014	101.2 ± 3.2
		$[target]_{exp}$ (weight%)	$[target]_{cert}$ (weight%)	recovery (%)
NIST SRM 1400 Bone Ash	P	17.69 ± 0.54	17.91 ± 0.19	98.8 ± 3.0
	Ca	38.20 ± 0.07	38.18 ± 0.13	100.0 ± 0.2
NIST SRM 1486 Bone Meal	P	12.21 ± 0.61	12.30 ± 0.19	99.3 ± 4.9
	Ca	26.59 ± 0.57	26.58 ± 0.24	100.1 ± 2.1

proven to be valuable [Klein *et al.*, 2004-b; Papadopoulou *et al.*, 2004]. The procedure that proved effective (table IV.4) was a microwave-assisted acid digestion derived from that described by Kennett *et al.* [Kennett *et al.*, 2002; Kennett *et al.*, 2004] and consisted of a 30 min microwave step after the addition of 3 mL HNO_3 + 1 mL HCl + 5 mL HF to 0.2 g of a powdered ceramics sample. After this step, the sample was transferred to a beaker and evaporated to nearly dry on a hotplate, followed by redissolution in concentrated nitric acid and dilution to 1 M HNO_3. The digestion procedure for ceramics was not validated using certified reference materials because (i) in NIST SRM 679 Brick Clay – presumably the best suited certified reference material for this purpose – the Pb content is not certified and (ii) to the best of the author's present knowledge, there is no similar reference material with a certified lead content. It was visually observed that a complete dissolution was obtained since no more particles were present in the solution after the entire digestion procedure.

Table V.4 – Digestion procedure for ceramics

ceramics digestion procedure (± 0.2 g)	
I. microwave-assisted acid digestion	
acid combination	microwave programme
3 mL HNO_3 + 1 mL HCl + 5 mL HF	10 min 250 W, 10 min 600 W, 10 min 250 W
II. transfer of digest to beaker, further digestion and evaporation on hotplate	
III. uptake of residue in 1 mL HNO_3 under ultrasonic agitation, and subsequent dilution to 1 M HNO_3 with milli-Q water	

V.4.5 – Metallic artefacts digestion procedure

For the digestion of metallic artefacts, a hotplate digestion approach was opted for. In order to dissolve pure lead fragments, an amount of lead curls was weighed in a beaker and 10 mL 1.4 M HNO_3 was added, followed by heating on a hotplate (table V.5.a).

Table V.5 – Digestion of metallic artefacts – (a) digestion procedure for lead fragments; (b) digestion procedure for metallic artefacts with a high Cu/Ag content; (c) experimental Pb recoveries for 7 separate digestions. Uncertainties represent 2s uncertainty intervals.

(a) Pb fragment digestion procedure (± 0.1 g)
addition of 10 mL 1.4 M HNO_3, dissolution by heating on hotplate

(b) Cu/Ag artefact digestion procedure (± 0.1 g)
I. addition of 2 mL HNO_3 + 6 mL HCl (+ 1 mL H_2SO_4 when > 50 % silver), heating and evaporation on hotplate
II. addition of 1 mL HNO_3, and subsequent dilution to 1 M HNO_3 with milli-Q water

(c) experimental recoveries

	$[Pb]_{exp}$ (µg g^{-1})	$[Pb]_{cert}$ (µg g^{-1})	recovery (%)
NBS SRM 500 Unalloyed Copper VII	130 ± 4	128 ± 5	101.6 ± 3.5
NBS SRM 875 Cupro-Nickel, 10 % "Doped"	91 ± 4	92 ± 5	98.5 ± 4.3
	$[Pb]_{exp}$ (weight%)	$[Pb]_{cert}$ (weight%)	recovery (%)
NBS SRM 872 Phosphor Bronze	4.14 ± 0.11	4.13 ± 0.03	100.2 ± 2.6

Besides lead fragments, also copper-based artefacts (unalloyed copper, brass and bronze) and silver objects were studied (chapter VIII). For the digestion of metallic artefacts rich in copper or silver, several combinations of HNO_3, HCl and HF were tested in a hotplate

digestion approach [Ekstroem and Gustavsson, 1993; Young *et al.*, 1997; Ponting and Segal, 1998; Klein *et al.*, 2004-b]. The use of 8 mL aqua regia (3:1 HCl/HNO_3, § V.3.2) succeeded in dissolving metals with a high copper content, but the samples with a high silver content (> 50 %) posed a problem to dissolve. With the addition of 1 mL of sulfuric acid however, complete dissolution was obtained (table V.5.b). For the certified reference materials NBS SRM 500 Unalloyed Copper VII, NBS SRM 872 Phosphor Bronze and NBS SRM 875 Cupro-Nickel 'doped', experimental Pb recoveries of 101.6 ± 3.5 %, 100.2 ± 2.6 % and 98.5 ± 4.3 % were retrieved, respectively (table V.5.c).

V.5 – Certification of Pb in bone candidate reference materials

In 2006, the New York State Department of Health conducted an interlaboratory study for the characterization of bone candidate reference materials from lead-dosed sources. Four samples, NYS RMs 01-04, were delivered. Two bone samples were of bovine (cow) origin, whilst two others were of caprine (goat) origin. In a first step of the characterization, the lead content was studied, and our laboratory participated in this study.

On two different days, triplicate digestion of the four samples along with triplicate digestion of NIST SRM 1400 Bone Ash and NIST SRM 1486 Bone Meal for validation purposes, were carried out. The bone samples were digested following the microwave-assisted acid digestion protocol described above (§ V.4.2). After digestion, elemental assay of the two sample batches obtained at the two different days was carried out, also on two different days. On the one day, the PerkinElmer SCIEX Elan 5000 was used, and on the other day the PerkinElmer SCIEX Elan DRC*plus* was used in vented mode. Standard addition was used as calibration technique (chapter II, § II.9.2.2). The Pb concentrations obtained for the four candidate reference material samples investigated are summarized in table V.6. After completion of the interlaboratory study, a consensus value, based on the Pb concentrations reported by all the participating labs, was established for every sample. These are summarized in table V.6. In figures V.4.a-d, the results obtained by all the participating labs are graphically displayed [Bellis *et al.*, 2008].

From figure V.4, it can be seen that the Pb concentrations found by our lab (lab 443) match within experimental uncertainty with the corresponding consensus value based on the results obtained by all the labs. However, a value that is systematically higher than the consensus value was obtained for samples NYS RM 02 to NYS RM 04. Nevertheless, our results are in perfect agreement with the results obtained by lab 429 that used

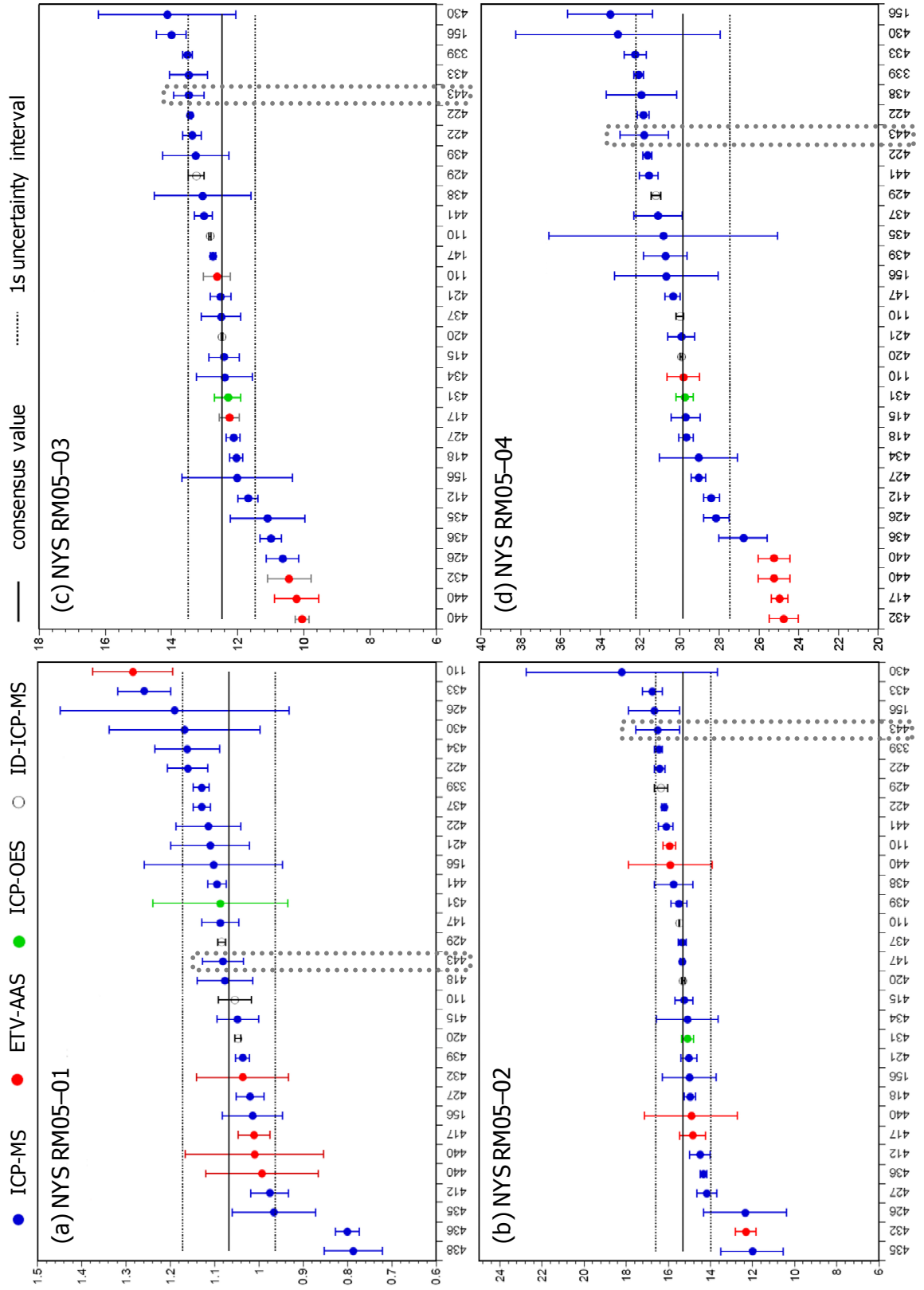

Figure V.4 – Experimental results for the Pb concentration in the NYS bone candidate reference materials obtained by the participating labs. Y-axis: Pb concentration (μg g^{-1}); X-axis: code for the participating labs. Our lab = 443; results are highlighted (dotted line).

Table V.6 – Pb concentration results obtained for the 4 NYS bone candidate reference materials. Consensus value and certified values taken from [Bellis *et al.*, 2008].

	[Pb] (µg g^{-1})			
	NYS RM 01	NYS RM 02	NYS RM 03	NYS RM 04
experimental result	1.08 ± 0.05	16.5 ± 0.8	13.5 ± 0.5	31.8 ± 1.1
consensus value	1.08 ± 0.08	15.3 ± 1.0	12.4 ± 1.0	29.9 ± 2.2
certified value	1.09 ± 0.06	16.1 ± 0.6	13.2 ± 0.6	31.5 ± 1.4

isotope dilution ICP – mass spectrometry (ID-ICP-MS) for concentration determination. On the other hand, two other labs (110 and 420) also used ID-ICP-MS and obtained a different (lower) result.

The organizers of the certification study subsequently assigned certified values to the investigated bone samples by applying double spike ID-ICP-MS. The certified values (table IV.6) are slightly higher than the consensus value obtained from the interlaboratory study, indicating a low bias in the results from the interlaboratory study [Bellis *et al.*, 2008]. Since the results obtained in our lab were slightly higher than the consensus values from the interlaboratory study, the match with the certified values is excellent. This observation confirms the ability of the digestion protocol developed for bone to give rise to a quantitative Pb recovery.

V.6 – Conclusions

The digestion procedures developed for the different archaeological artefacts under investigation – soil samples, bone and dental tissues, ceramics, lead and metallic artefacts – all give rise to a quantitative target element (Pb and/or P, Ca and Sr) recovery. Both microwave-assisted acid digestion and hotplate digestion have been proven as valuable to this purpose. From the observation that a quantitative Sr and/or Pb recovery was established, the occurrence of Sr and/or Pb isotopic fractionation during the sample pretreatment and digestion process can be excluded. Furthermore, the procedural blanks for Sr and Pb were found in the range of 1 to 10 ng L^{-1}, amounts that are negligible in comparison to the strontium or lead levels in the samples and giving rise to signal intensities that are < 0.1 % of the signal intensities encountered for standards and samples. This observation can be taken as a proof that the sample pretreatment procedures, the pulverization step by means of a microdismembrator, the sampling method for metallic objects by means of a miniature drill and the subsequent digestion procedures do not give rise to a significant amount of contamination.

CHAPTER VI

Isolation procedures for strontium and lead

For an accurate and precise determination of the isotopic composition of a target element in a sample, it is important to avoid, or at least accurately correct for, spectral and non-spectral interferences, which are factors that might compromise the attainable accuracy and precision. The best way to cope with such interferences is to separate the target element from its concomitant matrix in a pure and quantitative way. Via this approach, the analyte is obtained free from interfering species, and the matrix of the sample can be carefully matched to that of the standard solutions. In this work, an extraction chromatographic separation was used, based on a commercially available crown ether-based resin. Both Sr- and Pb-specific columns were evaluated, and their use was optimized and validated for their ability to isolate Sr or Pb from the archaeological samples under investigation, as is described in this chapter.

VI.1 – Pitfalls in obtaining accurate and precise isotope ratio results

In what follows, important problems that may be encountered in the acquisition of precise and accurate isotope ratio data are discussed. These include spectral and non-spectral interferences or matrix effects (chapter II, § II.2), and the influence of instrumental settings, memory effects and blank contributions.

VI.1.1 – Spectral interferences

Isotopic measurements aim at resolving very small differences in isotopic composition, and are therefore particularly vulnerable to spectral interferences. Spectral interferences are a major concern, particularly below 80 u, both in quadrupole-based single-collector ICP-MS and multi-collector ICP-MS. The mass resolution of a quadrupole-based ICP – mass spectrometer is limited to ~ 300, and most MC-ICP-MS instruments are generally operated at a mass resolution of ~ 400 to produce flat peak sections that are sufficiently wide for high precision isotope ratio measurements [Rehkämper *et al.*, 2004]. A higher mass resolution and at the same time preserving flat-topped peak shapes is accomplished when operating under so-called pseudo-high resolution conditions (chapter III, § III.3.2) [Weyer and Schwieters, 2003; Vanhaecke and Moens, 2004]. At low-resolution conditions, the mass spectrometer is unable to resolve interferences between the analyte and other ions with similar mass-to-charge ratio. Spectral interferences are generated by ions derived from the plasma, the sample solvent and the sample matrix (chapter II, § II.2). In order to

obtain accurate isotope ratio data, the influence of spectrally interfering ions should be either insignificant, or reduced to tolerable levels so that an accurate correction can be applied. In most cases, this can be achieved by (i) chemical separation of the analyte element from the sample matrix and/or (ii) the application of appropriate measurement protocols.

Isobaric interferences from other elements can be corrected for by monitoring an isotope of the interfering element and the application of a suitable mathematical interference correction [Halliday *et al.*, 1995]. Nonetheless, the maximum level of contamination giving rise to isobaric interferences that can be tolerated for accurate isotope ratio measurements needs to be evaluated. To avoid the measurement uncertainties that are associated with such interferences, the majority of the published MC-ICP-MS isotope data for geological samples have been collected either (i) on 'clean' samples that were processed through a chemical separation step prior to the mass spectrometry, or (ii) by direct analysis of major elements in a single phase, *e.g.*, Ca in carbonates [Halicz *et al.*, 1999] and Cu in ore samples [Zhu *et al.*, 2000-a].

Corrections for spectral interferences from polyatomic ions such as hydrides, oxides, nitrides or argides is less straightforward. In many cases, such interferences can be avoided by the chemical separation of the analyte prior to the mass spectrometry, *e.g.*, in the case of metal argides. The production of hydrides and oxides is furthermore greatly reduced when a desolvating nebulizer (chapter II, § II.2.2) is applied for sample introduction. The development of methods for the measurement of Fe isotopic compositions has been particularly difficult by the interferences of different argon-containing ions (ArN^+, $ArNH^+$, ArO^+, $ArOH^+$). However, as is demonstrated by published data [Anbar *et al.*, 2000; Belshaw *et al.*, 2000; Zhu *et al.*, 2000-b], precise data can be nevertheless obtained for this element when appropriate analytical protocols are followed [Weyer and Schwieters, 2003].

Interferences from refractory oxides and hydroxides (MO^+ and MOH^+, where M is a rare earth element) are often not a severe problem in MC-ICP-MS, since they can be avoided by chemical separation and because oxide formation can be greatly reduced in many cases by the use of a desolvating nebulizer.

Collision – and reaction cells [Feldmann *et al.*, 1999-a; Feldmann *et al.*, 1999-b; Tanner *et al.*, 2002; Koppenaal *et al.*, 2004] (chapter II, § II.6) which are used in quadrupole-based ICP-MS instruments and in the IsoProbe MC-ICP-MS instrument, have also been proven as valuable alternatives to reduce polyatomic [Baranov and Tanner, 1999] and isobaric [Moens *et al.*, 2001] spectral interferences. Furthermore, dynamic bandpass tuning (DBT, chapter II,

§ II.6.2.2.5) via the quadrupole assembly in a dynamic reaction cell allows an efficient control of the sequential chemistry [Latino *et al.*, 2001].

VI.1.2 – Matrix effects

Correction of instrumental mass discrimination by external standardization (chapter III, § III.4.2.2.2) requires that the mass discrimination of the analyte element is identical for both the sample and the standard. Similarly, external normalization (chapter III, § III.4.2.2.1) assumes that the relative mass bias encountered by the analyte and the reference element are indistinguishable for the samples and the isotopic standard [Rehkämper *et al.*, 2004]. A number of studies conducted with both ICP-Q-(DRC-)MS and MC-ICP-MS have shown that the instrumental mass discrimination can vary considerably with the analyte matrix and that the response of two elements of similar mass to a different matrix may not be sufficiently correlated [Douglas and Tanner, 1998; Horlick and Montaser, 1998; Galy *et al.*, 2001; Vanhaecke *et al.*, 2003]. This indicates that precise measurements of small differences in an isotopic composition are particularly prone to the generation of artefacts, and should preferably be conducted on target elements that have been chemically isolated from the sample matrix. Unfortunately, no chemical separation is perfect, but a number of MC-ICP-MS studies demonstrated that remaining matrix constituents do not have a detrimental effect on data quality, either by influencing the mass bias behavior, or through the formation of spectral interferences [Halicz *et al.*, 1999; Zhu *et al.*, 2000-a].

The accuracy of stable isotope ratio measurements may furthermore be affected by the concentration of the analyte or the relative concentrations of the analyte and normalizing element, as has been demonstrated for Pb with Tl as normalizing element, as well as the type and strength of the acid matrix of the sample and standard solutions [Rehkämper and Halliday, 1999; Rehkämper and Mezger, 2000; Kamenov *et al.*, 2004].

VI.1.3 – Other factors

A number of MC-ICP-MS stable isotope studies have noted that instrumental operating conditions (gas flow rates, focusing lens settings, acceleration lens potentials) must remain constant during an analytical session because even small changes in these parameters may result in changes in mass discrimination [Hirata, 1997; Rehkämper and Halliday, 1999]. Memory effects have been reported as a problem for elemental concentration measurements by ICP-Q-MS, particularly for the analysis of samples with highly variable

analyte abundances. In the case of isotope ratio measurements by MC-ICP-MS, memory problems are often less severe, because most analyses are conducted with 'clean' solutions of separated elements, and large variations in the concentrations of the analyte solutions should be avoided in any case [Rehkämper and Halliday, 1999]. Because samples and standards typically display only small differences in isotopic composition, the contribution of the instrumental blank is further decreased. It has been observed that memory effects are typically more pronounced for desolvating nebulizers compared to other sample introduction systems. This advantage can be overcome, however, by using appropriate washout protocols. In the case of severe memory problems (*e.g.*, B, Os), isotopic analysis requires the use of a designated sample introduction system and/or special cleaning procedures [Montaser *et al.*, 1998-a].

VI.2 – Analyte separation prior to isotopic analysis

VI.2.1 – Interferences on strontium and lead

An overview of the possible mass spectral interferences on Sr and Pb isotopes, potentially encountered when analyzing these elements by means of ICP – mass spectrometry, is given in table VI.1.

Since ^{87}Sr is formed by the beta-decay of ^{87}Rb (chapter IV, § IV.1.1), rubidium and strontium are often co-present, leading to an isobaric interference ($^{87}Rb^+$) on the $^{87}Sr^+$ signal. The mass resolution of ~ 300 000 that is required to resolve these isobaric ions is beyond the resolving capacities of all present-day mass spectrometers. Only chemical resolution in a dynamic reaction cell succeeds in the separation of these isobars (chapter II, § II.6.2.2.5) [Moens *et al.*, 2001]. This implies that a separation method for Sr from its guiding matrix should at the same time be successful in separating Rb from Sr. Next to rubidium, also krypton, that is present as impurities in argon gas, can lead to isobaric interferences on the ^{84}Sr and ^{86}Sr isotopes. Besides the interferences arising from Rb and Kr, also the interference from $ArCa^+$ molecular ions (table VI.1.a) should be taken care of, especially when analyzing bone and dental tissues. The potential interferences on Sr isotopes that arise from doubly charged ions (table VI.1.a) will be negligible, because the parent elements are low abundant, and since the operating parameters of an ICP – mass spectrometer are set in such a way that the occurrence of doubly charged ions in the mass spectrum is low (< 3 %).

Table VI.1 – Spectral interferences potentially encountered when analyzing the isotopic composition of (a) Sr and (b) Pb by means of ICP – mass spectrometry. M^+: isobaric interfering ion, MX^+: molecular interfering ion, M^{2+}: doubly charged interfering ion.

(a) Sr	isotopes:	$^{84}Sr^+$	$^{86}Sr^+$	$^{87}Sr^+$	$^{88}Sr^+$
	M^+	$^{84}Kr^+$	$^{86}Kr^+$	$^{87}Rb^+$	–
	MX^+	$^{36}Ar^{48}Ca^+$, $^{38}Ar^{46}Ca^+$, $^{40}Ar^{44}Ca^+$, $^{36}Ar^{48}Ti^+$, $^{38}Ar^{46}Ti^+$, $^{66}Zn^{18}O^+$, $^{67}Zn^{17}O^+$, $^{68}Zn^{16}O^+$	$^{38}Ar^{48}Ca^+$, $^{40}Ar^{46}Ca^+$, $^{36}Ar^{50}Ti^+$, $^{38}Ar^{48}Ti^+$, $^{40}Ar^{46}Ti^+$, $^{36}Ar^{50}Cr^+$, $^{68}Zn^{18}O^+$, $^{70}Zn^{16}O^+$, $^{69}Ga^{17}O^+$, $^{70}Ge^{16}O^+$	$^{38}Ar^{49}Ti^+$, $^{40}Ar^{47}Ti^+$, $^{36}Ar^{51}V^+$, $^{70}Zn^{17}O^+$, $^{69}Ga^{18}O^+$, $^{71}Ga^{16}O^+$, $^{70}Ge^{17}O^+$	$^{40}Ar^{48}Ca^+$, $^{38}Ar^{50}Ti^+$, $^{40}Ar^{48}Ti^+$, $^{38}Ar^{50}V^+$, $^{38}Ar^{50}Cr^+$, $^{70}Zn^{18}O^+$, $^{71}Ga^{17}O^+$, $^{70}Ge^{18}O^+$, $^{72}Ge^{16}O^+$
	M^{2+}	$^{168}Er^{2+}$, $^{168}Yb^{2+}$	$^{172}Yb^{2+}$	$^{174}Yb^{2+}$, $^{174}Hf^{2+}$	$^{176}Yb^{2+}$, $^{176}Lu^{2+}$, $^{176}Hf^{2+}$

(b) Pb	isotopes:	$^{204}Pb^+$	$^{206}Pb^+$	$^{207}Pb^+$	$^{208}Pb^+$
	M^+	$^{204}Hg^+$	–	–	–
	MX^+	$^{186}W^{18}O^+$, $^{187}Re^{17}O^+$, $^{186}Os^{18}O^+$, $^{187}Os^{17}O^+$, $^{188}Os^{16}O^+$	$^{188}Os^{18}O^+$, $^{189}Os^{17}O^+$, $^{190}Os^{16}O^+$, $^{190}Pt^{16}O^+$	$^{189}Os^{18}O^+$, $^{190}Os^{17}O^+$, $^{191}Ir^{16}O^+$, $^{190}Pt^{17}O^+$	$^{190}Os^{18}O^+$, $^{192}Os^{16}O^+$, $^{191}Ir^{17}O^+$, $^{190}Pt^{18}O^+$, $^{192}Pt^{16}O^+$
	M^{2+}	–	–	–	–

In the case of Pb, the interference that is most likely originates from Hg (table VI.1.b). The isobaric interference ($^{204}Hg^+$) on the signal of $^{204}Pb^+$ can be mathematically corrected for by monitoring the intensity of the $^{202}Hg^+$ isotope. Next to Hg, also oxides of W, Re, Os, Ir and Pt potentially interfere the Pb isotopes, but either (i) these oxide ions are not formed due to the very low occurrence of the parent elements, (ii) the interferences can be mathematically corrected for by monitoring another isotope of the element involved, or (iii) the parent elements are already removed in the preliminary separation process.

VI.2.2 – Requirements for analyte isolation

As stated in previous paragraphs, matrix-related interferences negatively influence the accuracy and precision of the measured analyte isotope ratio. The most drastic way to cope with these interferences is to isolate the target element prior to isotope ratio analysis. Further, in the case of low analyte concentrations, a preliminary target element

isolation, and thus preconcentration, can improve the isotope ratio precision obtained. Following Poisson counting statistics, a higher precision is attainable at higher analyte concentrations and thus, count rates (chapter III, equations III.6 and III.7). Isolation methods preceding an isotopic analysis can introduce isotopic fractionation, as observed for elements such as Fe [Anbar *et al.*, 2000], Cu and Zn [Maréchal and Albarède, 2002], and Cd [Cloquet *et al.*, 2005]. As a consequence, several requirements are essential for a separation method to be used prior to isotope ratio analysis: (i) the method should isolate the element of interest in a high degree of purity, and preferentially totally pure, (ii) the chemical yield should be as high as possible, ideally 100 %, enabling small or depleted samples to be analysed and ensuring the absence of isotopic fractionation during the separation process, (iii) the procedural blanks should be negligible with respect to the quantities analyzed, (iv) the method should preferentially use a limited amount of reagents, that are easy to purify, and (v) the method should be simple, rapid and robust [Gale, 1996]. A variety of methods have been proposed for this type of separation, among them, solvent extraction [Zolotov *et al.*, 1986], ion exchange chromatography [Walton and Rocklin, 1990], extraction chromatography [Braun and Ghersini, 1975], precipitation [Alfassi and Wai, 1992] and combinations thereof [Nevissi, 1991]. In many instances, however, these methods suffer from one or more drawbacks which limit their utility. Solvent extraction is far too cumbersome for routine use. Similarly, the lack of selectivity of conventional ion exchange resins complicates separations where the matrix is complex, as is the case when dealing with archaeological artefacts.

VI.2.3 – Existing isolation techniques for strontium

The most commonly used separation technique for strontium involves cation exchange chromatography in HCl medium using the AG50W-X8 ion exchange resin [Darbyshire and Sewell, 1997; Almeida and Vasconcelos, 2001; Vanhaecke *et al.*, 2001; Barbaste *et al.*, 2002]. On this strongly acidic cation exchange resin, strontium is retained more than the major bone and soil matrix elements in 2 M HCl medium [Strelow, 1960]. Ideally, all rubidium will elute from the ion exchange column before strontium is collected, but in practice, and especially when working with high rubidium concentrations, a complete separation of Rb and Sr may be difficult to achieve [Latkoczy *et al.*, 2001]. Next to ion exchange chromatography, also extraction chromatography was described as a tool for Rb/Sr separation [Horwitz *et al.*, 1991; Horwitz *et al.*, 1992; Pin and Bassin, 1992]. Here, a solution of a crown ether in octanol sorbed onto an inert substrate accomplishes the extraction of Sr from nitric acid media. The

selective resin, commercially available from Eichrom Environment (France) as Sr spec™, is often used in microquantities packed onto microcolumns (< 1 mL resin) to purify Sr prior to its isotope ratio analysis [Deniel and Pin, 2001; Prohaska *et al.*, 2002; Pin *et al.*, 2003; Fortunato *et al.*, 2004]. Also a combined use of extraction chromatography either after cation exchange on AG50W-X [Waight *et al.*, 2002] or before cation exchange using titanium phosphate (PHOTI D) or zirconium phosphate (PHOZIR) slurried in 2 M HNO_3 and loaded onto a polystyrene carrier [Pin *et al.*, 2003] has been successfully applied to geological materials. Next to these manual separation techniques, also automated ion exchange procedures using high-performance ion chromatography (HPIC) and flow injection (FI) have been developed and even coupled online to (MC-)ICP-MS for subsequent Sr isotope ratio analysis [Latkoczy *et al.*, 2001; Meynadier *et al.*, 2006; Galler *et al.*, 2007; Garcia-Ruiz *et al.*, 2007]. Recently, the separation of Rb and Sr via selective vaporization in an ETV-unit coupled to an ICP – mass spectrometer (ETV-ICP-MS), has been described [Rowland *et al.*, 2008].

VI.2.4 – Existing isolation techniques for lead

For geochemical applications, an anion exchange chromatographic separation using HBr and HCl with AG1-X8 resin is considered as the standard method for Pb isolation [Manhès *et al.*, 1980; Rehkämper and Mezger, 2000; White *et al.*, 2000; Weiss *et al.*, 1999; Baker *et al.*, 2004; Cloquet *et al.*, 2006-b]. Next to this method, also the use of iminodiacetate cation exchange columns (MetPac CC-1) was demonstrated useful for Pb isolation from a bone matrix [Hinners *et al.*, 1998]. An extraction chromatographic resin, Pb spec™, which is derived from Sr spec™, has also been developed and commercialized by Eichrom Environment [Horwitz *et al.*, 1994; Gale, 1996].

VI.2.5 – Strontium and lead isolation techniques used in this work

In this work, for both the target elements Sr and Pb, an extraction chromatographic separation was evaluated. To this purpose, the commercially available resins Sr spec™ for Sr and Pb spec™ for Pb – already mentioned above – were purchased from Eichrom Environment under the form of 2 mL pre-packed columns. These columns are larger than the microcolumns discussed above (§ VI.2.3), and thus allow the loading of a relatively large amount of liquid sample with a complex matrix composition, such as bone tissue or soil digests. Miniaturized methods are likely to fail in the cases where the target element concentration is low and the matrix is heavy, as is the case for most of the samples investigated in this work. Further, the extraction chromatographic resins Sr spec™ and

Pb spec™ should allow the use of less harmful chemicals or more diluted acids than those used in standard Sr and Pb isolation methods (§ VI.2.3 and § VI.2.4). The performance of the resins in terms of recovery, purity of the target element fraction obtained and absence of isotopic fractionation after the separation process was evaluated, by applying a separation protocol to (i) solutions obtained after digestion of soil and bone certified reference materials (BCR CRM 141 Calcareous Loam Soil, BCR CRM 142 Light Sandy Soil, NIST SRM 1400 Bone Ash and NIST SRM 1486 Bone Meal) following the digestion procedures described in chapter V (§ V.4.1 and § V.4.2) and (ii) isotopic standards (NIST SRM 981 Common Lead and NIST SRM 987 $SrCO_3$). Also the possibility of regeneration of the resin, allowing multiple employment of the same column, was evaluated.

VI.3 – Extraction chromatography using Sr spec™

VI.3.1 – Description of the resin

In this work, the Sr spec™ crown ether-based resin was used as commercially available pre-packed 2 mL columns, packed with an inert polymeric carrier with a particle diameter of 100-150 µm. The crown ether, 4,4'(5')-di-*tert*-butylcyclohexane-18-crown-6 (figure VI.1) is present in a 1.0 M concentration in 1-octanol, and the inert chromatographic support is loaded with 40 % (w/w) of this organic solution. The specific combination of crown ether concentration and alcohol constitutes the resin's selectivity for strontium. Additional information on Sr spec™ resin can be found in dedicated sources, *e.g.*, [Horwitz *et al.*, 1991; Horwitz *et al.*, 1992; Pin and Bassin, 1992].

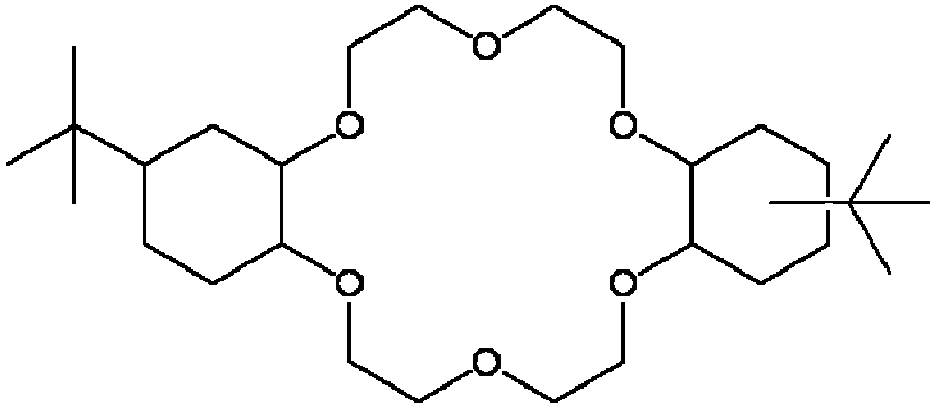

Figure VI.1 – Crown ether 4,4'(5')-di-*tert*-butylcyclohexane-18-crown-6, used in the Sr spec™ and Pb spec™ resins

VI.3.2 – Evaluation and optimization of the use of Sr spec™ resin

VI.3.2.1 – Isolation of Sr from its concomitant matrix

The binding properties of Sr, along with other elements (Na, K, Ca, Rb, Cs, Ba and Pb) on the Sr spec™ resin with increasing HNO_3 concentration are shown in figure VI.2 [Horwitz *et al.*, 1991; Horwitz *et al.*, 1992]. In column chromatography, a measure of the affinity of a target element for the stationary phase (in this case, the crown ether in 1-octanol loaded onto the polymeric carrier) is the retention factor or capacity factor *k'*, which is defined as the ratio of the number of moles of the target element in the stationary phase and in the mobile phase (in this case, the HNO_3 solution), respectively [Meyer, 2000].

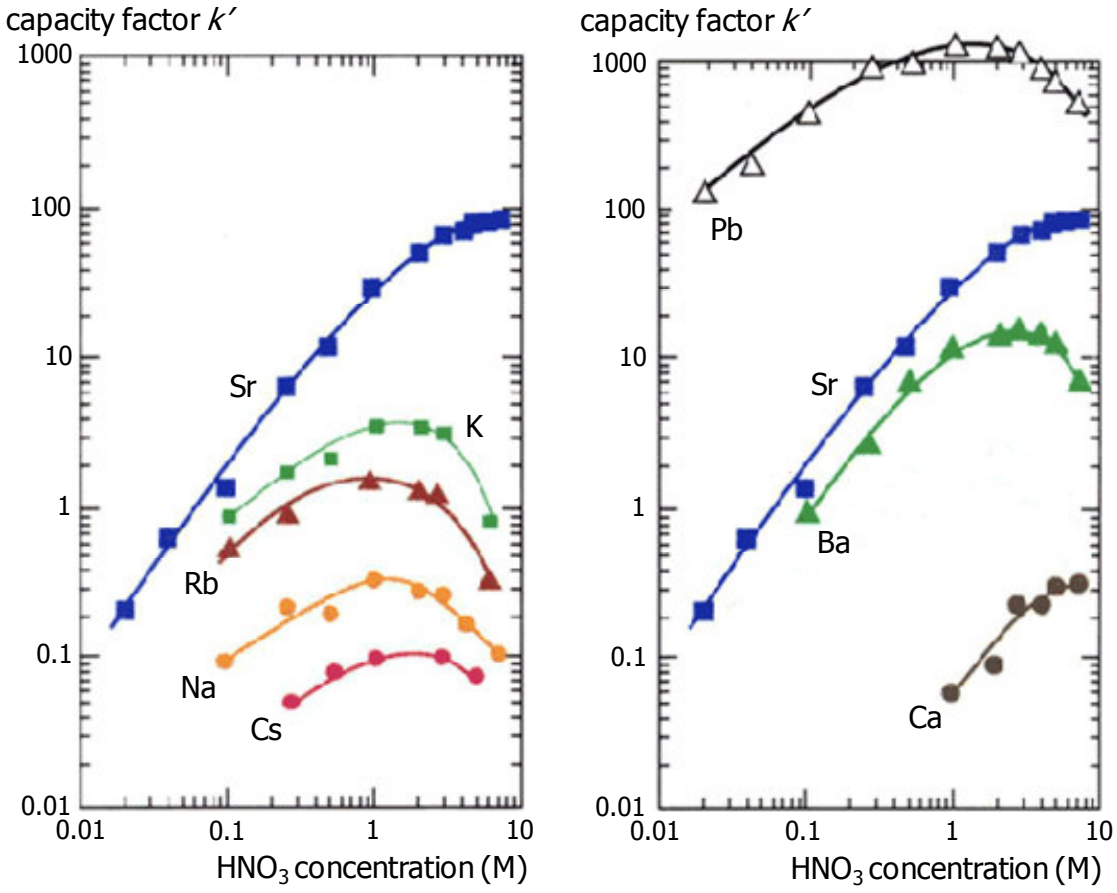

Figure VI.2 – Capacity factor *k'* of Sr and various other elements on Sr spec™ resin versus HNO_3 concentration

The higher the capacity factor *k'* for an element at a given HNO_3 concentration, the higher the affinity of the target element for the stationary phase and thus the better that element is retained by the column. In this work, bone and dental tissues are subjected to Sr isotopic analysis, and the elements that should thus be considered when optimizing a separation procedure preceding Sr isotopic analysis comprise (i) the target element Sr,

(ii) Rb, giving rise to the isobaric $^{87}Rb^+$ interference (table VI.1), (iii) Pb, that exhibits a behavior similar to that of Sr and is even better retained than Sr on the resin and (iv) the major constituents of the bone and tooth matrix, such as Na, Mg, P, K, Ca and Fe. Unfortunately, no information on the column behavior for, *e.g.*, Mg and Fe is available, and hence, this was experimentally evaluated.

The capacity factor for strontium, k'_{Sr}, reaches its maximum value ranging from 70 to 90 at a HNO_3 concentration ranging from 3 to 7 M (figure VI.2). In this concentration range, Pb displays an affinity that is even higher than that of Sr (~ 700), while all the other elements of interest display a k' value not higher than 3. Further, the capacity factor k' for bone matrix elements is decreasing by at least a factor of two when increasing the HNO_3 concentration from 3 to 7 M (Pb: 1 000 to 500, K: 3 to 1, Rb: 1 to 0.3, Na: 0.3 to 0.1), except for Ca of which k' stays constant around 0.3. From this observation, it can be concluded that the sample can be loaded onto the column in a 3 to 7 M HNO_3 medium, so that the Sr is retained by the column while the matrix elements, except for Pb, show only limited affinity for the column. Rinsing the column with an additional amount of 3 to 7 M HNO_3 can result in the slightly retained matrix elements being rinsed off the column. Lowering the HNO_3 concentration to, *e.g.*, 0.05 M results in a 100-fold decrease of the capacity factor of Sr, so that the Sr is released from the column. Under these conditions, also the capacity factor of Pb decreases from 500 to 300, but remains sufficiently high to retain Pb on the column. If required, later on, Pb can be eluted from the column using HCl [Deniel and Pin, 2001]. In view of the observations above, a strategy was suggested for the use of Sr spec^{TM}: (i) loading the sample in 3 to 7 M HNO_3 onto the column, (ii) rinsing the column with an arbitrary volume of 20 mL 3 to 7 M HNO_3 to remove slightly retained matrix elements and (iii) elution of the pure Sr fraction with an arbitrary volume of 20 mL 0.05 M HNO_3.

A first step in the optimization was to establish which HNO_3 concentration – 3 or 7 M – was the most efficient for sample loading and subsequent removal of the concomitant matrix elements. Hereto, a digest of NIST SRM 1400 Bone Ash was split into two aliquots, where one was diluted to 3 M HNO_3, and the other to 7 M HNO_3. An amount of these aliquots was brought onto an extraction chromatographic column, so that approximately 10 µg Sr was loaded onto the column. The column loaded with the aliquot in 3 M HNO_3 was subsequently rinsed with 20 mL 3 M HNO_3, while the column loaded with the 7 M HNO_3 aliquot was rinsed with 20 mL 7 M HNO_3, after which both Sr fractions were eluted using 20 mL 0.05 M HNO_3. After elution, the Sr recovery was determined by comparing the Sr concentrations retrieved in the original digest and in the eluted fraction.

This experiment was repeated 3 times, and the recovery in the 3 M HNO_3 setup appeared to be never higher than 20 %. Although 3 M HNO_3 is frequently used for sample loading and matrix removal on Sr spec™, the recovery was not reported [Prohaska *et al.*, 2002; Balcaen *et al.*, 2005], or was stated as not quantitative [Pin and Bassin, 1992; Galler *et al.*, 2007]. Using 7 M HNO_3 for sample loading and column rinsing resulted in an average quantitative Sr recovery for the 3 repetitions. As a consequence, 7 M HNO_3 was chosen as the optimum medium for sample loading onto and matrix removal from the column.

The second optimization step was the determination of the exact volumes of 7 M HNO_3 and 0.05 M HNO_3 solution required for complete removal of matrix elements (except for Pb) and quantitative Sr recovery, respectively, as the volume of 20 mL used in the first series of tests was only an arbitrary volume. This was done by loading approximately 10 µg Sr under the form of a NIST SRM 1400 Bone Ash digest in 7 M HNO_3 onto the column. Since nearly no Rb is present in NIST SRM 1400 Bone Ash, also 50 µg Rb under the form of a standard solution in 7 M HNO_3 was loaded onto the column. The solution that passed through the column after sample loading (effluent) was collected. Next, the column was rinsed with 20 mL 7 M HNO_3 in 1 mL aliquots, with every aliquot collected separately, followed by Sr elution with 20 mL 0.05 M HNO_3, where again the 1 mL aliquots were collected separately. The resulting 41 aliquots were semi-quantitatively analysed (chapter II, § II.9.1) for their Sr content and the presence of bone matrix elements using the Elan 5000 ICP – mass spectrometer. The elution profile thus obtained is displayed in figure VI.3. All the elements determined are slightly retained by the column, while for lead, no signal is observed for any fraction, what can be attributed to either (i) its low concentration in NIST SRM 1400 Bone Ash or (ii) the fact that the lead remains on the column during the whole experiment. This was not further investigated, but the second explanation seems more likely, since the combined Sr and Pb separation from silicate samples using Sr spec™ has already been described [Gale, 1996; Deniel and Pin, 2001]. It can be seen from figure VI.3 that the Rb/Sr separation and the removal of matrix elements is complete after rinsing the column with 10 mL of 7 M HNO_3, and that the complete Sr fraction is recovered after elution with 6 to 10 mL of 0.05 M HNO_3. An analogous experiment was performed using a BCR CRM 141 Calcareous Loam Soil digest, and exactly the same conclusions could be drawn from the elution profile.

The separation protocol developed, consisting of (i) conditioning the column with 3 mL 7 M HNO_3, followed by loading such an amount of sample in 7 M HNO_3 onto the column that 5 to 15 µg Sr is present , (ii) removal of slightly retained matrix elements by rinsing the column with 10 mL 7 M HNO_3 and (iii) elution of the purified Sr fraction with 10 mL

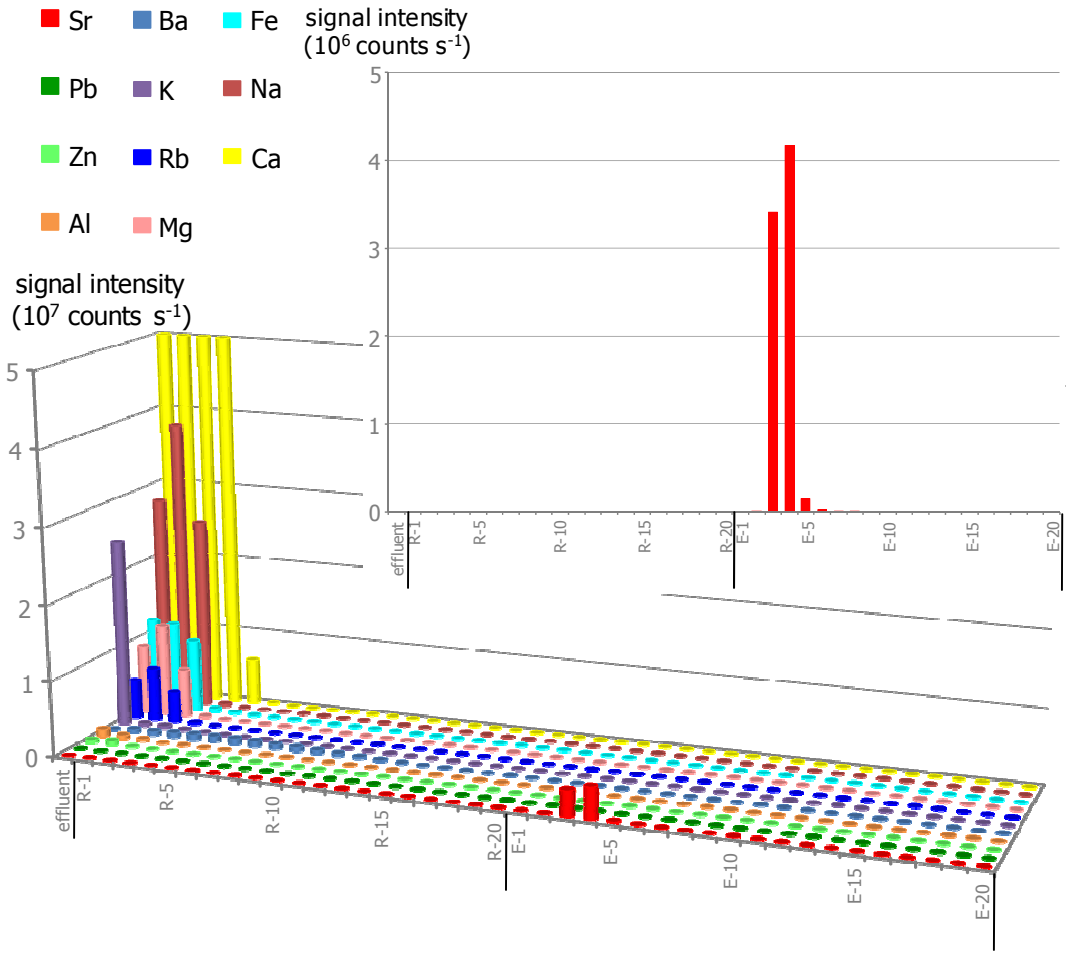

Figure VI.3 – Elution profile obtained for a NIST SRM 1400 Bone Ash digest loaded onto Sr spec™. An amount equivalent to 10 µg Sr was loaded and 50 µg Rb was additionally spiked onto the column. R-x = 1 mL 7 M HNO_3 rinse fraction x; E-x = 1 mL 0.05 M HNO_3 elution fraction x.

0.05 M HNO_3, was applied to the certified reference materials and the dental tissues under study. A Sr recovery with corresponding 2s uncertainty interval of 99.5 ± 2.3 % for soil (n=6), 100.0 ± 3.1 % for bone tissue (n=6) and 97.8 ± 4.4 % for dental tissues (enamel and dentine) (n=34) was obtained, resulting in an average Sr recovery of 99.1 ± 2.3 % on Sr spec™ resin.

VI.3.2.2 – Separation of rubidium and strontium

As was already observed from figure VI.3, the separation of Sr from the additionally spiked Rb was complete. However, an additional experiment was conducted in order to evaluate if the Rb/Sr separation efficiency depends on the relative amounts of Rb and Sr present. Hereto, standard solutions containing Rb and Sr in 7 M HNO_3, with a Sr/Rb ratio of 10, 1 and 0.1, were prepared. An amount equivalent to 10 µg Sr from each of these

three standard solutions was loaded onto three separate columns, followed by the rinsing and elution protocol described above, where every 1 mL fraction was collected separately. After semi-quantitative elemental assay of the fractions, the elution profiles displayed in figure VI.4 were obtained. It is clear that the separation of Rb and Sr is complete for every Sr/Rb ratio investigated. The amount of rubidium present in the purified strontium fractions of the three standard solutions was always below 0.4 µg L^{-1}, which is comparable to blank level.

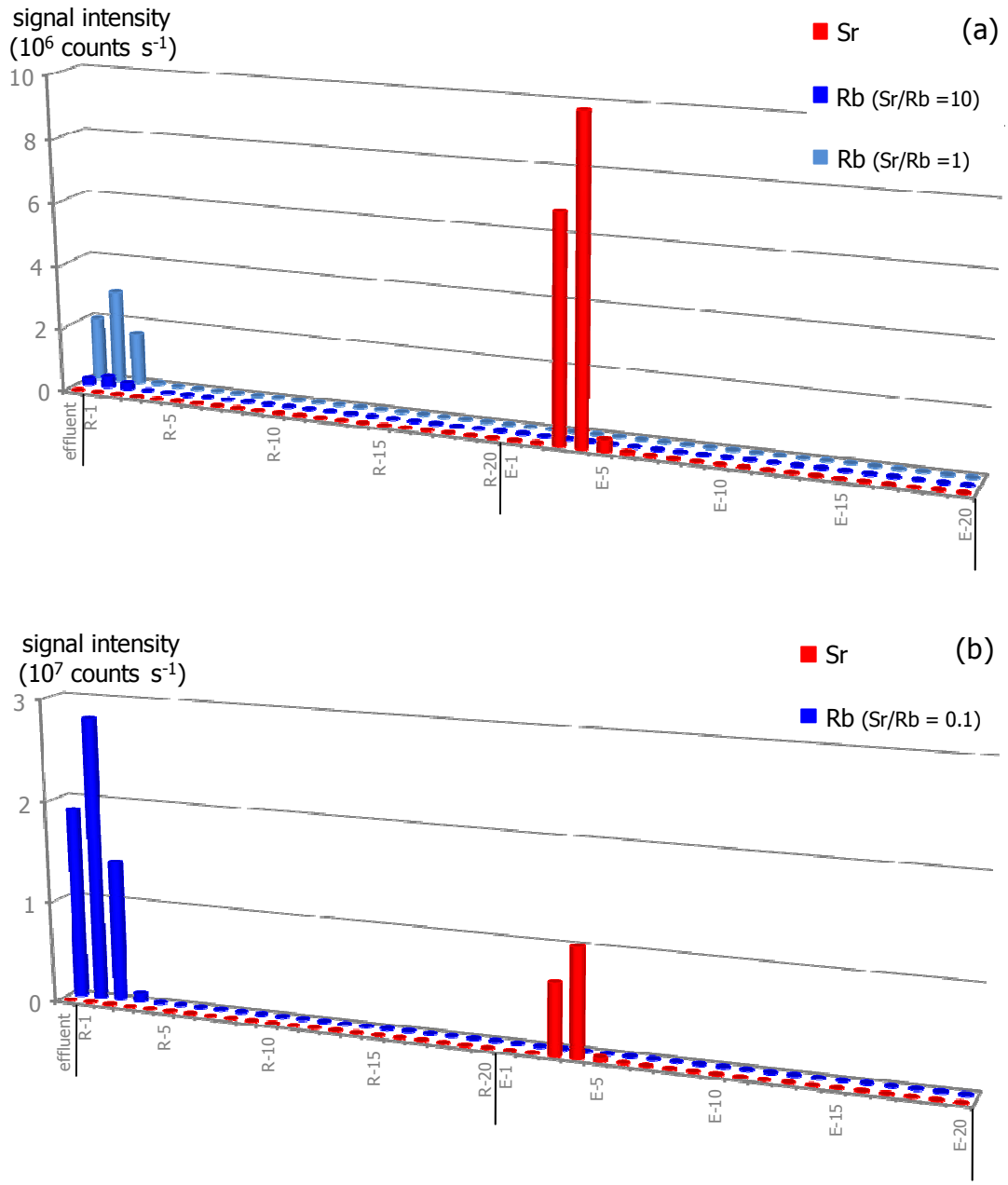

Figure VI.4 – Elution profiles obtained for standard solutions with varying Sr/Rb ratios – (a) Sr/Rb ratio = 10 and 1; (b) Sr/Rb ratio = 0.1. R-x = 1 mL 7 M HNO_3 rinse fraction x; E-x = 1 mL 0.05 M HNO_3 elution fraction x.

VI.4 – Extraction chromatography using Pb spec™

VI.4.1 – Description of the resin

The extraction chromatographic resin Sr spec™ (§ VI.3.1) was initially developed for the separation and preconcentration of Sr from HNO_3 solutions. It was noted that this material also exhibits extremely strong retention of Pb over a wide range of HNO_3 concentrations (figure VI.2), and even too strong for convenient stripping [Gale, 1996; Deniel and Pin, 2001]. From this observation, Pb spec™, a modified version of Sr spec™, was developed to achieve satisfactory lead retention from nitric acid containing aqueous phases, while at the same time readily permitting the stripping of the sorbed Pb. Lead extraction on the Pb spec™ resin is also accomplished by means of 4,4'(5')-di-*tert*-butylcyclohexane-18-crown-6 (figure VI.1) but the crown ether is present in a lower concentration (0.75 M) and dissolved in a higher molecular weight alcohol (isodecanol). Pb spec™ was also bought under the form of pre-packed 2 mL columns as Sr spec™. Additional information on Pb spec™ resin can be found in dedicated sources, *e.g.*, [Horwitz *et al.*, 1994].

VI.4.2 – Evaluation and optimization of the use of Pb spec™ resin

The capacity factor of Pb and various other elements on Pb spec™ resin with increasing HNO_3 concentration is available from the literature [Horwitz *et al.*, 1994] and shown in figure VI.5.

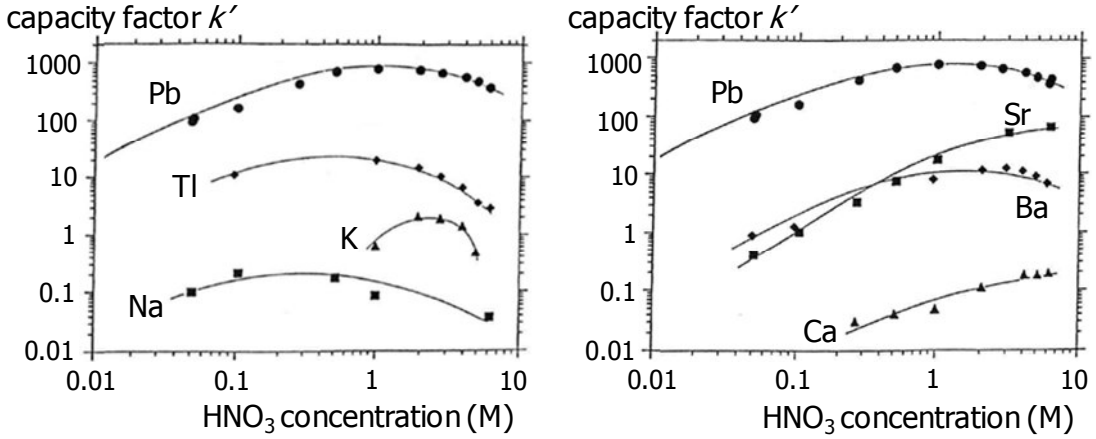

Figure VI.5 – Capacity factor *k´* of Pb and various other elements on Pb spec™ resin versus HNO_3 concentration

In view of the major elemental composition of the samples studied (soil, bone tissue, amphorae, metallic artefacts), especially the data available for Na, K, Ca, Sr and Ba,

besides Pb, are useful. Since Tl is often used in the case of Pb isotopic analysis for mass discrimination correction via external normalization (chapter III, § III.4.2.2.1) [Rehkämper and Mezger, 2000; White *et al.*, 2000; Kamenov *et al.*, 2004; Rehkämper *et al.*, 2004; Weiss *et al.*, 2004; Cloquet *et al.*, 2006-b], its absence in the sample fractions obtained after the Pb isolation procedure has to be guaranteed. Although Tl levels in bone and soil are (very) low, the efficiency of Tl removal has been experimentally evaluated when determining the Pb recoveries (see below). The capacity factor k' of Tl remains constant around 20 in the range of 0.2 to 1.0 M HNO_3 (figure VI.5). Na, K and especially Ca are major constituents of bone tissue, Sr is present in trace element range (although at a higher level than Pb) and Ba is present as a trace element in soils. The column shows an affinity for Sr and Ba that is comparable to that of Tl at 1.0 M HNO_3. The capacity factor k' is below 1 for K, below 0.2 for Na and below 0.1 for Ca in the HNO_3 concentration range of 0.1-1.0 M HNO_3 (figure VI.5). At 1.0 M HNO_3, K'_{Pb} reaches its maximum value (~ 1000), so this is the optimum HNO_3 concentration for sample loading and efficient sorption of Pb onto the resin. Sr and Ba are slightly retained under these conditions (K'_{Sr} ~ 20 and K'_{Ba} ~ 10), but they are removed by rinsing the column with 0.1 M HNO_3 (K'_{Sr} ~ 1 and K'_{Ba} ~ 2), while K'_{Pb} remains sufficiently high at ~ 500. As a consequence, the following strategy was suggested: (i) loading the sample in 1.0 M HNO_3 onto the column, (ii) rinsing the column with an arbitrary volume of 20 mL 0.1 M HNO_3 to remove slightly retained matrix elements (= matrix removal) and (iii) elution of the pure Pb fraction with an arbitrary volume of 20 mL of a suited eluent. No data are available on the capacity factors of, *e.g.*, Mg (bone tissue), Fe and Zn (soil), Al and Si (ceramics) and Cu and Ag (metallic artefacts); the behavior of these elements was experimentally evaluated after application of the proposed protocol.

In order to select a suited eluent, the following experiment was set up: 10 µg Pb from a Pb standard solution in 1.0 M HNO_3 was loaded onto an extraction chromatographic column, followed by column rinsing with 20 mL 0.1 M HNO_3. The performance in terms of recovery for several eluent candidates – milli-Q water, ethylenediamine tetra-acetate (EDTA) and ammonium oxalate [Horwitz *et al.*, 1994] – was evaluated. With 20 mL milli-Q water, only 0.38 % of the amount of Pb loaded onto the column was recovered. Next, 20 mL 0.1 M Na_4EDTA solution at pH 7.5 was tested. A major drawback of EDTA for the isolation of Pb is the strong complexing property of this organic compound. As a result, many metals were present as impurities in the eluted fraction, and Pb levels up to ~ 10 µg L^{-1} were retrieved in the blank solutions. Furthermore, due to its organic character, the presence of EDTA causes strong matrix effects (chapter II, § II.2) in ICP-

MS measurements. A signal suppression up to 35 % was observed for Pb. Hence, it was decided to opt for another eluent. The next candidate was a 0.05 M $(NH_4)_2C_2O_4$ solution. A Pb level below 0.5 µg L^{-1} was retrieved in the blank solutions, while other impurities were only present at negligible levels. The signal suppression observed on the Pb signal due to the presence of ammonium oxalate was below 0.5 % for 0.05 M $(NH_4)_2C_2O_4$ (the highest ammonium oxalate concentration used for Pb isotope ratio measurements). The first experiment with a 0.05 M $(NH_4)_2C_2O_4$ solution as eluent resulted in a quantitative Pb recovery. As a consequence, this eluent was selected as the best suited candidate for further employment.

The next step in the optimization was the determination of the volumes of 0.1 M HNO_3 and 0.05 M $(NH_4)_2C_2O_4$ solution required for complete matrix removal and quantitative Pb recovery. This was done in an experiment analogous to that described for Sr spec™ resin (§ VI.3.2.1). An amount of a soil (BCR CRM 141 Calcareous Loam Soil and BCR CRM 142 Light Sandy Soil) or bone (NIST SRM 1400 Bone Ash) digest in 1.0 M HNO_3 was loaded onto the column such that approximately 10 µg of Pb was present. The effluent was collected. Next, the column was rinsed with 20 mL 0.1 M HNO_3 and every 1 mL fraction was collected separately for individual analysis. Then, the Pb fraction was eluted with 20 mL 0.05 M $(NH_4)_2C_2O_4$ solution, where again every 1 mL fraction was collected separately. In the resulting 41 fractions (1 effluent, 20 rinse and 20 eluent fractions), Pb and a series of soil and bone matrix elements were determined semi-quantitatively (chapter II, § II.9.1) using the Elan 5000 ICP – mass spectrometer. The elution profile thus obtained for a BCR CRM 142 Light Sandy Soil digest is displayed in figure VI.6. The elements Mg and Fe display no affinity for the stationary phase. The elements Al, Si, K, Ca, Zn, Sr and Ba are retained by the column, but are completely removed during column rinsing. No Tl signal was observed during the optimization procedure since no detectable amount of Tl is present in BCR CRM 142 Light Sandy Soil. The removal of matrix elements is complete after rinsing with 10 mL 0.1 M HNO_3, and the pure Pb fraction is completely recovered after elution with 10 mL 0.05 M $(NH_4)_2C_2O_4$ solution. Exactly the same elution profile and conclusion was found for a BCR CRM 141 Calcareous Loam Soil and a NIST SRM 1400 Bone Ash digest.

Besides soil, bone tissue and ceramics, also metallic artefacts rich in copper and/or silver, were the subject of investigation. No data on the capacity factor *k'* of Cu or Ag, along with elements present in metallic artefacts (*e.g.*, As, Sn, Sb, Au, Bi) are available for Pb spec™. Further, in the digestion procedure developed for metallic artefacts with a high silver content (> 50 %) (chapter V, § V.4.5), 1 mL H_2SO_4 is added to the aqua regia in

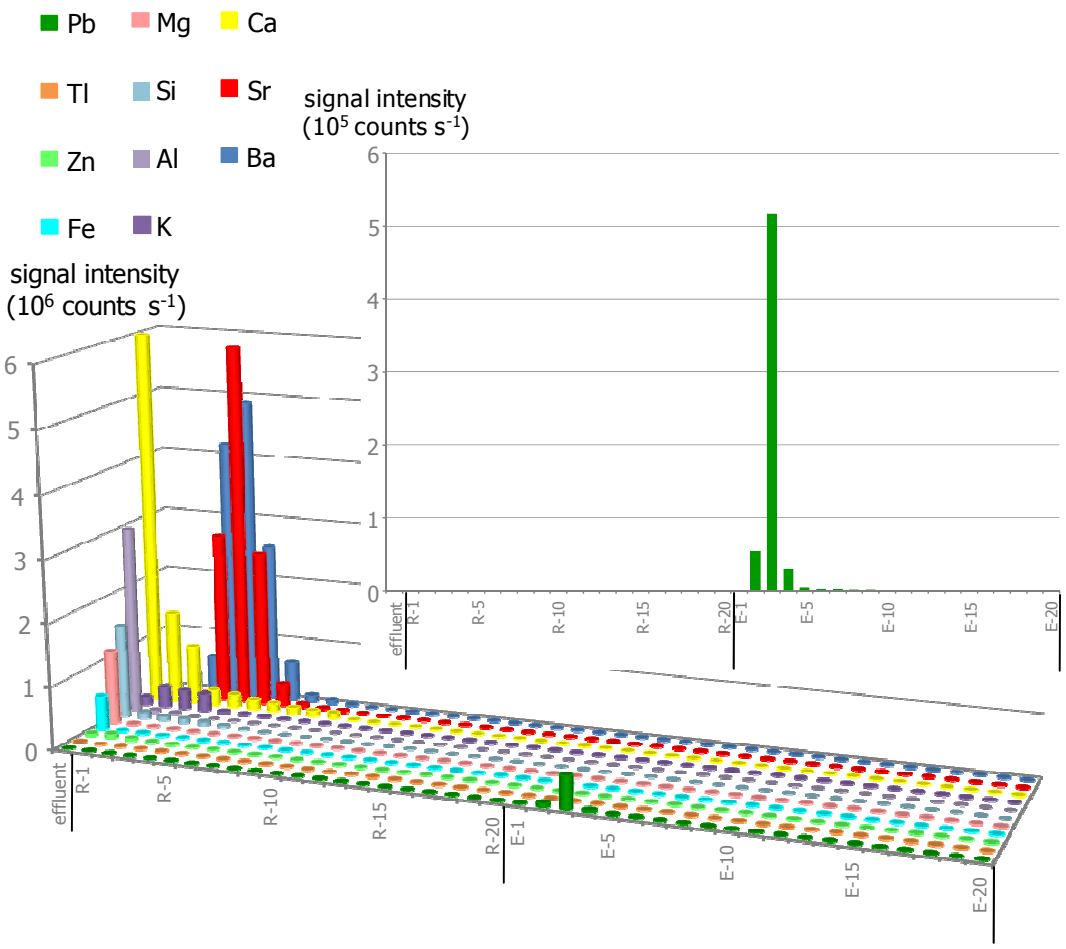

Figure VI.6 – Elution profile obtained for a BCR CRM 142 Light Sandy Soil digest loaded onto Pb spec™. An amount equivalent to 10 µg Pb was loaded onto the column. R-x = 1 mL 0.1 M HNO_3 rinse fraction x; E-x = 1 mL 0.05 M $(NH_4)_2C_2O_4$ elution fraction x.

order to complete the dissolution. Sulfuric acid cannot be completely evaporated since the boiling point of H_2SO_4 is higher than the melting point of the Teflon of which the beakers used in the sample digestion procedures are manufactured (chapter V, § V.3.4). As a consequence, there is always a residual amount of H_2SO_4 present in the digested samples with a high silver content. The Pb isolation protocol described for soil and bone tissue was also applied to metallic artefact digests that were diluted to 1.0 M HNO_3, regardless of the potential presence of residual amounts of H_2SO_4. An elution profile of a metallic fragment digest was recorded in an analogous way as described above, and is displayed in figure VI.7. Such an amount of a coin digest with a Cu/Ag ratio of ~ 1 and < 1 weight % of trace elements (*e.g.*, As, Sb, Sn, Pb) was brought onto the column that 10 µg Pb was loaded onto the column. The amounts of Cu and Ag loaded onto the column amounted to ~ 1 mg. It can be seen from figure VI.7 that none of the major and trace elements displays affinity for the stationary phase, and that, even when a residual amount of H_2SO_4 is present, the isolation of Pb from the metallic matrix remains efficient. Further, no

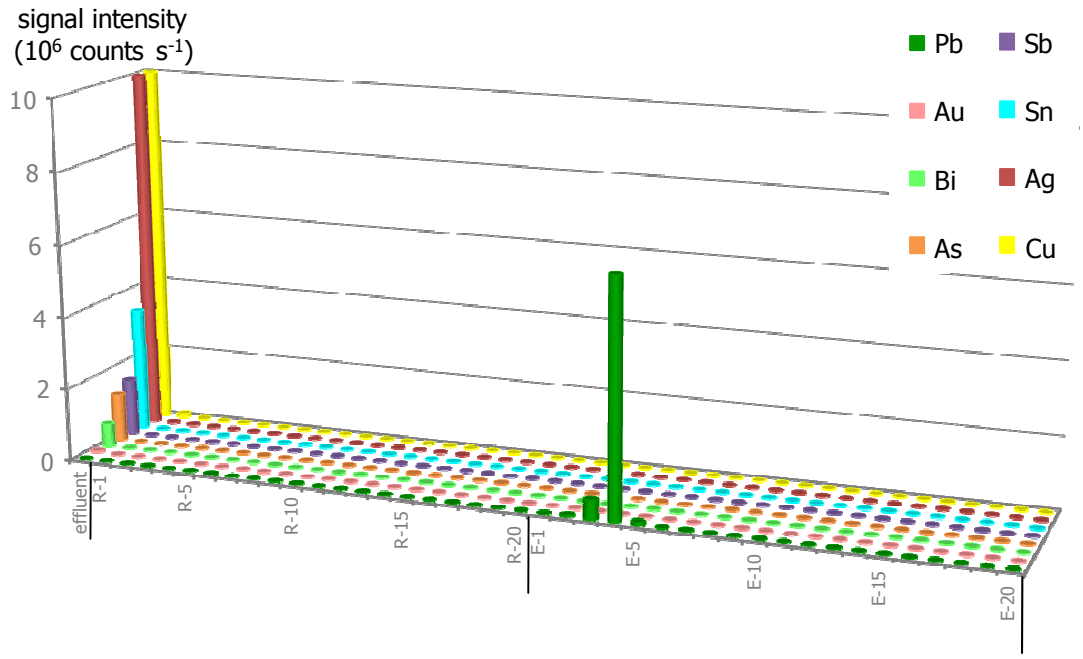

Figure VI.7 – Elution profile obtained for a metallic artefact digest with a Cu/Ag ratio of ~ 1 and less than 1 % trace elements. R-x = 1 mL 0.1 M HNO_3 rinse fraction x; E-x = 1 mL 0.05 M $(NH_4)_2C_2O_4$ elution fraction x.

detectable amounts of W – potentially introduced by the sampling using a tungsten-carbide miniature drill (chapter V, § V.1.3) – were found in the purified Pb fractions.

The Pb isolation method developed, was applied to the certified reference materials and archaeological samples under investigation. Between 5 and 15 µg of Pb, depending on the Pb concentration in the sample, was loaded onto the column. The column recoveries for the samples were determined by elemental assay using the Elan 5000 ICP – mass spectrometer followed by a comparison of the Pb concentration in the original digest and that in the Pb fraction after the isolation process. Besides Pb, also Tl was monitored in the Pb fractions, and the presence of Tl appeared to be limited to blank levels. The experimental Pb recovery and corresponding 2s uncertainty interval was determined as 99.8 ± 5.1 % for bone tissue (n=23), 100.3 ± 1.5 % for soil (n=22), 100.0 ± 2.0 % for ceramics (n=9), and 100.1 ± 2 % for metallic artefacts (n=42), resulting in an average Pb recovery of 100.1 ± 0.8 % on Pb spec™ resin.

VI.5 – Isotopic fractionation on the Sr and Pb resins

As stated higher, no isotopic fractionation is expected to occur in nature for Sr (chapter IV, § IV.1.1) and Pb (chapter IV, § IV.2.3). However, on-column fractionation has been occasionally reported for both Sr and Pb. In the case of Sr, separated using Sr spec™ resin, it was found that a minimal amount of mass-dependent isotopic

fractionation takes place during the course of the separation process, but that the cumulative isotope ratio after the separation procedure does not reflect detectable isotopic fractionation [Wakabayashi *et al.*, 2007]. The same observation was reported for Pb when using the standard HCl/HBr ion exchange technique, while again, the cumulative isotope ratio after the separation procedure matches within error to the certified value [Baker *et al.*, 2004]. It was suggested that the isotopic fractionation effects can be minimized by the use of small resin beds and collection of the Pb fraction in a sufficient amount of HCl. However, the pre-packed 2 mL columns used in this work are longer than the microcolumns used in standard methods for Sr and Pb isolations. Further, in this work, a large sample amount, ranging from 0.1 to 10 mL, depending on the target element concentration present, was loaded onto the column. In order to assess whether or not isotopic fractionation is introduced by the separation procedures developed for Sr and Pb, 10 µg of target element from an isotopic standard, NIST SRM 987 $SrCO_3$ for Sr and NIST SRM 981 Common Lead for Pb, was conducted through the respective isolation processes, followed by isotope ratio measurement using multi-collector ICP-MS (Thermo Electron's Neptune for Sr and Nu Instruments' Nu Plasma 500 for Pb) (chapter VII). Correction for mass discrimination was performed by external standardization (sample-standard bracketing) with a solution of NIST SRM 987 $SrCO_3$ for Sr isotope ratio measurements, and with a solution of NIST SRM 981 Common Lead for Pb isotope ratio measurements. A comparison of the isotope ratios obtained before and after the isolation procedure is given in table VI.2.

Table VI.2 – Experimental isotope ratios obtained for Sr and Pb isotopic standards before and after extraction chromatographic separation – (a) Sr results for NIST SRM 987 $SrCO_3$; (b) Pb results for NIST SRM 981 Common Lead. The uncertainty on the last digit is given in parentheses and represents a 2s uncertainty interval. Accepted values taken from [Nu, 2001] for Sr and from [Galer and Abouchami, 1998] for Pb.

(a) Sr	$^{84}Sr/^{86}Sr$	$^{84}Sr/^{88}Sr$	$^{87}Sr/^{86}Sr$
before	0.0565(2)	0.00674(2)	0.71022(3)
after	0.0564(2)	0.00673(2)	0.71023(3)
accepted	0.05649	0.006748	0.710248

(b) Pb	$^{206}Pb/^{204}Pb$	$^{207}Pb/^{204}Pb$	$^{208}Pb/^{204}Pb$	$^{207}Pb/^{206}Pb$	$^{208}Pb/^{206}Pb$	$^{208}Pb/^{207}Pb$
before	16.940(8)	15.496(6)	36.716(10)	0.9148(1)	2.1674(4)	2.3698(2)
after	16.949(10)	15.508(13)	36.741(25)	0.9148(2)	2.1678(6)	2.3699(3)
accepted	16.9405	15.4963	36.7219	0.91475	2.16771	2.3697

A good agreement, within experimental error, between the Sr isotope ratios obtained for NIST SRM 987 $SrCO_3$ before and after the isolation process is established (table VI.2.a). Further, within the external precision of the Sr measurement protocol using MC-ICP-MS, the experimental values are in very good agreement with the accepted values for NIST SRM 987 $SrCO_3$ as obtained via multi-collector ICP-MS [Thirlwall, 1991; Walder and Freedman, 1992; Nu, 2001; Faure and Mensing, 2005]. As a consequence, it can be concluded that no detectable isotopic fractionation is introduced by the extraction chromatographic isolation procedure via Sr spec™ resin. The Pb isotope ratios obtained before and after the isolation process for NIST SRM 981 Common Lead (table VI.2.b) match within experimental error and are in agreement with the accepted values for NIST SRM 981 Common Lead obtained via triple spike TI-MS [Galer and Abouchami, 1998]. Although the ratios with ^{204}Pb display a slight shift to higher values after the isolation process, they stay within experimental uncertainty of the isotope ratios before the isolation process. In view of the very good agreement for isotope ratios without ^{204}Pb, it can be concluded that no Pb isotopic fractionation is introduced by the isolation process using Pb spec™ resin. The quantitative recovery established for Sr on Sr spec™ (§ VI.3.2.1) and for Pb on Pb spec™ (§ VI.4.2) already pointed towards this conclusion.

VI.6 – Multiple use of extraction chromatographic resins

An experiment was set up to (i) assess the performance of the extraction chromatographic resins Sr spec™ and Pb spec™ after being regenerated, so when it is used a second time, and (ii) to test whether or not there is a change in recovery and/or isotope ratio when the same column, after regeneration, is applied for a second time for a matrix different from that when the column was used for the first time. For both Sr spec™ and Pb spec™, an analogous experiment was carried out, involving several columns as summarized in table VI.3. In a first batch (pass 1), an amount of NIST SRM 987 $SrCO_3$, a NIST SRM 1400 Bone Ash or a NIST SRM 1486 Bone Meal digest was loaded onto a new Sr spec™ column (table VI.3.a), and an amount of a digest of BCR CRM 141 Calcareous Loam Soil, BCR CRM 142 Light Sandy Soil or NIST SRM 1400 Bone Ash was loaded onto a new Pb spec™ column (table VI.3.b). After the respective Sr or Pb isolation procedure, the column was washed with 100 mL milli-Q water in order to regenerate the resins. This regeneration procedure was suggested for Pb spec™ resin [Horwitz *et al.*, 1994], but since bone and soil are characterized by a complex matrix composition (chapter IV, § IV.4.1

Table VI.3 – Experiment for column regeneration using certified reference materials. $SrCO_3$: NIST SRM 987 $SrCO_3$; BA: NIST SRM 1400 Bone Ash; BM: NIST SRM 1486 Bone Meal; CLS: BCR CRM 141 Calcareous Loam Soil; LSS: BCR CRM 142 Light Sandy Soil

(a) Sr	column 1	column 2	column 3	column 4
pass 1	$SrCO_3$	BA	BM	BM
pass 2	BA	BM	BA	BA

(b) Pb	column 1	column 2	column 3	column 4	column 5
pass 1	BA	BA	CLS	LSS	LSS
pass 2	BA	BA	CLS	CLS	LSS

and § IV.4.2), it was not taken for granted that this regeneration step is sufficiently sufficient. Hence, its efficiency was evaluated for both Sr spec™ and Pb spec™. In a second batch (pass 2), an amount of digest of the same certified reference materials as that used in the first batch was conducted through the respective Sr and Pb isolation procedure using the regenerated resins. Some columns were loaded with a digest of the same certified reference material as that loaded onto the column in the first batch, and some columns were loaded with a digest of a certified reference material that is different from that loaded in the first batch. It was stated that, in the case of a second use of Pb spec™, the Pb elution profile broadens, so that complete elution is accomplished at a higher eluent volume (shift ≤ 1 mL) [Horwitz *et al.*, 1994]. The Sr or Pb recovery on the regenerated resins was determined and established as quantitative, what was expected since 10 mL eluent is used for the elution of the purified Sr or Pb fractions. After the resin regeneration experiment, the Sr isotopic composition of the Sr fractions obtained was determined via MC-ICP-MS, and the Pb isotopic composition of the Pb fractions obtained was determined via SC-ICP-DRC-MS (chapter VII). The isotope ratio results thus obtained, reported as the average and corresponding 2s uncertainty interval obtained for two duplicate analyses, are summarized in table VI.4 and table VI.5, respectively.

For both Sr spec™ and Pb spec™, no systematic difference is observed between the isotope ratio results obtained for a digest of a certain certified reference material after the use of a new column or one that was used once before. Further, the isotope ratio results obtained for a digest of a certain certified reference material processed by a column that was previously used to process a digest of another certified reference material, are not significantly different from that obtained upon use of a new column. Moreover, the $^{87}Sr/^{86}Sr$ ratio obtained for every NIST SRM 1400 Bone Ash and NIST SRM 1486 Bone

Table VI.4 – Sr isotope ratio results obtained for certified reference materials using new and regenerated Sr spec™ resin. * reported by [Galler *et al.*, 2007]

	$^{87}Sr/^{86}Sr$	
	R	2s
NIST SRM 1400 Bone Ash		
col. 1 – pass 2	0.71300	0.00024
col. 2 – pass 1	0.71301	0.00027
col. 3 – pass 2	0.71299	0.00003
col. 4 – pass 2	0.71301	0.00004
average	*0.71301*	*0.00002*
MC-ICP-MS*	0.71315	0.00016
NIST SRM 1486 Bone Meal		
col. 2 – pass 2	0.70928	0.00005
col. 3 – pass 1	0.70931	0.00016
col. 4 – pass 1	0.70930	0.00007
average	*0.70929*	*0.00003*
MC-ICP-MS*	0.70931	0.00006

Meal digest (table VI.4) is, within experimental uncertainty, in excellent agreement with the previously reported $^{87}Sr/^{86}Sr$ ratio for these certified reference materials, obtained via multi-collector ICP-MS [Galler *et al.*, 2007]. Also the Pb isotope ratios retrieved for NIST SRM 1400 Bone Ash (table VI.5) display a good agreement with the previously reported values [Hinners *et al.*, 1998] normalized to the accepted [Galer and Abouchami, 1998] values for NIST SRM 981 Common Lead (for further discussion, see chapter VII, § VII.5.3.3). Thus, it can be concluded that, even when complex matrices are the subject of study, the Sr spec™ and Pb spec™ resins can be successfully regenerated and reused, as no effect on either recovery or isotope ratios could be established. A second and higher regeneration of the resins has not been tested. In these cases, one has to check to which extent the Sr or Pb elution profile further broadens and at which eluent volume the quantitative Sr or Pb elution is complete. From the observation that, when using a new column, the complete Sr fraction is recovered from Sr spec™ after elution with ~ 7 mL 0.05 M HNO_3 (figure VI.3) and that the complete Pb fraction is recovered from Pb spec™ after elution with ~ 6 mL 0.05 M $(NH_4)_2C_2O_4$ solution (figure VI.6), and given the fact that the maximum volume needed for complete elution shifts to a higher volume per regeneration (shift ≤ 1 mL), a 2nd and probably 3rd regeneration of the column is expected to display the same performance when 10 mL eluent is used.

Table VI.5 – Pb isotope ratio results obtained for certified reference materials using new and regenerated Pb spec™ resin. * renormalized from [Hinners *et al.*, 1998]

	$^{206}Pb/^{204}Pb$		$^{207}Pb/^{204}Pb$		$^{208}Pb/^{204}Pb$		$^{207}Pb/^{206}Pb$		$^{208}Pb/^{206}Pb$		$^{208}Pb/^{207}Pb$	
	R	2s	R	2s	R	2s	R	2s	R	2s	R	2s
NIST SRM 1400 Bone Ash												
col. 1 – pass 1	18.368	0.071	15.680	0.075	38.626	0.207	0.8536	0.0008	2.1031	0.0026	2.4635	0.0014
col. 1 – pass 2	18.333	0.044	15.655	0.030	38.561	0.013	0.8546	0.0018	2.1047	0.0019	2.4631	0.0039
col. 2 – pass 1	18.357	0.053	15.684	0.030	38.604	0.150	0.8543	0.0008	2.1026	0.0008	2.4605	0.0019
col. 2 – pass 2	18.363	0.069	15.676	0.039	38.631	0.062	0.8537	0.0011	2.1038	0.0046	2.4644	0.0022
average	*18.355*	*0.031*	*15.674*	*0.025*	*38.606*	*0.064*	*0.8541*	*0.0010*	*2.1036*	*0.0019*	*2.4629*	*0.0033*
TI-MS*	18.371	0.014	15.675	0.012	38.625	0.040	0.8532	0.0002	2.1025	0.0007	2.4642	0.0003
BCR CRM 141 Calcareous Loam Soil												
col. 3 – pass 1	18.607	0.097	15.670	0.078	38.637	0.186	0.8421	0.0002	2.0762	0.0002	2.4663	0.0011
col. 3 – pass 2	18.604	0.076	15.688	0.082	38.715	0.188	0.8433	0.0010	2.0803	0.0004	2.4673	0.0025
col. 4 – pass 2	18.589	0.044	15.643	0.041	38.578	0.044	0.8419	0.0013	2.0766	0.0050	2.4667	0.0077
average	*18.600*	*0.019*	*15.667*	*0.046*	*38.643*	*0.138*	*0.8424*	*0.0015*	*2.0777*	*0.0045*	*2.4667*	*0.0010*
BCR CRM 142 Light Sandy Soil												
col. 4 – pass 1	18.546	0.020	15.638	0.014	38.585	0.050	0.8432	0.0002	2.0810	0.0006	2.4674	0.0011
col. 5 – pass 1	18.529	0.073	15.666	0.049	38.625	0.152	0.8454	0.0009	2.0842	0.0010	2.4653	0.0044
col. 5 – pass 2	18.530	0.029	15.653	0.034	38.537	0.078	0.8446	0.0002	2.0791	0.0015	2.4610	0.0040
average	*18.535*	*0.019*	*15.652*	*0.028*	*38.582*	*0.089*	*0.8444*	*0.0022*	*2.0814*	*0.0051*	*2.4646*	*0.0065*

VI.7 – Conclusions

The performance of commercially available pre-packed 2 mL extraction chromatographic columns, containing a crown ether-based resin, was evaluated for the pure and quantitative isolation of Sr and Pb from heavy and complex matrices of archaeological artefacts. For Sr isolation and simultaneous separation of Rb and Sr, Sr spec™ was used, while for Pb isolation, Pb spec™ was used. Both resins are based on the crown ether 4,4'(5')-di-*tert*-butylcyclohexane-18-crown-6, while the selectivity of the resin for Sr or Pb is obtained by changing the crown ether concentration in combination with a change in the type of alcohol as solvent. It was demonstrated that the proper use of Sr spec™ and Pb spec™ results in a quantitative Sr or Pb recovery, and that the separation of Rb and Sr is complete on Sr spec™. A benefit of using these resins is that less harmful and more diluted chemicals can be used than those used in standard Sr and Pb isolation methods. Further, it was demonstrated that the isolation of Sr by means of Sr spec™ and the isolation of Pb by means of Pb spec™ does not introduce isotopic fractionation of Sr and Pb. The possibility of regenerating the resins, allowing multiple use of the same column, preserving a quantitative target element recovery and without influence on the measured isotope ratios, was demonstrated. As a consequence, it can be stated that the use of extraction chromatographic columns based on the resins Sr spec™ and Pb spec™ prior to isotopic analysis via single-collector – and multi-collector ICP-MS is a valuable alternative for the isolation processes that were previously adopted as standard methods in the field of geochemistry.

CHAPTER VII

Single-collector – and multi-collector ICP-MS measurement protocols

In this work, ICP-MS was used for the determination of (i) (trace) element concentrations and (ii) isotopic compositions. Several ICP-MS instruments have been used (Chapter II, § II.8) for this purpose. A quadrupole-based PerkinElmer SCIEX Elan 5000 was used for (semi-)quantitative elemental assay of Pb and various matrix elements in dissolved archaeological samples, while a quadrupole-based PerkinElmer SCIEX Elan DRC*plus*, equipped with a dynamic reaction cell (DRC), was used for quantitative elemental assay of P, Ca and Sr in dental tissue of archaeological interest. This single-collector ICP – dynamic reaction cell – mass spectrometer was also optimized for Pb isotope ratio analysis of archaeological artefacts. Further, also two multi-collector ICP-MS instruments were used in this work for isotope ratio analysis, namely, (i) a Nu Instruments Nu Plasma 500 for Pb isotope ratio analysis and (ii) a Thermo Electron Neptune for Sr isotopic analysis. This chapter presents a description of the measurement protocols developed for elemental assay and isotope ratio analysis using the instruments mentioned above.

VII.1 – Quadrupole-based ICP-MS – elemental assay

For semi-quantitative analysis (chapter II, § II.9.1), performed on the PerkinElmer Elan 5000 ICP – mass spectrometer, the calibration standard used consisted of the elements Be, Co, Rh, In, Pb and Th, each present in a concentration of 50 µg L^{-1}, and of which the intensities corresponding to the isotopes ^{9}Be, ^{59}Co, ^{103}Rh, ^{115}In, ^{208}Pb and ^{232}Th were monitored to calculate the corresponding relative sensitivity factors. For quantitative element determinations, several standards with the analytes of interest at different concentration levels were prepared. The instrumental settings and data acquisition parameters of the Elan 5000 used for both semi-quantitative and quantitative analysis are summarized in table VII.1.

VII.2 – ICP-DRC-MS – P, Ca and Sr determination

The Servatius – project (chapter X) focuses on Sr isotope ratio analysis of dental tissues of archaeological interest. As already stated higher (chapter IV, § IV.3.1), it is important to verify that the Sr analyzed at present is a reflection of the biogenic strontium in the dental tissues, and that the Sr isotope ratios are not altered by diagenetic Sr arising from contamination during burial. Bone and dentine are susceptible to diagenesis, while enamel is more resistant [Kohn *et al.*, 1999; Budd *et al.*, 2000]. One way to assess the significance of diagenesis is by monitoring the Ca/P ratio of the calcified tissue investigated [Bentley, 2006].

Table VII.1 – (semi-)quantitative analysis using the Elan 5000 ICP – mass spectrometer – (a) instrumental settings; (b) data acquisition parameters

(a) instrumental settings	
RF power	1000 W
plasma gas flow rate	15 L min^{-1}
auxiliary gas flow rate	0.8 L min^{-1}
nebulizer gas flow rate	0.80 – 0.85 L min^{-1}*
sampling cone	Ni, aperture diameter 1.0 mm
skimmer	Ni, aperture diameter 1.0 mm
sample delivery	peristaltic pump
sample uptake rate	1 mL min^{-1}
(b) data acquisition parameters	
scanning mode	peak hopping
dwell time	50 ms
settling time	5 ms
number of acquisition points per spectral peak	1
number of sweeps	20
number of readings	3
number of replicates	5
replicate time	~ 17 s per isotope
detector dead time	69 ns

* daily optimized for (i) maximum sensitivity and (ii) minimal oxide formation

It was argued that if the Ca/P ratio is near its biogenic value, what remains in the bone tissue is largely the biogenic calcium and strontium [Price *et al.*, 1994; Hoppe *et al.*, 2003; Bentley, 2006]. Besides the Ca/P ratio, also the Sr concentration had to be determined. A methodology was hence developed that allowed a simultaneous determination of P, Ca and Sr in a single instrumental run, so that in the same time, the Sr concentrations of the digested dental tissues could be determined, along with the Ca/P ratios to evaluate the occurrence of diagenesis.

VII.2.1 – Selection of the target isotopes of P, Ca and Sr

Dental tissues are largely composed of inorganic carbonate hydroxyapaptite (chapter IV, § IV.4.2), which implies that Ca and P are major elements in these tissues. The exact elemental composition of these tissues is susceptible to variation, but a value of

~ 370 000 µg g^{-1} (37 weight %), can be taken as the average Ca content [Kohn *et al.*, 1999]. The Ca/P ratio in biogenic enamel and dentine is ~ 2.1. The elemental composition of dental tissues is well reflected in that of the two certified bone reference materials NIST SRM 1400 Bone Ash and NIST SRM 1486 Bone Meal, which is summarized in table VII.2. It is clear that a significant amount of C is present in the bone matrix, and that also Na, Mg and Si are major elements, although their concentration is at least a factor of ~ 30 and ~ 60 lower than that of P and Ca, respectively.

Table VII.2 – Certified and indicative (in brackets) element concentrations in the certified bone reference materials used in this work – (a) NIST SRM 1400 Bone Ash; (b) NIST SRM 1486 Bone Meal; (c) element concentrations in a matrix-matched standard solution with the Sr concentration adjusted to 25 µg L^{-1}

	(a) NIST SRM 1400 Bone Ash	(b) NIST SRM 1486 Bone Meal	(c) matrix-matched standard
major elements (weight %)			*µg L^{-1}*
C	(n.a.)*	(18.6)	--
Na	(0.6)	(0.5)	600
Mg	0.684 ± 0.013	0.466 ± 0.017	700
Si	(0.13)	(< 0.02)	130
P	17.91 ± 0.19	12.30 ± 0.19	20 000
Ca	38.18 ± 0.13	26.58 ± 0.24	40 000
trace elements (µg g^{-1})			*µg L^{-1}*
Al	(530)	(< 1)	50
K	186 ± 6	412 ± 4	40
Fe	660 ± 27	99 ± 8	70
Zn	181 ± 3	147 ± 16	20
Sr	249 ± 7	264 ± 7	*25*
Pb	9.07 ± 0.12	1.335 ± 0.014	1

* n.a.: not available

Table VII.3 summarizes the naturally occuring isotopes of the elements P and Ca and Sr, their ionization energy and the potentially interfering ions. Calcium and strontium have several isotopes, and both elements have highly (^{40}Ca, ^{88}Sr) and lowly abundant (^{42}Ca, ^{43}Ca, ^{44}Ca, ^{46}Ca and ^{48}Ca, ^{84}Sr) isotopes. Regarding the Ca/Sr ratio of 1 000-1 500 in calcified tissues (table VII.2) and the aim of a simultaneous determination of Ca and Sr in this matrix, the combination of lowly abundant Ca isotopes and highly abundant Sr

isotopes should result in easily measurable count rates that are not excessively high for either element. The Ca/P ratio of 2.1 implies that also high P concentrations need to be measured on the only P isotope available. Phosphorus however, is ionized to a much lesser extent in the ICP because of its very high first ionization energy compared to that of Ca and Sr (table VII.3), resulting in a much lower P sensitivity. On the basis of these considerations, it was expected that the simultaneous determination of the mono-isotopic P, Ca via its low abundant isotopes and Sr via its higher abundant isotopes could be accomplished.

Table VII.3 – Ionization energy and representative isotopic composition of P, Ca and Sr, potentially interfering ions in Ar ICP-MS and their background-equivalent concentration. Ionization energies from [Moore, 1970]; isotopic abundances from [De Laeter *et al.*, 2003].

	ionization energy (eV)	isotope(s)	abundance (%)	potential interfering ion(s)	BEC (%)
(a) P	10.486	^{31}P	100	$^{14}N^{16}O^{1}H^{+}$, $^{15}N^{16}O^{+}$	20
(b) Ca	6.113	^{40}Ca	96.941	$^{40}Ar^{+}$, $^{40}K^{+}$	n.d.
		^{42}Ca	0.647	$^{14}N_3^{+}$, $^{26}Mg^{16}O^{+}$, $^{40}Ar^{1}H_2^{+}$, $^{84}Sr^{2+}$	20
		^{43}Ca	0.135	$^{14}N_3{}^{1}H^{+}$, $^{27}Al^{16}O^{+}$, $^{86}Sr^{2+}$	3
		^{44}Ca	2.086	$^{12}C^{16}O_2^{+}$, $^{14}N_2{}^{16}O^{+}$, $^{28}Si^{16}O^{+}$, $^{88}Sr^{2+}$	6
		^{46}Ca	0.004	$^{14}N^{16}O_2^{+}$	n.d.
		^{48}Ca	0.187	$^{31}P^{16}O^{1}H^{+}$, $^{36}Ar^{12}C^{+}$	n.d.
(c) Sr	5.695	^{84}Sr	0.56	see chapter VI, table VI.1.a	n.d.
		^{86}Sr	9.86		8
		^{87}Sr	7.00		n.d.
		^{88}Sr	82.58		9

* n.d.: not determined

Phosphorus suffers from N- and O- based interferences at its m/z ratio of 31. The most abundant Ca isotope, ^{40}Ca, is spectrally interfered by the intense $^{40}Ar^{+}$ peak. The mass resolution required to resolve these isobaric ions is ~ 200 000, making the ^{40}Ca isotope inaccessible for determination via standard quadrupole-based and even high resolution ICP-MS instrumentation. The use of NH_3 in a dynamic reaction cell was shown to result in separation of these isobaric interferences [Hattendorf *et al.*, 2005; Boulyga *et al.*, 2007]. Besides the ^{40}Ca isotope, also the five other much lower abundant Ca isotopes suffer from spectral interferences. All of these isotopes are hindered by plasma- and solvent-related interferences (*e.g.*, ArH_2^{+}, N_2O^{+}, NO_2^{+}). Because of the very low abundance of ^{46}Ca, and

the potentially important P-based interference (POH^+) on ^{48}Ca, it was decided not to consider the ^{46}Ca and ^{48}Ca isotopes for elemental assay. The isotopes ^{42}Ca, ^{43}Ca and ^{44}Ca were selected as target Ca isotopes. The interference from Sr^{2+} on the selected Ca isotopes was expected as negligible regarding (i) the much lower Sr abundance compared to the Ca abundance (Ca/Sr = 1 000-1 500) and (ii) the low amount of Sr^{2+} ions formed in the ICP (chapter II, § II.9). The importance of the other potentially interfering ions was experimentally evaluated. The N-, O- and Ar-based interferences were expected to be more important than the matrix-based interferences (*e.g.*, MgO^+, AlO^+) because of the very high relative Ca concentrations.

The low abundance of ^{84}Sr and the isobaric ^{87}Rb interference on ^{87}Sr exclude the use of these isotopes, leaving ^{86}Sr and ^{88}Sr as target Sr isotopes. These isotopes may be spectrally interfered by $ArCa^+$ molecular ions (chapter VI, table VI.1.a) and Ca_2^+ dimers, especially in the case of dental tissues, where Ca is the major matrix constituent.

In order to obtain a clear insight into the extent to which spectral interferences are potential problems in the determination of the target elements via the selected isotopes (^{31}P, ^{42}Ca, ^{43}Ca, ^{44}Ca, ^{86}Sr and ^{88}Sr), so-called 'background-equivalent concentrations' (BEC) were determined. The background-equivalent concentration represents the contribution of interfering ion(s) to the analyte signals, and is expressed as the apparent analyte concentration caused by the interfering ion(s). The signal intensities at the m/z ratios corresponding to the Ca isotopes in a matrix-matched standard (table VII.2.c) in which no Ca is present, can be translated into Ca-equivalent concentrations using the sensitivity for Ca. An analogous approach was followed for P and Sr, and the background-equivalent concentrations can be expressed relative to the concentration present, as summarized in table VII.3. It can be seen that the major interference affects the use of the ^{31}P and ^{42}Ca isotopes, and amounts to ~ 20 % of the analyte concentration, while the magnitude of interference is similar (~ 10 % of the analyte concentration) for ^{44}Ca, ^{86}Sr and ^{88}Sr. Obviously, a measurement protocol is required that provides interference-free conditions for the determination of the target isotopes.

VII.2.2 – Optimization of ICP-DRC-MS for P, Ca and Sr determination

The use of a quadrupole-based ICP-MS instrument, equipped with a dynamic reaction cell, allows chemical resolution via selective ion-molecule reactions (chapter II, § II.6.2), as has already been described for the determination of Ca and P. Methane (CH_4) has been shown as a suitable reaction gas for Ca concentration [Chen and Jiang, 2002; Wu *et al.*, 2003]

and isotope ratio determinations [Stürup *et al.*, 2006], while ammonia (NH_3) has been reported as useful in the measurement of the $^{44}Ca/^{40}Ca$ ratio [Hattendorf *et al.*, 2005; Boulyga *et al.*, 2007]. However, the efficiency of NH_3 in removing spectral interferences on other isotopes than ^{40}Ca and ^{44}Ca was not reported yet. Phosphorus determination can be performed by the oxidation of P^+ to PO^+ by means of using oxygen (O_2) in the dynamic reaction cell, followed by P determination on m/z 47, corresponding to the $^{31}P^{16}O^+$ signal [Wu *et al.*, 2003; Bandura *et al.*, 2004; Yang and Jiang, 2004]. Since the performance of CH_4 had already been studied in detail for Ca isotope ratio determinations [Stürup *et al.*, 2006], ammonia (NH_3) was selected to play the role of reaction gas, and its suitability for interference-free determination of the Ca isotopes and for the elimination of interfering molecular ions on $^{31}P^+$, $^{86}Sr^+$ and $^{88}Sr^+$ was evaluated.

When NH_3 is used in the dynamic reaction cell, the dominating reaction mechanism that takes place is a charge-transfer reaction (chapter II, § II.6.2.2.3). Whether or not a reaction will take place can be estimated by means of the relative first ionization energies. The ionization energy of Ca and Sr (table VII.3) is lower than that of NH_3 (10.3 eV), so that no charge transfer between Ca^+ and Sr^+ on one hand and NH_3 on the other hand, can take place. The ionization energies of C, N, O, Ar and molecules that are a combination of these elements are in the range of 11-16 eV, so that positively charged ions consisting of the cited atoms can transfer their charge to a neutral NH_3 molecule. In the case of Ar, the Ar^+ ions formed in the ICP will react with NH_3 in the dynamic reaction cell, resulting in Ar and NH_3^+. Next to thermodynamic conditions, also kinetic conditions must be favorable (chapter II, § II.6.2.2.2). However, it can be taken as a guideline that in the case of charge transfer reactions, a spontaneous reaction will proceed at a sufficiently high reaction rate. Interference on Sr is mainly due to $ArCa^+$ ions, and their reaction behavior with NH_3 was experimentally evaluated. Phosphorus has a first ionization energy that is slightly higher than that of NH_3 (table VII.3), so that it is expected from thermodynamics that P^+ will react with NH_3 to form P and NH_3^+. For this reason, it was expected that a different reaction gas (*e.g.*, O_2) would be required for P determination, so that in what follows below, no optimization for P is described.

VII.2.2.1 – Optimization of the NH_3 gas flow rate

The optimum reaction gas flow rate is found where the signal arising from the analyte ion is maximized with respect to the signal arising from the interfering ion(s). In what follows, the signal corresponding to the analyte and that corresponding to the interfering ion will

be referred to as 'signal' and 'background', respectively. Optimizing the reaction gas flow rate hence consists in determining the maximal signal-to-background ratio, and implies the fundamental requirement that the analyte and the background show a different behavior relative to the reaction gas. The ion signal obtained is not a linear function of the reaction gas flow (pressure). The signal profiles obtained for the analyte, Ca in this case, are the result of two combined phenomena: (i) collisional focusing/scattering and (ii) sequential damping of ion energies [Bandura *et al.*, 2001]. As the reaction gas flow rate, and thus, the pressure in the cell, is increased, the ions migrate towards the axis of the quadrupole, resulting in an increase in ion transmission efficiency. The detected ion signal thus increases until scattering losses dominate. Collisions with the gas at higher pressure cause sequential damping of the ion energy, and the number of collisions that an ion experiences increases because of a lower velocity of the ions, resulting in a decreasing ion signal. The background signal will remain nearly unchanged at low gas flow rates, but with an increasing pressure inside the cell, the interfering ions will react with the reaction gas, resulting in a decreasing ion signal [Bandura *et al.*, 2001; Tanner *et al.*, 2002].

First, the optimum reaction gas flow rate was determined for Ca. Hereto, an 800 µg L^{-1} Ca standard solution in 0.14 M HNO_3 was prepared (resulting intensities are referred to as 'signal'). An 0.14 M HNO_3 solution was used to monitor the 'background' signals, since the major interferences expected are N- and O- based and hence arise from the HNO_3 matrix and the ambient air. The NH_3 gas flow rate was increased in steps of 0.1 mL min^{-1} in the range of 0 to 1 mL min^{-1}. All gas flow rates are expressed in Ar-equivalent units (chapter II, § II.6.2.1); the conversion factor for NH_3 equals 0.56. The experimental findings are displayed in figure VII.1. As can be seen in these figures, the signal/background ratio increases with increasing NH_3 flow rates. The most drastic improvement in the signal to background ratio is observed for ^{42}Ca. At NH_3 flow rates above 0.5 mL min^{-1}, the ratio is improved with a factor of ~ 200 compared to vented mode. The improvement is less pronounced for the other Ca isotopes. An improvement with a factor of ~ 20 is observed for ^{43}Ca at a flow rate higher than 0.6 mL min^{-1}, while the signal/background ratio at m/z 44 increases with a factor of ~ 10 over the optimization range.

A similar optimization was performed for Sr. Hereto, a 25 µg L^{-1} Sr standard solution and a 40 mg L^{-1} Ca background solution, both in 0.14 M HNO_3, were prepared and monitored with increasing NH_3 flow rate. The results are displayed in figure VII.2. An improvement in the signal/background ratio over a factor of 10 is observed for both Sr isotopes at a gas flow rate of 1 mL min^{-1} compared to vented mode.

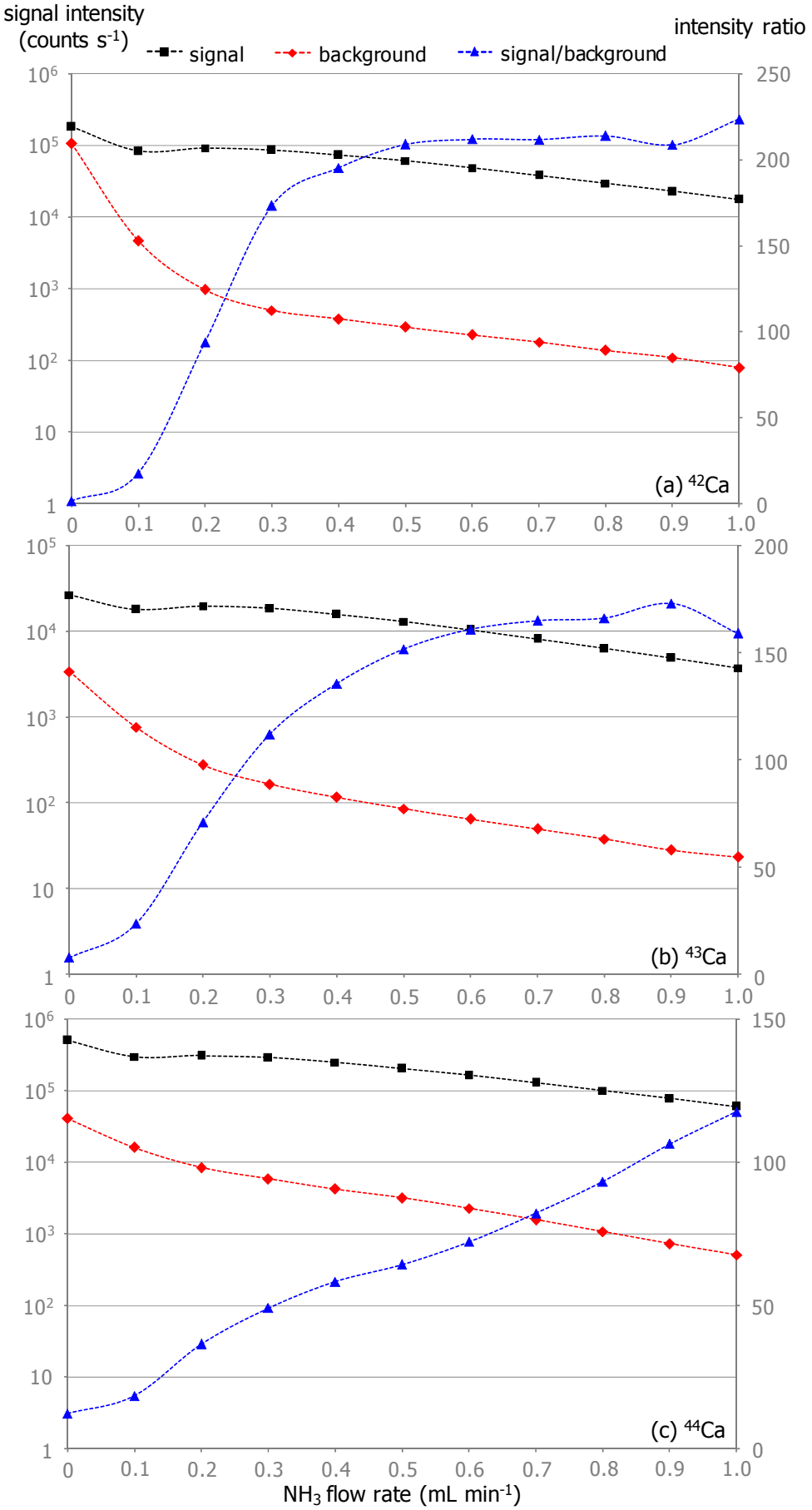

Figure VII.1 – Signal intensities of Ca and interfering ions versus the NH_3 flow rate

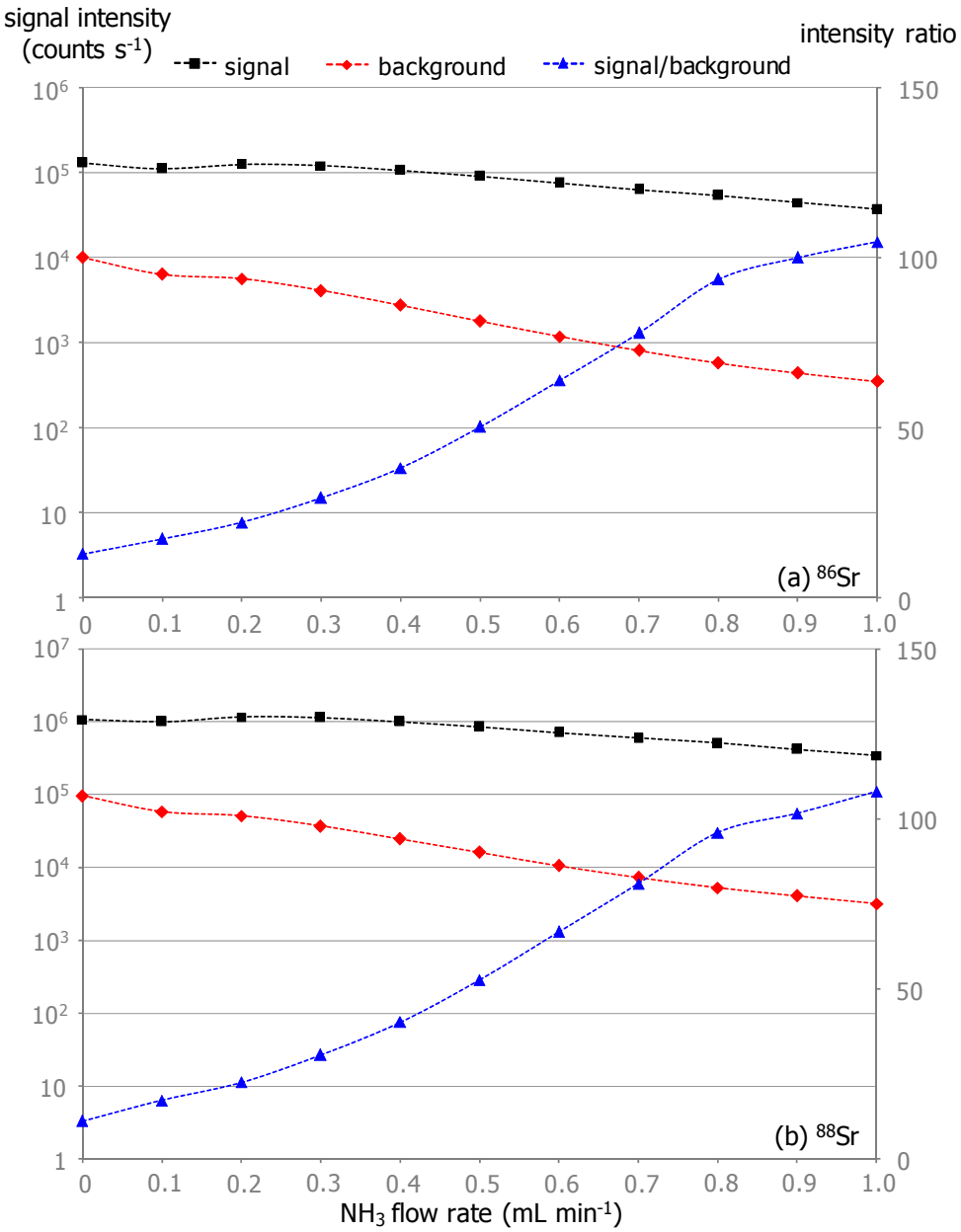

Figure VII.2 – Signal intensities of Sr and interfering ions versus the NH_3 flow rate

From the experimental data obtained for the lowly abundant Ca and the highly abundant Sr isotopes, a compromise value had to be determined for the NH_3 flow rate, since the aim is the simultaneous determination of Ca and Sr. The most significant improvement in signal-to-background ratio is observed for the ^{42}Ca and ^{43}Ca isotopes, while the improvement is less pronounced for the ^{44}Ca, ^{86}Sr and ^{88}Sr isotopes. The optimal NH_3 flow rate is found from 0.6 mL min^{-1} onwards for Ca, while for Sr, a continuous increase of the signal/background ratio was established, which becomes less pronounced from 0.8 mL min^{-1}. Herefrom, an NH_3 flow rate of 0.8 mL min^{-1} was taken as the compromise value. Under these conditions, the signal/background ratios are improved with a factor of ~ 200 for ^{42}Ca, ~ 20 for ^{43}Ca and ~ 10 for ^{44}Ca, ^{86}Sr and ^{88}Sr.

VII.2.2.2 – Optimization of the rejection parameter q (RPq)

The setting of the rejection parameter q (RPq) allows to remove newly formed ions in the dynamic reaction cell (Chapter II, § II.6.2.2.5). The measurements for optimization of the NH_3 gas flow rate were performed at an RPq setting of 0.45, which is the standard value. However, in order to remove molecular interfering ions potentially formed inside the dynamic reaction cell, an optimization of the RPq was carried out. Increasing the RPq value implies that the low-mass cutoff boundary of the DRC quadrupole bandpass window is increased. As a consequence, parent ions that give rise to new interfering ions and with an m/z ratio higher than that removed at an RPq setting of 0.45, are eliminated from the DRC quadrupole. In order to determine the optimal RPq setting, two matrix-matched standards (table VII.2) were prepared, and in each standard, either Ca or Sr were omitted since the aim of the optimization is to obtain the signals arising from interfering ions on the m/z ratios of these elements. Instead of Ca and Sr, Sc and Rh were respectively added to the standard in a concentration of 25 µg L^{-1}. The Sc signal at m/z 45 was used as the reference signal for Ca, while the Rh signal at m/z 103 was used as the reference signal for Sr. The signal corresponding to Sc and Rh can be referred to as 'signal', while the signal corresponding to interfering ions on m/z ratios of Ca and Sr are referred to as 'background'. The optimum RPq value is found there where the signal/background ratio reaches its maximum value. The ion intensities for Sc, Rh and interfering ions on m/z ratios corresponding to the selected Ca and Sr isotopes were monitored with an RPq setting ranging from 0.35 to 0.75 in steps of 0.1, and resulted in the diagrams presented in figure VII.3. A general trend is that the signal/background ratio increases with the RPq value. Increasing the RPq has the largest influence on the m/z ratio 43. Here, an improvement of the signal/background ratio of ~ 20 is achieved in the RPq range monitored. A large jump in the ratio of signal to background is observed at an RPq value of 0.65, corresponding to the removal of a precursor ion with an m/z ratio around 30. Suggested candidates are Al, Si and P, that might respectively form $^{27}Al^{16}O^+$, $^{29}Si^{14}N^+$ and $^{31}P^{12}C^+$ in the DRC. The latter seems the least likely since no C was added to the matrix-matched standard (table VII.2). The identification of the interfering ion was beyond the aim of this work and hence, not further investigated. The increase in RPq has a smaller effect on the other m/z values for Ca, and results in an improvement of the signal/background ratio with a factor of ~ 7 for ^{42}Ca and ~ 15 for ^{44}Ca. The improvement on the ^{86}Sr and ^{88}Sr isotopes is limited to a factor of ~ 1.5. It follows that the best signal-to-background ratio is obtained at an RPq value of 0.75 for all target isotopes. However,

the limits of the bandpass window in the DRC quadrupole are not sharply defined, so that the risk of analyte loss increases with increasing RPq. Therefore, 0.65 was taken as the optimum RPq setting.

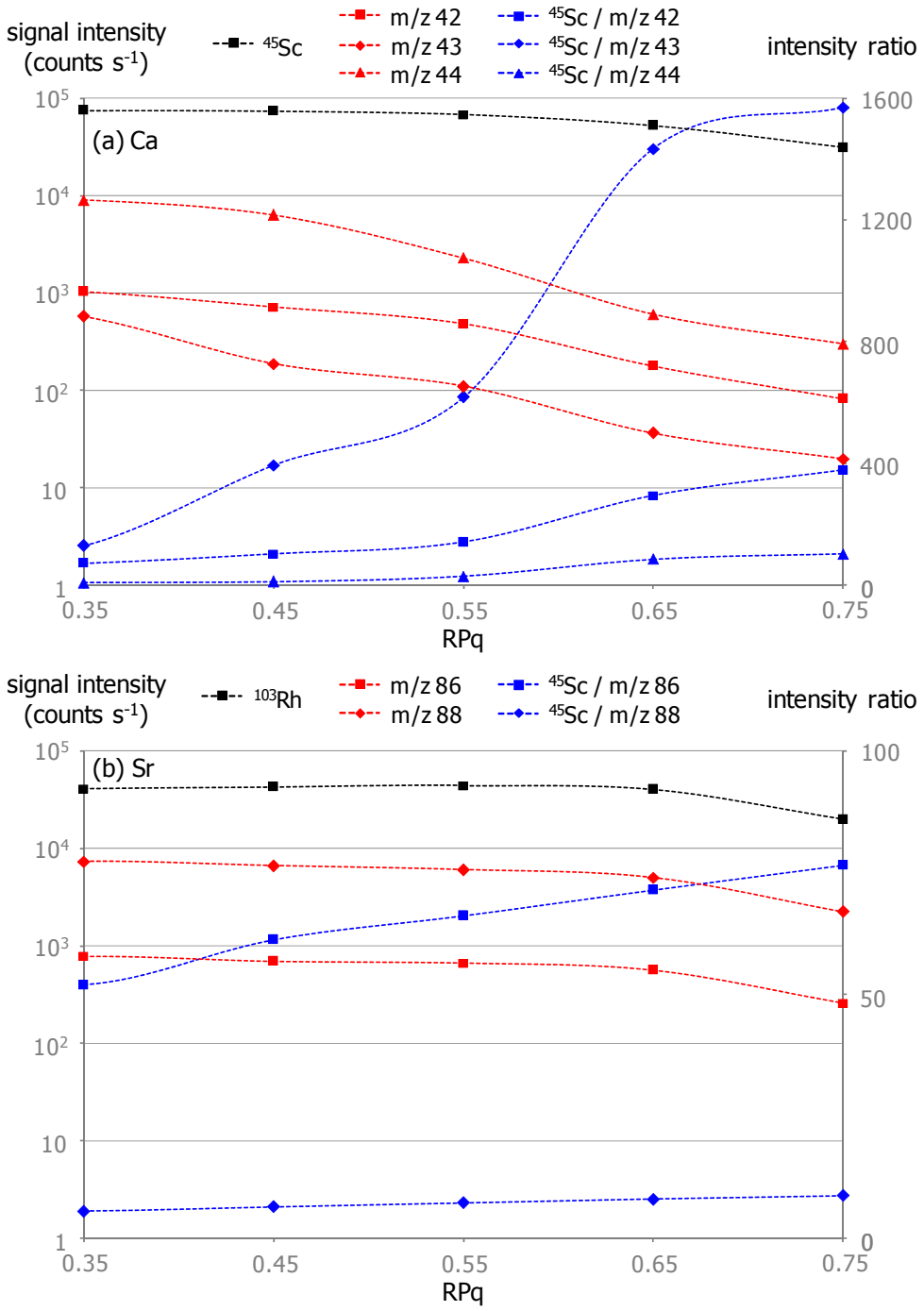

Figure VII.3 – Optimization of the rejection parameter q (RPq) for (a) Ca and (b) Sr

VII.2.2.3 – Determination of phosphorus

As already stated before, the reaction of P^+ and NH_3 is thermodynamically favored, so that phosphorus is expected to be lost from the DRC quadrupole. This would imply the

need of using a different reaction gas, *e.g.*, O_2. However, the measurement of standard solutions containing phosphorus with NH_3 in the dynamic reaction cell, introduced at a flow rate of 0.8 mL min^{-1}, resulted in a linear relation between signal intensity and concentration. From this observation, it was expected that the determination of phosphorus is also possible via the measurement protocol developed. A thermodynamical explanation for the experimental observation could be that the ionization energy of NH_3 (10.3 eV) is only slightly lower than that of P (10.5 eV), so that an equilibrium condition is reached in the conversion of P^+ to P. From a kinetic point of view, it seems likely that the reaction rate of the conversion of NO^+ and NOH^+ is higher than the conversion rate of P^+ to P with NH_3, resulting in a suppression of the interfering signal relative to the P^+ signal. A detailed study on the P^+ and NO^+/NOH^+ behavior in the DRC pressurized with NH_3 was beyond the aim of this study, but P was also experimentally determined under the same conditions as Ca and Sr.

VII.2.3 – Validation of the ICP-DRC-MS measurement protocol

The measurement protocol developed was applied to the simultaneous determination of P, Ca and Sr in digested certified bone reference materials NIST SRM 1400 Bone Ash and NIST SRM 1486 Bone Meal. Vanadium and rhodium were selected as internal standards, where the ^{51}V isotope served as internal standard for P and Ca, while the Sr signals were referenced to the ^{103}Rh signal. The instrumental settings and data acquisition parameters for the simultaneous determination of P, Ca and Sr via ICP-DRC-MS with NH_3 as a reaction gas are summarized in table VII.4.

The experimentally obtained P, Ca and Sr concentrations and recoveries for the certified bone reference materials NIST SRM 1400 Bone Ash and NIST SRM 1486 Bone Meal have already been summarized in chapter V, table V.3. As can be seen there, the agreement between the experimental results and the certified values is excellent. The concentrations reported are the average value of the concentrations found via the individual isotopes, and the agreement between the individual results is excellent. This implies that a simultaneous and interference-free determination of the Ca and Sr isotopes is possible, and that the various interfering molecular ions are successfully removed in the dynamic reaction cell via chemical resolution. It has not been proven that the interferences on P^+ are resolved, but the experimental results show that P determination is nevertheless successful. Detection limits of the measurement protocol for a bone matrix were found more than sufficient for the application presented here, and were established as 3 µg L^{-1}

for P, 2 µg L^{-1} for Ca via its ^{42}Ca, ^{43}Ca and ^{44}Ca isotopes, and 200 ng L^{-1} for Sr determined via its ^{86}Sr and ^{88}Sr isotopes.

Table VII.4 – Simultaneous determination of P, Ca and Sr using the Elan DRC*plus* ICP – mass spectrometer – (a) instrumental settings;(b) data acquisition parameters; (c) DRC parameters

(a) instrumental settings	
RF power	1200 W
plasma gas flow rate	17 L min^{-1}
auxiliary gas flow rate	1.2 L min^{-1}
nebulizer gas flow rate	0.95 – 1.00 L min^{-1}*
sampling cone	Ni, aperture diameter 1.1 mm
skimmer	Ni, aperture diameter 0.9 mm
extraction lens voltage	10 – 12 V*
sample delivery	peristaltic pump
sample uptake rate	1 mL min^{-1}
(b) data acquisition parameters	
isotopes monitored	^{31}P, ^{42}Ca, ^{43}Ca, ^{44}Ca, ^{51}V, ^{86}Sr, ^{88}Sr, ^{103}Rh
scanning mode	peak hopping
dwell time	50 ms
settling time	3 ms
number of acquisition points per spectral peak	1
number of sweeps	20
number of readings	3
number of replicates	5
replicate time	~ 16 s per isotope
(c) DRC parameters	
NH_3 gas flow rate	0.8 mL $min^{-1\$}$
RPa	0
RPq	0.65

* daily optimized for maximum sensitivity and < 3% oxide formation
$ gas flow rate in Ar-equivalent units. The conversion factor for NH_3 equals 0.56.

VII.2.4 – Conclusions

A measurement protocol was developed for the simultaneous determination of P, Ca and Sr in dental tissues. Hereto, NH_3 was used as a reaction gas in the dynamic reaction cell

of a DRC-equipped quadrupole-based ICP – mass spectrometer. It was shown that, compared to vented mode, a significant improvement of the signal-to-background ratio is obtained at a gas flow rate of 0.8 mL min^{-1} in combination with an RPq setting of 0.65, and that the detection limits for P, Ca and Sr are improved by at least a factor of 10. The method was validated by application to certified bone reference materials and demonstrated accurate and reliable. The method was applied to determine the Ca/P ratio of dental tissues of archaeological interest to evaluate the biogenic integrity of these tissues after burial (chapter X).

VII.3 – MC-ICP-MS – Sr isotopic composition

After extraction chromatographic isolation of Sr (chapter VI, § VI.3.2.1), the purified Sr fraction of the archaeological samples was present in 0.05 M HNO_3. The Sr concentration was subsequently adjusted to ~ 200 µg L^{-1} by dilution with 0.14 M HNO_3 and the diluted samples were subsequently submitted to strontium isotope ratio analysis using a Thermo Electron Neptune (chapter II, § II.8). Instrumental settings and data acquisition parameters for this instrument are summarized in table VII.5. The instrument was operated at low resolution mode (R = 400). Strontium isotope ratios were measured using static multicollection where the cups Low 3, Low 2, Low 1, Axial, High 1 and High 2 were used to monitor the ion intensities corresponding to ^{83}Kr, $^{84}Sr + ^{84}Kr$, ^{85}Rb, $^{86}Sr + ^{86}Kr$, $^{87}Sr + ^{87}Rb$ and ^{88}Sr, respectively (table VII.5.b). Data acquisition was done in 30 cycles of 5 s integration, grouped in blocks of 5 cycles. Outliers were removed by the software on the basis of a 2s-test (95 % confidence interval). A solution of 200 µg L^{-1} Sr resulted in a typical total Sr ion beam of 8-10 V. The samples were run using the sample-standard bracketing technique with a 200 µg L^{-1} Sr isotopic standard solution of NIST SRM 987 $SrCO_3$, that was previously conducted through the extraction chromatographic isolation procedure. Blank Sr signals were always negligible compared to the Sr intensities encountered for standards and samples (< 0.1 %). Between consecutive runs, the sample introduction system was rinsed a few minutes with 0.14 M HNO_3 in order to minimize memory effects.

Russell's law (chapter III, equation III.11) was used for mass discrimination correction on the basis of the invariant $^{86}Sr/^{88}Sr$ ratio (= 0.1194). The intensity obtained for ^{83}Kr was used to correct the intensities obtained at m/z 84 and 86 for Kr interferences, using the numerical $^{84}Kr/^{83}Kr$ and $^{86}Kr/^{83}Kr$ ratios of 4.95652 and 1.50435, respectively, and taking into account mass discrimination on these experimental ratios. The average difference

between the uncorrected and the Kr-corrected $^{87}Sr/^{86}Sr$ ratio amounts to ~ 540 ppm. The intensity obtained on m/z 87 was corrected for the ^{87}Rb contribution using a numerical $^{87}Rb/^{85}Rb$ ratio of 0.38565 and the signal obtained for ^{85}Rb, taking into account mass discrimination on this experimental ratio. Rubidium correction resulted in an average shift of the $^{87}Sr/^{86}Sr$ ratio over ~ 140 ppm.

Table VII.5 – Sr isotopic analysis using the Neptune multi-collector ICP – mass spectrometer – (a) instrumental settings; (b) cup configuration; (c) data acquisition parameters; (d) experimental values, external precision and accepted [Nu, 2001] values for NIST SRM 987 $SrCO_3$.

(a) instrumental settings

RF power	1200 W
plasma gas flow rate	13 L min^{-1}
auxiliary gas flow rate	0.7 L min^{-1}
nebulizer gas flow rate	1.0 L min^{-1}*
sampling cone	Ni, aperture diameter 1.1 mm
skimmer	Ni, aperture diameter 0.9 mm
extraction lens voltage	4 V*
mass resolution	400
sample delivery	auto aspiration
sample uptake rate	50 µL min^{-1}

(b) cup configuration

L3	L2	L1	Ax	H1	H2
^{83}Kr	^{84}Sr ^{84}Kr	^{85}Rb	^{86}Sr ^{86}Kr	^{87}Sr ^{87}Rb	^{88}Sr

(c) data acquisition parameters

magnet delay time	3 s
integration time	5 s
number of cycles	5 per block
number of blocks	6
measurement time	150 s

(d) experimental and accepted values for NIST SRM 987 $SrCO_3$

ratio	experimental	2s	RSD (%)	accepted
$^{84}Sr/^{86}Sr$	0.05640	0.00016	0.14	0.05649
$^{84}Sr/^{88}Sr$	0.006734	0.000020	0.14	0.006748
$^{87}Sr/^{86}Sr$	0.710230	0.000044	0.0030	0.710248

* daily optimized for maximum ^{88}Sr sensitivity

The external precision of the measurement protocol was calculated on the basis of the mass discrimination corrected values retrieved for the NIST SRM 987 $SrCO_3$ isotopic standard throughout the entire measurement session (3 days). An external precision of 30 ppm (0.003 % RSD) was established on the $^{87}Sr/^{86}Sr$ ratio, and of 1 400 ppm (0.14 % RSD) on the $^{84}Sr/^{86}Sr$ and $^{84}Sr/^{88}Sr$ ratios (table VII.5.d). Within the external precision, the experimental values retrieved for NIST SRM 987 $SrCO_3$ are in excellent agreement with the accepted literature values [Thirlwall, 1991; Walder and Freedman, 1992; Nu, 2001; Faure and Mensing, 2005].

VII.4 – MC-ICP-MS – Pb isotopic composition

After the Pb isolation procedure (chapter VI, § VI.4.2), the Pb fraction of the archaeological samples was present in a 0.05 M $(NH_4)_2C_2O_4$ solution. In order to remove the ammonium oxalate present in the Pb fractions prior to multi-collector ICP-MS Pb isotope ratio analysis, an aliquot of the sample was evaporated to dryness, followed by addition of 1 mL 14 M HNO_3 + 1 mL 10 M H_2O_2. After a few hours, the sample was evaporated to dryness again. Finally, the residue was taken up in 0.5 M HNO_3 + 0.2 M HF, thereby adjusting the Pb concentration to ~ 30 µg L^{-1}. Thallium (NIST SRM 997 Thallium isotopic standard) was added in a concentration of ~ 7.5 µg L^{-1}, resulting in a Pb/Tl ratio of ~ 4.

The Pb isotope ratios reported in this work were obtained using a Nu Instruments' Nu Plasma 500 (chapter II, § II.8). Instrumental settings and data acquisition parameters for this instrument are summarized in table VII.6. The instrument was run at a standard mass resolution of 450. Lead isotope ratio measurements were carried out by static multicollection, where the detectors Low 4, Low 3, Low 2, Low 1, Axial, High 1 and High 2 were used to record the ion intensities of ^{202}Hg, ^{203}Tl, ^{204}Pb + ^{204}Hg, ^{205}Tl, ^{206}Pb, ^{207}Pb and ^{208}Pb, respectively. Data acquisition was done in 60 cycles of 5 s integration, grouped in blocks of 20 cycles. Outliers were removed by the software on the basis of a 2s-test (95 % confidence interval). A 30 µg L^{-1} Pb solution doped with 7.5 µg L^{-1} Tl typically yielded a Pb total ion beam intensity of 5-7 10^{-11} A. The samples were run using the sample-standard bracketing technique with a 30 µg L^{-1} Pb isotopic standard solution of NIST SRM 981 Common Lead, that was previously conducted through the extraction chromatographic isolation procedure, doped with 7.5 µg L^{-1} Tl (NIST SRM 997 Thallium isotopic standard). The intensity measured at m/z 204 was corrected for the ^{204}Hg interference using a $^{204}Hg/^{202}Hg$ ratio of 0.229. The $^{204}Hg/^{204}Pb$ ratio was found as

Table VII.6 – Pb isotopic analysis using the Nu Plasma 500 multi-collector ICP – mass spectrometer – (a) instrumental settings; (b) cup configuration; (c) data acquisition parameters; (d) experimental values, external precision and accepted [Galer and Abouchami, 1998] values for NIST SRM 981 Common Lead.

(a) instrumental settings

RF power	1300 W
plasma gas flow rate	13 L min^{-1}
auxiliary gas flow rate	0.7 L min^{-1}
nebulizer gas flow rate	1.0 L min^{-1}*
sampling cone	Ni, aperture diameter 1.1 mm
skimmer	Ni, aperture diameter 0.9 mm
extraction lens voltage	4 V*
mass resolution	450
sample delivery	auto aspiration (Aridus)
sample uptake rate	80 µL min^{-1}

(b) cup configuration

L4	L3	L2	L1	Ax	H1	H2
^{202}Hg	^{203}Tl	^{204}Pb ^{204}Hg	^{205}Tl	^{206}Pb	^{207}Pb	^{208}Pb

(c) data acquisition parameters

magnet delay time	3 s
integration time	5 s
number of cycles	20 per block
number of blocks	3
measurement time	300 s

(d) experimental and accepted values for NIST SRM 981 Common Lead

ratio	experimental	2s	RSD (%)	accepted
$^{206}Pb/^{204}Pb$	16.9436	0.0064	0.0188	16.9405
$^{207}Pb/^{204}Pb$	15.4995	0.0054	0.0176	15.4963
$^{208}Pb/^{204}Pb$	36.7305	0.0139	0.0189	36.7219
$^{207}Pb/^{206}Pb$	0.91478	0.00009	0.0050	0.91475
$^{208}Pb/^{206}Pb$	2.16771	0.00019	0.0044	2.16771
$^{208}Pb/^{207}Pb$	2.3697	0.0002	0.0039	2.3697

* daily optimized for maximum ^{208}Pb sensitivity

negligible in all the samples investigated (average: 4 10^{-5}). Blank Pb signals always were below 1 %, and in most cases, even less than 0.1 % of the Pb signals encountered for samples and standards. Thus, blank contributions could be neglected, but for the sake of

consistency, a blank correction was always performed. Between two consecutive runs, the sample introduction system was rinsed with 0.5 M HNO_3 for a few minutes in order to minimize memory effects.

Mass discrimination correction was performed via Russell's law (chapter III, equation III.11) following the empirical method first described for Cu and Zn isotopes [Maréchal *et al.*, 1999] applied to Pb and Tl isotopes [White *et al.*, 2000]. Russell's equation was used to calculate the mass discrimination factors β_{Tl} and β_{Pb} using the certified $^{205}Tl/^{203}Tl$ ratio of 2.38714 for NIST SRM 997 Thallium isotopic standard and the accepted $^{208}Pb/^{206}Pb$ ratio of 2.16771 for NIST SRM 981 Common Lead [Galer and Abouchami, 1998], respectively. Plotting β_{Pb} versus β_{Tl} for the standard solution, obtained throughout the entire measurement session resulted in a linear relation. This relation was used to calculate the mass discrimination factor β_{Pb} for every unknown sample from the corresponding experimentally determined β_{Tl} value for that sample, and the mass discrimination factor β_{Pb} was subsequently used to calculate the true Pb isotope ratios.

The external precision reported on the samples was calculated by means of the Pb isotope ratios obtained for the NIST SRM 981 Common Lead standard during the entire measurement session (5 days), and was established to be 180-190 ppm (0.018-0.019 % RSD) for the ratios with ^{204}Pb, and 40-50 ppm (0.004-0.005 % RSD) for the other ratios (table VII.6.d). Within the external precision, the average Pb isotope ratios obtained for NIST SRM 981 Common Lead throughout the entire session match the accepted values [Galer and Abouchami, 1998] very well.

VII.5 – SC-ICP-DRC-MS – Pb isotopic composition

As already discussed higher (chapter III, § III.3.1), the use of a non-reactive collision gas (*e.g.*, Ne, Ar) in the dynamic reaction cell of a single-collector quadrupole-based ICP-MS instrument results in an improved isotope ratio precision [Bandura and Tanner, 1999; Bandura *et al.*, 2000]. Ions extracted from the ICP on slightly different moments are mixed in the cell, thereby mitigating the effect of short-term fluctuations on the measured isotope ratio and resulting in a better isotope ratio precision [Bandura and Tanner, 1999; Bandura *et al.*, 2000]. A measurement protocol for Pb isotope ratio determination via single-collector ICP – dynamic reaction cell – MS (SC-ICP-DRC-MS) was developed, on the basis of the use of a collision gas in the DRC in order to obtain improved isotope ratio precisions (< 0.2 % RSD) on Pb isotopic compositions compared to the precision attainable with standard quadrupole-based ICP-MS.

VII.5.1 – Selection of a collision gas and optimization of the flow rate

Two inert gases, Ne and Ar, were examined as candidate collision gases. The effect of three parameters on the Pb signal intensities measured and the Pb isotope ratio precisions obtained, was investigated by registering the signals for ^{206}Pb, ^{207}Pb and ^{208}Pb while monitoring a 25 µg L^{-1} NIST SRM 981 Common Lead standard solution. The influence of the collision gas flow rate on the Pb intensity was evaluated by varying the gas flow rate from 0.1 to 0.7 mL min^{-1} in steps of 0.1 mL min^{-1} (figure VII.4). In the case of Ne and Ar, that are both noble gases, the conversion factor between the Ar-equivalent gas flow rate and the actual flow rate equals 1, so that all the gas flow rates given below represent the actual gas flow rates. At a flow rate of 0.1 mL min^{-1}, a signal decrease, compared to vented mode (no collision gas in the DRC), of 13 % with Ar and 4 % with Ne, was observed. The higher the flow rate, the more Ar suppresses the Pb signals compared to Ne: at 0.7 mL min^{-1}, the suppression by Ar is 98 % compared to only 20 % by Ne. This effect can most likely be attributed to the higher mass of Ar (~ 40 u) compared to that of Ne (~ 20 u): scattering losses of Pb ions are less pronounced with the lighter collision gas Ne.

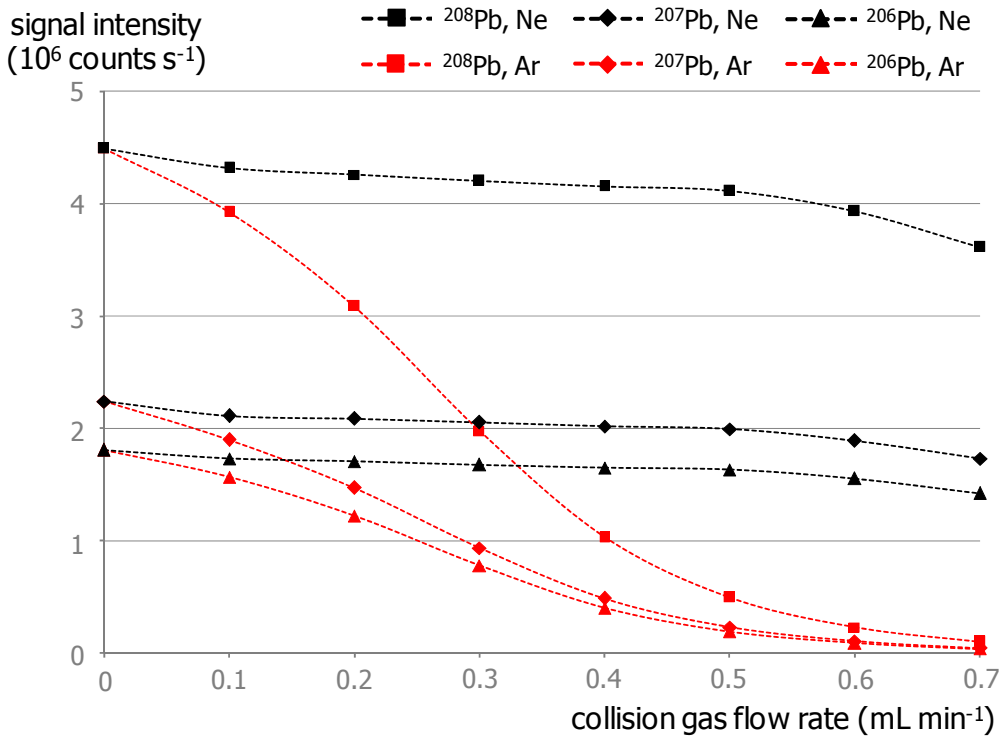

Figure VII.4 – Pb signal intensity as a function of the Ne – and Ar gas flow rate

Then, the isotope ratio precision attainable with a Ne- or Ar-pressurized cell was compared to that typical for vented mode. The % RSD-values as a function of the Ne –

and Ar gas flow rate (0.1 to 0.7 mL min^{-1} in steps of 0.1 mL min^{-1}) were determined for the $^{207}Pb/^{206}Pb$ and $^{208}Pb/^{206}Pb$ ratios (figure VII.5), and follow the same pattern. With Ar, the Pb isotope ratio precision deteriorates with increasing flow rate, but at 0.1 mL min^{-1}, the precision is similar to that obtained with Ne at the same flow rate. In the case of Ne, the precision is optimum at 0.1 mL min^{-1} (~ 0.11 % RSD), but from a gas flow rate of 0.3 mL min^{-1} onwards, the precision deteriorates to ≥ 0.17 % RSD for the $^{207}Pb/^{206}Pb$ ratio and to ≥ 0.12 % RSD for the $^{208}Pb/^{206}Pb$ ratio.

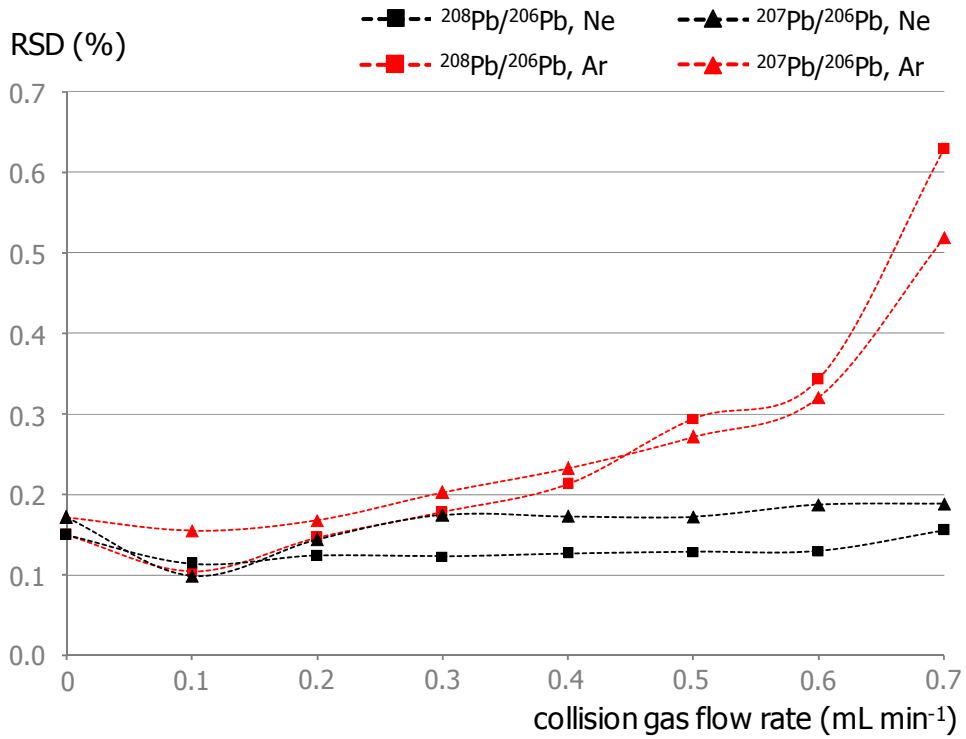

Figure VII.5 – Precision attainable on the $^{207}Pb/^{206}Pb$ and $^{208}Pb/^{206}Pb$ ratios as a function of the Ne – and Ar gas flow rate

Finally, also the mass discrimination effect due to the presence of a collision gas in the dynamic reaction cell [Vanhaecke *et al.*, 2003] was evaluated (figure VII.6). At 0.1 mL min^{-1}, the raw $^{208}Pb/^{206}Pb$ ratio is – compared to vented mode – increased with 2 % when Ne is used, and with 3 % when Ar is used, and becomes higher at higher flow rates for both Ar and Ne. Since the isotopic standards and samples are measured under the same DRC-conditions, this observation can be accurately corrected for, as is described below (§ VII.5.2).

It can be concluded that (i) Ne is preferred over Ar owing to the (much) lower scattering losses, (ii) with Ne, the same level of precision is obtained at the lower gas flow rate, minimizing both scattering losses and gas consumption, and (iii) the mass discrimination effect introduced by the use of a collision gas in the DRC is the lowest for Ne. As a

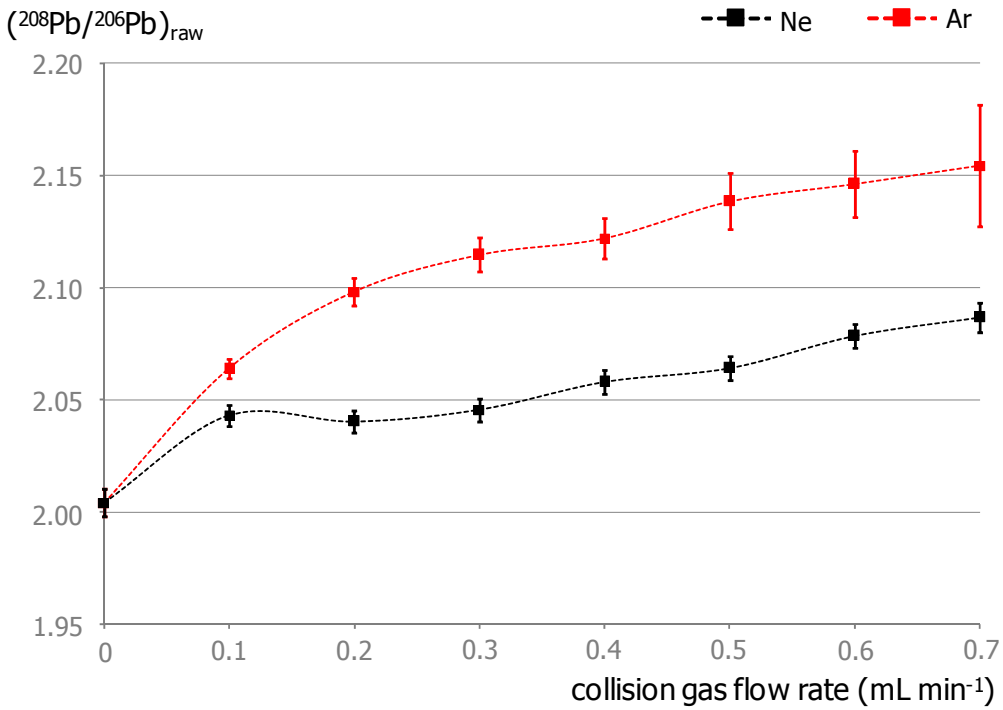

Figure VII.6 – Raw $^{208}Pb/^{206}Pb$ ratio as a function of the Ne – and Ar gas flow rate

consequence, Ne was selected as collision gas and was introduced into the DRC at a flow rate of 0.1 mL min^{-1}. No new interfering ions are formed inside the DRC when Ne is used, so that the RPq was maintained at its standard value of 0.45, this setting was also used during the optimization of the gas flow rate. Next to the collision gas flow rate, also the detector dead time was determined (chapter III, § III.4.5.2) and subsequently set at 61 ns, resulting in entirely optimized conditions for Pb isotope ratio determination by means of single-collector ICP – dynamic reaction cell – MS.

VII.5.2 – Measurement protocol

After extraction chromatographic isolation of Pb (chapter VI, § VI.4.2), the Pb fraction of the archaeological samples was present in 0.05 M $(NH_4)_2C_2O_4$ solution. The Pb fractions were diluted with 0.14 M HNO_3 to obtain a Pb concentration between 25 and 50 µg L^{-1}, and subsequently analyzed for their Pb isotopic composition using a PerkinElmer SCIEX Elan DRC*plus*. The instrumental settings and data acquisition parameters for Pb isotope ratio determination using single-collector ICP – dynamic reaction cell – MS are summarized in table VII.7. The samples were monitored in a sample-standard bracketing approach using a 25 µg L^{-1} Pb isotopic standard solution of NIST SRM 981 Common Lead in 0.14 M HNO_3. The procedural blank Pb intensities were always negligible (< 0.1 %) compared to the Pb intensities encountered for the samples and the standards. It was

Table VII.7 – Pb isotopic analysis using the Elan DRC*plus* ICP – mass spectrometer – (a) instrumental settings; (b) data acquisition parameters; (c) DRC parameters; (d) experimental values, external precision and accepted [Galer and Abouchami, 1998] values for NIST SRM 981 Common Lead.

(a) instrumental settings	
RF power	1200 W
plasma gas flow rate	17 L min^{-1}
auxiliary gas flow rate	1.2 L min^{-1}
nebulizer gas flow rate	0.95 – 1.00 L min^{-1}*
sampling cone	Ni, aperture diameter 1.1 mm
skimmer	Ni, aperture diameter 0.9 mm
extraction lens voltage	10 – 12 V*
sample delivery	peristaltic pump
sample uptake rate	1 mL min^{-1}
(b) data acquisition parameters	
isotopes monitored	^{204}Pb, ^{206}Pb, ^{207}Pb, ^{208}Pb
scanning mode	peak hopping
dwell time	2 ms
settling time	200 µs
number of acquitition points per spectral peak	1
number of sweeps	500
number of readings	10
number of replicates	15, final 10 taken into account
replicate time	~ 46 s
detector dead time	61 ns
(c) DRC parameters	
Ne gas flow rate	0.1 mL $min^{-1\$}$
RPa	0
RPq	0.45

(d) experimental and accepted values for NIST SRM 981 Common Lead

ratio	experimental	2s	RSD (%)	accepted
$^{206}Pb/^{204}Pb$	16.9410	0.0537	0.16	16.9405
$^{207}Pb/^{204}Pb$	15.4967	0.0469	0.15	15.4963
$^{208}Pb/^{204}Pb$	36.7230	0.1228	0.17	36.7219
$^{207}Pb/^{206}Pb$	0.91474	0.00172	0.09	0.91475
$^{208}Pb/^{206}Pb$	2.16771	0.00256	0.06	2.16771
$^{208}Pb/^{207}Pb$	2.3698	0.0036	0.08	2.3697

* daily optimized for maximum ^{208}Pb sensitivity; $ actual gas flow rate

observed that the same isotope ratios were obtained with and without blank correction. However, a blank correction was always consistently performed.

Data acquisition consisted of 15 replicates of ~ 46 s each, establishing a total sample measurement time of ~ 11 min. When the DRC is pressurized, the cell opens/closes at the start/end of every sample measurement, causing a 'delay time' before a homogeneous pressure within the cell is established again. As a consequence, considerable signal fluctuations can occur during the first 2-4 replicates, resulting in an isotope ratio precision that is up to 0.04 % RSD better when only the final 10 replicates are considered. Thus, only replicates 6 to 15 were used for isotope ratio calculations, and the measurement time for the first 5 replicates should be regarded as a stabilization time. The $^{206}Pb/^{204}Pb$, $^{207}Pb/^{204}Pb$, $^{208}Pb/^{204}Pb$, $^{207}Pb/^{206}Pb$, $^{208}Pb/^{206}Pb$ and $^{208}Pb/^{207}Pb$ intensity ratios for the 10 replicates for both standards and samples were calculated. A Q-test on the 95 % confidence interval was performed, but the occurrence of outliers was sporadic. The average and the corresponding 2s uncertainty interval and relative standard deviation (% RSD) were calculated from the 10 replicates for every sample and standard. Mass discrimination correction was performed by external standardization (sample-standard bracketing, chapter III, § III.4.2.2.2), and the sample ratios were calculated using equation III.13, with the accepted values for NIST SRM 981 Common Lead [Galer and Abouchami, 1998] as reference values.

The external precision of the measurement protocol was calculated on the basis of the mass discrimination corrected Pb isotope ratios for the NIST SRM 981 Common Lead standard. As the Pb concentration for the measured samples (25-50 µg L^{-1}) is equal to or higher than that for the isotopic standard (25 µg L^{-1}), the external precision calculated from the standards can be regarded as a 'worst case' limit for the precision attainable for the samples (counting statistics). The external precision was established to be typically 0.15-0.17 % RSD for ratios with ^{204}Pb ($^{206}Pb/^{204}Pb$, $^{207}Pb/^{204}Pb$ and $^{208}Pb/^{204}Pb$), and 0.06-0.09 % RSD for the ratios $^{207}Pb/^{206}Pb$, $^{208}Pb/^{206}Pb$ and $^{208}Pb/^{207}Pb$ (table VII.7.d).

VII.5.3 – Validation of the SC-ICP-DRC-MS measurement protocol

The accuracy of the single-collector ICP-DRC-MS measurement protocol developed has been validated by comparing the data obtained to the corresponding values obtained via multi-collector ICP-MS. The accuracy and reproducibility of the entire method developed for Pb isotope ratio analysis (Pb isolation (chapter VI, § VI.4.2) + single-collector ICP-DRC-MS measurement) has been validated by (i) duplicate analyses of bone and soil

samples using single-collector ICP-DRC-MS and (ii) application of the method to the Pb isotope ratio determination of two certified reference materials, BCR CRM 482 Lichen and NIST SRM 1400 Bone Ash, for which Pb isotope data are available in literature. Further, the Pb isotopic composition of two certified soil reference materials, BCR CRM 141 Calcareous Loam Soil and BCR CRM 142 Light Sandy Soil, that had not been previously reported in literature, was determined.

VII.5.3.1 – Duplicate analyses

The results of duplicate Pb isotope ratio analysis via SC-ICP-DRC-MS of some bone, soil and garum samples under investigation in the context of the Roman Bone – project (chapter IX), and selected for duplicate analysis on the basis of their different isotopic composition relative to each other, are summarized in table VII.8. For every sample, the single-collector ICP-DRC-MS duplicate analyses match within experimental error. An average bias of 0.18 % for $^{206}Pb/^{204}Pb$, 0.22 % for $^{207}Pb/^{204}Pb$, 0.16 % for $^{208}Pb/^{204}Pb$, 0.10 % for $^{207}Pb/^{206}Pb$, 0.15 % for $^{208}Pb/^{206}Pb$ and 0.15 % for $^{208}Pb/^{207}Pb$ is observed. The bias between duplicate analyses is within the external precision of the method. Nevertheless, for one sample (soil 1-140-165, table VII.8), a bias between duplicate results of 0.39 % on the $^{208}Pb/^{206}Pb$ ratio was observed. This bias can most likely be attributed to the heterogeneity of the samples since, as is shown below, the method can be considered as accurate and reproducible.

VII.5.3.2 – Comparison of single-collector – and multi-collector ICP-MS results

All the samples under investigation in the context of the Roman Bone – project (chapter IX) have been analyzed using both single-collector ICP-DRC-MS and multi-collector ICP-MS. A comparison of the Pb isotope ratio results thus obtained for selected bone, soil, amphora and lead fragment samples, chosen on the basis of their relative difference in Pb isotopic composition, is given in table VII.9. It is observed that, within external precision, every single isotope ratio obtained via SC-ICP-DRC-MS matches the corresponding MC-ICP-MS result, including the isotope ratios with ^{204}Pb. When the results obtained via SC-ICP-DRC-MS and MC-ICP-MS are compared for the entire set of samples investigated in the context of the Roman Bone – project – soil (n=21), bone (n=22), garum (n=1), amphora (n=8), pottery (n=1) and lead fragment (n=10) samples – the average bias between single-collector ICP-DRC-MS and multi-collector ICP-MS results was

Table VII.8 – Results of duplicate Pb isotope ratio analysis via SC-ICP-DRC-MS of selected samples investigated in the context of the Roman Bone – project

		$^{206}Pb/^{204}Pb$	$^{207}Pb/^{204}Pb$	$^{208}Pb/^{204}Pb$	$^{207}Pb/^{206}Pb$	$^{208}Pb/^{206}Pb$	$^{208}Pb/^{207}Pb$
2s		0.054	0.047	0.123	0.0017	0.0026	0.0036
soil samples							
1-140-165	1	18.899	15.693	38.803	0.8300	2.0527	2.4721
	2	18.819	15.652	38.794	0.8317	2.0607	2.4777
6-265-328	1	18.815	15.626	38.695	0.8324	2.0566	2.4722
	2	18.764	15.617	38.729	0.8323	2.0605	2.4756
59-43-63	1	18.809	15.677	38.770	0.8331	2.0611	2.4741
	2	18.781	15.633	38.721	0.8343	2.0629	2.4704
bone samples							
1-140-165	1	18.557	15.692	38.489	0.8437	2.0742	2.4627
	2	18.565	15.640	38.591	0.8425	2.0780	2.4666
6-265-328	1	18.644	15.688	38.537	0.8408	2.0671	2.4586
	2	18.590	15.615	38.478	0.8399	2.0684	2.4626
51-54-165	1	18.415	15.613	38.467	0.8473	2.0792	2.4484
	2	18.438	15.639	38.376	0.8482	2.0810	2.4539
59-43-63	1	18.509	15.631	38.308	0.8445	2.0733	2.4588
	2	18.508	15.612	38.436	0.8438	2.0768	2.4620
garum							
13-2-236	1	18.416	15.635	38.438	0.8489	2.0853	2.4564
	2	18.436	15.647	38.430	0.8487	2.0845	2.4561

Table VII.9 – Comparison of SC-ICP-DRC-MS results to the corresponding MC-ICP-MS results of selected samples investigated in the context of the Roman Bone – project

	$^{206}Pb/^{204}Pb$		$^{207}Pb/^{204}Pb$		$^{208}Pb/^{204}Pb$		$^{207}Pb/^{206}Pb$		$^{208}Pb/^{206}Pb$		$^{208}Pb/^{207}Pb$	
	SC	MC	SC	MC	SC	MC	SC	MC	SC	MC	SC	MC
2s	0.054	0.006	0.047	0.005	0.123	0.014	0.0017	0.0001	0.0026	0.0002	0.0036	0.0002
soil samples												
6-99-128	18.384	18.385	15.626	15.624	38.383	38.380	0.8497	0.8499	2.0878	2.0871	2.4567	2.4557
14-173-242	18.679	18.684	15.665	15.658	38.660	38.687	0.8387	0.8381	2.0698	2.0706	2.4680	2.4707
51-60-176	18.730	18.784	15.639	15.665	38.673	38.772	0.8350	0.8340	2.0634	2.0640	2.4722	2.4750
59-96-204	18.709	18.715	15.626	15.643	38.642	38.670	0.8352	0.8359	2.0654	2.0662	2.4723	2.4720
71-29-54	18.730	18.718	15.667	15.661	38.746	38.748	0.8365	0.8367	2.0683	2.0701	2.4731	2.4742
bone samples												
6-99-128	18.388	18.396	15.635	15.633	38.329	38.390	0.8501	0.8498	2.0846	2.0869	2.4516	2.4557
14-173-242	18.645	18.684	15.620	15.661	38.520	38.658	0.8378	0.8382	2.0684	2.0690	2.4685	2.4684
51-60-176	18.506	18.529	15.625	15.652	38.473	38.566	0.8445	0.8448	2.0799	2.0815	2.4634	2.4640
59-96-204	18.541	18.536	15.643	15.643	38.532	38.518	0.8437	0.8439	2.0783	2.0781	2.4633	2.4624
71-29-54	18.631	18.584	15.689	15.656	38.682	38.628	0.8422	0.8424	2.0762	2.0785	2.4655	2.4673
amphora samples												
218-48	18.622	18.641	15.655	15.658	38.614	38.635	0.8407	0.8400	2.0723	2.0726	2.4656	2.4674
C-3656	18.599	18.569	15.671	15.654	38.600	38.587	0.8429	0.8430	2.0780	2.0780	2.4653	2.4650
IV-C-166	18.765	18.771	15.660	15.669	38.760	38.766	0.8347	0.8348	2.0648	2.0652	2.4741	2.4741
lead fragments												
3-2-32	18.414	18.408	15.640	15.636	38.416	38.415	0.8494	0.8494	2.0880	2.0869	2.4583	2.4569
6-62-20	18.398	18.395	15.627	15.624	38.414	38.394	0.8499	0.8498	2.0877	2.0872	2.4568	2.4565
7-547-971	18.380	18.381	15.611	15.631	38.332	38.373	0.8494	0.8504	2.0855	2.0876	2.4553	2.4551

established to be 0.1 % for ratios with ^{204}Pb, and 0.05 % for the other ratios, values that are well within the external precision of the single-collector ICP-DRC-MS measurement protocol (table VII.7.d). Further, the dispersion of Pb isotope ratios among the displayed set (table VII.8 and table VII.9) and the entire set (chapter IX, tables IX.1-IX.3) of samples under investigation in the context of the Roman Bone – project is larger than the attainable precision via SC-ICP-DRC-MS (table VII.7.d). Also for Pb isotope ratio analysis of metallic artefacts in the context of the ed-Dur – project (chapter VIII), the Pb isotope ratio precision offered by the SC-ICP-DRC-MS measurement protocol is sufficient. As a conclusion, it can be stated that the single-collector ICP-DRC-MS measurement protocol, developed for the purpose of Pb isotope ratio analysis of archaeological artefacts, leads to accurate results and is fit-for-purpose.

VII.5.3.3 – Pb isotope ratio determination in certified reference materials

The Pb isotope ratio results obtained via SC-ICP-DRC-MS for the selected certified reference materials after digestion and Pb isolation are summarized in table VII.10. The Pb isotopic compostion of NIST SRM 1400 Bone ash has already been determined via TI-MS [Hinners *et al.*, 1998]. The double spike TI-MS values reported for NIST SRM 981 Common Lead [Woodhead *et al.*, 1995] were used in the work of Hinners *et al.* as reference values. To be consistent with the normalization used throughout this work, the experimental values for NIST SRM 1400 Bone Ash reported by Hinners *et al.* have been recalculated using the triple spike TI-MS values for NIST SRM 981 Common Lead [Galer and Abouchami, 1998] used throughout this work. As can be seen in table VII.10.a, the average single-collector ICP-DRC-MS results obtained for NIST SRM 1400 Bone Ash via the Pb methodology developed, are in very good agreement with the results obtained via TI-MS following a different sample pretreatment [Hinners *et al.*, 1998]. This confirms the developed method's reliability for Pb isotope ratio analysis. The replicate results are given in chapter VI, table VI.5, as a part of the regeneration experiment of Pb spec^{TM} resin.

The Pb isotopic composition of the certified soil reference materials BCR CRM 141 Calcareous Loam Soil and BCR CRM 142 Light Sandy Soil has not been reported yet. In table VII.10.b-c, the average Pb isotope ratio data obtained via the SC-ICP-DRC-MS protocol are summarized. The replicate results are given chapter VI, table VI.5, as a part of the regeneration experiment of Pb spec^{TM} resin.

The Pb isolation procedure and single-collector ICP-DRC-MS measurement protocol was further applied to a certified reference material with a matrix composition that is also

Table VII.10 – Pb isotope ratio results obtained via single-collector ICP-DRC-MS for selected certified reference materials. Literature data are taken from [Hinners *et al.*, 1998] (bone) and [Cloquet *et al.*, 2006-b] (lichen). The replicate results for certified bone and soil reference materials are given in chapter VI, table VI.5

	$^{206}Pb/^{204}Pb$	$^{207}Pb/^{204}Pb$	$^{208}Pb/^{204}Pb$	$^{207}Pb/^{206}Pb$	$^{208}Pb/^{206}Pb$	$^{208}Pb/^{207}Pb$
(a) NIST SRM 1400 Bone Ash						
SC-ICP-DRC-MS (n=4)	18.355	15.674	38.606	0.8541	2.1036	2.4629
2s	0.031	0.025	0.064	0.0010	0.0019	0.0033
TI-MS (n=7)*	18.371	15.675	38.625	0.8532	2.1025	2.4642
2s	0.014	0.012	0.040	0.0002	0.0007	0.0003
(b) BCR CRM 141 Calcareous Loam Soil						
SC-ICP-DRC-MS (n=3)	18.600	15.667	38.643	0.8424	2.0777	2.4667
2s	0.019	0.046	0.138	0.0015	0.0045	0.0010
(c) BCR CRM 142 Light Sandy Soil						
SC-ICP-DRC-MS (n=4)	18.535	15.652	38.582	0.8444	2.0814	2.4646
2s	0.019	0.028	0.089	0.0022	0.0051	0.0065
(d) BCR CRM 482 Lichen						
SC-ICP-DRC-MS (n=3)	17.607	15.568	37.495	0.8842	2.1296	2.4085
2s	0.114	0.061	0.235	0.0024	0.0012	0.0047
MC-ICP-MS (n=4)*	17.611	15.570	37.490	0.8841	2.1288	2.4078
2s	0.007	0.007	0.020	0.0001	0.0003	0.0004

complex, but different from that of bone tissue and soils. For the certified reference material BCR CRM 482 Lichen, Pb isotope ratios, obtained via multi-collector ICP-MS, have been reported [Cloquet *et al.*, 2006-b]. After digestion of this reference material according to the method described in the work cited above, the digest was conducted through the extraction chromatographic separation procedure used throughout this work (chapter VI, § VI.4.2) and analyzed for its Pb isotopic composition using SC-ICP-DRC-MS. As can be seen from table VII.10.d, there is an excellent agreement between the results obtained via single-collector ICP-DRC-MS and multi-collector ICP-MS. This agreement suggests that the method developed is suitable for a wide range of applications involving Pb isotopic analysis of complex matrices.

VII.5.4 – Conclusions

A methodology, consisting of an extraction chromatographic Pb isolation procedure, followed by Pb isotope ratio measurement using single-collector ICP – dynamic reaction cell – MS, has been developed for the purpose of Pb isotope ratio analysis of archaeological artefacts. It has been proven that the methodology is applicable for a wide range of applications of Pb isotope ratio analysis, even when very complex matrices are the subject of study, and for which an excellent isotope ratio precision, as offered by MC-ICP-MS, is not mandatory.

Literature Pb isotope ratio precision values obtained via single-collector sector field ICP-MS cover the range of 0.04-0.27 % RSD [Woolard *et al.*, 1998; De Wannemacker *et al.*, 2000; Krachler *et al.*, 2004]. The use of ICP-DRC-MS for Pb isotope ratio measurements in peat cores, making use of an Ar/H_2 mixture at a gas flow rate of 0.5 mL min^{-1} [Jackson *et al.*, 2004] resulted in a Pb isotope ratio precision below 0.5 % RSD for the ratios without ^{204}Pb for the samples, and below 0.1 % RSD for the $^{206}Pb/^{207}Pb$ ratio of the NIST SRM 981 Common Lead isotopic standard. The single-collector ICP-DRC-MS measurement protocol developed in this work, using Ne as a collision gas in a dynamic reaction cell (DRC), is more precise than 'traditional' quadrupole-based ICP-MS and offers a Pb isotope ratio precision that is similar to or better than the best results reported for sector field ICP-MS and ICP-DRC-MS. Further, the method was shown as accurate and reproducible, with Pb isotope ratio results similar to multi-collector ICP-MS and TI-MS results, also for the ratios with ^{204}Pb.

CHAPTER VIII

Provenancing pre-Islamic metallic artefacts excavated at ed-Dur and Khor Rori

This chapter presents and discusses Pb isotope ratio data that were obtained for metallic artefacts excavated at the sites of ed-Dur (Emirate of Umm al-Qaiwain, United Arab Emirates) and Khor Rori (Oman). The collection of metallic artefacts investigated, consists of copper-based (unalloyed copper, brass, bronze), lead-based (lead and litharge) and silver fragments and objects. Also a set of local South-East Arabian coins, manufactured from a copper-silver alloy, were investigated. The metallic artefacts were studied to obtain insight into the trade relations between the Roman Empire and the Indian subcontinent during the period 1st century BC – 1st half 2nd century AD, and the position of ed-Dur in this trading network.

In what follows, the sites of ed-Dur and Khor Rori and the artefacts investigated are shortly discussed, followed by a presentation of the Pb isotope ratio results. These are subsequently compared to literature Pb isotope ratios for copper and silver/lead ores, with the aim of determining the provenance of the metallic artefacts. The analytical findings are then translated into the most important archaeological implications. A detailed discussion of the entire archaeological context is beyond the scope of this chapter; the interested reader is referred to a PhD thesis entirely devoted to this topic [Delrue, 2008].

VIII.1 – Geography, history and archaeology

VIII.1.1 – The archaeological site of ed-Dur

The site of ed-Dur is situated on the west coast of the Oman Peninsula, near the sheltered lagoon of Khor al-Beidah in the Emirate of Umm al-Qaiwain, United Arab Emirates (figure VIII.1). The site extends to about 1 kilometer inland and is hidden behind a dune that protects it from winds coming from the sea. The true extent of the site during its heydays is hard to determine as shards were found over a vast area, but it is believed that the spread was at least 2-3 square kilometers [Haerinck, 2001; Delrue, 2008].

Ed-Dur is the only large coastal site identified so far between Qatar and the Strait of Hormuz, which connects the Persian Gulf and the Gulf of Oman (figure VIII.1), with a main occupation phase dating between the 1st century BC and the 1st half of the 2nd century AD. The settlement must have profited from its position, as the coast itself between Umm al-Qaiwain and Dubai is renowned for its dangerous shoals and reefs. The proximity of the lagoon provided the possibility of fishing and collecting shellfish, while the sea itself permitted fishing in open sea and international commercial traffic. Next to the sea, also traditional routes via land were important. One of these led to the fertile

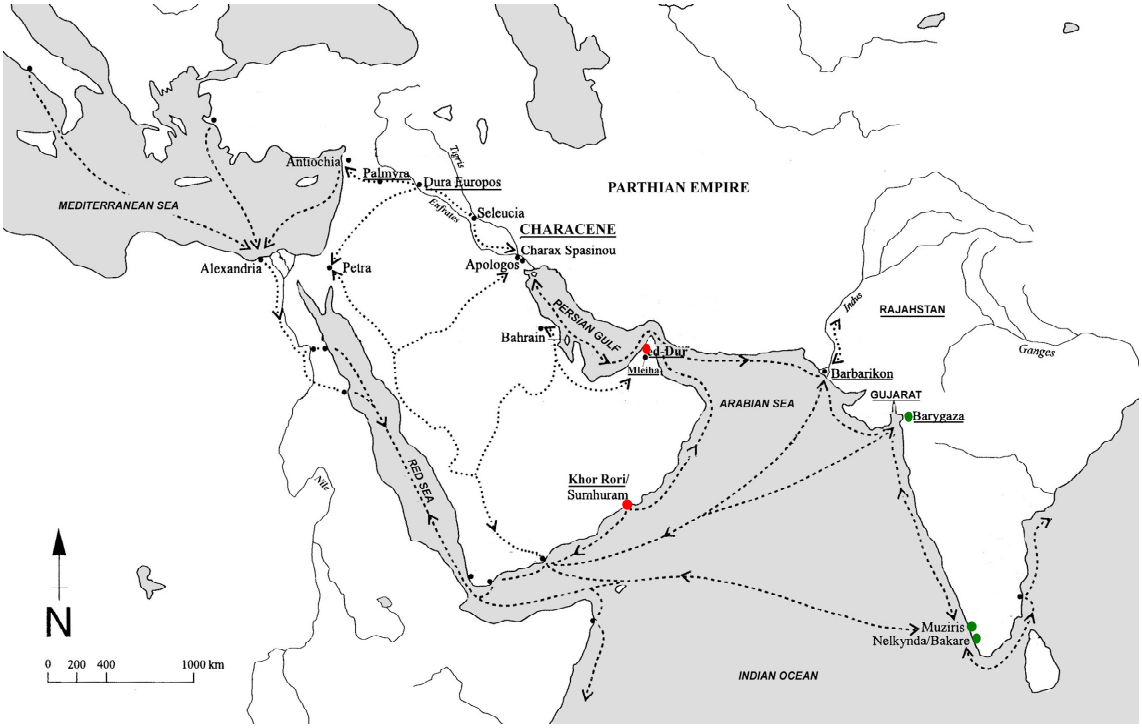

Figure VIII.1 – Map of the region of interest. The sites of ed-Dur and Khor Rori are indicated in red; the Indian harbors Barygaza, Muziris and Nelkynda are indicated in green. Dashed lines are trade routes in the period 1st century BC – 2nd century AD

inland plain of al-Madam, where the site of Mleiha is located (Emirate of Sharjah, United Arab Emirates) (figure VIII.1). The site of Mleiha is another important site in the trading network, because here, several land routes converge [Boucharlat *et al.*, 1988; Delrue, 2008].

The site of ed-Dur was discovered by an Iraqi team in 1973 during an archaeological survey of the United Arab Emirates. A small square fort was discovered, and the investigation of the surface collections of ceramics and coins revealed the presence of Characenean coins, glazed Parthian pottery and Roman glasswork, indicating an international orientation [Salles, 1980]. In 1986, a European consortium of four countries (Belgium, Denmark, France and Great Britain) was created to conduct full-scale excavations. Over time however, only the Belgian team remained for nine continuous seasons at ed-Dur between 1987 and 1995, with eight excavation campaigns and a final study season [Haerinck, 2001].

An enormous treasure of imported goods was found at ed-Dur, witnessing an extensive trading network existing at that time. Besides the metallic artefacts with copper, silver or lead as the major element that were investigated in this work for their Pb isotopic composition, a large collection of other imported artefacts were also excavated. Among these are glass vessels and glass fragments, all of these having abundant parallels in the Roman Empire [Whitehouse, 1998]. Also a huge number of ceramics was excavated [Rutten,

2006]. Some of these were shown to be produced locally, while the largest group (72 %) was imported. Southern Mesopotamia and North-East Arabia were identified as the main providers. Further, also stone vessels [Zutterman, 2003], human and animal figurines [Daems, 2004-a; Daems, 2004-b] and beads [Haerinck, 2003] witness an international trade system of ed-Dur with the Mediterranean region, the Roman Empire, the Parthian Empire, Arabia and the Indian subcontinent [Delrue, 2008].

VIII.1.2 – The archaeological site of Khor Rori

Next to metallic artefacts originating from the archaeological site of ed-Dur, also a few metallic artefacts originating from the archaeological site of Khor Rori, were investigated. The coastal settlement of Khor Rori was founded on the Dhofar Coast (Oman) (figure VIII.1) in the early 1st century AD [Sedov, 1996] and its foundation was connected to the increase in maritime trade between the Roman Empire and the Indian subcontinent at the beginning of the era. It was a port that was mainly used for trade in incense. Possibly, Khor Rori was built on top of an earlier settlement that may have been a stopping place on the ancient sea routes to India or Oman for trade in everyday goods and metals. Although the importance of the site of Khor Rori for metal production and/or trade is not well-known, there is evidence of iron and bronze working during the history of Khor Rori and a northern route that connects Khor Rori to inland Oman is hypothesized to be linked to the copper trade [Avanzini, 2002; Delrue, 2008].

VIII.1.3 – Historical written sources on trade

The goal of the study presented here was to provenance the metallic artefacts investigated, in order to contribute to a more profound insight in the trade system between the Roman Empire and the Indian subcontinent at the period of occupation of the site of ed-Dur, and to further clarify the commercial routes via which the trade system took place. Two important historical sources, the *Periplus Maris Erythraei* (Periplus of the Erythraean Sea) and Plinius' *Naturalis Historia* (Natural History) were written during the time that ed-Dur was inhabited and provide direct information concerning the trade between the Roman Empire and the Indian subcontinent, such as the goods shipped, the itineraries followed and the harboring places. Next to this textual information, there is a growing body of archaeological evidence to support (or reject) the statements in these sources.

The *Naturalis Historia* [Plinius] can be considered as an encyclopedia on the knowledge in the 1st century AD and was composed by Pliny (Plinius) the Elder. This work is further referred to as 'Plinius'. The *Periplus Maris Erythraei* [Periplus] (further in the text referred to as 'Periplus') is a Greek commercial trade handbook generally accepted to date from the 1st century AD or shortly thereafter. The anonymous author, probably an Egyptian Greek, wrote it as a technical guide for merchants and sailors who set sail from the ports of Roman Egypt at the Red Sea to the coast of Africa, the western and southern coasts of Arabia and the western coast of India. The detailed information on the traded goods in this work is rather atypical, since a periplus is foremost a guide for seamen, whereas the Periplus considered here is in the first place a guide for merchants. This is what makes this Periplus such an exceptional and valuable document [Delrue, 2008].

VIII.2 – Samples investigated in this work

The metallic artefacts that were available for lead isotope ratio analysis can be divided into three groups, according to the metal that is the major component of the object/fragment: (i) copper-based artefacts, (ii) lead-based artefacts and (iii) silver objects. An overview of the samples investigated, their physical appearance and lead concentration is given in tables VIII.1-4. The lead concentrations, as determined using SEM-EDX (scanning electron microscopy – electron dispersive X-ray spectrometry) were provided with the samples. Preceding Pb isotope ratio analysis, the Pb concentrations were also determined using quadrupole-based ICP-MS (PerkinElmer SCIEX Elan 5000), and the ICP-MS results were in most cases lower, but matched largely within 50 % with the SEM-EDX values. The discrepancy can be attributed to the facts that (i) SEM-EDX is a semi-quantitative technique only and (ii) the objects investigated do not show a homogeneous distribution of lead, as was also demonstrated by surface analysis using SEM and optical microscopy. However, the SEM-EDX results provide an accuracy that is sufficient to distinguish leaded (> 4 % Pb, chapter IV, § IV.4.4) from non-leaded alloys.

Twenty-one copper-based artefacts were investigated (table VIII.1). The set comprises 3 unalloyed copper, 5 brass and 13 bronze artefacts (chapter IV, § IV.4.4). Of these 13 bronze objects, SEM-EDX analysis revealed that 10 of them can be classified as leaded bronze (table VIII.1). Six samples from the copper-based artefacts set originate from the site of Khor Rori (KR in sample code): 1 unalloyed copper, 2 bronze and 3 leaded bronze fragments. The other copper-based artefacts originate from the site of ed-Dur.

The lead-based fragments are summarized in table VIII.2 and consist of 18 items, which were all found at the site of ed-Dur. Most of these (15) were provided as fragments. Three lead fragments – BS 269 (bulla) and S 0024 and Z 019 (assumed to be ingots) – were supposed to be particularly important, and hence indicated as 'lead proxies' (table VIII.2). A bulla is an Indian imitation of a Roman coin that was manufactured in clay, gold, silver, faience, or, as is the case here, lead. Its use was primarily as a decorative pendant. The fact that item BS 269 was certainly made in India [Delrue, 2008] makes it a valuable object. Lead fragment S 0024 was supposed to be an ingot, which is a tradable form of lead. It has a monogram imprinted that can provide a clue for provenancing this object. Also fragment Z 019 was supposed to be an ingot, but without a clue towards its origin. Next to 15 lead fragments, also 3 litharge fragments were provided, testifying of the extraction of silver from a copper-silver alloy on the site of ed-Dur [Delrue, 2008], since litharge fragments are always man-made [Tylecote, 1976].

Table VIII.3 summarizes the 12 silver objects found at the site of ed-Dur. The set consists of 5 pieces of jewelry and 7 coins. The coins can be divided into obols and tetradrachms. Obols are smaller than tetradrachms, implying a lower monetary value. Four silver obols and three silver tetradrachms were investigated. Besides silver tetradrachms, also a set of 18 tetradrachms consisting of a copper-silver alloy (billon) were analyzed (table VIII.4).

VIII.3 – Analytical methodology

The copper- and silver-based artefacts were sampled by the use of a tungstencarbide miniature drill (chapter V, § V.1.3), while the lead fragments were sampled by scraping an amount of lead off the object (chapter V, § V.1.1). The powdered samples or pieces were consequently digested according to the digestion procedures developed for this purpose (chapter V, § V.4.5). After the digestion step, the lead fraction of the digests (except for the lead fragments) was isolated from its metallic matrix by means of extraction chromatography (chapter VI, § VI.4.2). Finally, the purified lead solutions were submitted to lead isotope ratio analysis following the single-collector ICP-DRC-MS measurement protocol developed (chapter VII, § VII.5.2). The use of Ne as a collision gas in the dynamic reaction cell resulted in an external precision below 0.17 % RSD for the ratios with ^{204}Pb ($^{206}Pb/^{204}Pb$, $^{207}Pb/^{204}Pb$, $^{208}Pb/^{204}Pb$), and below 0.09 % RSD for the other ($^{207}Pb/^{206}Pb$, $^{208}Pb/^{206}Pb$ and $^{208}Pb/^{207}Pb$) ratios, and this precision proved sufficient in grouping and distinguishing objects on the basis of their experimentally determined Pb isotope ratios.

Table VIII.1 – Pb concentration and Pb isotopic composition of copper-based artefacts from the sites of ed-Dur and Khor Rori

		[Pb] (%)	$^{206}Pb/^{204}Pb$	$^{207}Pb/^{204}Pb$	$^{208}Pb/^{204}Pb$	$^{207}Pb/^{206}Pb$	$^{208}Pb/^{206}Pb$	$^{208}Pb/^{207}Pb$
external precision (2s)		--	0.054	0.047	0.123	0.0017	0.0026	0.0036
unalloyed copper								
BS 169	coin (tetradrachm)	1.4	18.263	15.638	38.275	0.8560	2.0958	2.4476
N 138	altar	2.3	18.709	15.654	38.848	0.8367	2.0765	2.4817
KR 012	fragment	1.7	18.533	15.791	38.484	0.8520	2.0773	2.4381
brass								
AT 013	ring-pommel dagger	2.3	18.413	15.663	38.555	0.8504	2.0936	2.4599
AV 083	large rivet	2.1	18.347	15.655	38.432	0.8536	2.0948	2.4551
AW 063-4	ring-pommel dagger	1.5	18.322	15.638	38.344	0.8535	2.0926	2.4520
BL 014	ring-pommel dagger	1.6	18.371	15.678	38.377	0.8525	2.0890	2.4504
BO 029	bell pendant	2.7	18.582	15.700	38.851	0.8442	2.0912	2.4769
bronze								
AV 115	ladle fragment	2.8	18.640	15.676	38.911	0.8409	2.0882	2.4838
KR 009	fragment	2.8	16.928	15.711	37.063	0.9297	2.1899	2.3574
KR 010	fragment	2.7	17.845	15.684	37.998	0.8789	2.1294	2.4234
leaded bronze								
AV 005	ram's head *patera*	17	18.800	15.716	38.986	0.8360	2.0734	2.4793
AV 104	horse applic	22	18.809	15.718	38.940	0.8364	2.0708	2.4752
C 079	handle vessel	12	18.547	15.680	38.610	0.8446	2.0838	2.4672
K 203	handle vessel	12	18.296	15.680	38.366	0.8570	2.0986	2.4492
M 007	pedestal statuette	22	18.628	15.700	38.688	0.8428	2.0757	2.4642
N 118	bead	13	18.586	15.698	38.856	0.8431	2.0868	2.4753
S 020	female head applic	22	18.796	15.713	38.950	0.8360	2.0716	2.4789
KR 007	fragment	12	18.511	15.763	38.734	0.8515	2.0946	2.4598
KR 008	fragment	16	18.315	15.684	38.629	0.8564	2.1079	2.4629
KR 011	fragment	13	17.886	15.734	38.057	0.8785	2.1274	2.4244

Table VIII.2 – Pb concentration and Pb isotopic composition of lead and litharge fragments from the site of ed-Dur. Lead fragments assumed to be 100 % lead.

		[Pb] (%)	$^{206}Pb/^{204}Pb$	$^{207}Pb/^{204}Pb$	$^{208}Pb/^{204}Pb$	$^{207}Pb/^{206}Pb$	$^{208}Pb/^{206}Pb$	$^{208}Pb/^{207}Pb$
external precision (2s)		--	0.054	0.047	0.123	0.0017	0.0026	0.0036
lead proxies								
BS 269	bulla	100	18.703	15.942	38.857	0.8516	2.0776	2.4397
S 0024	ingot ?	100	18.081	15.710	38.355	0.8682	2.1213	2.4429
Z 19	ingot ?	100	16.949	15.723	37.029	0.9277	2.1844	2.3552
lead fragments								
BK 1238 B	fragment	100	18.091	15.707	38.334	0.8682	2.1188	2.4406
BM 1225 B	fragment	100	18.132	15.738	38.432	0.8684	2.1195	2.4419
BM 1225 C	fragment	100	18.138	15.666	38.369	0.8639	2.1154	2.4487
BM 1225 D	fragment	100	18.019	15.658	38.222	0.8692	2.1213	2.4413
BS 1139 A	fragment	100	18.151	15.725	38.462	0.8663	2.1190	2.4459
BS 1360	fragment	100	18.066	15.702	38.299	0.8692	2.1200	2.4389
BS 1441 A	fragment	100	18.130	15.763	38.452	0.8694	2.1204	2.4393
BS 1453 A	fragment	100	18.106	15.736	38.422	0.8692	2.1216	2.4416
BS 1453 B	fragment	100	18.097	15.702	38.343	0.8676	2.1187	2.4420
BS 1466	fragment	100	17.109	15.791	37.258	0.9230	2.1777	2.3595
ED 1309	fragment	100	18.081	15.720	38.403	0.8700	2.1227	2.4389
S 0010 C	fragment	100	18.112	15.686	38.286	0.8661	2.1155	2.4426
litharge fragments								
AW 13	fragment	57	18.052	15.668	38.299	0.8679	2.1216	2.4445
BO 722	fragment	57	18.099	15.706	38.289	0.8678	2.1155	2.4377
BO 724 A	fragment	55	18.057	15.658	38.205	0.8671	2.1158	2.4379

Table VIII.3 – Pb concentration and Pb isotopic composition of silver objects from the site of ed-Dur

		[Pb] (%)	$^{206}Pb/^{204}Pb$	$^{207}Pb/^{204}Pb$	$^{208}Pb/^{204}Pb$	$^{207}Pb/^{206}Pb$	$^{208}Pb/^{206}Pb$	$^{208}Pb/^{207}Pb$
external precision (2s)		--	0.054	0.047	0.123	0.0017	0.0026	0.0036
AG 003	coin (tetradrachm)	1.9	18.070	15.624	38.139	0.8648	2.1106	2.4411
AV 161	coin (obol)	1.5	18.410	15.632	38.436	0.8487	2.0877	2.4587
BQ 041	coin (obol)	1.8	18.396	15.698	38.538	0.8534	2.0952	2.4550
BQ 125	coin (obol)	1.5	18.323	15.611	38.323	0.8533	2.0947	2.4540
BQ 136	coin (tetradrachm)	1.7	18.202	15.698	38.294	0.8631	2.1069	2.4411
BQ 142	coin (tetradrachm)	1.7	18.351	15.672	38.475	0.8550	2.0979	2.4545
F 107	bracelet	0.8	18.510	15.673	38.660	0.8465	2.0886	2.4666
F 108	bracelet	1.9	18.525	15.673	38.549	0.8460	2.0791	2.4584
F 113	finger ring	1.3	18.359	15.824	38.722	0.8619	2.1091	2.4480
K 205	finger ring	1.6	18.645	15.711	38.846	0.8430	2.0835	2.4726
N 036	coin (obol)	1.7	18.503	15.626	38.382	0.8445	2.0744	2.4563
N 301	small twisted wire	1.3	18.324	15.665	38.527	0.8549	2.1026	2.4625

Table VIII.4 – Pb concentration and Pb isotopic composition of copper-silver alloy coins from the site of ed-Dur

		[Pb] (%)	$^{206}Pb/^{204}Pb$	$^{207}Pb/^{204}Pb$	$^{208}Pb/^{204}Pb$	$^{207}Pb/^{206}Pb$	$^{208}Pb/^{206}Pb$	$^{208}Pb/^{207}Pb$
external precision (2s)		--	0.054	0.047	0.123	0.0017	0.0026	0.0036
AD 025	coin (tetradrachm)	1.6	18.339	15.687	38.514	0.8554	2.1008	2.4551
AV 023	coin (tetradrachm)	2.2	18.486	15.671	38.558	0.8476	2.0858	2.4604
BM 026	coin (tetradrachm)	2.7	18.470	15.634	38.580	0.8463	2.0886	2.4679
BO 043	coin (tetradrachm)	1.7	18.546	15.745	38.739	0.8486	2.0886	2.4604
BQ 005	coin (tetradrachm)	1.4	18.448	15.674	38.524	0.8496	2.0882	2.4572
BR 106	coin (tetradrachm)	0.8	18.424	15.701	38.606	0.8522	2.0954	2.4588
BS 043	coin (tetradrachm)	1.7	18.312	15.648	38.366	0.8545	2.0952	2.4516
BS 080	coin (tetradrachm)	2.0	18.096	15.618	38.147	0.8631	2.1081	2.4427
BS 097	coin (tetradrachm)	1.9	18.223	15.623	38.136	0.8573	2.0927	2.4417
BS 148	coin (tetradrachm)	1.2	18.321	15.626	38.388	0.8521	2.0933	2.4567
BS 172	coin (tetradrachm)	2.2	18.203	15.594	38.167	0.8564	2.0975	2.4464
BS 235	coin (tetradrachm)	1.7	18.410	15.613	38.239	0.8481	2.0771	2.4492
BS 236	coin (tetradrachm)	1.4	18.363	15.746	38.600	0.8575	2.1021	2.4514
BS 237	coin (tetradrachm)	2.1	18.319	15.664	38.366	0.8551	2.0943	2.4493
BS 254	coin (tetradrachm)	1.9	18.357	15.658	38.324	0.8529	2.0877	2.4477
BS 284	coin (tetradrachm)	1.8	18.546	15.694	38.629	0.8462	2.0829	2.4614
ED 005	coin (tetradrachm)	1.6	18.310	15.666	38.496	0.8553	2.1013	2.4581
N 310	coin (tetradrachm)	1.6	18.447	15.661	38.693	0.8486	2.0964	2.4712

VIII.4 – Pb isotope ratio results

In tables VIII.1-4, the Pb isotope ratio results, obtained for the metallic artefacts investigated, are summarized. Graphical representations of the $^{208}Pb/^{206}Pb$ ratio versus the $^{207}Pb/^{206}Pb$ ratio and the $^{208}Pb/^{204}Pb$ ratio versus the $^{206}Pb/^{204}Pb$ ratio are given in figure VIII.2. At first sight, two distinct isotope ratio fields can be discerned. Most of the objects investigated are to be found in a field showing a relatively large range in isotopic composition, covering a $^{208}Pb/^{206}Pb$ ratio between 2.07 and 2.13 (figure VIII.2.a), and a $^{206}Pb/^{204}Pb$ ratio between 17.85 and 18.80 (figure VIII.2.b). The copper-based objects show the largest dispersion in Pb isotopic composition and cover the isotope ratio ranges given above. A compact group of lead and litharge fragments is found at a $^{208}Pb/^{206}Pb$ ratio of 2.115 – 2.123 and a $^{206}Pb/^{204}Pb$ ratio of 18.02 – 18.15, while one lead object (bulla BS 269) is outside this compact group and displays a more radiogenic Pb isotopic composition. The silver objects cover a $^{208}Pb/^{206}Pb$ ratio range of 2.075 – 2.110 and a $^{206}Pb/^{204}Pb$ ratio range of 18.07 – 18.64. The copper-silver alloy coins form an intermingled group with the silver objects and range between 2.077 and 2.108 in $^{208}Pb/^{206}Pb$ ratio and between 18.10 and 18.55 in $^{206}Pb/^{204}Pb$ ratio. The overlap of the silver objects with the coins suggests that silver of the same origin was used for the objects as for the coins. Further, the proximity of some silver objects to the compact group of lead objects suggests the use of a common ore, *e.g.*, silver-bearing galena.
The second field is made up by 3 fragments that are much less radiogenic and characterized by a $^{208}Pb/^{206}Pb$ ratio in the 2.177 – 2.190 range (figure VIII.2.a) and a $^{206}Pb/^{204}Pb$ ratio in the 16.93 – 17.11 range (figure VIII.2.b). This field is made up by a bronze fragment originating from Khor Rori (KR 009), and two lead fragments originating from ed-Dur (BS 1466 and Z 019).

VIII.5 – Provenance determination of artefacts

In what follows, an attempt was made to provenance the metallic objects investigated, on the basis of their Pb isotopic composition. Provenancing can be translated as tracing the origin of the copper ores and silver/lead ores that were used to respectively refine the copper and silver/lead from, that was subsequently used to manufacture the artefacts investigated in this work. For this purpose, the experimental Pb isotope ratios were compared to an extensive Pb isotope ratio database, consisting of several thousands of literature data concerning the Pb isotopic composition of copper and silver/lead ore

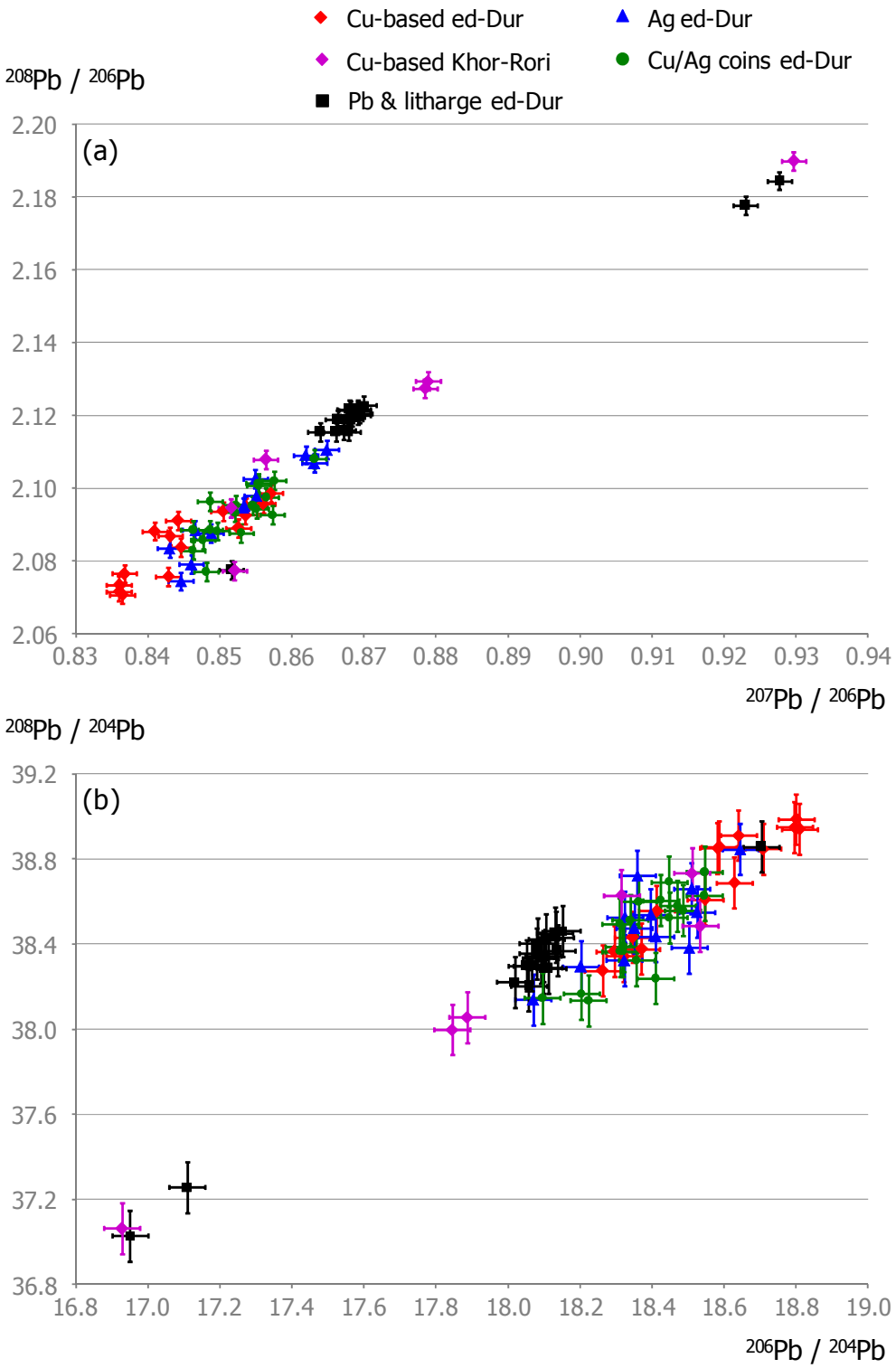

Figure VIII.2 – Pb isotope ratios obtained for metallic artefacts from ed-Dur and Khor Rori – (a) $^{208}Pb/^{206}Pb$ ratio versus $^{207}Pb/^{206}Pb$ ratio; (b) $^{208}Pb/^{204}Pb$ ratio versus $^{206}Pb/^{204}Pb$ ratio. Error bars represent 2s uncertainty intervals (external precision).

deposits from all over the old world. This database was provided by dr. P. Delrue (Ghent University) and was used for comparison purposes in this work. It was not the intention to thoroughly check all the data in this database and hence, only the relevant references in

this database were checked. An extended list containing all the literature references making up the database can be found in [Delrue, 2008]. The best documented part of the world is the Mediterranean region. To a lesser extent, data on ores from the Parthian world and India were present, while Pb isotope ratio data on material from South-East Arabia were rather limited. A drawback of the use of this database is that the dataset contains some old data and that the results have been obtained via different techniques with a different precision. However, the use of the database is supported by the observation that different literature sources report very similar isotope ratio values for a certain place of origin. Further, it should be stressed that provenance studies on the basis of Pb isotope ratios often only allow a 'negative' conclusion, *i.e.*, these studies allow to exclude a certain ore field as a potential ore source, and that via this approach, it is not possible to attribute an artefact to a single ore source with 100 % certainty.

Evidently, the isotope ratios obtained for copper-based artefacts were compared to data on copper ores, while the isotope ratios obtained for silver and lead artefacts were compared to silver/lead ores. However, it can be questioned to which extent the Pb isotopic signature of, *e.g.*, silver, brass and bronze, compares to that of the original silver/lead or copper ore. The main lead mineral is galena. Secondary lead minerals, such as cerussite and anglesite, have the same isotopic composition as that of the galena from which they are derived. The lead isotopic composition of these minerals shows a complex range of variations, inherent to their particular geological history (chapter IV, § IV.2). In antiquity, almost all silver was extracted from silver-bearing galena, and always retained some of the parent material, thus reflecting its Pb isotopic composition. However, silver is a precious metal, so that recycling and remelting must have been common practice. Mixing silver from different origin distorts the original Pb isotopic signature. Further, silver is very often debased by the addition of copper, that brings its own Pb isotopic signature [Gale and Stos-Gale, 2000]. A third point is that litharge fragments were found at ed-Dur, which are potential residues of silver extraction from a copper-silver alloy involving the addition of lead to the system. It has been shown that the addition of lead to silver prior to cupellation seriously distorts the original Pb isotopic signature of the silver [Ortiz, 2003]. However, it is not known to what extent this process was used. Copper is alloyed with tin to produce bronze. The potential contribution of lead from tin or cassiterite (SnO_2), which is found relatively pure in nature, is seen as minimal since tin deposits rarely contain any lead [Gale and Stos-Gale, 2000; Ortiz, 2003]. Leaded bronze, in this work defined as containing > 4 % lead, will mainly reflect the Pb isotopic composition of the lead added. Smelting experiments and analyses of batches of raw copper have shown that certain copper ores

can generate smelted copper with a lead content up to 4-5 %. It has been stated that copper alloy artefacts that contain less than 4 % lead can be provenanced on the basis of their copper Pb isotopic signature [Gale and Stos-Gale, 2000; Ortiz, 2003]. Provenancing brass via its Pb isotopic composition is not an easy task, since lead is always associated with zinc ores. Adding zinc to copper results in a mixing of the Pb isotopic signatures of the copper and the zinc. However, the brasses found at ed-Dur display a very low zinc and lead level, indicating that they are rather 'pure' and not the result of extensive recycling. From this point of view, lead isotope ratios are valuable for intra-site comparison of the brass artefacts.

For the purpose of provenance determination, the isotope ratios $^{207}Pb/^{206}Pb$ and $^{208}Pb/^{206}Pb$ are used in the discussion below, since these ratios can be most precisely determined using the single-collector ICP – dynamic reaction cell – MS measurement protocol developed, compared to the Pb isotope ratios with ^{204}Pb. However, the conclusions based on the $^{207}Pb/^{206}Pb$ and $^{208}Pb/^{206}Pb$ ratios are the same as that established with diagrams where the $^{206}Pb/^{204}Pb$ and $^{208}Pb/^{204}Pb$ ratios are plotted with respect to each other. Another reason is that ratios with ^{204}Pb are less frequently documented in the database than the ratios consisting of the most abundant Pb isotopes. In following paragraphs, first the field consisting of the three artefacts with a $^{208}Pb/^{206}Pb$ ratio of 2.177 – 2.190 are considered, followed by the copper-based artefacts. After that, the lead and silver artefacts are treated together.

VIII.5.1 – Fragments BS 1466 and Z 019 (lead) and KR 009 (bronze)

First, the field formed by the two lead fragments BS 1466 and Z 019 from ed-Dur and the bronze fragment KR 009 from Khor Rori (figure VII.2) is considered. The fragments in this group are characterized by a Pb isotopic composition that is significantly less radiogenic than that of the other metallic artefacts investigated. A scatterplot of the $^{208}Pb/^{206}Pb$ ratio versus the $^{207}Pb/^{206}Pb$ ratio for these three samples is given in figure VIII.3. The bronze object KR 009 was found as not intentionally leaded (table VIII.1), and thus it can be assumed that its Pb isotopic composition reflects mainly that of its copper ore. The fragments BS 1466 and Z 019 are lead fragments. Both of these contain traces of silver, in accordance with lead that was de-silvered. The fragment Z 019 was taken from a rather large piece of lead (12 x 7 x 3 cm) with a rough bottom side, that might indicate molten lead being poured into a roughly hewn stone hollow, and hence suggests that this fragment might be an ingot [Delrue, 2008].

In figure VIII.3, the Pb isotope ratio data corresponding to copper and silver/lead ores from the database that display a similar Pb isotopic composition are superposed onto the experimental data. Although there is no overlap, the only relevant matches for both copper and lead fragments appear to be ores from the Indian subcontinent. Not much data on Indian ores are available however. The most closely related ores are these from the region or Rajasthan (figure VIII.1), that are characterized by a $^{208}Pb/^{206}Pb$ ratio of 2.19 – 2.25 [Ericson and Shirahata, 1985; Srinivasan, 1999], while the ores from the region of Gujarat (figure VIII.1) display a $^{208}Pb/^{206}Pb$ ratio 2.15 – 2.16 [Ericson and Shirahata, 1985; Srinivasan, 1999]. The Rajasthan ores are polymetallic, containing lead and zinc, and both copper and silver deposits are present [Ericson and Shirahata, 1985], explaining the fact that some copper and silver/lead ore data points plot in the same place (figure VIII.3).

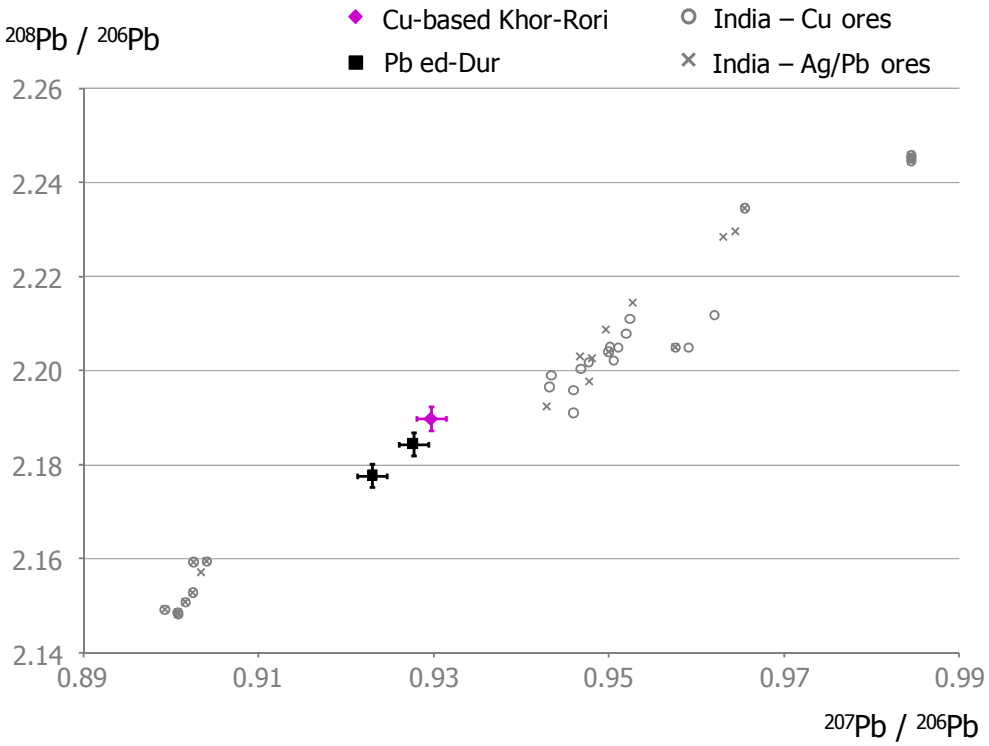

Figure VIII.3 – $^{208}Pb/^{206}Pb$ ratio versus $^{207}Pb/^{206}Pb$ ratio for bronze fragments KR 009 (Khor Rori) and lead fragments BS 1466 and Z 019 (ed-Dur), and literature data (references: see text) for Indian copper and silver/lead ores. Error bars represent 2s uncertainty intervals (external precision).

The Pb isotopic composition of the bronze fragment KR 009 does not exactly overlap with the Indian copper ore data (figure VIII.3), but the copper can be a mix of different ore sources of Indian origin. Another possibility is that the copper ore at the origin of the object is, as yet, still unidentified regarding the vastness of the Indian subcontinent and the relatively few Pb isotope ratio data available for this region. In any case, the origin of the copper in the bronze fragment is most likely Indian, an assumption that is supported

by historical evidence that ore sources in Rajasthan were exploited at 'early times' [Chakraborti, 1966].

The provenance of the two ed-Dur lead fragments BS 1466 and Z 019 can be derived in the same way as the bronze fragment from Khor Rori, and is most probably linked to Indian silver/lead ores from the region of Rajasthan. Again, no overlap is observed, which leads to different suggestions. First, the lead can be a mix of (i) lead originating from several regions in India, or (ii) lead originating from India and lead originating from the Roman Empire (see § VIII.5.3). Second, the ore source at the origin of these objects may still remain to be identified. Based on the physical appearance of the object Z 019 and its Pb isotopic signature, it can be suggested that this object is a lead ingot of Indian origin.

An additional argument for assigning a non-European origin to the fragments KR 009, BS 1466 and Z 019, is found in their high $^{207}Pb/^{206}Pb$ ratios (0.923 – 0.930), indicating an age of 1.2-1.3 billion years according to the Stacey-Kramers growth curve [Stacey and Kramers, 1975], an age that is older than that of most of the European Pb deposits.

VIII.5.2 – Copper-based artefacts

A scatterplot representing the $^{208}Pb/^{206}Pb$ ratio versus the $^{207}Pb/^{206}Pb$ ratio for the copper-based artefacts – unalloyed copper, brass and bronze (table VIII.1) – is given in figure VIII.4. The bronze fragment KR 009 was discussed above (§ VIII.5.1) and is not further considered here.

Two bronze fragments originating from Khor Rori (KR 010 and KR 011) display a $^{208}Pb/^{206}Pb$ ratio of 2.127 – 2.129 (figure VIII.4). One of these fragments (KR 011) is leaded (table VIII.1), what leads to the expectation that its Pb signature is originating from the lead added rather than from the copper. The rest of the bronze artefacts occur in a lower $^{208}Pb/^{206}Pb$ ratio range of 2.07 – 2.11 and are scattered throughout this isotope ratio range (figure VIII.4). The brass objects are found at a $^{208}Pb/^{206}Pb$ ratio of 2.089 – 2.095 and form a relatively compact group. Apart from the fact that brass is hard to provenance by comparing its Pb isotopic composition to that of copper ores due to the zinc added, it can be concluded that the brass is derived from the same basic materials. The three unalloyed-copper objects appear to be rather different in Pb isotopic composition.

The fact that some bronze artefacts were leaded and that the Pb isotopic signature of brass can be biased by Pb coming from the zinc, implies that care should be taken when comparing to copper ore data. From a comparison of the experimental results to the

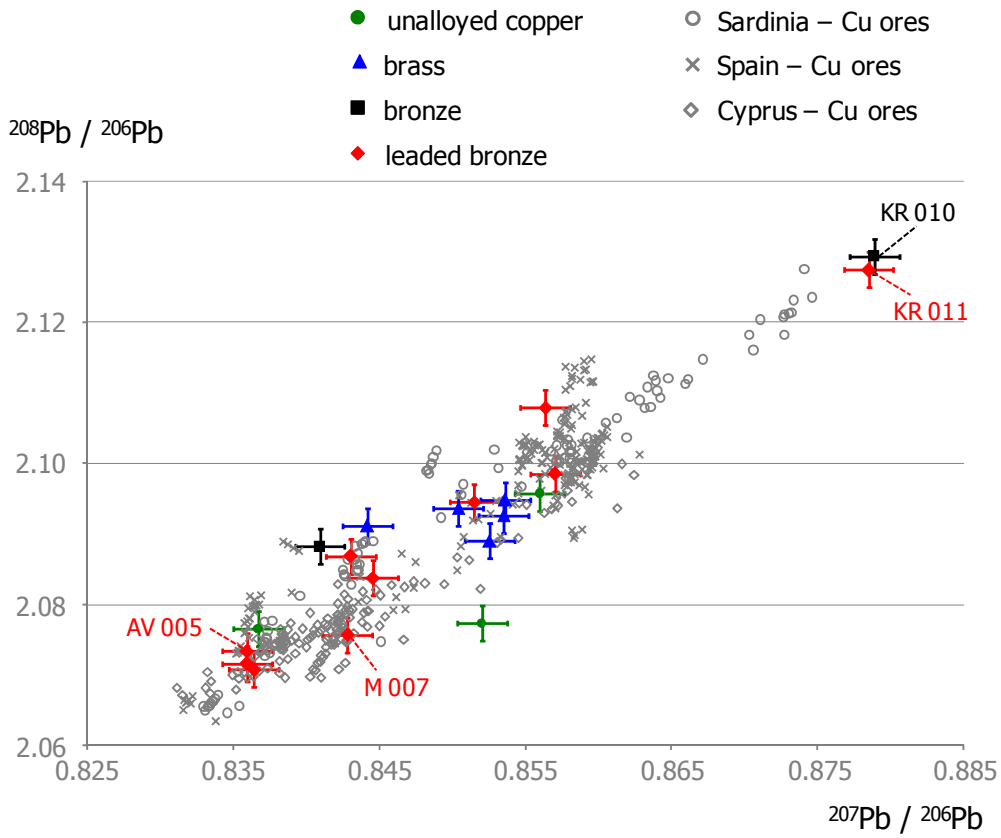

Figure VIII.4 – $^{208}Pb/^{206}Pb$ ratio versus $^{207}Pb/^{206}Pb$ ratio for copper-based artefacts from ed-Dur and Khor Rori, and literature data (references: see text) for Sardinian, Spanish and Cypriot copper ores. Error bars represent 2s uncertainty intervals (external precision).

database, it was established that many ore fields resulted in overlap with the experimental data to at least some extent. This is the case for ores originating from, *e.g.*, Bulgaria, Greece, Italy and Turkey (figure VIII.6). However, the best agreement was found with copper ore sources from Cyprus, Sardinia and Spain, regions that are known as important sources of copper to the Roman Empire [Delrue, 2008]. The Pb isotope ratio data for Cypriot, Sardinian and Spanish copper ores are superposed on the experimental data in figure VIII.4. The Cypriot copper ores are mainly found at a $^{208}Pb/^{206}Pb$ ratio of 2.07 – 2.08 [Stos-Gale *et al.*, 1986; Gale *et al.*, 1997; Stos-Gale *et al.*, 1997; Stos-Gale *et al.*, 1998-a; Attanasio *et al.*, 2001; Ortiz, 2003], while the bulk of the Spanish ores is found between 2.09 and 2.11 in $^{208}Pb/^{206}Pb$ ratio [Stos-Gale *et al.*, 1995; Attanasio *et al.*, 2001; Ortiz, 2003]. The Sardinian copper ores show a Pb isotopic composition that is rather dispersed among the experimental $^{208}Pb/^{206}Pb$ ratio range [Gale and Stos-Gale, 1987; Stos-Gale *et al.*, 1995; Stos-Gale *et al.*, 1997; Attanasio *et al.*, 2001; Begemann *et al.*, 2001]. From the match with Cypriot, Sardinian and Spanish copper ores, a Mediterranean/Roman origin of the copper in the investigated objects from ed-Dur is put forward. This assumption is archaeologically supported by the knowledge that Sardinia and Spain were extensively mined by the Romans until ca.

50 AD. Further archaeological evidence is provided by the Pb isotopic composition observed for the bronze patera (AV 005) and pedestal statuette (M 007), matching mainly Mediterranean copper ores (figure VIII.4 and figure VIII.6). A patera is a bowl or pan with a long, round, frequently ribbed handle. Often, this handle is decorated with a ram's head. These vessels became widespread in the Roman Empire during the 1st century AD and served mainly for cooking and serving food. It is unquestionable that this object is of Mediterranean/Roman origin [Delrue, 2008]. The pedestal statuette (M 007) was found together with two more Roman objects. Little information is available on this object. However, two similar pedestals have been reported, both in Roman context. From this, it can be suggested that the pedestal is also Roman [Delrue, 2008]. An attribution of the ore sources to Roman provenance indicates that these objects of Roman manufacture are made from copper originating from Roman ore sources.

For the two bronze Khor Rori fragments with a $^{208}Pb/^{206}Pb$ ratio of 2.127 – 2.129 (KR 010 and KR 011), no agreement is found with the Cypriot, Sardinian and Spanish copper ores (figure VIII.4). However, their Pb isotopic composition may be explained by mixing of copper stemming from Indian and Roman ore sources. It might be argued, at least for the unleaded fragment KR 010, that it contains copper from the Indian subcontinent, so that its Pb isotopic signature shifts towards Indian ores. Combining the facts that bronze fragment KR 009 (figure VIII.3) is probably Indian and that crucibles used for copper melting were retrieved at Khor Rori [Delrue, 2008], suggests that copper from both source regions (Mediterranean and Indian) were mixed. Considering the collection of bronze fragments originating from Khor Rori as a whole (figure VIII.2 and table VIII.1), their Pb isotope ratios reveal that most of these are rather atypical compared to the bronze artefacts originating from ed-Dur. This observation might imply that the metal supply to the site of Khor Rori was different from that to the site of ed-Dur.

VIII.5.3 – Silver and lead artefacts

A scatterplot representing the $^{208}Pb/^{206}Pb$ ratio versus the $^{207}Pb/^{206}Pb$ ratio for the lead and litharge fragments and silver objects investigated in this work is given in figure VIII.5. The leaded bronze fragments discussed above (§ VIII.5.2) are also shown in figure VIII.5 since the Pb isotopic signature is probably closer to that of the lead added than to the copper in the bronze artefact. The lead fragments BS 1466 and Z 019 with a less radiogenic Pb isotopic composition have been discussed and provenanced in § VIII.5.1 and are not further discussed below.

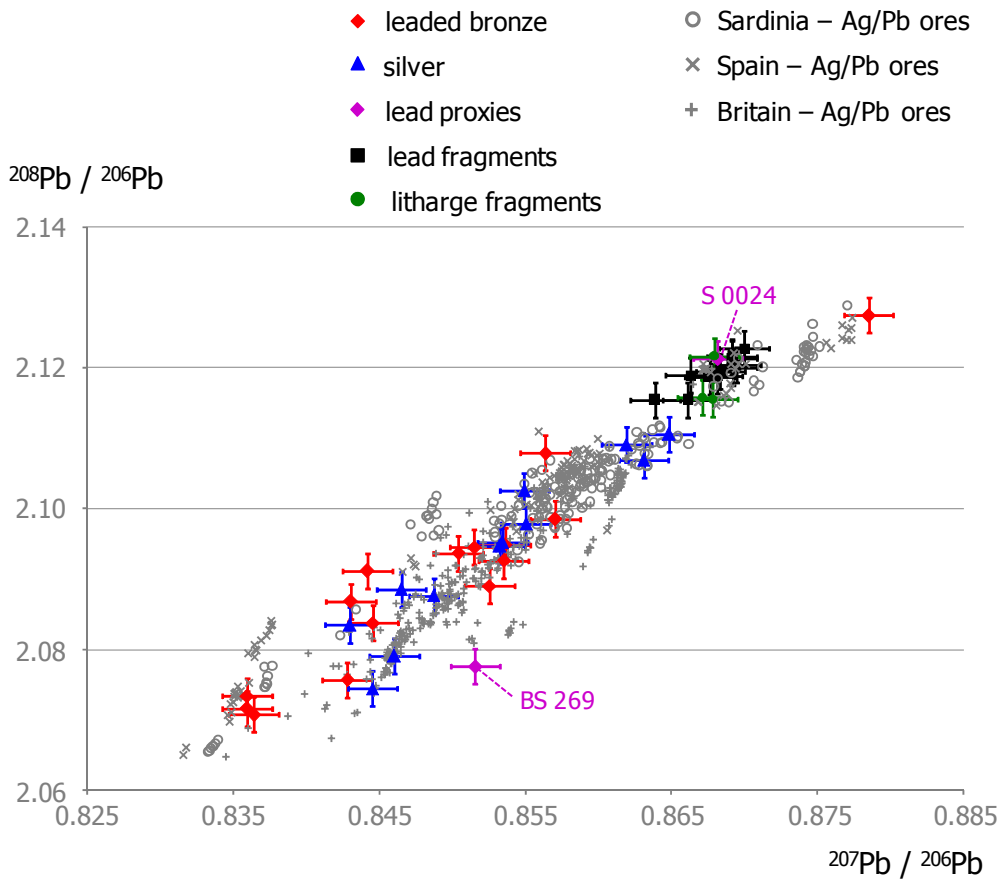

Figure VIII.5 – $^{208}Pb/^{206}Pb$ ratio versus $^{207}Pb/^{206}Pb$ ratio for silver, lead and litharge (ed-Dur) and leaded bronze (ed-Dur and Khor Rori) fragments, and literature data (references: see text) for Sardinian, Spanish and British silver/lead ores. Error bars represent 2s uncertainty intervals (external precision).

The Pb isotopic composition of the leaded bronze objects covers the $^{208}Pb/^{206}Pb$ ratio range of 2.07 – 2.11, while one bronze object from Khor Rori (KR 011) displays a $^{208}Pb/^{206}Pb$ ratio of 2.127. The silver objects display a $^{208}Pb/^{206}Pb$ ratio between 2.074 and 2.110 and form a rather dispersed group, although three distinct groups can be discerned on the basis of the $^{207}Pb/^{206}Pb$ ratio. The lead and litharge fragments constitute a compact group, situated in the range 2.115 – 2.123 in $^{208}Pb/^{206}Pb$ ratio (figure VIII.5). Only the lead fragment BS 269 (bulla) is not included in this group and is characterized by a lower $^{208}Pb/^{206}Pb$ ratio of 2.078. Remarkably, the three lead fragments initially denoted as 'lead proxies' – BS 269 (bulla) and S 0024 (figure VIII.5) and Z 019 (figure VIII.3) (assumed to be ingots) – all show a different Pb isotopic composition (table VIII.2). The compact group of lead and litharge fragments is centered around lead fragment S 0024 (figure VIII.5), which supports the assumption that lead fragment S 0024 indeed is an ingot. Further, it shows that the other lead fragments originate from the same lead source and provides evidence that lead was imported in 'bulk' to ed-Dur and used to

manufacture the desired lead objects on-site. Moreover, the litharge fragments centered around the ingot S 0024 show that lead from the same source as for the ingot was used in the cupellation process for the purification of silver. The bulla BS 269 shows a Pb isotopic composition that is quite different from that of the ingot S 0024 and that of the lead and litharge fragments (figure VIII.5). Since the bulla BS 269 was certainly not produced at ed-Dur, but is beyond doubt of Indian manufacture [Delrue, 2008], such a result could be expected. Unfortunately, bulla BS 269 is neither linked to ingot Z 019 to which an Indian provenance was attributed (§ VIII.4.1). However, an agreement with an unalloyed copper fragment (KR 012) is observed (figure VIII.2 and figure VIII.4). This bronze fragment originates from Khor Rori and it was concluded from the provenance of the copper-based artefacts (§ VIII.4.2) that the metal supply to the site of Khor Rori is probably different from that to the site of ed-Dur.

Comparison of the Pb isotope ratio data obtained for the silver and leaded bronze artefacts with silver/lead ore source regions revealed that, for the objects with a $^{208}Pb/^{206}Pb$ ratio above 2.09, there is an excellent overlap with Sardinian and Spanish ores (figure VIII.5), compared to other source regions. Most part of the literature data on the Pb isotopic composition of Sardinian [Gale and Stos-Gale, 1987; Stos-Gale *et al.*, 1995; Stos-Gale *et al.*, 1997; Begemann *et al.*, 2001] and Spanish [Stos-Gale *et al.*, 1995; Pernicka *et al.*, 1998; Santos Zalduegui *et al.*, 2004] silver/lead ores report a $^{208}Pb/^{206}Pb$ ratio in the range of 2.09 – 2.13, although also values around 2.07 are documented to a lesser extent. Sardinia and Spain were already put forward as the most probable ore sources for the leaded bronze artefacts on the basis of comparison to copper ore data (§ VIII.4.2). However, with only Sardinia and Spain as ore source fields, the silver objects with a $^{208}Pb/^{206}Pb$ below 2.09 remain barely explained, suggesting that an additional source field was required. Further comparison to the Pb isotope data in the database indeed showed that the ore sources of the United Kingdom and Wales complete the source attribution of all the silver objects investigated. The $^{208}Pb/^{206}Pb$ ratio ranges between 2.07 and 2.10 for the silver/lead ores from the United Kingdom [Rohl, 1996], and between 2.09 and 2.11 for the silver/lead ores from Wales [Rohl, 1996] (figure VIII.5). Next to Sardinia, Spain, the United Kingdom and Wales, also Bulgaria, France and Italy show overlap to a certain extent (figure VIII.6) and hence, cannot be excluded as additional potential ore source regions. The source attribution to Sardinia and Spain on the one hand, and to the United Kingdom and Wales on the other hand, can be explained on the basis of archaeological data. Possibly, a chronological factor is at play here. It is known that the Romans extensively mined the Sardinian and Spanish ores during the 1st century AD. After the annexation of Great

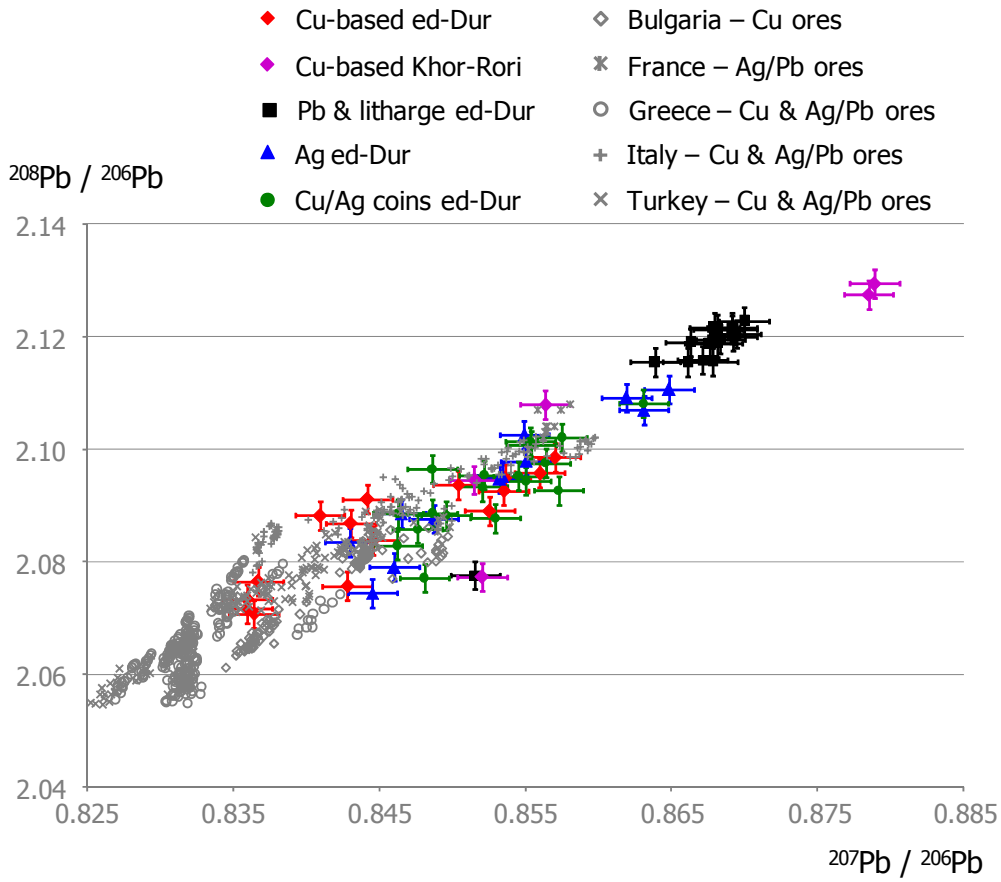

Figure VIII.6 – $^{208}Pb/^{206}Pb$ ratio versus $^{207}Pb/^{206}Pb$ ratio for metallic artefacts from ed-Dur and Khor Rori, and literature data for Bulgarian [Stos-Gale *et al.*, 1998-b; Gale *et al.*, 2003], French [Trincherini *et al.*, 2001], Greek [Barnes *et al.*, 1974; Stos-Gale *et al.*, 1996; Stos-Gale *et al.*, 1997], Italian [Stos-Gale *et al.*, 1995; Boni *et al.*, 2000; Ortiz, 2003; Klein *et al.*, 2004-a] and Turkish [Yener *et al.*, 1991; Sayre *et al.*, 2001] copper and/or silver/lead ores. Error bars represent 2s uncertainty intervals (external precision).

Britain to the Roman Empire, British lead ores, that were more easily accessible, became available. By ca. 70 AD, the British ore fields had become the main providers of lead and silver ores [Delrue, 2008]. These data fall well within the occupation phase of ed-Dur (1^{st} century BC – 1^{st} half 2^{nd} century AD). Some silver objects that have been attributed to British silver/lead ore source fields indeed date from a later time [Delrue, 2008]. In any case, the provenance of the silver and leaded bronze fragments is most likely Roman.

A similar comparison of the experimental Pb isotope ratios obtained for the lead and litharge fragments with the database showed an excellent agreement with the Sardinian and Spanish silver/lead ores. As a consequence, the ingot S 0024 and most of the lead fragments found at ed-Dur can, with a high degree of certainty, be identified as of Mediterranean/Roman origin. The isotopic composition of the bulla BS 269, which is certainly produced in India [Delrue, 2008], does not appear to be Sardinian or Spanish as is ingot S 0024, and neither Indian as is ingot Z 019. The best match for bulla BS 269 is

with British silver/lead ores. This observation could be explained by assuming that the bulla was manufactured in India with lead imported from the Roman Empire, and was subsequently exported from India to ed-Dur.

The tetradrachm coins (table VIII.4), manufactured from a copper-silver alloy (billon) form an intermingled group with the copper-based and silver artefacts (figure VIII.2). The attribution of Roman ore sources to the copper-based and silver artefacts implies that also the local South-East Arabian coins are manufactured from Roman ores.

VIII.6 – Conclusions and implications on trade

Provenancing copper-based artefacts excavated at the site of ed-Dur showed that the Pb isotopic signature is linked to ore sources from Cyprus, Sardinia and Spain, which implies that the ed-Dur objects are made from Roman copper. Three bronze samples (KR 009, KR 010 and KR 011), excavated at the site of Khor Rori, deviate in Pb isotopic composition from the samples excavated at ed-Dur. One of these samples (KR 009) can be linked to Indian copper ores. The attribution of the sample from Khor Rori to an Indian origin is intriguing. The Periplus and Pliny both state that copper was imported into India from the Roman world and suggest that no local copper was produced in India [Periplus; Plinius; Delrue, 2008]. The findings here rather contradict this and suggest that at least to some extent, copper was produced in India and, apparently, exported to Oman. There is evidence that sources in Rajasthan were exploited at 'early times' [Chakraborti, 1966]. This region would have had an outlet via the harbor of Barygaza. Barygaza is indeed mentioned in the Periplus, as sending shipments of copper to the Gulf. The dependence of India on imported Roman copper might have been less significant than suggested in the Periplus and Pliny, and rather meant to create a surplus than to fill a shortage [Delrue, 2008]. Further, the bronze fragments from Khor Rori are observed as atypical in Pb isotopic composition compared to the objects from ed-Dur, implying that the metal supply to the site of ed-Dur was different from that to the site of Khor Rori [Delrue, 2008].

The lead fragments investigated, except for 3 items, all show a very similar Pb isotopic composition and are grouped around an ingot (S 0024) with a stamped monogram. The very good agreement with Sardinian and Spanish ores allows the conclusion that this lead is of Roman origin. However, two lead fragments (BS 1466 and Z 019), of which one (Z 019) probably is an ingot, show a Pb isotopic composition similar to that of the deviating bronze fragment from Khor Rori, and can probably be attributed to India. The identification of two objects as Indian can be explained by a chronological factor that is at

play, namely that these objects date from the 2nd half of the 1st century AD [Delrue, 2008]. In this period, the Indian mines of Rajasthan were opened, as evidenced by a study of the Indian coinage [Seeley and Turner, 1984]. It was observed that in the second half of the 1st century AD, the Pb isotopic signature drastically changed from a Mediterranean (Sardinia and Spain) into an Indian (Rajasthan) signature. As a consequence, the provenancing of lead fragments found at ed-Dur fits the idea that India was producing and even exporting lead to some extent. In any case, the two samples from ed-Dur are the first to demonstrate that India was exporting, and thus also producing, lead before the 2nd century AD [Delrue, 2008]. Also one of the Khor Rori bronzes seems to originate from the same Indian region. The lead from fragment BS 269 (bulla) that is certainly of Indian manufacture [Delrue, 2008], does not show a correlation with Indian lead ores, but rather appears to be of British origin.

The litharge fragments show a Pb isotopic composition that is similar to that of the Roman ingot and the lead fragments, which implies that the same lead is used in the cupellation process to obtain silver. The silver objects were established as stemming from Sardinian and Spanish ores, but these ore source fields do not explain the isotopic composition of all the silver objects investigated. Including the British ore source fields, exploited by the Romans from ca. 50 AD and dominating from ca. 70 AD onwards, leads to a complete source attribution to the silver objects, and the conclusion that the silver is originating from the Roman Empire. The local South-East Arabian coins are manufactured from a copper-silver alloy (billon) and form an intermingled group with the copper-based and silver artefacts, from which it can be concluded that also these coins were made from Roman ores.

The results from Pb isotope ratio analysis and provenancing of metallic artefacts from ed-Dur and Khor Rori can be considered in the light of the trade relations and routes operated in the period between the 1st century BC – 1st half 2nd century AD. It is known from the Periplus that, during the 1st century AD, the Romans were exporting lead towards the Indian subcontinent, which apparently also ended up at ed-Dur. The question remains via which trade channel ed-Dur was provided with lead. Three possible routes can be suggested, based on textual and archaeological research [Delrue, 2008]. The main trade route between the Roman Empire and the Indian subcontinent was via the Red Sea along the South-Arabian coast, past the mouth of the Gulf, towards India (figure VIII.1). Later on, a direct route across the open sea was opened. The lead arrived in the Indian subcontinent via the harbors of Barygaza on the north-west coast, and Muziris and Nelkynda on the south-west coast of India. The metal that arrived in India could then be

re-exported towards the Gulf, as is illustrated in the Periplus for copper metal, but not for lead. Theoretically however, it is entirely possible that also lead was shipped to the Gulf region via this route [Delrue, 2008].

A second possibility is that Roman lead was already disembarked in one of the South-Arabian ports and then transported to the Gulf via local trade routes by ship or across land (figure VIII.1). However, there is scarce evidence of contacts between South Arabia and ed-Dur, which makes this possibility less probable [Delrue, 2008].

The third option is that the lead came from an entirely different direction, namely via the Palmyrene-Characenean network (figure VIII.1). This implies that the metal travelled from the Eastern Mediterranean across Syria, to Palmyra. There, it was taken on the Euphrates and travelled downstream to the city of Characene, and continuing its route down the Gulf to eventually reach ed-Dur [Delrue, 2008].

This puzzle can be solved by considering the lead isotope ratio data obtained for the ingot S 0024 and the bulla BS 269. The lead of the ingot S 0024 was provenanced as Roman, and an interesting feature of this ingot is the stamped monogram on it. Similar and even the same monograms were found on some South-East Arabian coins and some pottery shards. It resembles monograms on coins from Characene and Seleucia, and an intaglio of a Characenean finger-ring. The meaning of this monogram is unfortunately unknown, but it could be the abbreviation of Attambelos, who was a Characenean king [Delrue, 2008]. When the hypothesis is assumed that this monogram indeed is Characenean, it indicates that the lead metal passed through the city of Characene. It is known that the links between ed-Dur and Characene were tight. This is evidenced by the large amount of South Mesopotamian ceramics and coins originating from Characene found at ed-Dur. Moreover, a more general link between ed-Dur and the Parthian culture is found in the appearance of ring-pommel daggers [Delrue, 2006], and the similarity in some iron objects [Delrue, 2008]. Combining the strong link between ed-Dur and Characene, the appearance of a monogram possibly of Characenean origin on the ingot S 0024 and the absence of lead listed as an export product in the otherwise detailed Periplus, leads to the conclusion that an itinerary of the lead ingot via the Palmyrene-Characenean network is very plausible [Delrue, 2008].

The lead of the bulla, on the other hand, shows correlation with the British ore sources and can probably be identified as Roman. However, this bulla is certainly made in India [Delrue, 2008]. When the lead in the bulla indeed is Roman, this demonstrates the use of the first trade route suggested above, where the lead was shipped from the Roman Empire to India, processed and used to manufacture artefacts from, that were

subsequently shipped to the Gulf region. The reason why this itinerary is not mentioned in the Periplus remains unclear.

CHAPTER IX

Investigation of infant exposure to lead during the Roman Era

This chapter summarizes and discusses Pb isotope ratio data that were obtained in the framework of a multidisciplinary study, involving the fields of archaeology, toxicology and analytical chemistry, investigating the cause of high infant lead exposure in the Roman Era. The goal of the study was to identify the sources of the high lead levels retrieved in inhumed infant bone tissue samples, and more specifically to find out whether the high lead concentration in bone can be attributed to diagenesis. A detailed discussion on the toxicological and archaeological context and implications is largely beyond the scope of this chapter, and the interested reader is referred to two papers entirely devoted to these topics [de Wolff *et al.*, 2008; Smits *et al.*, 2008].

IX.1 – Toxicological and historical background

IX.1.1 – Toxicology of lead

Lead is a widely used metal, *e.g.*, in ancient times, for manufacturing trays and kitchen utensils and in more recent times, for the production of electric batteries for vehicles, as an additive in gasoline and in paints. At the same time, lead is a versatile, insidious and persistent poison. Metallic lead has belonged to the human environment for over 5 000 years [Philip and Gerson, 1994-a]. Effects of lead toxicity, which manifests itself by, *e.g.*, anemia, nephrotoxicity and nervous system disorders, have already been described by Hippocrates in 370 BC [Philip and Gerson, 1994-a]. Many more negative effects of lead are known at present. Organic (tetraethyl) lead affects the nervous system [Gidlow, 2004], while inorganic lead acts on different body functions and systems, *e.g.*, heme synthesis [Piomelli, 2002], reproduction [Hu, 1991], nervous system and kidneys [Philip and Gerson, 1994-b]. From epidemiological studies, inconclusive evidence has been found as to a causal relation between lead exposure and the incidence of cancer. At present, there are insufficient data for suggesting that lead compounds are carcinogenic to humans [IARC, 1987]. Especially children and pregnant women are vulnerable to the negative effects of lead. Additional and more detailed information on lead toxicity can be found in dedicated sources, *e.g.*, [Gidlow, 2004; Papanikolaou *et al.*, 2005].

Lead can enter the body via different pathways: by absorption through the intestines after oral ingestion, by inhalation through the lungs, by direct swallowing, and through the skin [Philip and Gerson, 1994-a]. Inorganic lead absorption takes place throughout the respiratory and gastrointestinal tracts, while organic (tetraethyl) lead can be absorbed via the skin. After lead exposure, the lead is absorbed into the blood and transported to other tissues.

Lead predominantly accumulates in three compartments: blood, soft tissues, and bone [Rabinowitz, 1991]. Approximately 99 % of the lead in blood is found in the erythrocytes, leaving about 1 % in the plasma. More than 95 % of lead is deposited in skeletal bone as insoluble phosphate [Rabinowitz, 1991]. In adults, 80 to 95 % of the total body burden of lead is found in the skeleton; for children, this is only 73 %. Lead has an estimated half-life of 20 to 30 years in bone tissue [Rabinowitz *et al.*, 1976; Papanikolaou *et al.*, 2005] and its concentration in bone and teeth increases as a function of age. In general, lead is excreted extremely slowly from the body. Its biological half-life is estimated at 10 years [Philip and Gerson, 1994-a].

IX.1.2 – The use of lead in the Roman Era

In the Roman Era, lead was used for a variety of applications. Next to the manufacturing of water pipes and lead tools, lead-containing food additives have been described, such as *sapa* and *defrutum* [Smits, 2006]. These are derived from grapes, and boiled in vessels made of lead or leaded bronze [Columella; Plinius]. From experiments with ancient recipes, it was estimated that *sapa* and *defrutum* would have contained 240-1 000 µg L^{-1} of lead [Kobert, 1909; Eisinger, 1977]. This syrup was added to numerous dishes for its sweet taste to, *e.g.*, *garum*, a fermented fish sauce, and for conservation purposes of, *e.g.*, wine and fruits. It was estimated that the lead level in wine by the addition of *sapa* would amount to 15-30 µg L^{-1} [Hofmann, 1883], and even (much) higher [Nriagu, 1983-a; Needleman, 2004].
The mental and physical health of a number of emperors, as evidenced from written sources, could point towards lead poisoning [Suetonius]. Claudius was walking with unequal steps and dragged his right foot, displayed involuntary movements of the head and spoke and laughed with a strange-sounding voice. Tiberius suffered from encephalopathy and was famous for his drinking habits. Also Caligula and Nero were alcoholics. Extravagance, immorality, intolerance, paranoia and cruelty featured their behavior. Most of the emperors also suffered from saturnine gout [Celsus], a likely symptom of lead poisoning due to the inhibited excretion of uric acid and the deposition of urate crystals in the joints. Also the low number of offspring from the aristocracy [Suetonius] can be attributed to a decreasing fertility as a consequence of lead poisoning. The downfall of the Roman Empire has even been suggested as a direct or indirect consequence of excessive lead uptake [Gilfillan, 1965; Nriagu, 1983-a; Nriagu, 1983-b].

IX.2 – Sampling site and history of research

The study presented here focuses on the cemetery of a Roman settlement, excavated in the village of Valkenburg, situated on the Southern shore of the river Rhine a few kilometres west of the city of Leiden (*Lugdunum Batavorum*), in the West of The Netherlands close to the North Sea (figure IX.1). The river Rhine marked the Northern frontier in this part of the Roman Empire. This frontier was defended by many military fortresses connected by the Roman road. In the period 1st – 3rd century AD, several military forces were settled in a fortress at Valkenburg, at that time known as *Pretorium Agrippinae*. In the vicinity, archaeological excavations uncovered the remains of a civilian settlement and a large cemetery [Bult and Hallewas, 1986; Bult and Hallewas, 1987; Bult and Hallewas, 1990]. This cemetery yielded many cremation graves, as older children and adults were customarily cremated in Roman days. However, the Roman rule also stipulated that young infants (without teeth) should be buried instead of being cremated [Plinius]. Approximately 35 % of the total population (on the basis of the cremation and inhumation graves) died before the age of fourteen, while approximately 14 % even died in the first year of life [Smits, 2006].

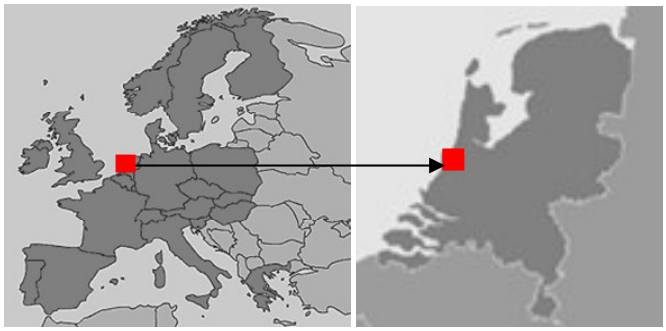

Figure IX.1 – Geographical location of Valkenburg (The Netherlands, Europe)

In most Roman cemeteries, the remains of very young infants (buried in inhumation graves) are mostly absent because of the fragility of the remains and the acidic soil conditions that often did not favor the preservation of bone tissue. Moreover, these small and fragile bones are easily missed as a result of the archaeological excavation methods typically used in the field. At Valkenburg however, an exceptionally high number of infant graves was discovered, even providing a fair insight into the percentage of infant graves in relation to the total cemetery population. The excavations at the grave field resulted in the discovery of the remains of a total of 683 individuals in 520 cremation graves and 134 inhumation graves. The age and/or sex could be determined for 503 individuals. In 176 graves – 81 cremation graves and 95 inhumation graves – skeletal remains of

children between 0 and 14 years of age were discovered. It was established that 84 of the 95 inhumed infant skeletons found, stemmed from infants younger than 1 year [Smits, 2006]. These skeletons are relatively well-preserved as the soil in that region is alkaline due to deposition of sea shells. To investigate the cause of this high infant mortality, self-evidently, only the skeletal remains are accessible. In paleopathology, the cause of death can seldom be detected from the bone material. In this case however, the availability of infant remains in association with the existing theories of the abundant use of lead during the Roman period instigated a chemical-toxicological study of the infant bones to discover whether the ingestion of lead during pregnancy might have been contributing to or even be at the origin of the death of these infants.

A preliminary study, in which the lead concentration in the femora of 33 neonates was determined using electrothermal AAS after acid digestion, showed that the bones of all individuals displayed a considerable lead concentration, ranging between 12 and 388 µg g^{-1} with an average of 103 ± 87 µg g^{-1}. The surrounding soil showed a much lower lead concentration of 18 ± 7 µg g^{-1} [de Wolff *et al.*, 2001]. From these observations, it could not be a priori excluded that diagenesis – post-mortem lead exchange between bone and surrounding soil – is the main source of the lead found in the bones. Therefore, a new study, carried out within the scope of this thesis, was designed, with the intention to reveal the source(s) of the lead found in the bones via lead isotope ratio analysis. The aim was to clarify if the bone lead has entered the bone via diagenesis (from the soil) or via another mechanism, *e.g.*, ante-mortem lead uptake via lead-rich food consumed by the mother. Therefore, in addition to the infant bone tissue, also soil and other potential sources of bone lead such as *garum*, lead objects and amphorae were investigated for their Pb isotopic composition.

IX.3 – Samples investigated in this work

A set of 22 infant bone tissue samples, taken throughout the entire excavation site, was subject to Pb isotopic analysis. The bone samples were taken from femora of deceased and stillborn Roman infants of which the sex is, as yet, not determined. The cortical bone tissue (hard outer tissue) was sampled. This area is free of foreign material – and thus provides the most accurate results – in contradiction to trabecular bone (inner tissue in which the bone metabolism occurs), which contains excessive amounts of intruded soil particles and hence, is less reliable. Every bone sample was accompanied by a sample from the surrounding soil from which the bone was excavated, thus leading to 22 pairs of

bone tissue and soil. Only small sample amounts (≤ 1 g) of bone and soil were available. Potential sources of bone lead, next to soil, consisted of a sample of fish bones, 10 lead fragments, 1 pottery fragment and 8 amphora samples. The fish bones originate from a large earthenware bowl, which was excavated at the site and which was filled with hundreds of fish bones. This find was interpreted as the remains of the well-known Roman dish *garum* (§ IX.1.2). In the following text, this fish bone sample will always be referred to as 'garum'. Of the 10 lead fragments supplied, one was mounted onto a pottery shard, in a construction that resembles a mill. This object was identified as stemming from a container for food conservation. The pottery fragment was also sampled. Further, 8 amphora samples were provided. These amphorae, as opposed to the other samples that were excavated at Valkenburg, originate from an archaeological site in Nijmegen, but date from the same period.

IX.4 – Analytical methodology

After the suited sample pretreatment of the bone tissue, garum, soil, amphora, pottery and lead fragment samples (chapter V, § V.1.1 and § V.1.2), the powdered samples were digested according to the corresponding digestion procedures (chapter V, § V.4.1, § V.4.2, § V.4.4 and § V.4.5). After the digestion step, the lead fraction of the digests (except for lead fragments) was isolated from the concomitant matrix by means of extraction chromatography (chapter VI, § VI.4.2). Finally, the purified lead solutions were submitted to lead isotope ratio analysis using a Nu Plasma 500 multi-collector ICP-MS instrument (ETH Zürich) (chapter VII, § VII.4).

IX.5 – Pb concentration and Pb isotope ratio results

IX.5.1 – Pb concentration results

The Pb concentration retrieved in the artefacts investigated is summarized in table IX.1-3. The soil Pb content (table VII.1) ranges from 13 to 71 μg g^{-1} (< 5 % RSD) with an average of 28 μg g^{-1}, being a normal range for lead in soil, although distinguishing background Pb levels from levels affected by anthropogenic activities is difficult. Average lead levels for different soil types range from 10 to 67 μg g^{-1}, with an average of 32 μg g^{-1} [Kabata-Pendias and Pendias, 1984-c], while the Pb concentration in the upper continental crust equals 20 μg g^{-1} [Taylor and McLennan, 1995] (chapter IV, § IV.4.1). The Pb concentration for

Table IX.1 – Pb concentration and Pb isotopic composition of soil samples from *Pretorium Agrippinae*. * typical uncertainty < 5 % RSD. n.d.: not determined

	[Pb] (µg g^{-1})*	$^{206}Pb/^{204}Pb$	$^{207}Pb/^{204}Pb$	$^{208}Pb/^{204}Pb$	$^{207}Pb/^{206}Pb$	$^{208}Pb/^{206}Pb$	$^{208}Pb/^{207}Pb$
external precision (2s)		0.006	0.005	0.014	0.0001	0.0002	0.0002
1-140-165	17	18.845	15.662	38.847	0.8311	2.0614	2.4804
6-53-75	23	18.640	15.654	38.600	0.8398	2.0708	2.4659
6-99-128	3 800	18.385	15.624	38.380	0.8499	2.0871	2.4557
6-100-146	24	18.756	15.663	38.743	0.8351	2.0656	2.4735
6-130-190	44	18.724	15.659	38.700	0.8363	2.0669	2.4715
6-133-196	22	18.677	15.659	38.692	0.8384	2.0717	2.4710
6-147-235	39	18.647	15.655	38.665	0.8396	2.0736	2.4698
6-265-328	17	18.834	15.654	38.782	0.8315	2.0592	2.4775
14-116-188	71	18.589	15.663	38.689	0.8426	2.0812	2.4701
14-120-193	29	18.710	15.656	38.726	0.8368	2.0698	2.4735
14-152-202	2	n.d.	n.d.	n.d.	n.d.	n.d.	n.d.
14-173-242	24	18.684	15.658	38.687	0.8381	2.0706	2.4707
51-54-165	27	18.628	15.656	38.679	0.8404	2.0764	2.4706
51-60-176	20	18.784	15.665	38.772	0.8340	2.0640	2.4750
59--169	13	18.704	15.656	38.756	0.8370	2.0721	2.4756
59-41-41	25	18.386	15.646	38.424	0.8510	2.0899	2.4558
59-43-63	20	18.795	15.648	38.739	0.8326	2.0611	2.4756
59-76-110	38	18.719	15.655	38.689	0.8363	2.0668	2.4714
59-96-204	24	18.715	15.643	38.670	0.8359	2.0662	2.4720
71-26-45	26	18.581	15.644	38.588	0.8419	2.0767	2.4667
71-29-54	23	18.718	15.661	38.748	0.8367	2.0701	2.4742
73-53-79	22	18.600	15.648	38.572	0.8413	2.0738	2.4650

Table IX.2 – Pb concentration and Pb isotopic composition of bone and garum samples from *Pretorium Agrippinae*. * typical uncertainty < 5 % RSD

	[Pb] (µg g^{-1})*	$^{206}Pb/^{204}Pb$	$^{207}Pb/^{204}Pb$	$^{208}Pb/^{204}Pb$	$^{207}Pb/^{206}Pb$	$^{208}Pb/^{206}Pb$	$^{208}Pb/^{207}Pb$
external precision (2s)		0.006	0.005	0.014	0.0001	0.0002	0.0002
bone							
1-140-165	110	18.581	15.665	38.616	0.8431	2.0783	2.4652
6-53-75	79	18.630	15.659	38.631	0.8405	2.0736	2.4670
6-99-128	32 000	18.396	15.633	38.390	0.8498	2.0869	2.4557
6-100-146	150	18.575	15.660	38.629	0.8431	2.0796	2.4667
6-130-190	64	18.647	15.654	38.613	0.8395	2.0707	2.4666
6-133-196	31	18.591	15.652	38.577	0.8420	2.0751	2.4646
6-147-235	170	18.640	15.660	38.646	0.8402	2.0734	2.4678
6-265-328	160	18.632	15.644	38.577	0.8397	2.0705	2.4659
14-116-188	320	18.540	15.659	38.623	0.8446	2.0832	2.4665
14-120-193	200	18.561	15.648	38.573	0.8430	2.0781	2.4651
14-152-202	29	18.599	15.654	38.609	0.8416	2.0757	2.4662
14-173-242	44	18.684	15.661	38.658	0.8382	2.0690	2.4684
51-54-165	300	18.428	15.629	38.413	0.8481	2.0845	2.4578
51-60-176	340	18.529	15.652	38.566	0.8448	2.0815	2.4640
59--169	59	18.705	15.653	38.663	0.8369	2.0670	2.4698
59-41-41	120	18.592	15.660	38.609	0.8423	2.0767	2.4654
59-43-63	120	18.525	15.636	38.502	0.8441	2.0784	2.4624
59-76-110	88	18.617	15.658	38.651	0.8410	2.0761	2.4685
59-96-204	47	18.536	15.643	38.518	0.8439	2.0781	2.4624
71-26-45	23	18.589	15.650	38.581	0.8419	2.0754	2.4652
71-29-54	160	18.584	15.656	38.628	0.8424	2.0785	2.4673
73-53-79	75	18.498	15.645	38.529	0.8457	2.0827	2.4628
garum							
13-2-236	670	18.435	15.638	38.436	0.8483	2.0849	2.4578

Table IX.3 – Pb concentration and Pb isotopic composition of amphora, pottery and lead fragment samples from *Pretorium Agrippinae*. * typical uncertainty < 5 % RSD. § lead fragments assumed to be 100 % lead

	[Pb] (µg g^{-1})*	$^{206}Pb/^{204}Pb$	$^{207}Pb/^{204}Pb$	$^{208}Pb/^{204}Pb$	$^{207}Pb/^{206}Pb$	$^{208}Pb/^{206}Pb$	$^{208}Pb/^{207}Pb$
external precision (2s)		0.006	0.005	0.014	0.0001	0.0002	0.0002
amphorae							
C-3656	45	18.569	15.654	38.587	0.8430	2.0780	2.4650
C-3668	28	18.795	15.669	38.793	0.8337	2.0640	2.4758
C-3675	31	18.623	15.659	38.629	0.8408	2.0742	2.4669
IV-C-166	31	18.771	15.669	38.766	0.8348	2.0652	2.4741
IV-C-173	41	18.501	15.665	38.533	0.8467	2.0827	2.4598
212-65	29	18.680	15.661	38.687	0.8384	2.0710	2.4702
218-48	32	18.641	15.658	38.635	0.8400	2.0726	2.4674
GM-3	31	18.579	15.671	38.643	0.8434	2.0799	2.4659
pottery							
5-67-499	3 000	18.551	15.641	38.474	0.8431	2.0740	2.4599
lead fragments§							
1-14-35	1 000 000	18.430	15.647	38.449	0.8490	2.0862	2.4573
2-24-10	1 000 000	18.388	15.630	38.378	0.8500	2.0872	2.4556
3-2-32	1 000 000	18.408	15.636	38.415	0.8494	2.0869	2.4569
4-55-99	1 000 000	18.403	15.635	38.412	0.8496	2.0873	2.4567
5-67-499	1 000 000	18.386	15.627	38.379	0.8499	2.0873	2.4560
6-62-20	1 000 000	18.395	15.624	38.394	0.8498	2.0872	2.4565
7-547-971	1 000 000	18.381	15.631	38.373	0.8504	2.0876	2.4551
8-41-1048	1 000 000	18.408	15.637	38.408	0.8495	2.0865	2.4563
9-63-60	1 000 000	18.382	15.624	38.367	0.8499	2.0871	2.4556
10--5185	1 000 000	18.426	15.637	38.442	0.8486	2.0863	2.4585

the bones (table IX.2) ranges between 23 and 340 μg g^{-1} (< 5 % RSD) with an average of 129 μg g^{-1}. This is remarkably close to the previous results obtained for 33 neonates with AAS [de Wolff *et al.*, 2001] (§ IX.2). As a comparison, the bone lead level for non-occupationally exposed 'modern' teenagers, obtained via X-ray fluorescence spectrometry, was found to range up to 14.2 μg Pb per gram bone mineral, with an average of 4.0 ± 4.4 μg g^{-1} [Hoppin *et al.*, 1997; Farias *et al.*, 1998]. For every bone-soil pair, the Pb concentration in the bone is higher by a factor of 2 to 10 compared to the corresponding soil. One soil sample (14-152-202, table IX.1) shows a very low Pb concentration (only 2 μg g^{-1}), while the corresponding bone sample contains 29 μg g^{-1} of Pb (table IX.2), which is not the lowest Pb concentration found for the entire set of bones. The bone-soil pair 6-99-128 (tables IX.1-2), on the other hand, shows an exceptionally high lead concentration compared to the other samples. The reason for the high lead concentration displayed by this pair remains unclear, as no lead objects were found inside this grave. Most of the amphorae display a similar Pb concentration in the range of 28 to 32 μg g^{-1} (< 5 % RSD), while two display a slightly higher Pb concentration of 41 and 45 μg g^{-1} (table IX.3). The average Pb concentration of the amphorae equals 34 μg g^{-1}, which is in the range of normal Pb levels for soil. Since ceramics are derived from soil, a similar lead content for both could have been expected. Unlike the amphorae, the pottery fragment is characterized by a very high Pb concentration of 3 000 μg g^{-1} (table IX.3). The use of laser ablation ICP-MS (chapter II, § II.2.3.2) for Pb determination on the inner and outer surface of the shard revealed that the lead is mainly present in a thin layer on both the inner and outer surface. The lead is inhomogeneously distributed over both the inner and outer surface, and the Pb concentration on the inner surface (the side that was in contact with food) is up to factor of ~ 500 higher than the Pb concentration on the outer surface, indicating a contamination of the inner surface of the bowl with lead. Also the garum contains the considerable amount of 670 μg g^{-1} lead (table IX.2). The lead fragments were assumed to be 100 % lead (table IX.3).

Controversy exists concerning the origin of high lead concentrations as retrieved in bone tissue dating from the Roman – or in general, any historical – era. Lead levels higher than biogenic ranges found in Roman bone tissue were, on the one hand considered as the result of dietary uptake or uptake by inhalation [Martinez-Garcia *et al.*, 2005], and on the other hand ascribed to diagenesis as the most important process leading to these high Pb concentrations [Millard, 2006; Zapata *et al.*, 2006]. In the samples studied here, it was found that (i) the Pb levels are 2 to 10 times higher in the bone than in the surrounding soil, and (ii) one soil (14-152-202) has a very low Pb concentration (2 μg g^{-1}) compared to a

much higher Pb concentration of the corresponding bone (29 μg g^{-1}). On the one hand, it seems unlikely that all the lead present in the soil has moved into the bone, although this cannot be excluded since the specific structure of bone might allow the incorporation of Pb in the bone against a concentration gradient. On the other hand, the observation that samples linked to food (pottery as a food container and garum as a lead-enriched fish sauce) display elevated Pb concentrations, suggests that Pb uptake from food appears to be likely. However, this statement is only based on lead concentrations, while lead isotope ratios can provide a more profound insight into the relative contribution of diagenesis to the Pb found in the bones at present [Millard, 2006].

IX.5.2 – Pb isotope ratio results

The Pb isotope ratio results obtained for the samples investigated are summarized in table IX.1-3. Graphical representations of the $^{208}Pb/^{206}Pb$ ratio versus the $^{207}Pb/^{206}Pb$ ratio and the $^{206}Pb/^{204}Pb$ ratio versus the $^{208}Pb/^{204}Pb$ ratio are given in figure IX.2. Due to the very small amount of soil 14-152-202 available (~ 10 mg), in combination with the very low Pb concentration (table IX.1), no reliable Pb isotope ratio measurement could be performed on this sample. In figures IX.2.a-b, three groups can be distinguished: (i) a compact group of lead fragments with a $^{206}Pb/^{204}Pb$ ratio between 18.38 and 18.43 and a $^{208}Pb/^{206}Pb$ ratio between 2.086 and 2.088, (ii) a group of soil samples, covering a $^{206}Pb/^{204}Pb$ ratio range between 18.58 and 18.85 and a $^{208}Pb/^{206}Pb$ ratio range between 2.059 and 2.081 (soil samples 6-99-128 and 59-41-41 excluded) and (iii) a group of bone samples, located in-between the groups of lead objects on one side, and soil samples on the other side, in a $^{206}Pb/^{204}Pb$ ratio range of 18.50 – 18.70 and a $^{208}Pb/^{206}Pb$ ratio range of 2.067 – 2.083 (bone samples 6-99-128 and 51-54-165 excluded). The lead in the soil samples is more radiogenic than that in the bones, which is again more radiogenic than the lead of the fragments. The bone-soil pair 6-99-128 is characterized by a Pb isotopic composition similar to that of the lead fragments, as are the soil 59-41-41 and the bone 51-54-165 (figure IX.2). The garum displays a Pb isotopic composition that is between that of the lead fragments and the bone samples but close to that of the lead fragments with a $^{206}Pb/^{204}Pb$ ratio of 18.44 and a $^{208}Pb/^{206}Pb$ ratio of 2.085 (figure IX.2). The amphorae excavated at Nijmegen all show a Pb isotopic composition that is similar to that of the soil samples from Valkenburg, and can be divided in four subgroups, scattered throughout a $^{206}Pb/^{204}Pb$ ratio range of 18.50 – 18.80 and a $^{208}Pb/^{206}Pb$ ratio range between 2.064 and 2.083 (figure IX.2). The pottery fragment, found at a $^{206}Pb/^{204}Pb$ ratio

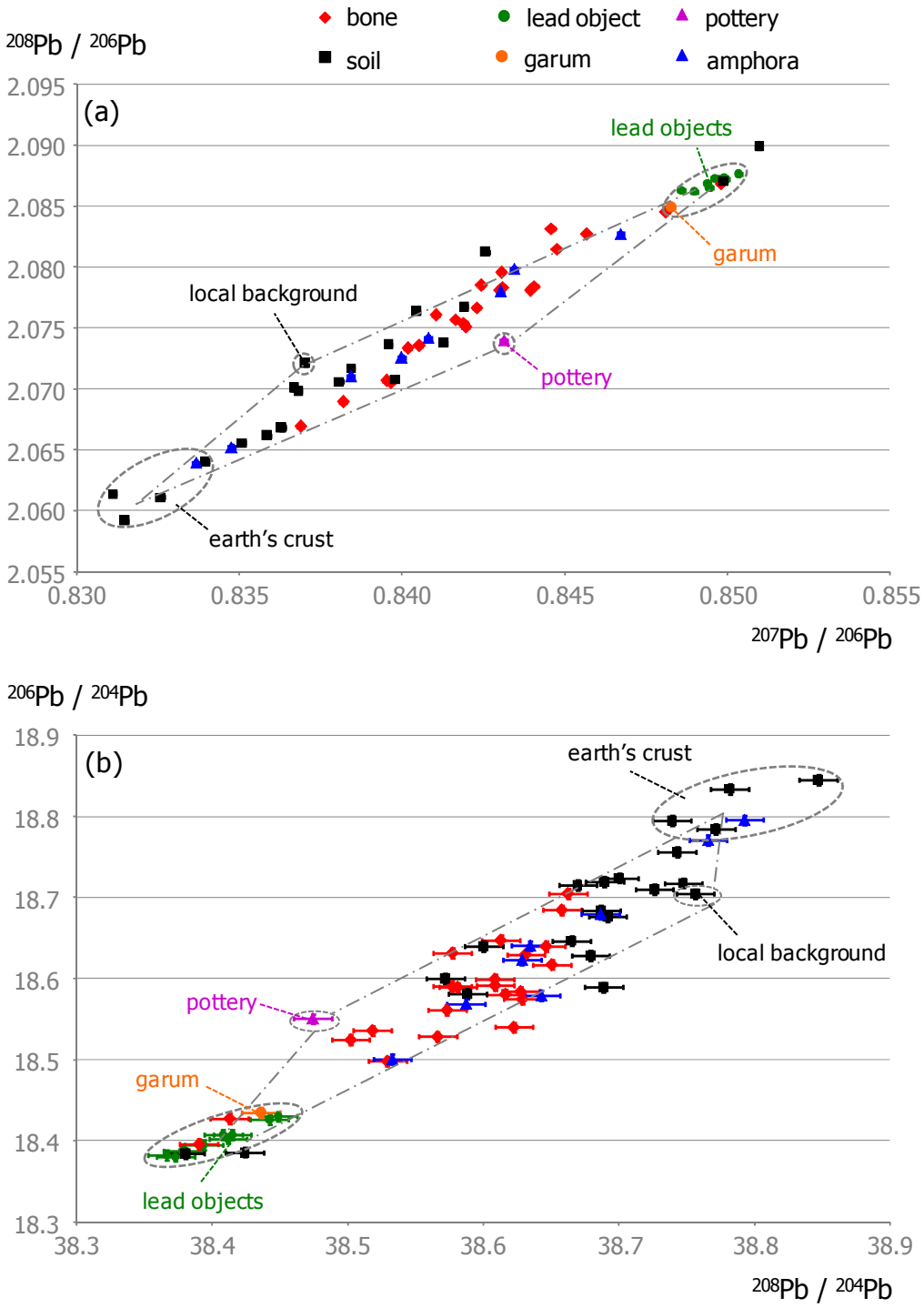

Figure IX.2 – Graphical representation of the Pb isotope ratio results – (a) $^{208}Pb/^{206}Pb$ ratio versus $^{207}Pb/^{206}Pb$ ratio; (b) $^{206}Pb/^{204}Pb$ ratio versus $^{208}Pb/^{204}Pb$ ratio. Error bars are included in the symbol size or represent 2s uncertainty intervals (external precision).

of 18.55 and a $^{208}Pb/^{206}Pb$ ratio of 2.074, displays a Pb isotopic composition that is different from that of the lead fragment that was attached to it (5-67-499). Further, this pottery fragment appears to be rather atypical in Pb isotopic composition and does not seem to fit in one of the groups as defined above (figure IX.2).

A comparison of the $^{208}Pb/^{206}Pb$ ratio for every bone-soil pair is presented in figure IX.3. It can be seen that most of the bone-soil pairs display a significantly different Pb isotopic composition for the bone and corresponding soil. The $^{208}Pb/^{206}Pb$ ratio is systematically higher for the bones than for the soils, except for six bone-soil pairs. Two of these six pairs (6-99-128 and 6-147-235) display the same $^{208}Pb/^{206}Pb$ ratio, while the other four pairs (14-173-242, 59--169, 59-41-41 and 71-26-45) display a $^{208}Pb/^{206}Pb$ ratio that is higher for the soils than for the bones. The spread in $^{208}Pb/^{206}Pb$ ratio is lower for the bones than for the soils. The procentual shift in $^{208}Pb/^{206}Pb$ isotope ratio from soil to bone (figure IX.3) varies between –0.64 % (bone-soil pair 59-41-41) and 0.84 % (bone-soil pair 51-60-176). However, no systematic correlation is observed between, on the one hand, the magnitude of the $^{208}Pb/^{206}Pb$ isotope ratio shift, and on the other hand, (i) the well where the sample was taken (indicated by the first number in the sample identification code, as given in tables IX.1-2) and (ii) the absolute values of the $^{208}Pb/^{206}Pb$ isotope ratios for bone and soil. Furthermore, no systematic trend could be discerned between the absolute difference in the $^{208}Pb/^{206}Pb$ ratio for bone and corresponding soil, on the one hand, and the absolute difference in concentration between bone and corresponding soil, on the other hand. The apparent lack of a systematic correlation between the difference in $^{208}Pb/^{206}Pb$ ratio and the difference in Pb concentration for bone and corresponding soil may be explained by a different Pb exposure and Pb uptake during life, but could, however, also be attributed to the process of diagenesis [Radosevich, 1993].

The graphical representation of the $^{208}Pb/^{206}Pb$ ratio versus the $^{207}Pb/^{206}Pb$ ratio (figure IX.2.a) displays an alignment of the bones with the soils, garum and lead fragments. This suggests that the bone lead is a mix between lead originating from at least 2 sources: (i) soils and (ii) lead fragments and/or garum, indicating that the process of diagenesis is probably not the only lead source for bone. Furthermore, owing to the high precision of the measurement, it could be deduced that at least one additional lead source is required for complete clarification (figure IX.2.a). This assumption is confirmed in the representation of the $^{206}Pb/^{204}Pb$ ratio versus the $^{208}Pb/^{204}Pb$ ratio (figure IX.2.b), where the spread of the samples is wider. The observation that the samples are no longer aligned (figure IX.2.b) indeed confirms the need of at least one additional lead source. The pottery fragment, displaying a Pb concentration of 3 000 µg g^{-1}, could be addressed as such.

A scatterplot where, respectively, the $^{208}Pb/^{206}Pb$ ratio and the $^{206}Pb/^{204}Pb$ ratio is plotted versus the inverse of the Pb concentration is given in figure IX.4. From these graphs, 2 soil endmembers can be clearly identified: (i) a group consisting of 4 soils: 1-140-165,

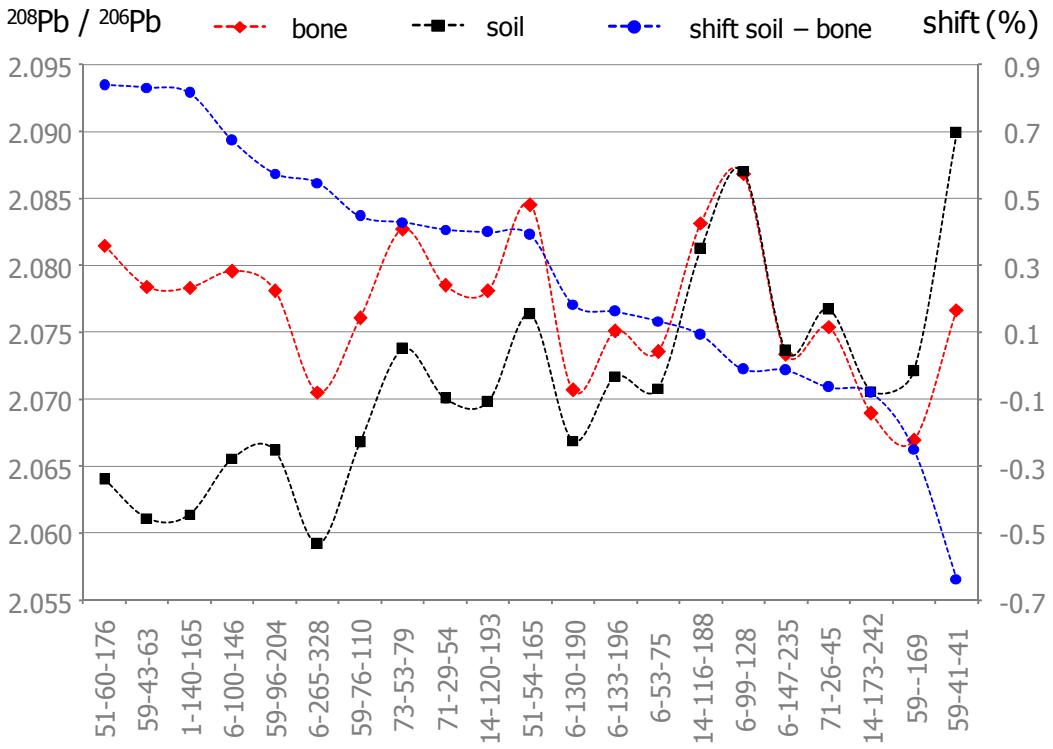

Figure IX.3 – $^{208}Pb/^{206}Pb$ ratios for the bone-soil pairs, organised according to decreasing difference (%) between the $^{208}Pb/^{206}Pb$ ratio for the soil and corresponding bone sample

6-265-328, 51-60-176 and 59-43-63, and (ii) soil 59--169. The first endmember is constituted of the group of 4 soils mentioned above, all of which were excavated at a different well (indicated by the first number in the sample identification code). The average Pb isotopic composition of this 4-soil group equals 18.81 for $^{206}Pb/^{204}Pb$, 15.66 for $^{207}Pb/^{204}Pb$, 38.79 for $^{208}Pb/^{204}Pb$, 0.832 for $^{207}Pb/^{206}Pb$ and 2.061 for $^{208}Pb/^{206}Pb$, which is in agreement with the range of Pb isotope ratio values given for North-West European continental crust and sediments [Elbaz-Poulichet *et al.*, 1984; Elbaz-Poulichet *et al.*, 1986; Weiss *et al.*, 1999]. Furthermore, these 4 soils display Pb concentrations between 17 and 20 µg g^{-1} (table IX.1), which is in the range of the Pb concentration of the upper continental crust [Taylor and McLennan, 1995]. As a consequence, this endmember may represent the earth's crust. The soil 59--169 displays a $^{208}Pb/^{206}Pb$ ratio of 2.072 and a Pb concentration of 13 µg g^{-1}, being the lowest Pb concentration after the atypically low Pb concentration for soil 14-152-202 (2 µg g^{-1}) (table IX.1). This soil, 59--169, appears to be different from the average earth's crust in terms of Pb concentration and Pb isotopic composition, as was confirmed by duplicate analysis. The difference might be attributed to a local variation, resulting from a variation in the mineral components of the local sediments. Another explanation might be that this soil sample was enriched in a specific mineral component. This second soil endmember, soil 59--169, is further referred to as a 'local background'.

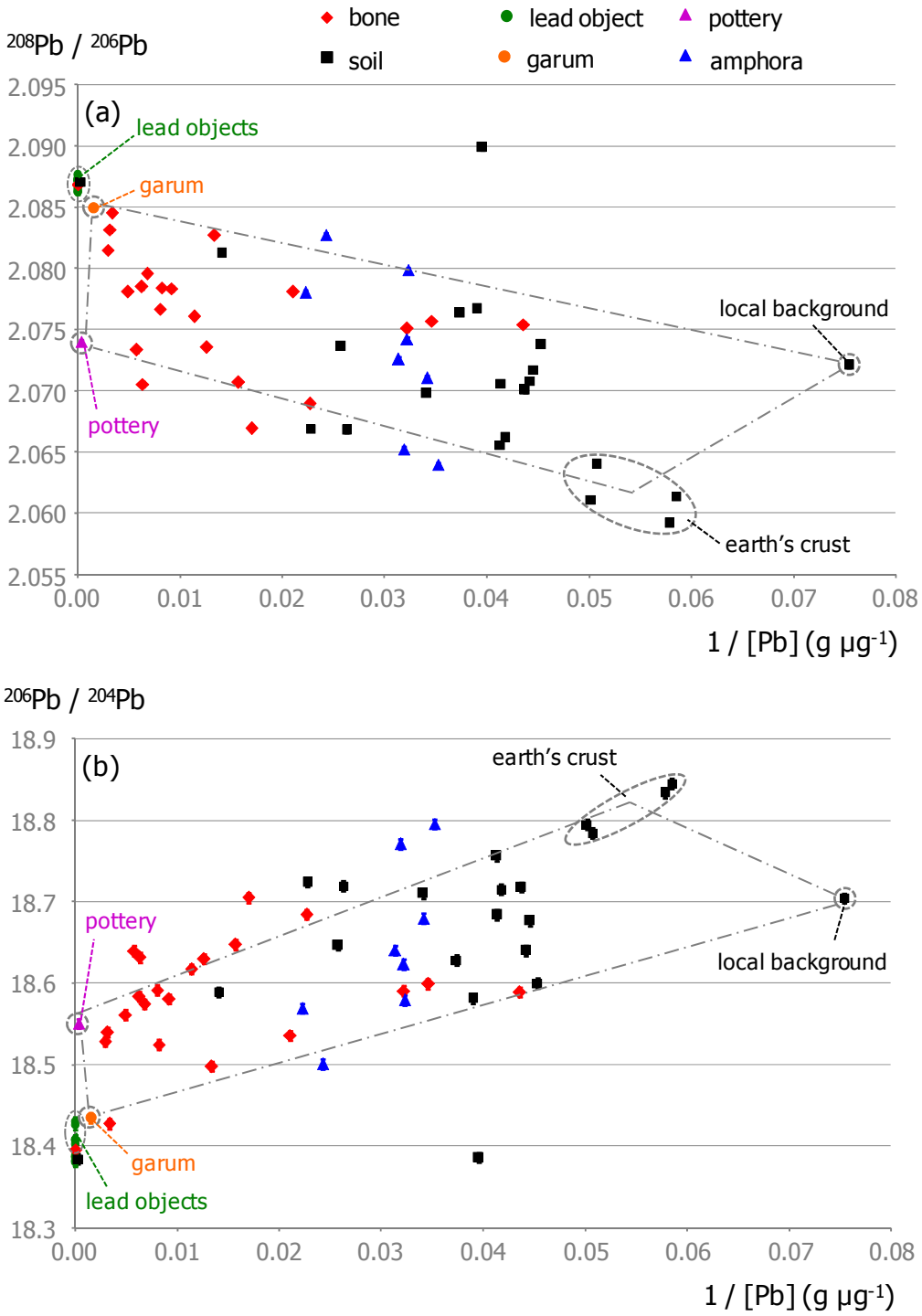

Figure IX.4 – $^{208}Pb/^{206}Pb$ ratio (a) and $^{206}Pb/^{204}Pb$ ratio (b) versus the inverse of the Pb concentration. Error bars are included in the symbol size.

Next to soil, the group of lead fragments and garum can be considered as a lead source (figure IX.4). For the garum, it was observed that (i) its isotopic composition approaches that of the Pb from the fragments (figure IX.2) and (ii) its Pb concentration amounts to 670 µg g^{-1} (table IX.2), a concentration that is twice as high as the highest bone lead concentration, found for sample 51-60-176 (6-99-128 excluded) (table IX.2). From this observation, the garum can be considered as contaminated with Pb coming from the lead

fragments, and thus represents a proxy for the lead fragments. Since the garum was ingested by the Romans as a fish sauce enriched with *sapa*, (§ IX.1.2) it makes sense to consider garum as a source of bone lead. Further, also lead coming from the lead fragments (by, *e.g.*, drinking water) is a likely source of bone lead. The observation that a higher bone lead concentration (lower 1/Pb value) is characterized by an isotopic composition approaching that of garum and lead objects, confirms the assumption of garum, on its turn contaminated by Pb coming from the lead fragments, as a third endmember.

The three endmembers identified so far – soil 59--169, group of soils 1-140-165, 6-265-328, 51-60-176 and 59-43-63 and lead fragments + garum – are indicated in figure IX.2 and figure IX.4. In figure IX.2, the Pb isotopic composition of most of the bone samples is explained by these 3 endmembers. However, this is not the case in figure IX.4, indicating that a fourth endmember is needed. Defining the pottery fragment 5-67-499, displaying a Pb concentration of 3 000 µg g^{-1} (table IX.3), enriched in Pb at its inner surface, and stemming from a bowl used for the conservation of food, as a fourth endmember, results in a quasi-complete source attribution of all the bone samples investigated.

An attempt was made to calculate the maximal amount of Pb that could be contributed to the bone lead levels by the process of diagenesis, by assuming that the lead retrieved in the bone tissue at present is a mix of lead originating from only two lead sources: (i) soil and (ii) lead fragments. The following (simplifying) assumptions were made: (i) the Pb isotopic composition of the bone tissue at the moment of death ($R_{bone,t=0}$) equals the average Pb isotopic composition of the lead fragments ($R_{lead\ fragments}$); in other words, lead from the lead fragments was the only source of bone lead before death, (ii) the Pb concentration and Pb isotopic composition of the bone tissue at present ($[bone]_{t=present}$ and $R_{bone,t=present}$, respectively) have evolved from the original Pb concentration and Pb isotopic composition of the bone ($[bone]_{t=0}$ and $R_{bone,t=0} = R_{lead\ fragments}$, respectively) by post-mortem diagenesis only; in other words, the process of diagenesis is the only source of bone lead after death, (iii) the Pb concentration of the soil does not change by the process of diagenesis, and (iv) only unidirectional diagenesis (from soil to bone) has taken place. In the case where the assumptions given above are not met, as it is in reality, diagenesis will have resulted in a lower relative contribution. As a consequence, with the assumptions made, the contribution of diagenesis calculated is always the maximal contribution possible. From the maximal amount of Pb arising from diagenesis, also the minimal bone lead concentration at the moment of death can be estimated. For

every bone-soil pair, the amount of Pb that was incorporated into the bone after death and that originates from the soil ($[\text{bone}]_{\text{from soil}}$), was calculated using an equation derived from isotope dilution analysis [Heumann, 1988; Vanhaecke *et al.*, 2006], as follows:

$$[\text{bone}]_{\text{from soil}} = \frac{[\text{bone}]_{\text{t=present}}}{1 + \frac{R_{\text{soil}} - R_{\text{bone,t=present}}}{R_{\text{bone,t=present}} - R_{\text{lead fragments}}}} \qquad \text{(equation IX.1)}$$

The difference between the Pb concentration at present in the bone ($[\text{bone}]_{\text{t=present}}$) and the maximal fraction that was contributed by the process of diagenesis ($[\text{bone}]_{\text{from soil}}$), yields the minimal Pb concentration that must have been present at the moment of death. The Pb contribution of the process of diagenesis to the lead retrieved in the bone at present can be expressed relative to the lead concentration of the bone at present as follows:

$$\%\ \text{diagenesis} = 100\ \frac{[\text{bone}]_{\text{from soil}}}{[\text{bone}]_{\text{t=present}}} \qquad \text{(equation IX.2)}$$

These calculations were carried out for every bone-soil pair, using every Pb isotope ratio determined (R = $^{206}Pb/^{204}Pb$, $^{207}Pb/^{204}Pb$, $^{208}Pb/^{204}Pb$, $^{207}Pb/^{206}Pb$, $^{208}Pb/^{206}Pb$ or $^{208}Pb/^{207}Pb$), and the results are summarized in table IX.4. In some cases, *e.g.*, in the exceptional case wherein the Pb isotope ratio of the bone is not in-between that of the corresponding soil and the average Pb isotope ratio of the lead fragments, contributions of diagenesis to the bone lead concentration below 0 % or above 100 % were obtained. These results were not further considered. Hence, the range given in table IX.4 is defined by the lowest and the highest value retrieved when only the percentages between 0 and 100 % are considered. For most of the bone-soil pairs, a spread lower than 20 % is obtained from calculations based on the different isotope ratios. Only for 5 bone-soil pairs (6-53-75, 6-147-235, 14-173-242, 59--169 and 71-26-45), the contribution of diagenesis to the bone lead is near to 100 %, while most of the other bone-soil pairs display a diagenesis contribution that is (well) below 80 %. The corresponding minimal bone lead concentrations at the moment of death are considerably higher than the bone lead level for non-occupationally exposed 'modern' teenagers that was found to range up to 14.2 µg Pb per gram bone mineral, with an average of 4.0 ± 4.4 µg g^{-1} [Hoppin *et al.*, 1997; Farias *et al.*, 1998]. As a consequence, it can be concluded that diagenesis is probably not the only source of bone lead, and thus it can be suggested that infant Pb exposure must have taken place at *Pretorium Agrippinae*.

As a conclusion, soil, lead fragments and pottery were established as sources of bone lead. Four endmembers, indicated in figure IX.2 and figure IX.4, have been identified:

Table IX.4 – maximal contribution of diagenesis to the Pb concentration as currently present in the bone, and corresponding minimal Pb concentration in the bone at the moment of death. -- : result < 0 % or > 100 % was obtained.

bone-soil pair	maximal contribution of diagenesis to the present bone Pb concentration (%)	minimal Pb concentration of the bone at the moment of decease (µg g^{-1})
1-140-165	33 – 49	56 – 73
6-53-75	83 – 96	3 – 14
6-99-128	28 – 69	9 600 – 23 000
6-100-146	34 – 89	16 – 97
6-130-190	67 – 81	12 – 21
6-133-196	56 – 78	7 – 14
6-147-235	85 – 97	5 – 26
6-265-328	45 – 59	65 – 87
14-116-188	66 – 86	46 – 110
14-120-193	51 – 64	74 – 100
14-152-202	--	--
14-173-242	84 – 99	0 – 7
51-54-165	4 – 23	230 – 290
51-60-176	24 – 60	140 – 260
59--169	70 – 91	6 – 18
59-41-41	--	--
59-43-63	21 – 33	82 – 96
59-76-110	54 – 87	12 – 41
59-96-204	38 – 44	27 – 29
71-26-45	85 – 96	1 – 3
71-29-54	50 – 81	30 – 81
73-53-79	32 – 80	15 – 51

(i) soil 59--169 as a local soil background, (ii) a group of 4 soils (1-140-165, 6-265-328, 51-60-176 and 59-43-63), which is representative for the upper continental crust, (iii) garum, contaminated with Pb from the lead fragments, and the lead fragments themselves, and (iv) the pottery fragment, stemming from a bowl for the conservation of food. These findings, and a calculation of the maximal Pb concentration contributed to the bone lead concentration by the process of diagenesis, allow the conclusion that the process of diagenesis is most likely not the only lead source for bone lead. The bone lead appears to be a mix between geogenic lead (soil lead) and dietary exposure lead, taken

up from *e.g.*, garum, drinking water and conserved food. It is likely that this dietary lead was taken up by the mother and was subsequently transferred to the foetus.

Four samples (bone and soil 6-99-128, bone 51-54-165 and soil 59-41-41) display a Pb isotopic composition that is similar to that of the lead objects and the garum (figure IX.2). Both the bone tissue and the soil for the sample set 6-99-128 show a very high lead concentration and an isotopic composition clearly deviating from that of the other bone-soil pairs (table IX.1-2), indicating a very high degree of contamination with lead from the lead fragments. In figure IX.4, the soil 59-41-41 is located far out of the range displayed by the other samples. For the moment, the reason why the soil 59-41-41 displays an isotopic composition clearly different from that of the other soil samples, remains unexplained.

IX.6 – Conclusions

The Pb isotopic investigation of infant bone tissue dating from the Roman Era, along with possible sources of bone lead such as the surrounding soil, garum, lead fragments, pottery and amphorae, has revealed that at least an important fraction of the lead present in the bones must already have been present at the moment of death. Two sources of bone lead have been identified, namely, soil and food. These sources are represented in four endmembers. Two endmembers are soils, a local background and a group representative of the upper continental crust. A third endmember consists of lead fragments and garum contaminated with lead from the lead fragments, and a fourth endmember is a pottery shard stemming from a bowl used for the conservation of food. It was shown that the process of diagenesis is not the only source of bone lead, but that the bone lead is a mixture of geogenic (soil) lead and dietary exposure lead taken up from, *e.g.*, garum, drinking water and conserved food. It is likely that this dietary lead was taken up by the mother, and subsequently transferred from the mother to the foetus during pregnancy.

Chapter X

Investigation of the grave field population around the Servatius complex

In this chapter, an explorative study is presented, in which the heterogeneity of the grave field population around the basilica dedicated to the Saint Servatius in Maastricht (The Netherlands) is investigated. For this purpose, the $^{87}Sr/^{86}Sr$ ratio of the dental tissues, enamel and dentine, from a number of individuals, excavated at the Pandhof site and the Vrijthof site, were determined and compared. The $^{87}Sr/^{86}Sr$ isotope ratio in dental tissues can provide insight into population migration in the past. Strontium passes unfractionated after intake from the food sources and the environment into the blood and is incorporated into the skeletal tissues. The strontium isotopic composition of tooth enamel, which is formed during childhood and is not remodeled throughout life, hence reflects the bioavailable $^{87}Sr/^{86}Sr$ ratio of the place of birth, while the strontium isotopic composition of tooth dentine, which remodels during life, reflects the $^{87}Sr/^{86}Sr$ ratio of the place of residence in the last years of life. A different $^{87}Sr/^{86}Sr$ ratio for enamel and dentine thus points at a relocation of an individual during his/her life history, under the condition that the biogenic Sr isotopic signature has not been blurred by post-mortem contamination with strontium from diagenetic (soil) origin (chapter IV, § IV.3.1). First, the archaeological background on the Servatius complex, the sites Pandhof and Vrijthof, and the samples investigated are briefly discussed. Then, the influence of the process of diagenesis on the strontium present in the dental tissues, is evaluated. Next, the Sr isotope ratio results are presented and discussed, followed by preliminary conclusions on the migration behavior of the individuals excavated on the sites of Pandhof and Vrijthof.

X.1 – History of Servatius

The Servatius basilica, located in Maastricht (The Netherlands) (figure X.1), was built in honor of Servatius, who was the bishop of Tongeren in the 4th century AD. The construction of the basilica was started in the 6th century AD, following the impulse of Monulfus, the bishop of Maastricht at that time. At present, the Servatius basilica is one of the most impressive monuments of the Low Countries and testifies of 1 600 years of religion, going back to the earliest Christianity in the valley of the river Maas in the late-antique era.

The rich history of the Servatius complex is well documented under the form of written sources, liturgical traditions and numerous objects preserved in the treasure of the basilica. However, excavations that started about 50 years ago in and around the Servatius complex revealed an, until then, 'hidden' archive, consisting of buildings and graves. A wealth of wall remains, sarcophagi, grave findings, fragments of architecture,

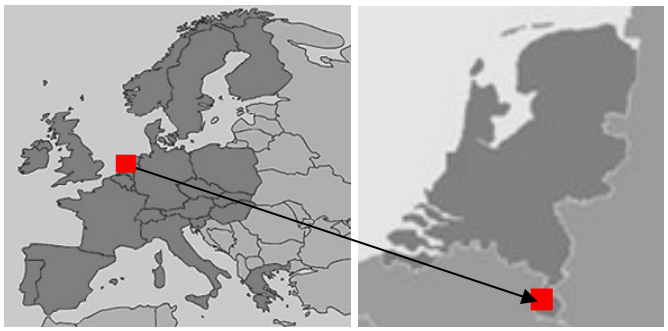

Figure X.1 – Geographical location of Maastricht (The Netherlands, Europe)

carvings and sculptures have been discovered, even magnifying the importance of the Servatius basilica as a monument.

An overview of the site covered by the Servatius complex is given in figure X.2. The excavations at the Servatius complex resulted in a large amount of well preserved skeletal remains that are useful for research. The sites that are considered in this work are the Pandhof site and the Vrijthof site (figure X.2). The excavations at the site Pandhof were carried out in the early 1950's. The underground of this site revealed a complex stratigraphy with graves dating back until the 4th century AD and the remains of fundaments of several buildings. In many graves, the skeletal material was well conserved. The Pandhof cemetery acquired fame due to the wealth of gifts found inside the graves. The site Vrijthof was excavated in the late 1960's. A complex structure, consisting of Roman roads, inhabitation layers and burial layers was discovered. This cemetery dates from the 6th – 7th century AD. In several cases, three to four layers of graves were found on top of each other. As on the Pandhof site, wealthy gifts were found in many graves.

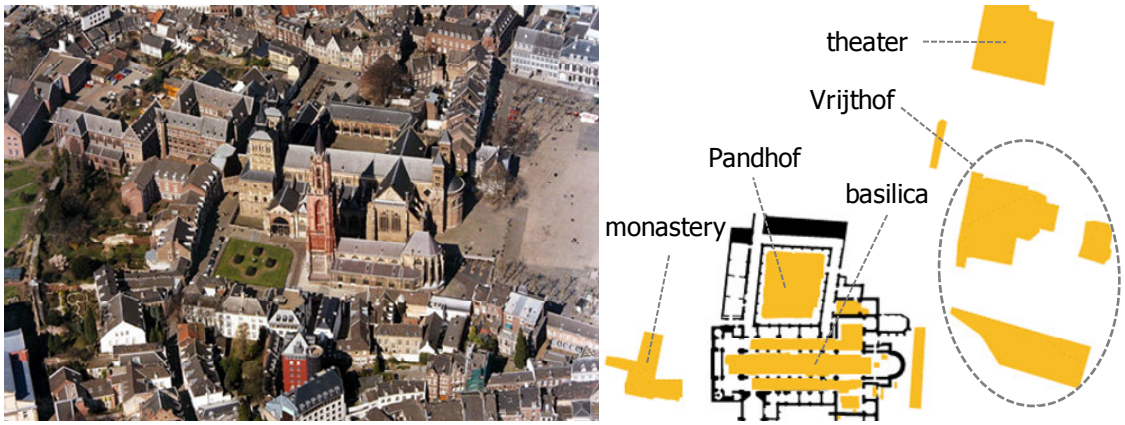

Figure X.2 – Overview of the Servatius complex in Maastricht (The Netherlands) – (left) picture of the site; (right) schematic map of the excavation site with an indication of the buildings and the grave fields Pandhof and Vrijthof

Two kinds of investigation can be performed on the skeletal remains excavated. In the first place, the skeletal material itself comprises information on the physical characteristics of the deceased population, such as age, sex, length and pathology of the teeth and the skeleton. In the second place, these data can be used to investigate the demographic structure, health and pathology of the buried population. Also the physical characteristics of the graves, the burial ritual and the gifts can be considered in a broader context, aiming at a cultural reconstruction of social entities.

The study presented in this work aims at obtaining insight into the heterogeneity of the grave field populations from the sites Pandhof and Vrijthof, and focuses on the dental remains of individuals excavated at these cemeteries. Strontium isotope ratio analysis can provide insight into population migration and thus allows to distinguish individuals that lived in the same area during their entire life and individuals that relocated to a geographically/geologically distinct area [Ericson, 1985; Sealy *et al.*, 1991; Bentley, 2006] (chapter IV, § IV.3.1). When the strontium isotopic composition of the dentine (figure X.3) is different from that of the enamel (figure X.3), it can be concluded that the individual under investigation has moved during his/her life from one geological area to another. The strontium isotopic composition of the dentine, namely, reflects the place of residence during the last years of life, while that of the enamel reflects the place of childhood.

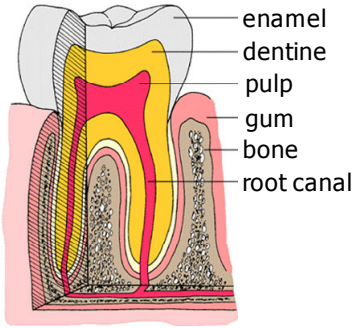

Figure X.3 – Schematic representation of a tooth

X.2 – Samples investigated in this work

An explorative study was conducted on a limited sample set consisting of 14 teeth that were taken from the skeletal remains of seven different individuals excavated at the Servatius complex, found in graves with a wealth of gifts. Two individuals were excavated at the Pandhof site (figure X.2). The first individual (108) is a child of 5-9 years of age of which the sex is not known, and the second individual (454) is a woman of 20-80 years of age. Five other individuals investigated were excavated at the Vrijthof site (figure X.2). All

of them are women and 20-35 years of age. Both an incisor and a molar from the seven individuals were available for investigation, hence forming a group of 4 teeth from the Pandhof site and a group of 10 teeth from the Vrijthof site.

X.3 – Analytical methodology

After leaching the whole teeth in 0.1 M acetic acid and carefully separating enamel and dentine (chapter V, § V.1.1), these tissues were digested according to the digestion protocol developed for this purpose (chapter V, § V.4.3). After digestion, the Sr content and the Ca/P ratio of the digests was determined following the ICP-DRC-MS measurement protocol developed hereto (chapter VII, § VII.2). Prior to the determination of the $^{87}Sr/^{86}Sr$ isotope ratios using a Neptune multi-collector ICP-MS instrument (chapter VII, § VII.3), the strontium fraction of the digests was isolated from the concomitant matrix by means of extraction chromatography (chapter VI, § VI.3.2).

X.4 – Evaluation of diagenetic alteration

As mentioned earlier (chapter IV, § IV.3.1), the occurrence of diagenesis may alter the biogenic element concentrations and, in the case of Sr, result in a $^{87}Sr/^{86}Sr$ ratio that is different from the biogenic $^{87}Sr/^{86}Sr$ ratio. When comparing the strontium isotopic composition of enamel and dentine, it is important to verify a priori that the biogenic Sr isotope ratios have not been altered by the addition of diagenetic strontium arising from contamination during burial. Bone and dentine are susceptible to diagenesis [Price *et al.*, 1992; Hedges, 2002; Nielsen-Marsh and Hedges, 2000-a], while enamel is more resistant [Kohn *et al.*, 1999; Budd *et al.*, 2000]. It has been argued that diagenetic strontium can be removed by proper sample cleaning, *e.g.*, with a weak acid [Price *et al.*, 1992; Sillen and Sealy, 1995; Nielsen-Marsh and Hedges, 2000-b]. The idea is that leaching skeletal tissue in 0.1-1 M acetic acid will dissolve the diagenetic strontium present in carbonate in the pore spaces, while retaining the original dietary strontium more strongly bound in the Ca site of the inorganic matrix [Price *et al.*, 1994; Ezzo *et al.*, 1997]. Several diagenetic proxies, or indicators, have been identified as useful for evaluating whether or not a significant diagenetic alteration has taken place, such as changes in crystallinity, carbonate content and the concentration of uranium and rare earth elements (REE) [Burton *et al.*, 1999; Balter *et al.*, 2002; Lee-Thorp and Sponheimer, 2003; Labs-Hochstein and MacFadden, 2006]. Because of the very low U and REE content in living organisms [Buseth *et al.*, 1998; Hinners *et al.*, 1998], elevated concentrations of

uranium and the rare earth elements have been proposed as indicative for chemical alteration by the process of diagenesis. These elements are believed to replace Ca in the specific crystal sites [Kohn *et al.*, 1999]. Another proxy for diagenesis is the Ca/P ratio of the calcified tissue investigated [Bentley, 2006]. It was argued that as long as the Ca/P ratio is near its biogenic value, what remains in the skeletal tissue is largely the biogenic calcium and strontium [Price *et al.*, 1994; Hoppe *et al.*, 2003; Bentley, 2006]. In this work, the Ca/P ratio of the dental tissues was chosen as the indicator to provide insight into the extent of diagenetic alteration. The Ca/P ratios obtained for the dental tissues under investigation are summarized in table X.1 and graphically displayed in figure X.4. The average Ca/P ratio obtained for the dentine equals 2.19 and ranges between 2.11 and 2.25. Within experimental uncertainty (< 5 % RSD), these values match with the biogenic Ca/P ratio of 2.1 – 2.2 for dentine [Hillson, 1996]. The enamel samples display a Ca/P ratio that is lower than that of the dentine samples, ranging between 1.91 and 2.07 with an average Ca/P ratio of 2.02, in agreement with the biogenic Ca/P ratio of 1.91 – 2.17 for enamel [Hillson, 1996]. A comparison of the experimentally obtained Ca/P ratios with the biogenic Ca/P ratios for enamel and dentine is given in figure X.4. It has been stated that diagenetic tests (Ca/P ratio, crystallinity, rare earth element content) can be passed or failed independently of whether the Sr reflects biological levels [Burton *et al.*, 1999]. However,

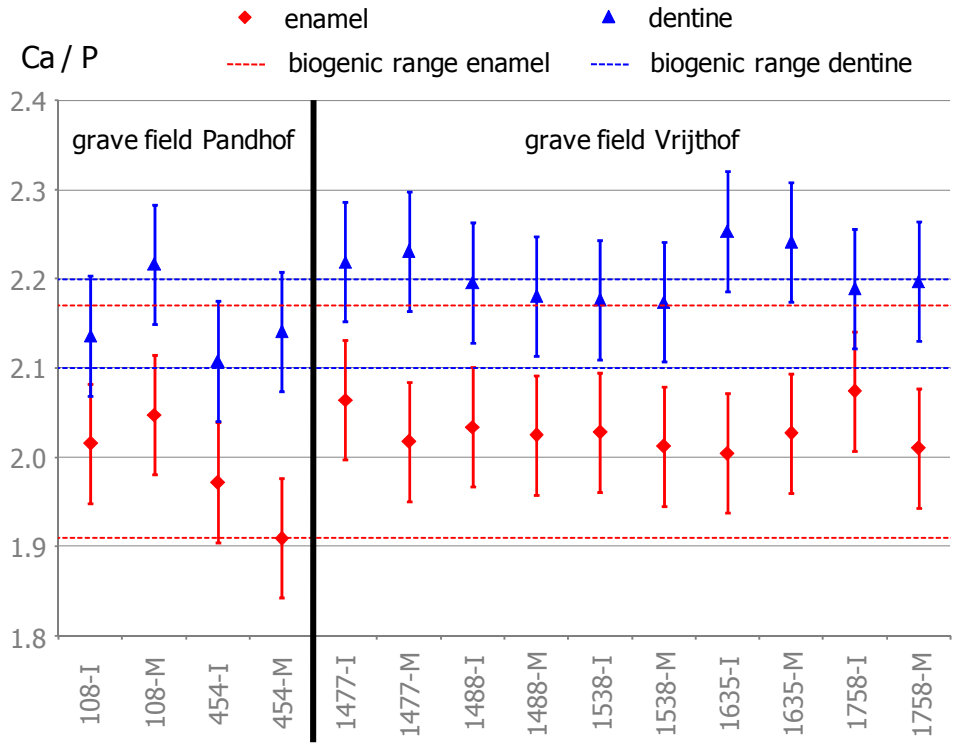

Figure X.4 – Ca/P ratio for the investigated incisors (I) and molars (M) from the sites of Pandhof and Vrijthof. Error bars represent average 2s uncertainty intervals. Data on the biogenic Ca/P range for enamel and dentine taken from [Hillson, 1996].

Table X.1 – Ca/P ratio, Sr concentration and $^{87}Sr/^{86}Sr$ ratio for the enamel and dentine samples from the grave field populations of the sites Pandhof and Vrijthof at the Servatius complex, Maastricht. * typical uncertainty < 5 % RSD

	tooth type	dentine			enamel		
		Ca/P	[Sr] (µg g^{-1})	$^{87}Sr/^{86}Sr$	Ca/P	[Sr] (µg g^{-1})	$^{87}Sr/^{86}Sr$
external precision (2s)		0.10	*	0.00004	0.10	*	0.00004
grave field Pandhof							
108	incisor	2.14	70	0.70963	2.02	390	0.70961
108	molar	2.22	550	0.70962	2.05	110	0.70964
454	incisor	2.11	350	0.70934	1.97	250	0.70933
454	molar	2.14	150	0.70931	1.91	110	0.70928
grave field Vrijthof							
1477	incisor	2.22	170	0.71024	2.06	140	0.70959
1477	molar	2.23	170	0.71028	2.02	90	0.70979
1488	incisor	2.20	220	0.71030	2.03	160	0.70994
1488	molar	2.18	190	0.71017	2.03	170	0.70978
1538	incisor	2.18	210	0.71043	2.03	130	0.70998
1538	molar	2.17	170	0.71051	2.01	130	0.71006
1635	incisor	2.25	200	0.71055	2.00	110	0.70960
1635	molar	2.24	200	0.71033	2.03	130	0.70941
1758	incisor	2.19	190	0.71051	2.07	120	0.71025
1758	molar	2.20	160	0.71024	2.01	130	0.70966

archaeological bone tissue that was demonstrated to be affected by diagenesis displayed a Ca/P ratio higher than 3 [Sillen and Sealy, 1995], which is significantly higher than the biogenic Ca/P ratio and the experimental Ca/P ratios obtained in this work. As a consequence, it can be assumed from the good agreement of the experimental Ca/P ratios with the biogenic Ca/P ratio range for both enamel and dentine, that the Ca and Sr present in these tissues are largely the biogenic fractions. Herefrom, it can be inferred that the subsequently determined $^{87}Sr/^{86}Sr$ isotope ratios are a reflection of the biogenic $^{87}Sr/^{86}Sr$ signatures of the dental tissues. This is a requirement when the specific aim is to identify the geological areas in which the studied individuals resided during childhood and in the last years of life. When a distinction between local people on the one hand and non-local people on the other hand is aimed at, the occurrence of diagenesis is less a problem. Diagenesis, namely, involves a local signature, so that when a non-local signal is obtained, this implies that the population is non-local [Schweissing and Grupe, 2003]. However, since distinct bone samples may display a different extent of diagenetic alteration [Radosevich, 1993], there is always a spread on the diagenetic signature that should be taken into account.

X.5 – Sr concentration and Sr isotope ratio results

The Sr concentrations and the $^{87}Sr/^{86}Sr$ isotope ratios obtained for the enamel and dentine of the teeth investigated are summarized in table X.1. The strontium concentration for teeth from the individuals of the Pandhof site is variable, and ranges between 70 and 550 µg g^{-1} for the dentine, and between 110 and 390 µg g^{-1} for the enamel. Except for incisor 108, the dentine displays a higher Sr concentration than the corresponding enamel (table X.1). Further, the highest Sr concentrations of the entire dataset (390 µg g^{-1} for dentine and 550 µg g^{-1} for enamel) are retrieved in the dental tissues of individual 108, a child of 5-9 years of age. Possibly, the dental tissues of children are more susceptible to diagenetic alteration than the dental tissues of adults, what could explain the higher strontium content of the former, despite the biogenic Ca/P ratios retrieved for the enamel and dentine of individual 108 (figure X.4). However, it is noted that the incisor and the molar of individual 108 display an inverse trend in Sr concentration for enamel and dentine. The highest Sr concentration for the dentine corresponds to the lowest Sr concentration in enamel and vice versa. If diagenesis has indeed occurred, the reason why either the enamel or the dentine of this individual's incisor and molar displays an elevated Sr concentration, remains unclear.

The teeth from the individuals of the Vrijthof site display similar Sr concentrations. The dentine Sr concentration ranges between 160 and 220 µg g^{-1} with an average of 190 µg g^{-1}. The corresponding enamel Sr concentrations are lower in every case and range between 90 and 170 µg g^{-1} with an average of 130 µg g^{-1}. The spread in Sr concentration is lower for the samples from the Vrijthof site than for the samples from the Pandhof site, although more samples were investigated from the Vrijthof site. The Sr concentrations observed are in agreement with the *in vivo* ranges in mammalian skeletal tissues of 50 – 500 µg g^{-1} in enamel and 100 – 1000 µg g^{-1} in bone and dentine [Elias *et al.*, 1982; Burton *et al.*, 1999; Kohn *et al.*, 1999; Bentley, 2006].

The $^{87}Sr/^{86}Sr$ ratios obtained for the dental tissues from the individuals of Pandhof and Vrijthof are summarized in table X.1 and displayed in figure X.5. The procentual shift in $^{87}Sr/^{86}Sr$ isotope ratio from enamel to dentine for every enamel-dentine pair is displayed in figure X.6. The samples from Pandhof and Vrijthof display a different trend in $^{87}Sr/^{86}Sr$ isotope ratio. When first the samples from Pandhof are considered, it can be seen that the enamel and dentine of both the incisor and the molar of the same individual display, within experimental error, the same $^{87}Sr/^{86}Sr$ ratio (figure X.5). The incisor and the molar of individual 108 both display a $^{87}Sr/^{86}Sr$ ratio of 0.7096, while the incisor and molar of individual 454 both display a $^{87}Sr/^{86}Sr$ ratio of 0.7093. For the samples from Pandhof, a shift of –0.003 to 0.004 % is observed from enamel to dentine (figure X.6), a shift that is

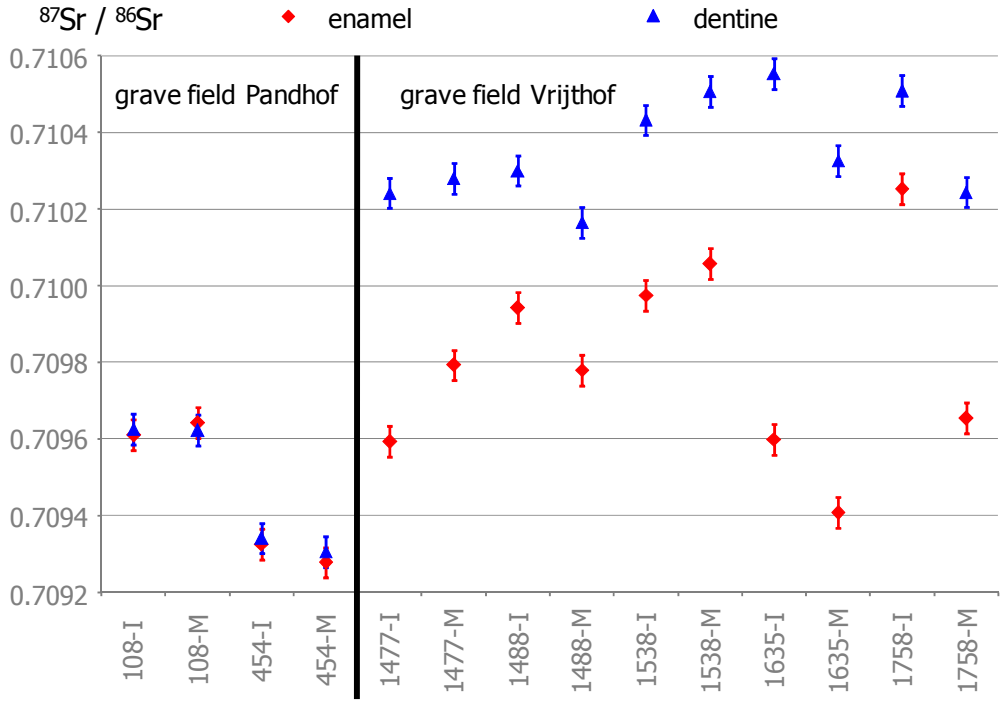

Figure X.5 – $^{87}Sr/^{86}Sr$ isotope ratio for the investigated incisors (I) and molars (M) from the sites of Pandhof and Vrijthof. Error bars represent 2s uncertainty intervals (external precision).

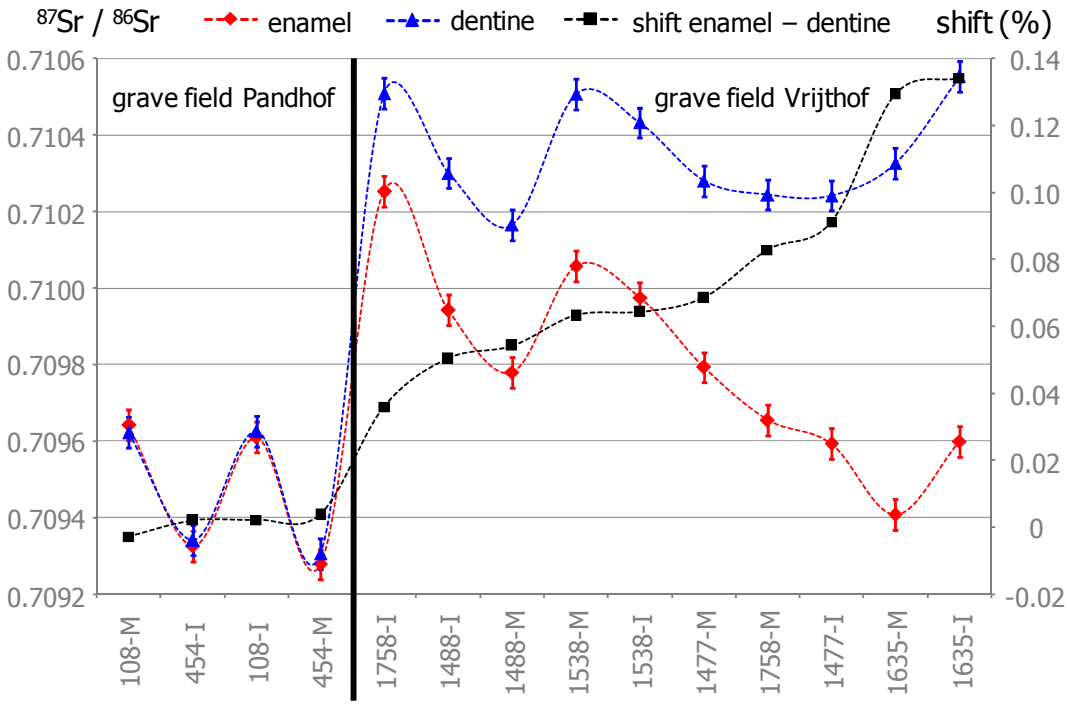

Figure X.6 – $^{87}Sr/^{86}Sr$ isotope ratio and $^{87}Sr/^{86}Sr$ ratio shift from enamel to dentine for the investigated incisors (I) and molars (M) from the sites of Pandhof and Vrijthof, organized according to increasing shift in $^{87}Sr/^{86}Sr$ ratio from enamel to dentine. Error bars represent 2s uncertainty intervals (external precision).

smaller than the external precision of the method (0.006 % 2 RSD). Thus, the $^{87}Sr/^{86}Sr$ ratios of the dental tissues of the individuals from the Pandhof site suggest that these individuals spent their entire life in the same geological area, since there is no indication that these individuals relocated.

For the individuals excavated at Vrijthof, it is clear that the dentine is always characterized by a $^{87}Sr/^{86}Sr$ ratio that is higher than that of the corresponding enamel (figure X.5). The enamel from the Vrijthof site displays a $^{87}Sr/^{86}Sr$ ratio range of 0.7094 – 0.7103, while the dentine from the Vrijthof site displays a $^{87}Sr/^{86}Sr$ ratio range of 0.7102 – 0.7106. The spread in $^{87}Sr/^{86}Sr$ ratio is higher for the enamel than for the corresponding dentine (figure X.5). When the incisor and the molar of the same individual are considered, it is observed that 2 individuals (1477 and 1538) display a higher $^{87}Sr/^{86}Sr$ ratio for the molar, while the other 3 individuals (1488, 1635 and 1758) display a higher $^{87}Sr/^{86}Sr$ ratio for the incisor. The procentual shift in $^{87}Sr/^{86}Sr$ ratio from enamel to dentine for the samples from the Vrijthof site (figure X.6) ranges between 0.036 and 0.134 %, a difference that is well above the external precision of the method (0.006 % 2 RSD). When the incisor and the molar of the same individual are considered, a similar shift in $^{87}Sr/^{86}Sr$ ratio is established, except for individuals 1477 and 1758, for which a significant difference in shift of respectively 0.023 and 0.047 % is observed. The observation that a

difference in $^{87}Sr/^{86}Sr$ ratio is established for the enamel and dentine of all the individuals from Vrijthof investigated, might suggest that the strontium present in both of these dental tissues is of different geological origin. Probably the most likely explanation is that the individuals excavated at the Vrijthof site resided, during the last years of life, in an area that is geologically distinct from the area they resided in during childhood and thus, that these individuals have relocated during their life history. Alternatively, but less likely, the different $^{87}Sr/^{86}Sr$ ratio of enamel and dentine can be attributed to the consumption of food from non-local origin.

A graphical presentation of the $^{87}Sr/^{86}Sr$ ratio versus the inverse of the Sr concentration is given in figure X.7. The dentine from the individuals at the Vrijthof site constitutes a rather compact group, while also the enamel samples can be considered as a rather widely dispersed group. As opposed to the samples from the Vrijthof site, the enamel and dentine samples from the Pandhof site form a widely dispersed and intermingled group with a more narrow spread in $^{87}Sr/^{86}Sr$ ratio, which can probably in part be attributed to the limited number of samples, but a wider Sr concentration range.

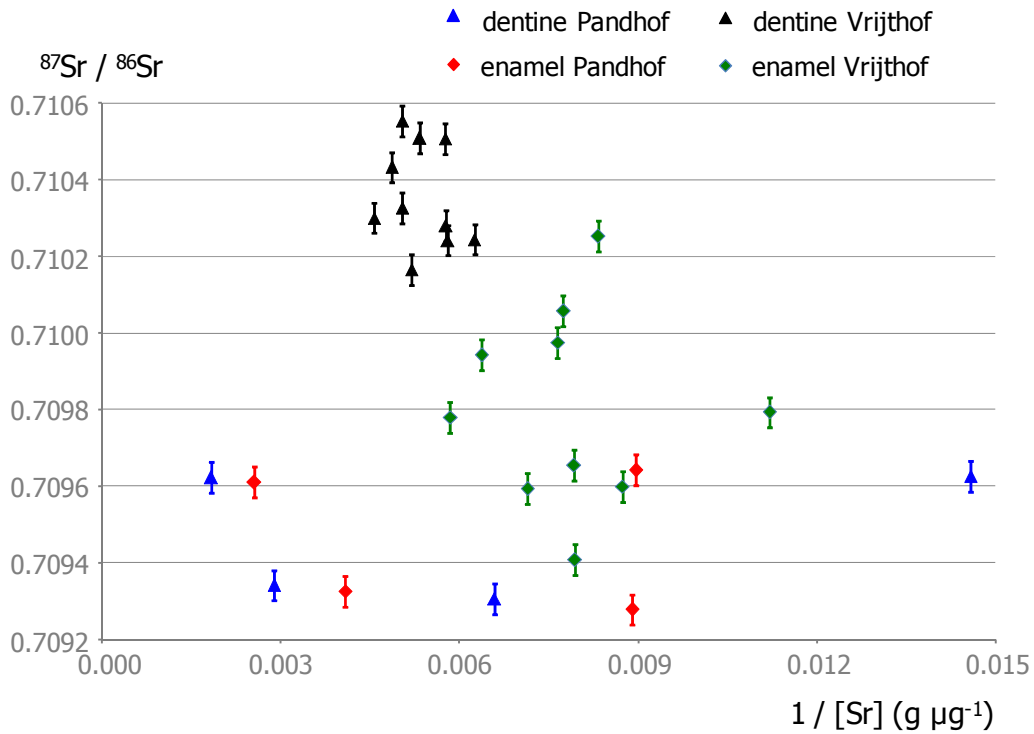

Figure X.7 – $^{87}Sr/^{86}Sr$ ratio versus the inverse of the Sr concentration for the dentine and enamel from the individuals of Pandhof and Vrijthof. Error bars represent 2s uncertainty intervals (external precision).

On the basis of the $^{87}Sr/^{86}Sr$ ratio versus the inverse of the Sr concentration (figure X.7) for the dentine samples, a clear difference is established between the individuals from Pandhof on the one hand and the individuals from Vrijthof on the other hand. It could be

suggested that the individuals from both grave fields resided in a distinct geological area during the last years of life.

The enamel samples from the Pandhof site display a $^{87}Sr/^{86}Sr$ ratio that overlaps with the $^{87}Sr/^{86}Sr$ ratio range displayed by the enamel samples from the Vrijthof site. Hence, on the basis of the $^{87}Sr/^{86}Sr$ ratio in enamel, the individuals from the Pandhof site and the Vrijthof site cannot be distinguished and thus it cannot be excluded that possibly all the individuals investigated spent their childhood in the same geological area. However, the Sr concentrations show a larger dispersion for the samples from the Pandhof site than for that from the Vrijthof site. On the one hand, the larger spread in Sr concentration for the samples from the Pandhof site is remarkable and when it would be considered as significant, it could be an argument in stating that the population on the Pandhof site is different from that on the Vrijthof site. On the other hand, the significance of the different Sr concentrations for the populations from Pandhof and Vrijthof can be doubted, since Sr concentrations in skeletal tissues are highly variable and susceptible to variations due to, *e.g.*, diet, so that the difference in concentration may not be linked to geological origin but rather to a specific individual's diet. Further, diagenesis may have had an influence on the biogenic signals, despite the fact that the experimentally determined Ca/P ratios reflect biogenic values. The analysis of more samples originating from the Pandhof site for diagenetic proxies, Sr concentration and $^{87}Sr/^{86}Sr$ isotope ratio is necessary to provide the answer to the question whether or not the differences in Sr concentration can be attributed to a different origin of the populations on the Pandhof and the Vrijthof site.

X.6 – Conclusions and future

The $^{87}Sr/^{86}Sr$ isotope ratio analysis of the dental remains of a limited number of individuals from the Pandhof site and the Vrijthof site on the Servatius complex in Maastricht (The Netherlands) suggest a difference between the populations of the two grave fields. From the analysis of the teeth of 2 individuals from the Pandhof site, it seems that this grave field has been used to bury individuals that did not move throughout their life history. The analysis of the teeth of 5 individuals excavated at the Vrijthof site revealed that probably these individuals have relocated during their life history. However, it cannot be deduced from the current data which dentine $^{87}Sr/^{86}Sr$ ratio is to be considered as the local (Maastricht) $^{87}Sr/^{86}Sr$ isotope ratio and thus which individuals spent their last years of life in the Maastricht area.

On the basis of the explorative $^{87}Sr/^{86}Sr$ isotope ratio study conducted on a small number of individuals, two hypotheses can be put forward concerning the migration behavior of the individuals investigated from these grave fields, be it without an identification of the local $^{87}Sr/^{86}Sr$ ratio and thus without an identification of the local individuals. It is stressed that further investigation is required to show which of the following hypotheses is a reflection of the reality, and to clarify to which extent the hypotheses suggested are applicable to the entire population of the Pandhof and Vrijthof sites.

One hypothesis may be that the dental tissues from Pandhof, characterized by an average $^{87}Sr/^{86}Sr$ ratio of 0.7095, stem from individuals that were born and spent their entire life in the area of Maastricht. In this case, the individuals from the Vrijthof site were born in either the Maastricht area, or a geologically slightly distinct area as reflected in their enamel with an average bioavailable $^{87}Sr/^{86}Sr$ ratio of 0.7098, and moved throughout their life to another geological area, different from the area of Maastricht, that is characterized by a local $^{87}Sr/^{86}Sr$ ratio of 0.7104 or higher, as reflected in the dentine of these individuals. As a consequence, it could be concluded that the Pandhof site was used to bury individuals that lived their entire life locally, while individuals that migrated to another area than Maastricht were transferred to the Servatius complex after death to be buried at the Vrijthof site. Alternatively, these individuals may have reintegrated into the Maastricht area but died very shortly after the reintegration.

Another hypothesis is based upon the assumption that the individuals excavated at the Vrijthof site spent their last years of life in the area of Maastricht and that these individuals moved only once from the place of birth to the Maastricht area. The average dentine $^{87}Sr/^{86}Sr$ ratio of 0.7104 has arisen from the mixing of Sr from their place of birth, reflected in their enamel strontium with an average $^{87}Sr/^{86}Sr$ ratio of 0.7098, and Sr from the Maastricht area, that should display a bioavailable $^{87}Sr/^{86}Sr$ ratio equal to or higher than 0.7104. The $^{87}Sr/^{86}Sr$ ratio of the dental tissues from the individuals at the Pandhof site would indicate in this case that these individuals spent their entire life in an area that is geologically distinct from the area in which the individuals from the Vrijthof site resided during their last years of life, and would lead to the conclusion that the individuals excavated at the Pandhof site were transferred to the Servatius complex after death to be buried at the Pandhof site.

More research is needed to elucidate which hypothesis is the most likely. More enamel and dentine samples from individuals from both grave fields should be analyzed for their $^{87}Sr/^{86}Sr$ ratios in order to clarify (i) if the individuals on the Pandhof site and the Vrijthof site share a common place of birth, in other words, if the enamel of the individuals from

both sites can be considered as one group in terms of its $^{87}Sr/^{86}Sr$ ratio and (ii) which population displays the local bioavailable $^{87}Sr/^{86}Sr$ ratio in its dentine, and thus which individuals resided in the Maastricht area during their last years of life. When the conclusions are to be extended to the entire populations on the Pandhof and Vrijthof sites, more research is required concerning the homogeneity of the population from each grave field in terms of dental $^{87}Sr/^{86}Sr$ ratios. It was observed for the individuals of the Vrijthof site that the incisor and the molar display the same trend in $^{87}Sr/^{86}Sr$ ratios, that are however slightly different in absolute value. From this observation, in combination with the knowledge that a specific diet (rich or poor in Sr) leads to a specific dentine $^{87}Sr/^{86}Sr$ ratio, it is likely that the uncertainty on the dental $^{87}Sr/^{86}Sr$ ratios has been underestimated, so that the intra-population spread on the $^{87}Sr/^{86}Sr$ ratio needs to be determined before concluding that a population has relocated. Further, also the evaluation of diagenetic alteration can be extended to several diagenetic proxies, such as the Ca/P ratio and the uranium and rare earth element contents. This will allow to obtain a more reliable conclusion on the occurrence of diagenesis and to evaluate the biogenic integrity of the experimental dental $^{87}Sr/^{86}Sr$ ratios with a higher degree of certainty.

In order to identify the local $^{87}Sr/^{86}Sr$ isotope ratio range, two approaches can be followed. In a first approach, the $^{87}Sr/^{86}Sr$ ratio of the bioavailable Sr of the soil can be determined, because this ratio characterizes the Sr that is taken up from local foods and infers a change in the $^{87}Sr/^{86}Sr$ ratio of dentine after moving to a geologically distinct area. A better approach to evaluate the local $^{87}Sr/^{86}Sr$ ratio is to use teeth instead of soil. In this case, the $^{87}Sr/^{86}Sr$ ratio of the enamel of local small mammals, *e.g.*, mice and rodents, can provide a fair estimation [Hoppe *et al.*, 1999; Price *et al.*, 2002]. It was shown that the variability in $^{87}Sr/^{86}Sr$ ratio is orders of magnitude smaller in animal bone and dental tissues than in whole rocks and soils [Ezzo *et al.*, 1997; Beard and Johnson, 2000; Price *et al.*, 2002]. The danger when sampling modern animals is that they may consume imported foods or local foods with 'exotic' strontium introduced through fertilizers or airborne sources of strontium. In this respect, some snail species that exclusively feed on moss and thus, reflect the local $^{87}Sr/^{86}Sr$ ratio in their shell, may be a better choice. Another, perhaps even more reliable, approach to characterize the bioavailable local strontium is to analyze archaeological teeth of an animal species that lived locally [Price *et al.*, 2002; Bentley *et al.*, 2004; Knudson *et al.*, 2004]. Domestic pigs are very useful in this respect, and the variability in $^{87}Sr/^{86}Sr$ ratio of pig enamel is half that of caprine and cattle, and even less than that in human bone [Price *et al.*, 2002; Bentley *et al.*, 2004; Bentley and Knipper, 2005].

CHAPTER XI

Summary and conclusions

The aim of this work was to answer specific archaeological questions by means of results obtained via isotopic analysis. The isotopic composition of strontium and lead, present in low amounts in archaeological artefacts, was used to this purpose. A powerful technique for isotope ratio analysis is inductively coupled plasma – mass spectrometry (ICP-MS). Single-collector ICP-MS (SC-ICP-MS), in which the instrument is equipped with one electron multiplier for ion detection, is suited for isotope ratio applications that do not require the ultimate isotope ratio precision. However, when very small variations in isotopic composition need to be addressed, multi-collector ICP-MS (MC-ICP-MS) is the method of choice. In this work, both single-collector – and multi-collector ICP-MS were used for isotope ratio analysis.

XI.1 – Analytical methodologies developed

A first phase of this work was devoted to the development of analytical methodologies for Pb and Sr isotope ratio analysis of archaeological artefacts. The collection of archaeological artefacts investigated consisted of a variety of materials: soil samples, bone and dental tissues, ceramics and metallic objects and fragments rich in copper, silver and/or lead.

Since ICP-MS is, in its standard configuration, suited for the analysis of sample solutions, the solid samples required to be dissolved prior to isotope ratio analysis. To this purpose, a specific digestion procedure was developed for every sample type involved. Sample digestion was performed by adding a well-chosen combination of concentrated mineral acids (*e.g.*, HNO_3, HCl, HF, $HClO_4$, H_2O_2) to a weighed amount ($\leq$ 0.5 g) of homogenized solid sample and submitting the sample-acid mixture to a microwave-assisted acid digestion step, a hotplate digestion step, or a combination of both. The digestion procedures developed for the various sample types succeeded in a complete dissolution of the respective solid samples and all gave rise to quantitative target element recoveries, as was proven by the digestion of certified reference materials with a matrix composition similar to that of the respective sample types and analysis of the digests thus obtained. The fact that a quantitative target element recovery was established for Sr and/or Pb, assures that no isotopic fractionation of Sr or Pb could have been introduced by the digestion process. Prior to acid digestion, the samples were cleaned, rinsed and prepared for the subsequent digestion step. Soil and bone tissues were powdered by the use of a microdismembrator, metallic objects were sampled by means of a miniature drill and teeth were carefully cut by the use of a dental saw to obtain the separate dentine and

enamel fractions. The levels of Sr and Pb in the procedural blanks were found to be negligible (< 0.1 %) compared to the levels of Sr and Pb present in the digested samples, so that it can be concluded that the pretreatment step does not lead to significant amounts of contamination.

Most of the sample types under investigation were characterized by a complex matrix composition. In order to obtain accurate and precise isotope ratio data, a preliminary isolation of the target element is required, especially when MC-ICP-MS will be subsequently used for isotope ratio measurements. Hence, the next step was to develop separation procedures that succeed in isolating Sr or Pb from the complex concomitant matrix, preferably in pure form and in a quantitative way. An extraction chromatographic separation, making use of a resin based on a crown ether (Sr spec^{TM} for Sr and Pb spec^{TM} for Pb) was evaluated in its capability to meet these requirements. The optimization of the separation procedure consisted of selecting suited reagents and determining the volumes required for the removal of the concomitant matrix elements after loading the digest onto the extraction chromatographic column, and for the subsequent elution of the purified Sr or Pb fraction. It was found that the isolation of Sr by means of Sr spec^{TM} is accomplished by (i) loading the digest in 7 M HNO_3 onto the column, (ii) rinsing the column with 10 mL 7 M HNO_3 for the removal of slightly retained concomitant matrix elements and (iii) eluting the purified Sr fraction with 10 mL 0.05 M HNO_3. This protocol was applied to the isolation of Sr from digests of soil samples, bone and dental tissues, and was shown to result in a quantitative Sr recovery, to allow the pure Sr fraction to be obtained and to succeed in the complete separation of Sr from Rb. When these two elements are not separated from one another, rubidium gives rise to an isobaric interference ($^{87}Rb^+$) on the $^{87}Sr^+$ signal. The isolation of Pb by means of Pb spec^{TM} was performed in an analogous manner. The digested sample, dissolved in 1 M HNO_3, was loaded onto the extraction chromatographic column. The removal of slightly retained concomitant matrix elements was performed by rinsing the column with 10 mL 0.1 M HNO_3 and the purified Pb fraction was subsequently stripped from the column using a 0.05 M $(NH_4)_2C_2O_4$ solution. This separation protocol was successfully applied to the isolation of Pb from digests of bone tissue, soil samples, ceramics and metallic objects, and for each of these sample types, a quantitative recovery was established. Further, the Pb fractions obtained were free of residual matrix components. The isolation protocols for Sr and Pb were also applied to isotopic standards, and the comparative Sr or Pb isotopic analysis of the respective isotopic standards before and after the respective isolation protocol showed that no Sr or Pb isotopic fractionation is introduced by the isolation process. Lastly, the possibility of

regenerating the extraction chromatographic resins, allowing multiple use of the same column, was explored. It was found that rinsing with 100 mL milli-Q water is efficient in regenerating the resin for at least a second use, without a loss in separation performance or an influence on isotopic composition. This has been demonstrated by Sr and Pb isotopic analysis of purified Sr or Pb fractions from certified reference materials that were obtained with new and regenerated columns.

Strontium isotope ratio measurements were carried out using multi-collector ICP-MS. For lead isotope ratio analysis, both single-collector ICP-MS and multi-collector ICP-MS were used. Single-collector quadrupole-based ICP-MS is characterized by an isotope ratio precision that is not sufficiently high for many isotope ratio applications. However, when the quadrupole-based ICP-MS instrument is equipped with a dynamic reaction cell (DRC), the use of a collision gas in the DRC allows an improved isotope ratio precision to be obtained. A measurement protocol for Pb isotope ratio analysis was developed, making use of Ne as a collision gas, introduced at a flow rate of 0.1 mL min^{-1} into the DRC of a quadrupole-based ICP-MS instrument. It was demonstrated that the SC-ICP-DRC-MS measurement protocol is more precise than traditional quadrupole-based ICP-MS, and yields a Pb isotope ratio precision that is similar to the best precision reported for single-collector sector field ICP-MS. A comparison of Pb isotope ratio results obtained via the SC-ICP-DRC-MS measurement protocol to the corresponding results obtained via multi-collector ICP-MS demonstrated that the single-collector measurement protocol provides accurate isotope ratio results. Further, certified reference materials with a Pb isotopic composition that is known from previous studies, were analyzed. The good agreement between the Pb isotope ratios obtained in this work and results published in literature for certified reference materials with a complex matrix composition confirms that the entire analytical methodology developed – consisting of sample digestion, Pb isolation via extraction chromatography, and isotope ratio measurement using single-collector ICP – dynamic reaction cell – MS – is reproducible and yields accurate results that are similar to those obtained via multi-collector ICP-MS and TI-MS, including the ratios with ^{204}Pb. Further, it is expected that this analytical methodology is applicable for a wide range of Pb isotope ratio applications focusing on samples with a complex matrix composition.

The use of a well-chosen collision gas in a dynamic reaction cell results in an improved isotope ratio precision. The introduction of a well-chosen reaction gas into the DRC allows the analyte signals to be freed from spectral overlap originating from plasma-based or matrix-based molecular ions via chemical resolution. A strategy was developed for the simultaneous determination of P, Ca and Sr in dental tissue digests, in order to evaluate

the biogenic integrity of these tissues. The determination of P by means of ICP-MS is hampered by the occurrence of NO^+/NOH^+ signals in the mass spectrum, Ca isotopes mainly suffer from spectral interferences caused by Ar-containing molecular ions, and when working with high Ca concentrations (as is the case for dental tissues), $ArCa^+$ molecular ions interfere with the Sr^+ signals. The use of NH_3 in the dynamic reaction cell, introduced at a flow rate of 0.8 mL min^{-1} and with an RPq setting of 0.65, resulted in a significant reduction of signals arising from interfering ions, and an improvement of the detection limit with at least a factor of 10 was established. The measurement protocol was validated by the determination of P, Ca and Sr in certified reference materials, and from the good agreement between certified concentrations and experimentally retrieved concentrations, it was concluded that the measurement protocol yields accurate results.

XI.2 – Archaeological projects

The analytical methodology developed for Sr and Pb isotopic analysis was, in a second phase of this work, applied to archaeological artefacts, in the framework of three distinct archaeological projects. Two projects focused on Pb isotope ratio analysis, in which, respectively, provenancing of metallic objects and investigation of infant lead exposure in the Roman Era were aimed at. A third project aimed at the use of Sr isotope ratios to obtain insight into the migration behavior of historical individuals.

A first study focused on the provenance determination of metallic artefacts, excavated on the archaeological sites of ed-Dur (Emirate of Umm al-Qaiwain, United Arab Emirates) and Khor Rori (Oman), aiming at obtaining insight into the trade relations between the Roman Empire and the Indian subcontinent in the period 1st century BC – 2nd century AD, and the position of ed-Dur in the metal-trading network. The collection of metallic artefacts studied consisted of silver objects and copper-based (unalloyed copper, brass and bronze) and lead-based (lead and litharge) fragments and objects, that were investigated for their Pb isotopic composition using single-collector ICP-DRC-MS. Provenancing the artefacts was performed by comparing the experimentally determined Pb isotope ratios to Pb isotope ratio data for copper and silver/lead ores from a wide range of geographical areas over the old world. The copper-based objects excavated at the site of ed-Dur are linked to ore sources from Cyprus, Sardinia and Spain, which implies that the ed-Dur objects are made from Roman copper. Three bronze samples, excavated at the site of Khor Rori, deviate in Pb isotopic composition from the samples excavated at ed-Dur. One of these samples can be linked to Indian copper ores. This observation implies that, at least to

some extent, copper was produced in India at that time. The lead and litharge fragments, except for 3 items, all show a very similar Pb isotopic composition and are grouped around an ingot with a stamped monogram. The very good agreement with Sardinian and Spanish ore sources allows the conclusion that this lead is of Roman origin. However, two lead fragments show a Pb isotopic composition similar to that of the deviating bronze sample from Khor Rori, and could be attributed to India. These two lead fragments from ed-Dur are the first to demonstrate that India was exporting, and thus also producing, lead before the 2nd century AD. The litharge fragments show a Pb isotopic composition that is similar to that of the Roman ingot and the lead fragments, what implies that the same lead is used in the cupellation process to obtain silver. The silver objects were identified as stemming from Sardinian, Spanish and British ores, thus attributing their provenance to the Roman Empire. Further, on the basis of the monogram imprinted on the Roman lead ingot, it was suggested that metal was exported from the Roman Empire to the Indian subcontinent via an itinerary from the Eastern Mediterranean across Syria, to Palmyra. There, it was taken on the Euphrates and travelled downstream to the city of Characene, and continuing its route down the Gulf to eventually reach ed-Dur for further transport or local employment in, *e.g.*, the purification of silver.

In a second study, the origin of high lead concentrations retrieved in infant bone tissue, excavated at a Roman settlement in the village of Valkenburg (The Netherlands) was investigated. The collection of samples consisted of infant bone tissue displaying elevated Pb concentrations, along with samples from the surrounding soil and additional potential sources of bone lead, such as fish bones, ceramics and lead fragments. The Pb isotopic investigation of these artefacts has revealed that an important fraction of the lead found at present in the bone tissue must already have been present at the moment of death, thus that diagenesis – post-mortem lead exchange between bone and soil – is not the main source of bone lead. Two sources of bone lead have been identified, namely, soil and food. These sources are represented in four endmembers. Two endmembers are soils that represent the upper continental crust and the local soil background. The lead fragments and *garum*, a fermented fish sauce enriched with a syrup having a high lead content, were identified as a third endmember. The fourth endmember was found to be a pottery sherd stemming from a bowl that was used for the conservation of food. The infant bone lead is a mixture of geogenic (soil) lead and dietary exposure lead, taken up from, *e.g.*, garum, drinking water and conserved food. It is likely that the infants have been exposed to lead that was taken up by the mother and subsequently transferred to the foetus during pregnancy.

The third project focused on the dental tissues (enamel and dentine) of the grave field population around the basilica dedicated to the Saint Servatius in Maastricht (The Netherlands). In an explorative study, the dental tissues of a small number of individuals excavated on two sites, Pandhof and Vrijthof, were studied. The strontium isotopic composition of enamel reflects the geological area of residence during childhood, while that of dentine reflects the geological area of residence during the last years of life. A difference in strontium isotopic composition of enamel and dentine hence implies that the individual under study has relocated throughout his/her life history. A comparison of $^{87}Sr/^{86}Sr$ isotope ratios of dentine and enamel from individuals from the Pandhof and the Vrijthof site suggests that the individuals buried on the Pandhof site did not relocate during their life history, while the individuals at the Vrijthof site migrated from one area to another geologically distinct area. From the enamel $^{87}Sr/^{86}Sr$ ratios, it cannot be excluded that the individuals from Pandhof and Vrijthof spent their childhood in the same geological area. However, the analysis of more samples from both the Pandhof and the Vrijthof site is required to confirm or reject this hypothesis and to obtain insight into the homogeneity of the populations of Pandhof and Vrijthof in terms of $^{87}Sr/^{86}Sr$ ratios. Within a population, individuals having a different diet (*e.g.*, poor or rich in Sr) will display a different dentine $^{87}Sr/^{86}Sr$ ratio. Further, from the present data it is not clear which individuals spent their last years of life in the Maastricht area. To clarify this, the local bioavailable $^{87}Sr/^{86}Sr$ ratio needs to be determined. This can be performed by determining the bioavailable $^{87}Sr/^{86}Sr$ ratio from the soil, because this ratio characterizes the strontium that is taken up from the food. Another, and better, way to evaluate the local bioavailable $^{87}Sr/^{86}Sr$ ratio is the determination of the $^{87}Sr/^{86}Sr$ ratio of the enamel of local small mammals such as mice and rodents, or that of the shell of snail species that exclusively feed on moss. The best approach for characterizing the bioavailable local strontium is to analyze the enamel of an archaeological animal species that certainly lived locally during the same period, such as domestic pigs.

HOOFDSTUK XII

Samenvatting en besluit

Het doel van dit werk bestond erin een antwoord te bieden op archeologische vragen door middel van strontium- en looodisotopenanalyse. Een krachtige techniek voor de bepaling van isotopenverhoudingen is inductief gekoppeld plasma – massaspectrometrie (ICP-MS). Een ICP-MS instrument uitgerust met slechts één elektronenvermenigvuldiger voor iondetectie (single-collector ICP-MS) is geschikt voor deze toepassingen waar een uitmuntende isotopenprecisie niet vereist is. Wanneer echter heel kleine verschillen in isotopische samenstelling dienen vastgesteld te worden, is multi-collector ICP-MS de aangewezen techniek. In dit werk werden zowel single-collector – als multi-collector ICP-MS aangewend voor isotopenanalyse.

XII.1 – Ontwikkelde analytische strategie

Een eerste fase van dit werk was gewijd aan het ontwikkelen van analytische strategieën voor strontium- en loodisotopenanalyse van archeologische artefacten. De verzameling bestudeerde archeologische artefacten bestond uit bodemstalen, bot- en tandweefsels, aardewerk en metallische objecten met een hoog koper-, zilver- en/of loodgehalte.
Gezien ICP-MS in de standaardconfiguratie geschikt is voor de analyse van vloeibare monsters, was het noodzakelijk de aangeleverde artefacten vooraf in oplossing te brengen. Hiertoe werd voor ieder type monster een specifieke digestieprocedure op punt gesteld. De procedure bestond erin een welgekozen combinatie van minerale zuren (HNO_3, HCl, HF, $HClO_4$, H_2O_2) toe te voegen aan een afgewogen hoeveelheid ($\leq$ 0.5 g) homogeen vast monster, en dit geheel te onderwerpen aan een microgolf-geassisteerde zure digestie, een digestie in een beker op een verwarmplaat, of een combinatie van beide. Elk type monster kon volledig in oplossing worden gebracht door het te onderwerpen aan de geschikte digestieprocedure. De ontwikkelde digestieprocedures werden gevalideerd door het toepassen van deze methoden voor digestie van gecertificeerde referentiematerialen met een matrixsamenstelling gelijkaardig aan die van het type monster waarvoor de procedure werd op punt gesteld, en de daaropvolgende analyse wees op een kwantitatieve recovery van de targetelementen. Op basis van de kwantitatieve recovery voor strontium en/of lood kon besloten worden dat er geen isotopische fractionatie van strontium of lood werd geïntroduceerd door de digestiestap. Voorafgaand aan de zure digestie werden de artefacten op een geschikte manier schoongemaakt en gehomogeniseerd. Bodemmonsters en botweefsel werden verpulverd door gebruik te maken van een microdismembrator, metallische artefacten werden bemonsterd aan de hand van een miniatuur-boor en met behulp van aangepast

gereedschap werd van de aangeleverde tanden het tandglazuur gescheiden van de dentine. De gehaltes aan strontium en lood teruggevonden in de procedureblanco's was verwaarloosbaar (< 0.1 %) in vergelijking met de gehaltes aan strontium en lood in de in oplossing gebrachte artefacten. Hieruit werd besloten dat er tijdens de monstervoorbehandeling en de daaropvolgende digestie geen significante hoeveelheid contaminatie optreedt.

Het merendeel van de onderzochte artefacten werd gekenmerkt door een complexe matrixsamenstelling. Voorafgaand aan isotopische analyse, en vooral bij gebruik van multi-collector ICP-MS, was het dan ook aangewezen het strontium of het lood te isoleren van de begeleidende matrix. Bijgevolg was de volgende stap in de analytische strategie het ontwikkelen van isolatieprocedures die er bij voorkeur in slagen het targetelement kwantitatief en zuiver te isoleren van de begeleidende matrix. Als isolatiemethode werd geopteerd voor een extractiechromatografische scheiding, gebruik makend van een hars waarop zich een kroonether bevindt (Sr spec^{TM} voor Sr en Pb spec^{TM} voor Pb). De optimalisatie van de isolatieprocedure bestond erin de geschikte reagentia te selecteren die ervoor zorgen dat, in een eerste stap, het targetelement (Sr of Pb) sterk weerhouden wordt door het hars terwijl de begeleidende matrixelementen van de kolom worden gespoeld. De tweede stap bestaat er dan in door middel van een geschikt reagens de zuivere Sr of Pb fractie van de kolom te elueren. De isolatie van strontium door middel van Sr spec^{TM} werd bewerkstelligd door het opgeloste monster op te nemen in 7 M HNO_3 en vervolgens op de kolom te brengen, de begeleidende matrixelementen te verwijderen door de kolom te spoelen met 10 mL 7 M HNO_3, en uiteindelijk de zuivere Sr fractie te elueren met 10 mL 0.05 M HNO_3. Deze isolatieprocedure werd toegepast op opgeloste bodem- en botmonsters, en bleek efficiënt te zijn in het scheiden van Rb en Sr en verder te resulteren in de zuivere Sr fractie op kwantitatieve wijze. Op analoge wijze als voor Sr spec^{TM} werd Pb spec^{TM} geoptimaliseerd voor de isolatie van lood. Het opgeloste monster werd opgenomen in 1.0 M HNO_3 en op de kolom gebracht, de begeleidende matrixelementen werden van de kolom gespoeld met 10 mL 0.1 M HNO_3 en de gezuiverde Pb fractie werd gerecupereerd met 10 mL 0.05 M $(NH_4)_2C_2O_4$ in milli-Q water. Deze isolatieprocedure werd aangewend om lood te isoleren uit opgeloste bodemmonsters, botweefsel, aardewerk en metallische fragmenten, en voor ieder type monster werd vastgesteld dat de zuivere loodfractie, vrij van overtollige matrixelementen, op kwantitatieve wijze werd bekomen. De extractiechromatografische procedures ontwikkeld voor de isolatie van strontium en lood werden eveneens toegepast op isotopische standaarden, en uit de later bepaalde isotopenverhoudingen kon besloten worden dat de

isolatieprocedure voor zowel Sr als Pb geen isotopische fractionatie van Sr of Pb introduceert. Tenslotte werd ook nog nagegaan of eenzelfde extractiechromatografische kolom meerdere malen kan aangewend worden na regeneratie van het hars. De regeneratie bleek mogelijk te zijn door, na gebruik van de kolom, deze te spoelen met 100 mL milli-Q water. Het op deze wijze geregenereerde hars werd daarna aangewend voor de isolatie Sr of Pb uit een tweede opgelost bodem- of botmonster, en er werd vastgesteld via Sr en Pb isotopische analyse van referentiematerialen, waarbij de zuivere Sr of Pb fracties werden bekomen door gebruik van een nieuwe en een geregenereerde kolom, dat de isolatie met een geregenereerde kolom dezelfde efficiënt vertoont als een nieuwe kolom.

Multi-collector ICP-MS werd ingezet voor de bepaling van strontiumisotopenverhoudigen. Loodisotopenverhoudingen werden bepaald via zowel single-collector – als multi-collector ICP-MS. Single-collector ICP-MS geeft aanleiding tot een isotopenprecisie die niet voldoende is voor vele toepassingen van isotopenanalyse. Wanneer echter een quadrupool-gebaseerde ICP – massaspectrometer uitgerust is met een dynamische reactiecel (DRC), laat het gebruik van een botsingsgas in deze DRC toe een verbeterde isotopenprecisies te bekomen. In het kader van dit werk werd een meetprotocol ontwikkeld voor de bepaling van loodisotopenverhoudingen door middel van SC-ICP-DRC-MS. Wanneer neon wordt binnengeleid in de DRC aan een gasdebiet van 0.1 mL min^{-1}, werd vastgesteld dat isotopenprecisies werden bekomen die vergelijkbaar zijn met de beste resultaten gerapporteerd voor single-collector sector veld ICP-MS. Verder werd aangetoond, door het vergelijken van experimentele Pb isotopenverhoudingen bekomen via SC-ICP-DRC-MS en de corresponderende Pb isotopenverhoudingen bekomen via MC-ICP-MS, dat het ontwikkelde meetprotocol accurate resultaten oplevert. Daarnaast werden ook een aantal referentiematerialen met een gekende isotopische samenstelling geanalyseerd. Uit de uitstekende overeenkomst tussen de resultaten bekomen via de ontwikkelde methodologie en literatuurwaarden bekomen via MC-ICP-MS of TI-MS kan besloten worden dat de volledige analytische strategie, bestaande uit zure digestie, isolatie van de zuivere Pb fractie, en het daaropvolgende meetprotocol via SC-ICP-DRC-MS, aanleiding geeft tot accurate resultaten, die gelijkaardig zijn aan deze bekomen via MC-ICP-MS en TI-MS, zelfs voor de isotopenverhoudingen met ^{204}Pb. Het is heel waarschijnlijk dat de ontwikkelde strategie met succes kan toegepast worden op een brede waaier aan toepassingen waarin het bepalen van Pb isotopenverhoudingen in complexe matrices centraal staat.

Het gebruik van een geschikt botsingsgas in een dynamische reactiecel resulteert in een verbeterde isotopenprecisie. De introductie van een weloverwogen geselecteerd reactiegas in de dynamische reactiecel laat toe spectrale interferenties, veroorzaakt door matrix- of plasma-gerelateerde ionen, te onderdrukken via chemische resolutie. Een meetprotocol werd op punt gesteld voor de gelijktijdige bepaling van P, Ca en Sr in opgelost tandweefsel, met als doel de biogene integriteit van deze weefsels te beoordelen. De bepaling van P door middel van ICP-MS wordt bemoeilijkt door de signalen afkomstig van NO^+ en NOH^+ moleculaire ionen in het massaspectrum. De isotopen van calcium worden voornamelijk geïnterfereerd door Ar-bevattende moleculaire ionen, en wanneer gewerkt wordt met hoge Ca concentraties – zoals het geval is bij tandweefsel – veroorzaken $ArCa^+$ ionen spectrale overlap met de Sr^+ signalen. Het gebruik van NH_3 als reactiegas in de dynamische reactiecel, geïntroduceerd in de DRC met een debiet van 0.8 mL min^{-1} en met een RPq instelling van 0.65, zorgde voor een significante reductie van de signalen afkomstig van interfererende ionen en een verbetering van de detectielimiet met tenminste een factor 10. Het meetprotocol werd gevalideerd door de bepaling van P, Ca en Sr in opgeloste bot gecertificeerde referentiematerialen, en uit de goede overeenkomst tussen de gecertificeerde en de experimenteel bepaalde resultaten werd besloten dat het ontwikkelde meetprotocol leidt tot accurate resultaten.

XII.2 – Archeologische projecten

De analytische strategie ontwikkeld voor Sr en Pb isotopische analyse werd in een tweede fase van dit werk toegepast op archeologische artefacten. In twee projecten was lood het targetelement, en werd Pb isotopenanalyse ingezet voor, respectievelijk, de herkomstbepaling van metallische artefacten, en onderzoek naar blootstelling aan lood gedurende de kindertijd in het Romeinse tijdperk. In een derde project werd gepoogd inzicht te verkrijgen in migratie van individuen door middel van variaties in de strontium isotopische samenstelling van hun tandweefsels.

In een eerste studie werden loodisotopenverhoudingen aangewend voor de herkomstbepaling van metallische artefacten die blootgelegd werden op de archeologische sites ed-Dur (Emiraat van Umm al-Qaiwain, Verenigde Arabische Emiraten) en Khor Rori (Oman). Het doel van deze studie was een dieper inzicht te verschaffen in de handelsrelaties tussen het Romeinse Rijk en het Indische subcontinent en de positie van ed-Dur in dit netwerk gedurende de periode 1ste eeuw vC – 2^{e} eeuw nC.

De collectie metallische artefacten bestond uit fragmenten en objecten rijk in koper (zuiver koper, messing en brons), lood (lood en loodglit fragmenten) of zilver. De herkomstbepaling werd uitgevoerd door het vergelijken van de experimentele Pb isotopenverhoudingen met waarden voor koper en zilver/lood ertsen van vrijwel de gehele oude wereld. Dit wees uit dat de fragmenten rijk in koper gevonden op de site ed-Dur gelinkt zijn aan ertsen van Cyprus, Sardinië en Spanje, wat impliceert dat deze fragmenten vervaardigd zijn met Romeins koper. Drie bronzen fragmenten, gevonden op de site Khor Rori, vertonen een duidelijk verschillende Pb isotopische samenstelling en één van deze bronzen fragmenten kan met hoge waarschijnlijkheid gelinkt worden aan Indische koperertsen. Deze vaststelling suggereert dat India in deze tijd koper won uit ertsen en dat ook exporteerde. De loden en loodglit fragmenten vertonen een heel gelijkaardige isotopische samenstelling, en vormen een nauw veld dat gecentreerd is rond een verhandelbare blok lood (ingot). Twee loden fragmenten vertonen echter een Pb isotopische samenstelling gelijkaardig aan die van het, vermoedelijk Indische, bronzen fragment van Khor Rori, wat leidt tot de suggestie dat ook deze twee fragmenten van Indische oorsprong zijn. Deze twee fragmenten zijn de eerste aanwijzingen dat India voor de 2^{e} eeuw nC lood won uit loodertsen en dit lood ook exporteerde. De loodglit fragmenten worden gekarakteriseerd door een Pb isotopische samenstelling gelijkaardig aan die van de ingot en de andere loden fragmenten, wat erop wijst dat lood van dezelfde oorsprong werd gebruikt voor het zuiveringsproces van zilver. De zilveren objecten kunnen gelinkt worden aan ertsen van Sardinië, Spanje en het Verenigd Koninkrijk, wat erop wijst dat ook de oorsprong van deze objecten Romeins is. Verder kon, op basis van het monogram teruggevonden op de Romeinse ingot, een route gesuggereerd worden via dewelke lood geëxporteerd werd vanuit het Romeinse Rijk naar het Indische subcontinent. Met een grote waarschijnlijkheid werd het lood via de oostelijke Middellandse Zee getransporteerd doorheen Syrië tot Palmyra. Vanaf Palmyra werd het verscheept over de Eufraat naar de stad Characene en dan verder via de Golf naar ed-Dur. Eens aangekomen in ed-Dur werd het lood lokaal gebruikt, of getransporteerd richting India.

In een tweede studie werd de bron van hoge loodconcentraties, teruggevonden in het botweefsel van overleden pasgeboren Romeinse kinderen, onderzocht. De kinderskeletjes werden opgegraven in Valkenburg (Nederland). De collectie onderzochte artefacten bestond uit botweefsel met een verhoogde loodconcentratie, monsters van de omringende bodem en andere potentiële bronnen voor lood in het bot, zoals visgraten, aardewerk en loden fragmenten. De bepaling van de lood-isotopische samenstelling van

deze artefacten heeft uitgewezen dat een belangrijke fractie van het lood teruggevonden in het botweefsel daar reeds aanwezig was op het tijdstip van overlijden, en dus dat diagenese – de post-mortem lood uitwisseling tussen bodem en bot – niet de voornaamste bron is van het lood in het botweefsel. Twee bronnen voor lood in bot zijn geïdentificeerd, namelijk, de bodem en het voedsel. De bodem als bron voor bot-lood wordt vertegenwoordigd door de aardkorst en een bodem die representatief is voor de lokale geogene lood achtergrond. De voeding als bron wordt vertegenwoordigd door enerzijds de loden fragmenten, samen met *garum*, een gefermenteerde vissaus waaraan *sapa*, een zoete siroop met een hoog loodgehalte, werd toegevoegd, en anderzijds een potscherf, die afkomstig is van een kom van aardewerk waarin voedsel werd bewaard. Het lood teruggevonden in de kinderbotjes is een mengsel van geogeen (bodem) lood, en lood opgenomen via de voeding uit *garum*, drinkwater en bewaard voedsel. Het is waarschijnlijk dat de kinderen werden blootgesteld aan lood dat door de moeder werd opgenomen via de voeding, en vervolgens werd doorgegeven aan de foetus gedurende de zwangerschap.

Het derde project had als doel de strontium isotopische samenstelling te bepalen van tandweefsels (glazuur en dentine) van de grafveldpopulatie rond de basiliek opgedragen aan de Heilige Servatius (Maastricht, Nederland). In een verkennende studie werden de tanden van een klein aantal individuen, opgegraven op de sites Pandhof en Vrijthof, bestudeerd. De strontium isotopische samenstelling van het tandglazuur weerspiegelt het geologische gebied waarin een individu verbleef gedurende zijn/haar kindertijd, terwijl deze van dentine een weerspiegeling is van het geologische gebied waarin een individu de laatste jaren van zijn/haar leven doorbracht. Een verschil in strontium isotopische samenstelling voor tandglazuur en dentine wijst er dus op dat een individu gedurende zijn/haar leven gemigreerd heeft van een welbepaald geologisch gebied naar een ander, geologisch verchillend, gebied. Uit een vergelijking van de experimentele $^{87}Sr/^{86}Sr$ isotopenverhoudingen teruggevonden voor de individuen van Pandhof en Vrijthof kan gesuggereerd worden dat de individuen van Pandhof hun hele leven hebben doorgebracht in eenzelfde geologische streek, terwijl de individuen van Vrijthof migreerden naar een geologisch verschillende streek. Verder onderzoek is echter nodig om deze hypotheses te bevestigen, of te verwerpen. De analyse van bijkomende glazuur- en dentine monsters is nodig om een inzicht te verkrijgen in de homogeneïteit van de $^{87}Sr/^{86}Sr$ isotopenverhouding binnen de populaties van Pandhof en Vrijthof. Immers kan de dentine van individuen uit eenzelfde populatie een verschillende $^{87}Sr/^{86}Sr$ isotopenverhouding vertonen naar gelang het dieet van die persoon (vb. arm of rijk in Sr). Verder kan uit de

huidige data niet worden afgeleid welke onderzochte individuen hun laatste levensjaren doorbrachten in de streek van Maastricht. Om dit op te helderen dient de lokale biobeschikbare $^{87}Sr/^{86}Sr$ isotopenverhouding te worden bepaald. Dit kan gedaan worden door het biobeschikbare strontium te extraheren uit de bodem en de $^{87}Sr/^{86}Sr$ verhouding van deze fractie te bepalen, aangezien deze isotopenverhouding het strontium karakteriseert dat wordt opgenomen via de voeding. Een andere, en betere, manier om de biobeschikbare $^{87}Sr/^{86}Sr$ verhouding te achterhalen is de $^{87}Sr/^{86}Sr$ verhouding te bepalen van het tandglazuur van lokale zoogdieren, zoals muizen en knaagdieren, of deze van slakkenhuisjes van slakkensoorten die zich enkel voeden met mos. De beste manier, echter, is de $^{87}Sr/^{86}Sr$ analyse van het tandglazuur van archeologische dieren die met zekerheid lokaal verbleven gedurende dezelfde periode, zoals bijvoorbeeld varkens.

References

[Alfassi and Wai, 1992] – ZB Alfassi and CM Wai (1992) Preconcentration techniques for trace elements. CRC Press, Boston

[Almeida and Vasconcelos, 2001] – CM Almeida and MTSD Vasconcelos (2001) J Anal At Spectrom 16:607-611

[Anbar, 2004] – AD Anbar (2004) Molybdenum stable isotopes: observations, interpretations and directions. In: CM Johnson, BL Beard and F Albaréde (eds) Reviews in mineralogy & geochemistry, vol. 55. Geochemistry of non-traditional stable isotopes. Mineralogical Society of America, Washington:429-454

[Anbar *et al.*, 2000] – AD Anbar, JE Roe, J Barling and KH Nealson (2000) Science 288:126-128

[Anbar *et al.*, 2001] – AD Anbar, KA Knab and J Barling (2001) Anal Chem 73:1425-1431

[Andrén *et al.*, 2004] – H Andrén, I Rodushkin, A Stenberg, D Malinovsky and DC Baxter (2004) J Anal At Spectrom 19:1217-1224

[Anicich, 1993] – VG Anicich (1993) Astrophys J Suppl Ser 84:215-315

[Appelblad *et al.*, 2001] – PK Appelblad, I Rodushkin and DC Baxter (2001) Anal Chem 73:2911-2919

[Arnay-De-La-Rosa *et al.*, 1998] – M Arnay-De-La-Rosa, E Gonzalez-Reimers, J Velasco-Vazquez, L Galindo-Martin, E Delgado-Ureta, F Santolaria-Fernandez and N Barros-Lopez (1998) Sci Total Envir 209:107-111

[Attanasio *et al.*, 2001] – D Attanasio, G Bultrini and GM Ingo (2001) Archaeometry 43:529-547

[Aufderheide, 1989] – AC Aufderheide (1989) Chemical analysis of skeletal remains. In: MY Iscan and KAR Kennedy (eds) Reconstruction of like from the skeleton. Liss Inc., New York:237-260

[Avanzini, 2002] – A Avanzini (2002) Khor Rori report 1. In: A Avanzini (ed) Arabia antica. Universita di Pisa, Pisa

[Baker *et al.*, 2004] – J Baker, D Peate, T Waight and C Meyzen (2004) Chem Geol 211:275-303

[Baker *et al.*, 2006] – J Baker, S Stos and T Waight (2006) Archaeometry 48:45-56

[Balcaen *et al.*, 2005] – L Balcaen, I De Schrijver, L Moens and F Vanhaecke (2005) Int J Mass Spectrom 242:251-255

[Balter *et al.*, 2002] – V Balter, H Bocherens, A Person, N Labourdette, M Renard and B Vandermeersch (2002) Palaeogeogr Palaeoclimatol Palaeoecol 186:127-143

[Bandura and Tanner, 1999] – DR Bandura and SD Tanner (1999) At Spectrosc 20:69-72

[Bandura *et al.*, 2000] – DR Bandura, VI Baranov and SD Tanner (2000) J Anal At Spectrom 15:921-928

[Bandura *et al.*, 2001] – DR Bandura, VI Baranov and SD Tanner (2001) Fresenius J Anal Chem 370:454-470

[Bandura *et al.*, 2004] – DR Bandura, O Ornatsky and L Liao (2004) J Anal At Spectrom 19:96-100

[Baranov and Tanner, 1999] – VI Baranov and SD Tanner (1999) J Anal At Spectrom 14:1133-1142

[Barbaste *et al.*, 2002] – M Barbaste, K Robinson, S Guilfoyle, B Medina and R Lobinski (2002) J Anal At Spectrom 17:135-137

[Barnes *et al.*, 1974] – IL Barnes, WR Shields, TJ Murphy and RH Brill (1974) Isotopic analysis of Laurion lead ores. In: CW Beck (ed) Archaeological chemistry. American Chemical Society, Washington:1-10

[Barone, 1982] – JP Barone (1982) The role of hydroxyapatite in biological systems. In: LJ Anghileri and AM Tuffet-Anghileri (eds) The role of calcium in biological systems, volume 1. CRC Press, Boca Raton:27-40

[Barone *et al.*, 2004] – G Barone, V Crupi, S Galli, F Longo, D Majolino, P Mazzoleni and S Spagnolo (2004) Archaeometry 46:553-568

[Barone *et al.*, 2005] – G Barone, A Lo Giudice, P Mazzoleni, A Pezzino, D Barilaro, V Crupi and M Triscari (2005) Archaeometry 47:745-762

[Bashkin, 2002] – VN Bashkin (2002) Modern Biogeochemistry. Kluwer Academic, Dordrecht

[Beard and Johnson, 2000] – BL Beard and CM Johnson (2000) J Forensic Sci 45:1049-1061

[Beauchemin *et al.*, 1988] – D Beauchemin, JW McLaren and SS Berman (1988) J Anal At Spectrom 3:775-780

[Begemann *et al.*, 2001] – F Begemann, S Schmitt-Strecker, E Pernicka and F Lo Schiavo (2001) Eur J Archaeol 4:43-85

[Begley and Sharp, 1994] – IS Begley and BL Sharp (1994) J Anal At Spectrom 9:171-176

[Begley and Sharp, 1997] – IS Begley and BL Sharp (1997) J Anal At Spectrom 12:395-402

[Bellis *et al.*, 2008] – DJ Bellis, KM Hetter, MF Verostek and PJ Parsons (2008) J Anal At Spectrom 23:298-308

[Belshaw *et al.*, 1998] – NS Belshaw, PA Freedman, RK O'Nions, M Frank and Y Guo (1998) Int J Mass Spectrom 181:51-58

[Belshaw *et al.*, 2000] – NS Belshaw, XK Zhu, Y Guo and RK O'Nions (2000) Int J Mass Spectrom 197:191-195

[Bentley, 2006] – RA Bentley (2006) J Archaeol Method Theory 13:135-187

[Bentley and Knipper, 2005] – RA Bentley and C Knipper (2005) Archaeometry 47:629-644

[Bentley *et al.*, 2004] – RA Bentley, TD Price and E Stephan (2004) J Archaeol Sci 31:365-375

[Bettinelli *et al.*, 2000-a] – M Bettinelli, C Baffi, GM Beone and S Spezia (2000) At Spectrosc 21:50-59

[Bettinelli *et al.*, 2000-b] – M Bettinelli, GM Beone, S Spezia and C Baffi (2000) Anal Chim Acta 424:289-296

[Bigeleisen, 1998] – J Bigeleisen (1998) Proc Natl Acad Sci USA 95:4808-4809

[Bigeleisen and Mayer, 1947] – J Bigeleisen and MG Mayer (1947) J Chem Phys 15:261-267

[Bigi *et al.*, 1997] – A Bigi, G Cojazzi, S Panzavolta, A Ripamonti, N Roveri, M Romanello, KN Suarez and L Moro (1997) J Inorg Biochem 68:45-51

[Birck, 2004] – JL Birck (2004) An overview of isotopic anomalies in extraterrestrial materials and their nucleosynthetic heritage. In: CM Johnson, BL Beard and F Albaréde (eds) Reviews in mineralogy & geochemistry, vol. 55. Geochemistry of non-traditional stable isotopes. Mineralogical Society of America, Washington:25-64

[Blum *et al.*, 2000] – JD Blum, EH Taliaferro, MT Weisse and RT Holmes (2000) Biogeochemistry 49:87-101

[Boni *et al.*, 2000] – M Boni, G Di Maio, R Frei and IM Villa (2000) Archaeometry 42:201-208

[Botto and Zhu, 1994] – RI Botto and JJ Zhu (1994) J Anal At Spectrom 9: 905-912

[Boucharlat *et al.*, 1988] – R Boucharlat, E Haerinck, CS Phillips and DT Potts (1988) Akkadica 58:1-26

[Boulyga *et al.*, 2007] – SF Boulyga, U Klötzli, G Stingeder and T Prohaska (2007) Anal Chem 79:7753-7760

[Bower *et al.*, 2005] – NW Bower, SR Getty, CP Smith, ZR Simpson and JM Hoffman (2005) Int J Osteoarchaeol 15:360-370

[Bower *et al.*, 2007] – NW Bower, SA McCants, JM Custodio, ME Ketterer, SR Getty and JM Hoffman (2007) Sci Total Envir 372:463-473

[Brännvall *et al.*, 1999] – ML Brännvall, R Bindler, I Renberg, O Emteryd, J Bartnicki and K Billstrom (1999) Environ Sci Technol 33:4391-4395

[Braun and Ghersini, 1975] – T Braun and G Ghersini (1975) Extraction Chromatography. Elsevier, New York

[Brilli *et al.*, 2005] – M Brilli, G Cavazzini and B Turi (2005) J Archaeol Sci 32:1543-1551

[Budd *et al.*, 2000] – P Budd, J Montgomery, B Barreiro and RG Thomas (2000) Appl Geochem 15:687-694

[Bult and Hallewas, 1986] – EJ Bult and DP Hallewas (1986) Graven bij Valkenburg I: het archeologisch onderzoek in 1985. Delft

[Bult and Hallewas, 1987] – EJ Bult and DP Hallewas (1987) Graven bij Valkenburg II: het archeologisch onderzoek in 1986. Delft

[Bult and Hallewas, 1990] – EJ Bult and DP Hallewas (1990) Graven bij Valkenburg III: het archeologisch onderzoek in 1987 en 1988. Delft

[Burton *et al.*, 1999] – JH Burton, TD Price and WD Middleton (1999) J Archaeol Sci 26:609-616

[Busch *et al.*, 1988] – KL Busch, GL Glish and SA McLuckey (1988) Mass spectrometry: techniques and applications of tandem mass spectrometry. VCH, New York

[Buseth *et al.*, 1998] – E Buseth, G Wibetoe and I Martinsen (1998) J Anal At Spectrom 13:1039-1049

[Butler *et al.*, 1997] – WT Butler, HH Ritchie and ALJJ Bronckers (1997) Extracellular matrix proteins of dentine. In: DJ Chadwick and G Cardew (eds) Dental enamel. Wiley, Chichester:107-117

[Capo *et al.*, 1998] – RC Capo, BW Stewart and OA Chadwick (1998) Geoderma 82:197-225

[Carey and Caruso, 1992] – JM Carey and JA Caruso (1992) Crit Rev Anal Chem 23:397-439

[Carlson, 1996] – AK Carlson (1996) J Archaeol Sci 23:557-567

[Celsus] – Celsus, De Medicina. Translated in EH Warmington (1971) De Medicina. Harvard University Press, Cambridge

[Chakraborti, 1966] – H Chakraborti (1966) Trade and commerce of ancient India (c. 200 BC – c AD 650). Academic Publishers, Calcutta

[Chamberlain *et al.*, 1997] – CP Chamberlain, JD Blum, RT Holmes, XH Feng, TW Sherry and GR Graves (1997) Oecologia 109:132-141

[Chen and Jiang, 2002] – KL Chen and SJ Jiang (2002) Anal Chim Acta 470:223-228

[Chiaradia *et al.*, 2003] – M Chiaradia, A Gallay and W Todt (2003) Appl Geochem 18:353-370

[Cloquet *et al.*, 2005] – C Cloquet, O Rouxel, J Carignan and G Libourel (2005) Geostand Geoanal Res 29:95-106

[Cloquet *et al.*, 2006-a] – C Cloquet, J Carignan, G Libourel, T Sterckeman and E Perdrix (2006) Environ Sci Technol 40:2525-2530

[Cloquet *et al.*, 2006-b] – C Cloquet, J Carignan and G Libourel (2006) Atmos Environ 40:574-587

[Collerson *et al.*, 2002] – KD Collerson, BS Kamber and R Schoenberg (2002) Chem Geol 188:65-83

[Columella] – Columella, De Re Rustica. Translated in K Ahrens (1976) Über Landwirtschaft: ein Lehr- und Handbuch der gesamten Acker- und Viehwirtschaft aus dem 1. Jahrhundert u.Z.. Akad-Verlag, Berlin

[Coplen *et al.*, 2002] – TB Coplen, JK Böhlke, P De Bièvre, T Ding, NE Holden, JA Hopple, HR Krouse, A Lamberty, HS Peiser, K Révész, SE Rieder, KJR Rosman, E Roth, PDP Taylor, RD Vocke and YK Xiao (2002) Pure Appl Chem 74:1987-2017

[Craddock, 1995] – PT Craddock (1995) Early metal mining and production. Edinburgh University Press, Edinburgh

[Daems, 2004-a] – A Daems (2004) Arab Arch Epig 15:92-104

[Daems, 2004-b] – A Daems (2004) Arab Arch Epig 15:229-239

[Dams *et al.*, 1995] – RFJ Dams, J Goossens and L Moens (1995) Microchim Acta 119:277-286

[Darbyshire and Sewell, 1997] – DPF Darbyshire and RJ Sewell (1997) Chem Geol 143:81-93

[Darke and Tyson, 1994] – SA Darke and JF Tyson (1994) Microchem J 50:310-336

[Date and Gray, 1981] – AR Date and AL Gray (1981) Analyst 106:1255-1267

[Date and Gray, 1983-a] – AR Date and AL Gray (1983) Int J Mass Spectrom Ion Proc 48:357-360

[Date and Gray, 1983-b] – AR Date and AL Gray (1983) Analyst 108:159-165

[Date and Gray, 1983-c] – AR Date and AL Gray (1983) Spectrochim Acta B 38:29-37

[Date and Gray, 1985] – AR Date and AL Gray (1985) Spectrochim Acta B 40:115-122

[Davis *et al.*, 1990] – AM Davis, A Hashimoto, RN Clayton and TK Mayeda (1990) Nature 347:655-658

[De Bièvre *et al.*, 1993] – P De Bièvre, JR De Laeter, HS Peiser and WP Reed (1993) Mass Spectrom Rev 12:143-172

[De Hoffmann *et al.*, 1996] – E De Hoffmann, J Charette and V Stroobant (1996) Mass spectrometry. Masson, Paris:39-98

[De Laeter *et al.*, 2003] – JR De Laeter, JK Böhlke, P De Biévre, H Hidaka, HS Peiser, KJR Rosman and PDP Taylor (2003) Pure Appl Chem 75:683-800

[De Wannemacker *et al.*, 2000] – G De Wannemacker, F Vanhaecke, L Moens, A Van Mele and H Thoen (2000) J Anal At Spectrom 15:323-327

[de Wolff *et al.*, 2001] – FA de Wolff, TJ Hessing, E Smits and GB van der Voet (2001) Toxicol Sci suppl:60

[de Wolff *et al.*, 2008] – F de Wolff, E Smits, D De Muynck, C Cloquet, L Moens and F Vanhaecke (2008) in preparation

[Degryse *et al.*, 2006] – P Degryse, J Schneider, U Haack, V Lauwers, J Poblome, M Waelkens and P Muchez (2006) J Archaeol Sci 33:494-501

[Delrue, 2006] – P Delrue (2006) Arab Arch Epig 17:201-213

[Delrue, 2008] – P Delrue (2008) Archaeometallurgical analyses of pre-islamic artefacts from ed-Dur (Emirate of Umm al-Qaiwain, U.A.E.). PhD dissertation, Department of Languages and Cultures of the Near East and North Africa, Ghent University

[Delves and Campbell, 1993] – HT Delves and MJ Campbell (1993) Environ Geochem Health 15:75-84

[Deniel and Pin, 2001] – C Deniel and C Pin (2001) Anal Chim Acta 426:95-103

[Dietz, 1965] – LA Dietz (1965) Rev Sci Instr 36:1763-1770

[Douglas, 1989] – DJ Douglas (1989) Can J Spectrosc 34:38-49

[Douglas and Tanner, 1998] – DJ Douglas and SD Tanner (1998) Fundamental considerations in ICPMS. In: A Montaser (ed) Inductively coupled plasma mass spectrometry. Wiley-VCH, New York:615-679

[Driessens and Verbeeck, 1990] – FCM Driessens and RMH Verbeeck (1990) Biominerals. CRC Press, Boca Raton

[Eiden *et al.*, 1996] – GC Eiden, CJ Barinaga and DW Koppenaal (1996) J Anal At Spectrom 11:317-322

[Eisinger, 1977] – J Eisinger (1977) Trends Biochem Sci 2:147-150

[Ekstroem and Gustavsson, 1993] – H Ekstroem and I Gustavsson (1993) Application of ICP-MS to steel, other metals, and metal alloys. In: G Holland and AN Eaton (eds) Applications of plasma source mass spectrometry II. Royal Society of Chemistry, Cambridge:150-157

[Elbaz-Poulichet *et al.*, 1984] – F Elbaz-Poulichet, P Holliger, WW Huang and JM Martin (1984) Nature 308:409-411

[Elbaz-Poulichet *et al.*, 1986] – F Elbaz-Poulichet, P Holliger, JM Martin and D Petit (1986) Sci Total Envir 54:61-76

[Elias *et al.*, 1982] – RW Elias, Y Hirao and CC Patterson (1982) Geochim Cosmochim Acta 46:2561-2580

[Engström *et al.*, 2004] – E Engström, A Stenberg, DC Baxter, D Malinovsky, I Makinen, S Ponni and I Rodushkin (2004) J Anal At Spectrom 19:858-866

[Erel *et al.*, 1994] – YG Erel, Y Harlavan and JD Blum (1994) Geochim Cosmochim Acta 58:5299-5306

[Ericson, 1985] – JE Ericson (1985) J Hum Evol 14:503-514

[Ericson and Shirahata, 1985] – JE Ericson and H Shirahata (1985) Lead isotope analysis of ancient copper and base metal ore deposits in Western India. In: PA England and L van Zelst (eds) Application of science in examination of works of art. Museum of Fine Arts, Boston:207-212

[Erkkila *et al.*, 1992] – J Erkkila, R Armstrong, V Riihimaki, DR Chettle, A Paakkari, M Scott, L Somervaille, J Starck, B Kock and A Aitio (1992) Brit J Ind Med 49:631-644

[Ettler *et al.*, 2004] – V Ettler, M Mihaljevic and M Komarek (2004) Anal Bioanal Chem 378:311-317

[Evans and Giglio, 1993] – EH Evans and JJ Giglio (1993) J Anal At Spectrom 8:1-18

[Evans *et al.*, 1995] – EH Evans, JJ Giglio, TM Castillano and JA Caruso (1995) Inductively coupled and microwave induced plasma sources for mass spectrometry. Royal Society of Chemistry, Cambridge

[Ezzo *et al.*, 1997] – JA Ezzo, CM Johnson and TD Price (1997) J Archaeol Sci 24:447-466

[Falciani *et al.*, 2000] – R Falciani, E Novaro, M Marchesini and M Gucciardi (2000) J Anal At Spectrom 15:561-565

[Farias *et al.*, 1998] – P Farias, H Hu, E Rubenstein, F Meneses-Gonzalez, E Fishbein, E Palazuelos, A Aro and M Hernandez-Avila (1998) Environ Health Perspect 106:733-737

[Farmer *et al.*, 1994] – JG Farmer, CL Sugden, AB MacKenzie, GH Moody and M Fulton (1994) Environ Technol 15:593-599

[Faure, 1986-a] – G Faure (1986) Principles of isotope geology. Wiley, New York:117-140

[Faure, 1986-b] – G Faure (1986) Principles of isotope geology. Wiley, New York:282-308

[Faure, 1986-c] – G Faure (1987) Principles of isotope geology. Wiley, New York:309-340

[Faure and Mensing, 2005] – G Faure and TM Mensing (2005) Isotopes: principles and applications. Wiley, Hoboken:75-112

[Feldmann *et al.*, 1999-a] – I Feldmann, N Jakubowski and D Stuewer (1999) Fresenius J Anal Chem 365:415-421

[Feldmann *et al.*, 1999-b] – I Feldmann, N Jakubowski, C Thomas and D Stuewer (1999) Fresenius J Anal Chem 365:422-428

[Fortunato *et al.*, 2004] – G Fortunato, K Mumic, S Wunderli, L Pillonel, JO Bosset and G Gremaud (2004) J Anal At Spectrom 19:227-234

[Freestone *et al.*, 2003] – IC Freestone, KA Leslie, M Thirlwall and Y Gorin-Rosen (2003) Archaeometry 45:19-32

[Furuta, 1991] – N Furuta (1991) J Anal At Spectrom 6:199-203

[Gale, 1996] – NH Gale (1996) Anal Chim Acta 332:15-21

[Gale and Stos-Gale, 1987] – NH Gale and ZA Stos-Gale (1987) Oxhide ingots from Sardinia, Crete and Cyprus and the Bronze Age copper trade: new scientific evidence. In: MS Balmuth (ed) Studies in Sardinian archaeology III. Nuragic Sardinia and the Mycenaean World. Archaeopress, Oxford:159-198

[Gale and Stos-Gale, 2000] – NH Gale and Z Stos-Gale (2000) Lead isotope analysis applied to provenance studies. In: E Ciliberto and G Spoto (eds) Modern analytical methods in art and archaeology. Wiley, New York:503-584

[Gale *et al.*, 1997] – NH Gale, ZA Stos-Gale, G Maliotis and N Annetts (1997) Archaeometry 39:237-246

[Gale *et al.*, 2003] – NH Gale, ZA Stos-Gale, A Raduncheva, I Panayotov, I Ivanov, P Lilov and T Todorov (2003) Early metallurgy in Bulgaria. In: PT Craddock and J Lang (eds) Mining and metal production through the ages. British Museum Press, London:122-173

[Galer and Abouchami, 1998] – SJG Galer and W Abouchami (1998) Miner Mag 62A:491-492

[Galler *et al.*, 2007] – P Galler, A Limbeck, SF Boulyga, G Stingeder, T Hirata and T Prohaska (2007) Anal Chem 79:5023-5029

[Galy *et al.*, 2001] – A Galy, NS Belshaw, L Halicz and RK O'Nions (2001) Int J Mass Spectrom 208:89-98

[Garcia-Ruiz *et al.*, 2007] – S Garcia-Ruiz, M Moldovan and JIG Alonso (2007) J Chrom A 1149:274-281

[Ghazi, 1994] – AM Ghazi (1994) Appl Geochem 9:627-636

[Ghazi *et al.*, 1994] – AM Ghazi, KJ Reinhard, MA Holmes and E Durrance (1994) Amer J Phys Anthropol 95:427-434

[Gidlow, 2004] – DA Gidlow (2004) Occup-Med Oxford 54:76-81

[Giessmann and Greb, 1994] – U Giessmann and U Greb (1994) Fresenius J Anal Chem 350:186-193

[Gilfillan, 1965] – SC Gilfillan (1965) J Occup Med 7:53-60

[Graustein 1989] – WC Graustein (1989) $^{87}Sr/^{86}Sr$ ratios measure the sources and flow of strontium in terrestrial ecosystems. In: PW Rundel, JR Ehleringer and KA Nagy (eds) Stable isotopes in ecological research, vol. 68. Ecological studies. Springer, New York:491-512

[Gray, 1975] – AL Gray (1975) Analyst 100:289-299

[Gray, 1985] – AL Gray (1985) Analyst 110:551-556

[Gray, 1986] – AL Gray (1986) J Anal At Spectrom 1:403-405

[Gray, 1989] – AL Gray (1989) The origins, realization, and performance of ICP-MS systems. In: AR Date and AL Gray (eds) Applications of inductively coupled plasma mass spectrometry. Blackie, Glasgow:1-42

[Gray and Date, 1983] – AL Gray and AL Date (1983) Int J Mass Spectrom Ion Proc 46:7-10

[Gulson, 1996] – BL Gulson (1996) Environ Health Perspect 104:306-312

[Gulson and Gillings, 1997] – BL Gulson and BR Gillings (1997) Environ Health Perspect 105:820-824

[Gulson and Wilson, 1994] – B Gulson and D Wilson (1994) Arch Environ Health 49:279-283

[Gulson *et al.*, 1995] – BL Gulson, JJ Davis and J Bawdensmith (1995) Sci Total Envir 164:221-235

[Gulson *et al.*, 1997] – BL Gulson, CW Jameson and BR Gillings (1997) J Forensic Sci 42:787-791

[Günther *et al.*, 1999] – D Günther, SE Jackson and HP Longerich (1999) Spectrochim Acta B 54:381-409

[Habashi, 1994] – F Habashi (1994) A history of metallurgy. Métallurgie extractive Québec, Québec

[Habicht-Mauche *et al.*, 2002] – JA Habicht-Mauche, ST Glenn, MP Schmidt, R Franks, H Milford and AR Flegal (2002) J Archaeol Sci 29:1043-1053

[Haerinck, 2001] – E Haerinck (2001) Excavations at ed-Dur (Umm al-Qaiwain, United Arab Emirates), volume II: the tombs. Peeters, Leuven

[Haerinck, 2003] – E Haerinck (2003) Arab Arch Epig 14:88-94

[Halicz *et al.*, 1999] – L Halicz, A Galy, NS Belshaw and RK O'Nions (1999) J Anal At Spectrom 14:1835-1838

[Halliday *et al.*, 1995] – AN Halliday, DC Lee, JN Christensen, AJ Walder, PA Freedman, CE Jones, CM Hall, W Yi and D Teagle (1995) Int J Mass Spectrom Ion Proc 146-147:21-33

[Halliday *et al.*, 1998] – AN Halliday, DC Lee, JN Christensen, M Rehkämper, W Yi, X Luo, CM Hall, CJ Ballentine, T Pettke and C Stirling (1998) Geochim Cosmochim Acta 62:919-940

[Hattendorf *et al.*, 2005] – B Hattendorf, H Wanner, H Gu, S Dorn and D Günther (2005) Determination of Ca-44-isotope markers for parasitoid studies using dynamic reaction cell ICPMS. In: G Holland and DR Bandura (eds) Plasma source mass spectrometry: current trends and future developments. Royal Society of Chemistry, Cambridge:91-98

[Hedges, 2002] – REM Hedges (2002) Archaeometry 44:319-328

[Held and Taylor, 1999] – A Held and PDP Taylor (1999) J Anal At Spectrom 14:1075-1079

[Heumann, 1988] – KG Heumann (1988) Isotope dilution mass spectrometry. In: F Adams, R Gijbels and R van Grieken (eds) Inorganic mass spectrometry. Wiley, New York:301-376

[Heumann *et al.*, 1998] – KG Heumann, SM Gallus, G Rädlinger and J Vogl (1998) J Anal At Spectrom 13:1001-1008

[Hillson, 1986] – S Hillson (1986) Teeth. Cambridge University Press, Cambridge

[Hillson, 1996] – S Hillson (1996) Dental anthropology. Cambridge University Press, Cambridge

[Hinners *et al.*, 1998] – TA Hinners, R Hughes, PM Outridge, WJ Davis, K Simon and DR Woolard (1998) J Anal At Spectrom 13:963-970

[Hirata, 1996] – T Hirata (1996) Analyst 121:1407-1411

[Hirata, 1997] – T Hirata (1997) Geochim Cosmochim Acta 61:4439-4448

[Hobson, 1999] – KA Hobson (1999) Oecologia 120:314-326

[Hofmann, 1883] – KB Hofmann (1883) Die Getränke der Griechen und Römer vom hygienischen Standpunkte. Archiv für Geschichte der Medizin

[Hong *et al.*, 1994] – SM Hong, JP Candelone, CC Patterson and CF Boutron (1994) Science 265:1841-1843

[Hoogewerff *et al.*, 2001] – J Hoogewerff, W Papesch, M Kralik, M Berner, P Vroon, H Miesbauer, O Gaber, KH Künzel and J Kleinjans (2001) J Archaeol Sci 28:983-989

[Hoppe *et al.*, 1999] – KA Hoppe, PL Koch, RW Carlson and SD Webb (1999) Geology 27:439-442

[Hoppe *et al.*, 2003] – KA Hoppe, PL Koch and TT Furutani (2003) Int J Osteoarchaeol 13:20-28

[Hoppin *et al.*, 1997] – JA Hoppin, A Aro, H Hu and PB Ryan (1997) Pediatrics 100:365-370

[Horlick and Montaser, 1998] – G Horlick and A Montaser (1998) Analytical characteristics of ICPMS. In: A Montaser (ed) Inductively coupled plasma mass spectrometry. Wiley-VCH, New York:503-588

[Horwitz *et al.*, 1991] – EP Horwitz, ML Dietz and DE Fisher (1991) Anal Chem 63:522-525

[Horwitz *et al.*, 1992] – EP Horwitz, R Chiarizia and ML Dietz (1992) Solv Extr Ion Exch 10:313-336

[Horwitz *et al.*, 1994] – EP Horwitz, ML Dietz, S Rhoads, C Felinto, NH Gale and J Houghton (1994) Anal Chim Acta 292:263-273

[Houk *et al.*, 1980] – RS Houk, VA Fassel, GD Flesch, HJ Svec, AL Gray and CE Taylor (1980) Anal Chem 52:2283-2289

[Hu, 1991] – H Hu (1991) Am J Public Health 81:1070-1072

[IARC, 1987] – International Agency for Research on Cancer (1987) Monographs on the evaluation of the carcinogenic risk of chemicals to humans. Suppl. 6:230-232

[Ingle and Crouch, 1972] – JD Ingle and SR Crouch (1972) Anal Chem 44:777-784

[Ingle *et al.*, 2003] – CP Ingle, BL Sharp, MSA Horstwood, RR Parrish and DJ Lewis (2003) J Anal At Spectrom 18:219-229

[Iyengar, 1976] – GV Iyengar (1976) Radiochem Radioanal Lett 24:35-42

[Jackson, 2001] – TA Jackson (2001) Can J Fish Aquat Sci 58:185-196

[Jackson *et al.*, 2004] – BP Jackson, PV Winger and PJ Lasier (2004) Environ Pollut 130:445-451

[Jakubowski *et al.*, 1998] – N Jakubowski, L Moens and F Vanhaecke (1998) Spectrochim Acta B 53:1739-1763

[Jarvis *et al.*, 1992] – KE Jarvis, AL Gray and RS Houk (1992) Handbook of inductively coupled plasma mass spectrometry. Blackie, London

[Johnson *et al.*, 2004-a] – CM Johnson, BL Beard and F Albaréde (2004) Overview and general concepts. In: CM Johnson, BL Beard and F Albaréde (eds) Reviews in mineralogy & geochemistry, vol. 55. Geochemistry of non-traditional stable isotopes. Mineralogical Society of America, Washington:1-24

[Johnson *et al.*, 2004-b] – CM Johnson, BL Beard, EE Roden, DK Newman and KH Nealson (2004) Isotopic constraints on biogeochemical cycling of Fe. In: CM Johnson, BL Beard and F Albaréde (eds) Reviews in mineralogy & geochemistry, vol. 55. Geochemistry of non-traditional stable isotopes. Mineralogical Society of America, Washington:359-408

[Kabata-Pendias and Pendias, 1984-a] – A Kabata-Pendias and H Pendias (1984) Trace elements in soils and plants. CRC Press, Boca Raton:15-31

[Kabata-Pendias and Pendias, 1984-b] – A Kabata-Pendias and H Pendias (1984) Trace elements in soils and plants. CRC Press, Boca Raton:33-50

[Kabata-Pendias and Pendias, 1984-c] – A Kabata-Pendias and H Pendias (1984) Trace elements in soils and plants. CRC Press, Boca Raton:151-169

[Kabata-Pendias and Pendias, 1984-d] – A Kabata-Pendias and H Pendias (1984) Trace elements in soils and plants. CRC Press, Boca Raton:91-125

[Kamenov *et al.*, 2004] – GD Kamenov, PA Mueller and MR Perfit (2004) J Anal At Spectrom 19:1262-1267

[Keinonen, 1992] – M Keinonen (1992) Sci Total Envir 113:251-268

[Kennett *et al.*, 2002] – DJ Kennett, S Sakai, H Neff, R Gossett and DO Larson (2002) J Archaeol Sci 29:443-455

[Kennett *et al.*, 2004] – DJ Kennett, AJ Anderson, MJ Cruz, GR Clark and GR Summerhayes (2004) Archaeometry 46:35-46

[King and Harrison, 1989] – FL King and WW Harrison (1989) Int J Mass Spectrom Ion Proc 89:171-185

[King *et al.*, 1988] – FL King, AL McCormack and WW Harrison (1988) J Anal At Spectrom 3:883-886

[Kingston and Jassie, 1988] – HM Kingston and LB Jassie (1988) J Res Nat Bur Stand 93:269-274

[Kingston and Walter, 1998] – HM Kingston and PJ Walter (1998) The art and science of microwave sample preparations for trace and ultratrace elemental analysis. In: A Montaser (ed) Inductively coupled plasma mass spectrometry. Wiley-VCH, New York:33-81

[Klein *et al.*, 2004-a] – S Klein, Y Lahaye, GP Brey and HM Von Kaenel (2004) Archaeometry 46:469-480

[Klein *et al.*, 2004-b] – M Klein, F Jesse, HU Kasper and A Golden (2004) Archaeometry 46:339-356

[Kniseley *et al.*, 1974] – RN Kniseley, H Amenson, CC Butler and VA Fassel (1974) Appl Spectrosc 28:285-286

[Knudson *et al.*, 2004] – KJ Knudson, TD Price, JE Buikstra and DE Blom (2004) Archaeometry 46:5-18

[Knudson *et al.*, 2005] – KJ Knudson, TA Tung, KC Nystrom, TD Price and PD Fullagar (2005) J Archaeol Sci 32:903-913

[Kobert, 1909] – R Kobert (1909) Chronische Bleivergiftigung im klassischen Altertum. In: P Diergart (ed) Beiträge aus der Geschichte der Chemie. Franz Deuticke, Leipzig

[Koch *et al.*, 1992] – PL Koch, AN Halliday, LM Walter, RF Stearley, TJ Huston and GR Smith (1992) Earth Planet Sci Lett 108:277-287

[Koch *et al.*, 1995] – PL Koch, J Heisinger, C Moss, RW Carlson, ML Fogel and AK Behrensmeyer (1995) Science 267:1340-1343

[Kohn *et al.*, 1999] – MJ Kohn, MJ Schoeninger and WW Barker (1999) Geochim Cosmochim Acta 63:2737-2747

[Koirtyohann, 1994] – SR Koirtyohann (1994) Spectrochim Acta B 49:1305-1311

[Koppenaal *et al.*, 2004] – DW Koppenaal, GC Eiden and CJ Barinaga (2004) J Anal At Spectrom 19:561-570

[Krachler *et al.*, 2004] – M Krachler, G Le Roux, B Kober and W Shotyk (2004) J Anal At Spectrom 19:354-361

[Kurz, 1979] – EA Kurz (1979) Amer Lab 11:67-82

[Labs-Hochstein and MacFadden, 2006] – J Labs-Hochstein and BJ MacFadden (2006) Geochim Cosmochim Acta 70:4921-4932

[Latino *et al.*, 2001] – J Latino, K Neubauer and RE Wolf (2001) At Spectrosc 22:306-311

[Latkoczy *et al.*, 1998] – C Latkoczy, T Prohaska, G Stingeder and M Teschler-Nicola (1998) J Anal At Spectrom 13:561-566

[Latkoczy *et al.*, 2001] – C Latkoczy, T Prohaska, M Watkins, M Teschler-Nicola and G Stingeder (2001) J Anal At Spectrom 16:806-811

[Lee-Thorp and Sponheimer, 2003] – J Lee-Thorp and M Sponheimer (2003) J Anthropol Archaeol 22:208-216

[Leya *et al.*, 2000] – I Leya, R Wieler and AN Halliday (2000) Earth Planet Sci Lett 175:1-12

[Lindemann, 1919] – FA Lindemann (1919) Philosoph Mag 38:173-181

[Lindemann and Aston, 1919] – FA Lindemann and FW Aston (1919) Philosoph Mag 37:523-535

[Little *et al.*, 2004] – NC Little, LJ Kosakowsky, RJ Speakman, MD Glascock and JC Lohse (2004) J Radioanal Nucl Chem 262:103-110

[Longerich *et al.*, 1987] – HP Longerich, BJ Fryer and DF Strong (1987) Spectrochim Acta B 42:39-48

[Malinovskiy *et al.*, 2007] – D Malinovskiy, DC Baxter and I Rodushkin (2007) Environ Sci Technol 41:1596-1600

[Mallory-Greenough *et al.*, 1998] – LM Mallory-Greenough, JD Greenough and JV Owen (1998) J Archaeol Sci 25:85-97

[Manhès *et al.*, 1980] – G Manhès, CJ Allègre, B Dupré and B Hamelin (1980) Earth Planet Sci Lett 47:370-382

[Maréchal and Albarède, 2002] – C Maréchal and F Albarède (2002) Geochim Cosmochim Acta 66:1499-1509

[Maréchal *et al.*, 1999] – CN Maréchal, P Télouk and F Albarède (1999) Chem Geol 156:251-273

[Marengo *et al.*, 2005] – E Marengo, M Aceto, E Robotti, MC Liparota, M Bobba and G Panto (2005) Anal Chim Acta 537:359-375

[Marr, 1979] – IL Marr (1979) A Handbook of decomposition: methods in analytical chemistry. Wiley, New York

[Martinez-Garcia *et al.*, 2005] – MJ Martinez-Garcia, JM Moreno, J Moreno-Clavel, N Vergara, A Garcia-Sanchez, A Guillamon, M Porti and S Moreno-Grau (2005) Sci Total Envir 348:51-72

[Marzo *et al.*, 2007] – P Marzo, F Laborda and J Perez-Arantegui (2007) At Spectrosc 28:195-201

[May *et al.*, 1999] – TW May, RH Wiedmeyer, LD Brown and SW Casteel (1999) At Spectrosc 20:199-211

[McConnell, 1973] – D McConnell (1973) Apatite, its crystal chemistry, mineralogy, utilization and geologic and biologic occurrences. Springer, Vienna

[Meinhard *et al.*, 1992] – BA Meinhard, DK Brown and JE Meinhard (1992) Appl Spectrosc 46: 1134-1139

[Meyer, 2000] – VR Meyer (2000) Practical high-performance liquid chromatography. Wiley, Chichester:14-51

[Meynadier *et al.*, 2006] – L Meynadier, C Gorge, JL Birck and CJ Allegre (2006) Chem Geol 227:26-36

[Michiels and De Bièvre, 1983] – E Michiels and P De Bièvre (1983) Int J Mass Spectrom Ion Proc 48:369-372

[Millard, 2006] – A Millard (2006) Sci Total Envir 354:295-297

[Moens and Jakubowski, 1998] – L Moens and N Jakubowski (1998) Anal Chem 70:251-256

[Moens *et al.*, 1995] – L Moens, F Vanhaecke, J Riondato and R Dams (1995) J Anal At Spectrom 10:569-574

[Moens *et al.*, 2001] – LJ Moens, FF Vanhaecke, DR Bandura, VI Baranov and SD Tanner (2001) J Anal At Spectrom 16:991-994

[Montaser *et al.*, 1998-a] – A Montaser, MG Minnich, JA McLean, H Liu, JA Caruso and CW McLeod (1998) Sample introduction in ICPMS. In: A Montaser (ed) Inductively coupled plasma mass spectrometry. Wiley-VCH, New York:83-264

[Montaser *et al.*, 1998-b] – A Montaser, JA McLean, H Liu and JM Mermet (1998) An introduction to ICP spectrometries for elemental analysis. In: A Montaser (ed) Inductively coupled plasma mass spectrometry. Wiley-VCH, New York:1-31

[Moore, 1970] – CE Moore (1970) Ionization potentials and ionization limits derived from the analysis of optical spectra. In: DR Lide (ed) (1991) Handbook of chemistry and physics, 72nd edition. CRC Press, Boca Raton:10:211-212

[Moorey, 1994] – PRS Moorey (1994) Ancient Mesopotamian materials and industries. The archaeological evidence. Clarendon Press, Oxford

[Müller et al., 2003] – W Müller, H Fricke, AN Halliday, MT McCulloch and JA Wartho (2003) Science 302:862-866

[Myers *et al.*, 1994] – DP Myers, GLP Yang and GM Hieftje (1994) J Am Soc Mass Spectrom 5:1008-1016

[Myers *et al.*, 1995-a] – DP Myers, G Li, PP Mahoney and GM Hieftje (1995) J Am Soc Mass Spectrom 6:400-410

[Myers *et al.*, 1995-b] – DP Myers, G Li, PP Mahoney and GM Hieftje (1995) J Am Soc Mass Spectrom 6:411-420

[Needleman, 2004] – H Needleman (2004) Annu Rev Med 55:209-222

[Nelms *et al.*, 2001] – SM Nelms, CR Quétel, T Prohaska, J Vogl and PDP Taylor (2001) J Anal At Spectrom 16:333-338

[Nevissi, 1991] – AE Nevissi (1991) J Radioanal Nucl Chem 148:121-131

[Nielsen-Marsh and Hedges, 2000-a] – CM Nielsen-Marsh and REM Hedges (2000) J Archaeol Sci 27:1139-1150

[Nielsen-Marsh and Hedges, 2000-b] – CM Nielsen-Marsh and REM Hedges (2000) J Archaeol Sci 27:1151-1159

[Niu and Houk, 1996] – H Niu and RS Houk (1996) Spectrochim Acta B 51:779-815

[Nu, 2001] – Nu Instruments Ltd (2001) Isotopic standard ratios

[Nriagu, 1983-a] – JO Nriagu (1983) Lead and lead poisoning in antiquity. John Wiley & Sons, New York

[Nriagu, 1983-b] – JO Nriagu (1983) N Engl J Med 308:660-663

[O'Neil, 1986] – JR O'Neil (1986) Rev Mineral 16:1-40

[Olesik and Bates, 1995] – JW Olesik and LC Bates (1995) Spectrochim Acta B 50:285-303

[Ortiz, 2003] – MAH Ortiz (2003) Prehistoric mining and metallurgy in South West Iberian Peninsula. Archaeopress, Oxford

[Outridge *et al.*, 1996] – PM Outridge, RJ Hughes and RD Evans (1996) At Spectrosc 17:1-8

[Papadopoulou *et al.*, 2004] – DN Papadopoulou, GA Zachariadis, AN Anthemidis, NC Tsirliganis and JA Stratis (2004) Anal Chim Acta 505:173-181

[Papanikolaou *et al.*, 2005] – NC Papanikolaou, EG Hatzidaki, S Belivanis, GN Tzanakakis and AM Tsatsakis (2005) Med Sci Monit 11:329-336

[Park *et al.*, 2000] – CJ Park, KH Cho, JK Suh and MS Han (2000) J Anal At Spectrom 15:567-570

[Patterson *et al.*, 1991] – C Patterson, J Ericson, M Manea-Krichten and H Shirahata (1991) Sci Total Envir 107:205-236

[Periplus] – Periplus Maris Erythraei. Translated in L Casson (1989) The Periplus Maris Erythraei. Princeton University Press, Princeton

[Pernicka *et al.*, 1998] – A Pernicka, T Rehren and S Schmitt-Strecker (1998) Late Uruk silver production by cupellation at Habuba Kabira, Syria. In: T Rehren, A Hauptmann and JD Muhly (eds) Metallurgica Antiqua. Deutsches Bergbau-Museum, Bochum:123-134

[Peters and Beauchemin, 1993] – GR Peters and D Beauchemin (1993) Spectrochim Acta B 48:1481-1494

[Peters *et al.*, 1986] – GJ Peters, EJ Laurensse, A Leyva and HM Pinedo (1986) Clin Chim Acta 158:193-198

[Philip and Gerson, 1994-a] – AT Philip and B Gerson (1994) Clin Lab Med 14:423-444

[Philip and Gerson, 1994-b] – AT Philip and B Gerson (1994) Clin Lab Med 14:651-670

[Pin and Bassin, 1992] – C Pin and C Bassin (1992) Anal Chim Acta 269:249-255

[Pin *et al.*, 2003] – C Pin, S Joannon, C Bosq, B Le Fèvre and PJ Gauthier (2003) J Anal At Spectrom 18:135-141

[Piomelli, 2002] – S Piomelli (2002) Pediatr Clin N Am 49:1285-1304

[Platzner, 1997] – IT Platzner (1997) Modern isotope ratio mass spectrometry. Wiley, Chichester:403-447

[Plinius] – Plinius, Naturalis Historia. Translated in H Rackham (1947) Naturalis Historia. Harvard University Press, Cambridge

[Ponting, 2002] – MJ Ponting (2002) Archaeometry 44:555-571

[Ponting and Segal, 1998] – M Ponting and I Segal (1998) Archaeometry 40:109-122

[Price and Gestsdottir, 2006] – TD Price and H Gestsdottir (2006) Antiquity 80:130-144

[Price *et al.*, 1992] – TD Price, J Blitz, J Burton and JA Ezzo (1992) J Archaeol Sci 19:513-529

[Price *et al.*, 1994] – TD Price, CM Johnson, JA Ezzo, J Ericson and JH Burton (1994) J Archaeol Sci 21:315-330

[Price *et al.*, 2002] – TD Price, JH Burton and RA Bentley (2002) Archaeometry 44:117-135

[Price *et al.*, 2006] – TD Price, V Tiesler and JH Burton (2006) Amer J Phys Anthropol 130:485-490

[Prohaska *et al.*, 1999] – T Prohaska, S Hann, C Latkoczy and G Stingeder (1999) J Anal At Spectrom 14:1-8

[Prohaska *et al.*, 2002] – T Prohaska, C Latkoczy, G Schultheis, M Teschler-Nicola and G Stingeder (2002) J Anal At Spectrom 17:887-891

[Quétel *et al.*, 1997] – CR Quétel, B Thomas, OFX Donard and FE Grousset (1997) Spectrochim Acta B 52:177-187

[Quétel *et al.*, 2000] – CR Quétel, T Prohaska, M Hamester, W Kerl and PDP Taylor (2000) J Anal At Spectrom 15:353-358

[Rabinowitz, 1987] – MB Rabinowitz (1987) Biol Tr Elem Res 12:223-229

[Rabinowitz, 1991] – MB Rabinowitz (1991) Environ Health Perspect 91:33-37

[Rabinowitz *et al.*, 1976] – MB Rabinowitz, GW Wetherill and JD Kopple (1976) J Clin Invest 58:260-270

[Radosevich, 1993] – SC Radosevich (1993) The six deadly sins of trace element analysis: a case of wishful thinking in science. In: MK Sandford (ed) Investigations of ancient human tissue: chemical analyses in anthropology. Gordon & Breach, Philadelphia:269-332

[Rehkämper and Halliday, 1998] – M Rehkämper and AN Halliday (1998) Int J Mass Spectrom 181:123-133

[Rehkämper and Halliday, 1999] – M Rehkämper and AN Halliday (1999) Geochim Cosmochim Acta 63:935-944

[Rehkämper and Mezger, 2000] – M Rehkämper and K Mezger (2000) J Anal At Spectrom 15:1451-1460

[Rehkämper *et al.*, 2001] – M Rehkämper, M Schönbächler and CH Stirling (2001) Geostand Newslett-J Geost 25:23-40

[Rehkämper *et al.*, 2002] – M Rehkämper, M Frank, JR Hein, D Porcelli, A Halliday, J Ingri and V Liebetrau (2002) Earth Planet Sci Lett 197:65-81

[Rehkämper *et al.*, 2004] – M Rehkämper, F Wombacher and JK Aggarwal (2004) Stable isotope analysis by multiple collector ICP-MS. In: PA de Groot (ed) Handbook of stable isotope analytical techniques, vol. 1. Elsevier, Amsterdam:692-725

[Reinhard and Ghazi, 1992] – KJ Reinhard and AM Ghazi (1992) Amer J Phys Anthropol 89:183-195

[Resano *et al.*, 2005] – M Resano, J Perez-Arantegui, E Garcia-Ruiz and F Vanhaecke (2005) J Anal At Spectrom 20:508-514

[Richter *et al.*, 2006] – FM Richter, RA Mendybaev, JN Christensen, ID Hutcheon, RW Williams, NC Sturchio and AD Beloso (2006) Geochim Cosmochim Acta 70:277-289

[Riondato *et al.*, 2001] – J Riondato, F Vanhaecke, L Moens and R Dams (2001) Fresenius J Anal Chem 370:544-552

[Robinson *et al.*, 1995] – C Robinson, J Kirkham, SJ Brookes, WA Bonass and RC Shore (1995) Int J Dev Biol 39:145-152

[Rodushkin *et al.*, 2004] – I Rodushkin, A Stenberg, H Andrén, D Malinovskiy and DC Baxter (2004) Anal Chem 76:2148-2151

[Rohl, 1996] – BM Rohl (1996) Archaeometry 38:165-180

[Rokita *et al.*, 1993] – E Rokita, C Hermes, HF Nolting and J Ryczek (1993) J Cryst Growth 130:543-552

[Rosenfeld *et al.*, 1997] – A Rosenfeld, S Ilani and M Dvorachek (1997) J Archaeol Sci 24:857-864

[Roth, 1997] – E Roth (1997) Pure Appl Chem 69:1753-1828

[Rowan and Houk, 1989] – JT Rowan and RS Houk (1989) Appl Spectrosc 43:976-980

[Rowland *et al.*, 2008] – A Rowland, TB Housh and JA Holcombe (2008) J Anal At Spectrom 23:167-172

[Russ, 1989] – GP Russ III (1989) Isotope ratio measurements using ICP-MS. In: AR Date and AL Gray (eds) Applications of inductively coupled plasma mass spectrometry. Blackie, Glasgow:90-114

[Russ and Bazan, 1987] – GP Russ and JM Bazan (1987) Spectrochim Acta B 42:49-62

[Russell *et al.*, 1978] – WA Russell, DA Papanastassiou and TA Tombrello (1978) Geochim Cosmochim Acta 42:1075-1090

[Rutten, 2006] – K Rutten (2006) Het aardewerk van ed-Dur (Umm al-Qaiwain, V.A.E.) uit de late 1ste eeuw voor tot de vroege 2de eeuw na Christus. Technologische, typologische en vergelijkende studie met een analyse van de ruimtelijke verspreiding en handel in en voorbij de Perzische Golf. PhD dissertation, Department of Languages and Cultures of the Near East and North Africa, Ghent University

[Salles, 1980] – JF Salles (1980) Archaeol UAE 2-3:79-91

[Santos Zalduegui *et al.*, 2004] – JF Santos Zalduegui, S Garcia De Madinabeitia, JI Gil Ibarguchi and F Palero (2004) Archaeometry 46:625-634

[Sayre *et al.*, 2001] – EV Sayre, EC Joel, MJ Blackman, KA Yener and H Ozbal (2001) Archaeometry 43:77-115

[Schauble, 2004] – EA Schauble (2004) Applying stable isotope fractionation theory to new systems. In: CM Johnson, BL Beard and F Albaréde (eds) Reviews in mineralogy & geochemistry, vol. 55. Geochemistry of non-traditional stable isotopes. Mineralogical Society of America, Washington:65-111

[Schweissing and Grupe, 2003] – MM Schweissing and G Grupe (2003) J Archaeol Sci 30:1373-1383

[Scott *et al.*, 1974] – RH Scott, VA Fassel, RN Kniseley and DE Nixon (1974) Anal Chem 46:75-81

[Seah, 1995] – MP Seah (1995) Surf Interface Anal 23:729-732

[Sealy *et al.*, 1991] – JC Sealy, NJ Van der Merwe, A Sillen, FJ Kruger and HW Krueger (1991) J Archaeol Sci 18:399-416

[Sedov, 1996] – AV Sedov (1996) Qana' (Yemen) and the Indian Ocean: the archaeological evidence. In: HP Ray and JF Salles (eds) Tradition and archaeology, early maritime contacts in the Indian Ocean. Manohar, New Delhi:11-35

[Seeley and Turner, 1984] – NJ Seeley and PJ Turner (1984) Metallurgical investigation of three early Indian coinages: implications for metal trading and dynastic chronology. In: B Allchin (ed) South Asian archaeology 1981. Cambridge University Press, Cambridge:331-333

[Sheppard *et al.*, 1990] – BS Sheppard, WL Shen, TM Davidson and JA Caruso (1990) J Anal At Spectrom 5:697-700

[Shotyk *et al.*, 1998] – W Shotyk, D Weiss, PG Appleby, AK Cheburkin, R Frei, M Gloor, JD Kramers, S Reese and WO Van der Knaap (1998) Science 281:1635-1640

[Sillen and Sealy, 1995] – A Sillen and JC Sealy (1995) J Archaeol Sci 22:313-320

[Sillen *et al.*, 1995] – A Sillen, G Hall and R Armstrong (1995) J Hum Evol 28:277-285

[Sillen *et al.*, 1998] – A Sillen, G Hall, S Richardson and R Armstrong (1998) Geochim Cosmochim Acta 62:2463-2473

[Skulan *et al.*, 2002] – JL Skulan, BL Beard and CM Johnson (2002) Geochim Cosmochim Acta 66:2995-3015

[Smits, 2006] – E Smits (2006) Leven en sterven langs de Limes. PhD dissertation, University of Amsterdam

[Smits *et al.*, 2008] – E Smits, F de Wolff, D De Muynck, C Cloquet, L Moens and F Vanhaecke (2008) in preparation

[Srinivasan, 1999] – S Srinivasan (1999) Archaeometry 41:91-116

[Stacey and Kramers, 1975] – JS Stacey and JD Kramers (1975) Earth Planet Sci Lett 26:207-221

[Stos-Gale *et al.*, 1986] – ZA Stos-Gale, NH Gale and U Zwicker (1986) The copper trade in the South-East Mediterranean region. Preliminary scientific evidence. The department of Antiquities, Cyprus:122-144

[Stos-Gale *et al.*, 1995] – ZA Stos-Gale, NH Gale, J Houghton and R Speakman (1995) Archaeometry 37:407-415

[Stos-Gale *et al.*, 1996] – ZA Stos-Gale, NH Gale and N Annetts (1996) Archaeometry 38:381-390

[Stos-Gale *et al.*, 1997] – ZA Stos-Gale, G Maliotis, NH Gale and N Annetts (1997) Archaeometry 39:83-123

[Stos-Gale *et al.*, 1998-a] – ZA Stos-Gale, G Maliotis and NH Gale (1998) A preliminary survey of the Cypriot slag heaps and their contribution to the reconstruction of copper production in Cyprus. In: T Rehren, A Hauptmann and JD Muhly (eds) Metallurgica Antiqua. Deutsches Bergbau-Museum, Bochum:235-262

[Stos-Gale *et al.*, 1998-b] – ZA Stos-Gale, NH Gale, N Annetts, T Todorov, P Lilov, A Raduncheva and I Panayotov (1998) Archaeometry 40:217-226

[Strelow, 1960] – FWE Strelow (1960) Anal Chem 32:1185-1188

[Stürup *et al.*, 2006] – S Stürup, L Bendahl and B Gammelgaard (2006) J Anal At Spectrom 21:297-304

[Suetonius] – Suetonius, The twelve Caesars. Translated in M Grant (1975) The twelve Caesars. Charles Scribner's Sons, London

[Sulcek and Povondra, 1989] – Z Sulcek and P Povondra (1989) Methods of decomposition in inorganic analysis. CRC Press, Boca Raton

[Sun *et al.*, 1987] – XF Sun, BTG Ting, SH Zeisel and M Janghorbani (1987) Analyst 112:1223-1228

[Tanner and Baranov, 1999] – SD Tanner and VI Baranov (1999) At Spectrosc 20:45-52

[Tanner *et al.*, 1994] – SD Tanner, LM Cousins and DJ Douglas (1994) Appl Spectrosc 48:1367-1372

[Tanner *et al.*, 2002] – SD Tanner, VI Baranov and DR Bandura (2002) Spectrochim Acta B 57:1361-1452

[Taylor and McLennan, 1995] – SR Taylor and SM McLennan (1995) Rev Geophys 33:241-265

[Taylor *et al.*, 1995] – PDP Taylor, P De Bièvre, AJ Walder and A Entwistle (1995) J Anal At Spectrom 10:395-398

[Taylor *et al.*, 1998] – HE Taylor, RA Huff and A Montaser (1998) Novel applications of ICP-MS. In: A Montaser (ed) Inductively coupled plasma mass spectrometry. Wiley-VCH, New York:681-807

[Thirlwall, 1991] – MF Thirlwall (1991) Chem Geol 94:85-104

[Thornton and Ehlers, 2003] – CP Thornton and CB Ehlers (2003) IAMS Journal 23:3-8

[Tomascak *et al.*, 1999] – PB Tomascak, RW Carlson and SB Shirey (1999) Chem Geol 158:145-154

[Trickett *et al.*, 2003] – MA Trickett, P Budd, J Montgomery and J Evans (2003) Appl Geochem 18:653-658

[Trincherini *et al.*, 2001] – PR Trincherini, P Barbero, P Qurati, C Domergue and L Long (2001) Archaeometry 43:393-406

[Tunstall and Amarasiriwardena, 2002] – S Tunstall and D Amarasiriwardena (2002) Microchem J 73:335-347

[Turner *et al.*, 1997] – P Turner, T Merren, J Speakman and C Haines (1997) Interface studies in the ICP – mass spectrometer. In: G Holland and SD Tanner (eds) Plasma source mass spectrometry, developments and applications. Royal Society of Chemistry, Cambridge:28-34

[Turner *et al.*, 1998] – PJ Turner, DJ Mills, E Schröder, G Lapitajs, G Jung, LA Iacone, DA Haydar and A Montaser (1998) Instrumentation for low- and high resolution ICPMS. In: A Montaser (ed) Inductively coupled plasma mass spectrometry. Wiley-VCH, New York:421-501

[Tylecote, 1962] – RF Tylecote (1962) Metallurgy in archaeology: a prehistory of metallurgy in the British Isles. Edward Arnold Publishers Ltd, London

[Tylecote, 1976] – RF Tylecote (1976) A history of metallurgy. The metals society, London

[Underwood, 1977-a] – EJ Underwood (1977) Trace elements in human and animal nutrition. Academic Press, New York:430-458

[Underwood, 1977-b] – EJ Underwood (1977) Trace elements in human and animal nutrition. Academic Press, New York:410-423

[Urey, 1947] – HC Urey (1947) J Chem Soc (London):562-581

[Urey and Greiff, 1935] – HC Urey and LJ Greiff (1935) J Am Chem Soc 57:321-327

[Vandecasteele *et al.*, 1988] – C Vandecasteele, M Nagels, H Vanhoe and R Dams (1988) Anal Chim Acta 211:91-98

[Vanhaecke and Moens, 2004] – F Vanhaecke and L Moens (2004) Anal Bioanal Chem 378:232-240

[Vanhaecke *et al.*, 1992] – F Vanhaecke, H Vanhoe, R Dams and C Vandecasteele (1992) Talanta 39:737-742

[Vanhaecke *et al.*, 1996-a] – F Vanhaecke, M Van Holderbeke, L Moens and R Dams (1996) J Anal At Spectrom 11:543-548

[Vanhaecke *et al.*, 1996-b] – F Vanhaecke, L Moens, R Dams and P Taylor (1996) Anal Chem 68:567-569

[Vanhaecke *et al.*, 1997] – F Vanhaecke, L Moens, R Dams, I Papadakis and P Taylor (1997) Anal Chem 69:268-273

[Vanhaecke *et al.*, 1998] – F Vanhaecke, G De Wannemacker, L Moens, R Dams, C Latkoczy, T Prohaska and G Stingeder (1998) J Anal At Spectrom 13:567-571

[Vanhaecke *et al.*, 1999] – F Vanhaecke, L Moens, R Dams, L Allen and S Georgitis (1999) Anal Chem 71:3297-3303

[Vanhaecke *et al.*, 2001] – F Vanhaecke, G De Wannemacker, L Moens and P Van den Haute (2001) Fresenius J Anal Chem 371:915-920

[Vanhaecke *et al.*, 2003] – F Vanhaecke, L Balcaen, I Deconinck, I De Schrijver, CM Almeida and L Moens (2003) J Anal At Spectrom 18:1060-1065

[Vanhaecke *et al.*, 2006] – F Vanhaecke, L Balcaen and P Taylor (2006) Use of ICP-MS for isotope ratio measurements. In: S Hill (ed) Inductively coupled plasma mass spectrometry and its applications. Blackwell Publishing, Oxford:160-225

[Veillon and Margoshe, 1968] – C Veillon and M Margoshe (1968) Spectrochim Acta B 23:503-533

[Veis, 1989] – A Veis (1989) Biochemical studies of vertebrate tooth mineralization. In: S Mann, J Webb and RJP Williams (eds) Biomineralization: chemical and biochemical perspectives. VCH, New York:189-222

[Verstraete *et al.*, 1998] – D Verstraete, J Riondato, J Vercauteren, F Vanhaecke, L Moens, R Dams and M Verloo (1998) Sci Total Envir 218:153-160

[Vieira *et al.*, 1986] – PA Vieira, H Zhizhuang, SK Chan and A Montaser (1986) Appl Spectrosc 40:1141-1146

[Vukovic *et al.*, 1998] – Z Vukovic, S Lazic, I Tutunovic and S Raicevic (1998) J Serb Chem Soc 63:387-393

[Waight *et al.*, 2002] – T Waight, J Baker and D Peate (2002) Int J Mass Spectrom 221:229-244

[Wakabayashi *et al.*, 2007] – T Wakabayashi, T Ohno, Y Fukushi, T Komiya and T Hirata (2007) Geochim Cosmochim Acta 71S:A1079

[Walczyk, 2004] – T Walczyk (2004) Anal Bioanal Chem 378:229-231

[Walder and Freedman, 1992] – AJ Walder and PA Freedman (1992) J Anal At Spectrom 7:571-575

[Walder and Furuta, 1993] – AJ Walder and N Furuta (1993) Anal Sci 9:675-680

[Walder *et al.*, 1993] – AJ Walder, I Platzner and PA Freedman (1993) J Anal At Spectrom 8:19-23

[Wallach and Chausmer, 1990] – S Wallach and AB Chausmer (1990) Metabolism of trace metals in animals and man: part I: non-essential pollutant metals. In: ND Priest and FL Van de Vyver (eds) Trace metals and fluoride in bones and teeth. CRC Press, Boca Raton:231-252

[Walters and Barnardt, 1988] – PE Walters and CA Barnardt (1988) Spectrochim Acta B 43:325-337

[Walton and Rocklin, 1990] – HF Walton and RD Rocklin (1990) Ion exchange in analytical chemistry. CRC Press, Boston

[Weeks, 2004] – LR Weeks (2004) Arab Arch Epig 15:240-252

[Weiss *et al.*, 1999] – D Weiss, W Shotyk, JD Kramers and M Gloor (1999) Atmos Environ 33:3751-3763

[Weiss *et al.*, 2004] – DJ Weiss, B Kober, A Dolgopolova, K Gallagher, B Spiro, G Le Roux, TFD Mason, M Kylander and BJ Coles (2004) Int J Mass Spectrom 232:205-215

[Weyer and Schwieters, 2003] – S Weyer and JB Schwieters (2003) Int J Mass Spectrom 226:355-368

[White *et al.*, 2000] – WM White, F Albarède and P Télouk (2000) Chem Geol 167:257-270

[Whitehouse, 1998] – D Whitehouse (1998) Excavations at ed-Dur (Umm al-Qaiwain, United Arab Emirates), volume I: the glass vessels. Peeters, Leuven

[Wombacher and Rehkämper, 2003] – F Wombacher and M Rehkämper (2003) J Anal At Spectrom 18:1371-1375

[Woodhead *et al.*, 1995] – JD Woodhead, F Volker and MT McCulloch (1995) Analyst 120:35-39

[Woolard *et al.*, 1998] – D Woolard, R Franks and DR Smith (1998) J Anal At Spectrom 13:1015-1019

[Wopenka and Pasteris, 2005] – B Wopenka and JD Pasteris (2005) Mat Sci Eng C-Biomim Supram S 25:131-143

[Wu *et al.*, 2003] – MC Wu, SJ Jiang and TS Hsi (2003) Anal Bioanal Chem 377:154-158

[Yaffe *et al.*, 1983] – Y Yaffe, CP Flessel, JJ Wesolowski, A Del Rosario, GN Guirguis, V Matias, TE Degarmo, GC Coleman, JW Gramlich and WR Kelly (1983) Arch Environ Health 38:237-245

[Yang and Jiang, 2004] – CH Yang and SJ Jiang (2004) Spectrochim Acta B 59:1389-1394

[Yener *et al.*, 1991] – KA Yener, EV Sayre, EC Joel, H Ozbal, IL Barnes and RH Brill (1991) J Archaeol Sci 18:541-577

[Yoshinaga *et al.*, 1998] – J Yoshinaga, M Yoneda, M Morita and T Suzuki (1998) Appl Geochem 13:403-413

[Young *et al.*, 1997] – SMM Young, P Budd, R Haggerty and AM Pollard (1997) Archaeometry 39:379-392

[Young *et al.*, 2002] – ED Young, A Galy and H Nagahara (2002) Geochim Cosmochim Acta 66:1095-1104

[Zapata *et al.*, 2006] – J Zapata, C Perez-Sirvent, MJ Martinez-Sanchez and P Tovar (2006) Sci Total Envir 369:357-368

[Zhu *et al.*, 2000-a] – XK Zhu, RK O'Nions, Y Guo, NS Belshaw and D Rickard (2000) Chem Geol 163:139-149

[Zhu *et al.*, 2000-b] – XK Zhu, RK O'Nions, YL Guo and BC Reynolds (2000) Science 287:2000-2002

[Zolotov *et al.*, 1986] – YA Zolotov, NM Kuzmin, OM Petrukhin and BY Spivakov (1986) Anal Chim Acta 180:137-161

[Zoorob *et al.*, 1998] – GK Zoorob, JW McKiernan and JA Caruso (1998) Microchim Acta 128:145-168

[Zutterman, 2003] – C Zutterman (2003) Arab Arch Epig 14:81-87